Advanced Control of Reaction Selectivity via High-speed Micromixing Flow Processes: A Breakthrough Approach to Protein Functionalization

June 2023

Yuichi Nakahara

Department of Chemistry

Graduate School of Science

(Doctor's course)

HOKKAIDO UNIVERSITY

Contents

Chapter 1

General Introduction

1. Flow micro-process technology: importance in process chemistry

The remarkable progress of mankind has been substantially aided by advances in science and technology. Chemical materials serve an indispensable role in numerous sectors, including automotive, electronics, pharmaceuticals, consumer goods, and construction. Not only do these novel materials enhance human living standards, but they also increasingly address the rising demand for energy conservation and environmental harmony. As technology advances, a shift is observed from basic chemical substances towards functional substances. This implies an industrial use of high-molecular-weight compounds and biomacromolecules such as proteins and nucleic acids, extending beyond just simple low-molecular-weight compounds. A movement towards more complex functional chemicals, including composites, inorganic hybrids, and protein conjugates, is also evident.

In the context of semiconductor materials, miniaturization, a crucial factor for improving the performance of smartphones and semiconductors, necessitates the functionalization of chemical products. This emphasizes the importance of precision synthesis processes, such as elevating yields and curbing impurities. The escalation in energy costs and the evolution of environmentally sustainable processes are also significant considerations.

Another noteworthy advancement in functional chemicals is visible within the pharmaceutical industry. Proteins and their functional conjugates are rapidly becoming standard as biotechnological materials. The introduction and functionalization of new materials through chemical processes, like PEGylated drugs such as Pegasys and antibody-drug conjugates (ADCs) like Enhertu, have been creating blockbuster products consistently. The key to these achievements lies in the stable production of these complex biomolecules.

Reports on continuous manufacturing specific to the drug manufacturing process have been issued by the FDA. In parallel, the Japanese PMDA has established a working group on continuous manufacturing, indicating a shift towards this production model. A specific expectation held by the FDA for Contract Manufacturing Organizations

(CMOs) involves the establishment of continuous manufacturing systems. Flow microreactor technology can be particularly impactful in this context.

Flow microreactor technology

Flow microreactor (FMR) technology, utilizing microscale environments, represents a transformative approach to process chemistry. This technology, initially spearheaded by the Mainz Microengineering Institute and the Karlsruhe Central Research Institute in Germany, capitalizes on the unique physical and chemical phenomena present in micro spaces. The concept of using semiconductor miniaturization technology for chemical synthesis has been introduced, revolutionizing the perception and control of chemical reactions.

A defining feature of flow microreactor technology, when compared to traditional batch synthesis, is recognized as its capacity for rapid heat and mass transfer. Greater control over reactions is thus enabled, and even hazardous processes can be carried out safely. This control often leads to improved yields, reduced impurities, and enhanced safety standards.

The contribution of FMR technology extends beyond basic process chemistry. A significant contribution to the sophistication of chemical products is made, easing the transition from basic to highly functional chemicals, such as complex high molecular weight compounds, proteins, nucleic acids, and their conjugates.

This technology proves particularly compelling in the pharmaceutical sector, where the continuous manufacture of complex biomolecules gains increasing importance. The necessity for such manufacturing systems is emphasized by regulatory bodies like the FDA and PMDA, with FMR technology serving as a cornerstone in meeting these standards.

FMR technology offers a compelling solution as the drive for environmentally sustainable practices intensifies. Energy-efficient processes that meet modern environmental expectations are provided by this technology. The attention garnered by FMR technology in recent years is not confined to academia but extends into the industrial sector as well. Collaborative efforts to advance this technology are burgeoning, led by various academic and industrial entities such as the Kyoto University Microchemical Production Consortium, the Kinki Chemical Association Flow Microsynthesis Research Group, and the Chemical Engineering Society Reaction Engineering Department Microchemical Process Subcommittee.

Physical and chemical processes such as the mixing and diffusion of raw materials, along with heat transfer within and outside the reaction system, are entailed by chemical reactions. Both process chemistry research and

industrial applications demand a thorough analysis and understanding of these processes and the identification of rate-determining factors. The incorporation of microfluidic technology into process chemistry, as explored in this thesis, signifies a substantial step towards this understanding and optimized application.

2. The role of mixing in flow microprocess chemistry

Mixing operations, a fundamental technique in process chemistry, entail the homogenization of two different liquids, and are vital to enhancing reactions in chemical processes. Typically, mixing in batch reactions is seen as macro-mixing, comprising two basic operations:

(1) breaking fluid lumps into smaller, uniform dispersions

(2) dispersing the fluid to molecular size.

The macroscopic mixing process relies on agitation, shear forces, and other methods to reduce fluid lump sizes. Microscopic mixing, by contrast, is facilitated by molecular diffusion over time, which gradually reduces the concentration difference between two fluids until homogeneity is achieved.

Micromixing, an alternative approach, takes advantage of the laminar flow state where viscous forces dominate, thereby enabling direct mixing by molecular diffusion. This technique permits precise and rapid mixing without necessitating the homogenization of fluid lumps seen in macro-mixing. The rapid mixing offered by flow microreactors can inhibit side reactions triggered by mixing rate-determining steps in batch reactions. It also enables chemical processes design based on true reaction rate constants. Additionally, the control of residence time within microreactors allows precise generation and utilization of unstable reaction intermediates and active species, paving the way for innovative chemical processes unachievable in traditional batch processes.

In chemical reactions, elements such as mixing and diffusion of raw materials, heat transfer from reactions, and heat exchange with the external environment are integral. Analyses of these processes and understanding the rate-determining factors are crucial for both process chemistry research and industrial applications. While various methods, like fluid simulations in traditional batch reactors, have been suggested for these analyses, they pose substantial challenges, including scale dependencies. However, flow-type reaction devices, including FMRs, extend beyond mere manufacturing methods, enhancing the understanding of reactions and physicochemical phenomena, thus being essential tools in process chemistry research.

The purpose of this dissertation is to comprehend reaction selectivity based on the micro rapid mixing feature of flow microreactors, and to investigate its applicability in highly functionalized protein processes such as conjugation processes and protein refolding processes. Particularly, studies exploring rapid mixing, the starting point of reactions, to control unstable intermediates using flow microreactors are limited. Therefore, by building evaluation systems using actual chemical synthesis processes, performing fluid simulations based on mixing, and capturing diverse

physicochemical phenomena like reactions, diffusion, and heat transfer, research into microchemical processes can be accelerated. Applying these microchemical insights to protein high-functionalization processes using microreactors, a scarcely explored research field, has the potential to pioneer new areas of research and development.

Keeping this in mind, work has been undertaken on constructing fundamental theories of rapid reactions in flow microprocess chemistry. The focus is on assessing the impacts of mixing speed on the control of the functional group selectivity of organolithium species using ultra-short time reactions unachievable in batch reactors (Chapter 2), constructing a mixing speed evaluation method using the degree of dispersion of polystyrene synthesized by living anionic polymerization as an indicator (Chapter 3), and building a reaction heat flux evaluation model based on reaction speed analysis and mixing, and heat generation and retardation in the exothermic reaction of ionic liquid synthesis (Chapter 4). Building on these fundamental theories, the FMR process has been applied to the monodisperse PEGylation of proteins as an application of flow microprocess chemistry (Chapter 5), and an efficient protein refolding process has been performed through precise temporal and spatial control technologies (Chapter 6). Detailed summaries of each chapter are provided in the following sections of this dissertation. This dissertation aims to underscore the significant impact of mixing operations on the efficiency and outcomes of chemical processes.

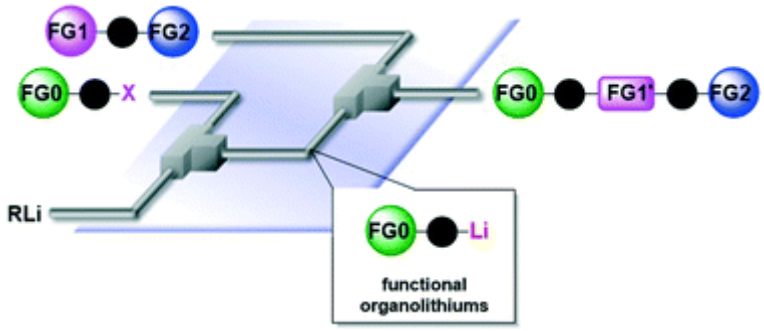

Figure 1. Illustration of chemoselective reactions of difunctional electrophiles with functional aryllithiums induced by micromixing

Chemical reactions involving functional groups are governed by the nucleophilicity or electrophilicity of each functional group, with their reaction rates typically addressed in terms of rate laws represented by rate constants. For compounds possessing multiple functional groups, it is expected that the functional group with the higher rate constant would preferentially react. Yet, in traditional batch reactors, reactions of functional groups with slower rate constants often proceed simultaneously. This concurrent occurrence is due to the simultaneous nature of mixing and reaction, frequently resulting in product ratios significantly deviating from predictions based on rate constants. Contrarily, FMR technology, utilizing micromixers, enables reduction of mixing time through molecular diffusion in microspaces.

Among FMR technologies, "flash chemistry" has been identified as a technique capable of actualizing ultra-short-time reactions. Given that the mixing speed of starting materials in reactions involving organic lithium species significantly influences the products, comprehension of the relationship between mixing speed and reaction rate becomes critical. In this research, the product ratio resulting from reactions of a dual-functionality electrophile (an aldehyde and a ketone) and phenyllithium (PhLi) was evaluated, considering reaction temperature, type of micromixer, and flow rate as indices of reaction selectivity. It was confirmed that by controlling the mixing speed, selective reaction of the aldehyde group occurs, while the reaction of the ketone group and subsequent reactions are suppressed. Additionally, the feasibility of condensation reactions was demonstrated through generation of short-lived organic lithium species and their rapid mixing under precise residence time control. These findings suggest that chemical processes based on inherent reaction rates of functional groups can be established by manipulation of the mixing rate.

Capter-3. Molecular Weight Distribution of Polymers Produced by Anionic Polymerization Enables Mixability Evaluation

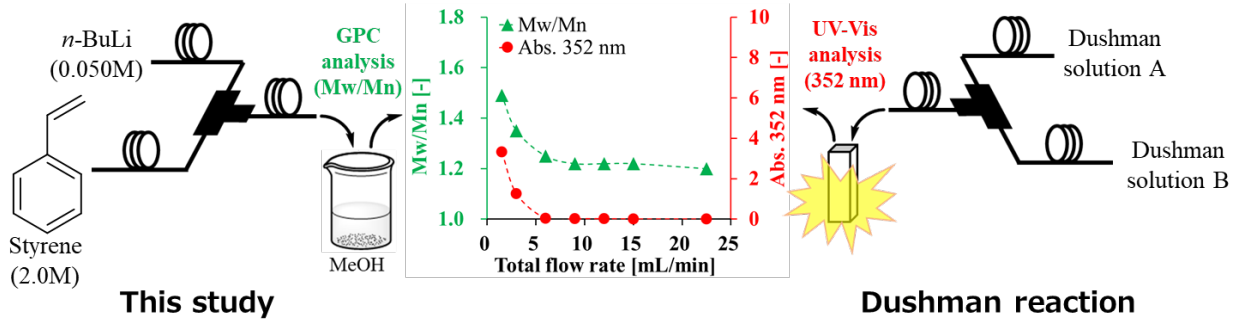

Figure 2. Illustration of mixability evaluation utilizing molecular weight distribution of polymers produced by anionic polymerization

In reaction processes utilizing FMR technology, the importance of mixing performance for precise reaction control is underscored. It is recognized that the type of micromixer employed significantly impacts the mixing process. Conventionally, the evaluation of mixing performance has been executed using a colorimetric reaction, leveraging a competitive reaction between a neutralization reaction, termed the Villermaux–Dushman reaction, and a redox reaction. However, due to these evaluations involving reactions with aqueous solutions, an assessment of mixing performance at temperatures below 0 °C has been unattainable. Furthermore, with the advancement of micromixer technology, a point has been reached whereby the Villermaux–Dushman reaction no longer suffices as a basis for contrasting mixing performance.

Addressing these challenges, a novel mixing performance evaluation system has been constructed, inspired by the observation that the molecular weight distribution of polystyrene synthesized by living anionic polymerization, an illustrative application of flow microreactors, is contingent on the mixing performance. The newly instituted evaluation system has been employed to demonstrate the feasibility of assessing mixing performance not only at temperatures below 0 °C, where traditional scoring methods fall short, but also for micromixers of differing internal diameters, which formerly exhibited insufficient performance divergence in the Villermaux–Dushman reactions. This achievement manifests the versatility and adaptability of the devised scoring system in evaluating mixing performance.

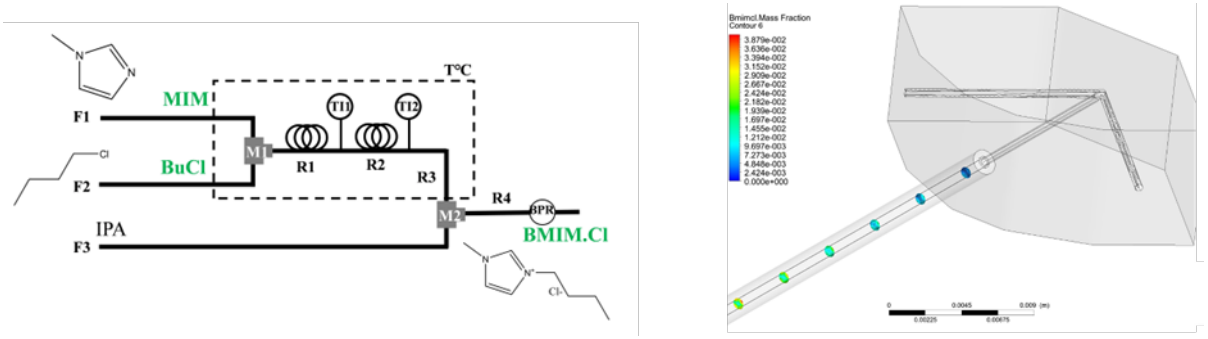

Figure 3. Illustration of ionic liquid synthesis produced by FMR: modeling and design of experiments

A reaction process is governed by a combination of several physicochemical processes, including the mixing of reactants, the chemical reaction itself, the generation of heat, and the diffusion of products. Not only the chemical reaction but also the physical processes associated with mixing and heat transfer are included. The reaction rate, being particularly affected by mixing and heat transfer, is quantified with these physical phenomena taken into consideration.

In the study discussed, the process of synthesizing an ionic liquid, an exothermic reaction, is examined using a flow microreactor. The reaction rate is calculated and a fluid simulation model is constructed to model a series of processes occurring within the microreactor, including mixing, reaction, heat generation, and heat dissipation. This model enables an understanding of the internal dynamics of the reaction. It allows for the prediction of changes in the reaction rate due to differences in mixing performance caused by different micromixers, and for forecasting the temperature distribution within the microreactor. When the inner diameter of the microreactor is increased, a decrease in reaction rate is observed in actual reactions. The cause of this phenomenon is identified as an increase in viscosity due to the produced ionic liquid, which subsequently reduces the diffusion of the reactants. This finding underscores the importance of considering the physicochemical changes in the reaction environment during reactor scale-up.

Capter-5. A Manufacturing Strategy Utilizing a Continuous Mode Reactor toward Homogeneous PEGylated Bioconjugate Production

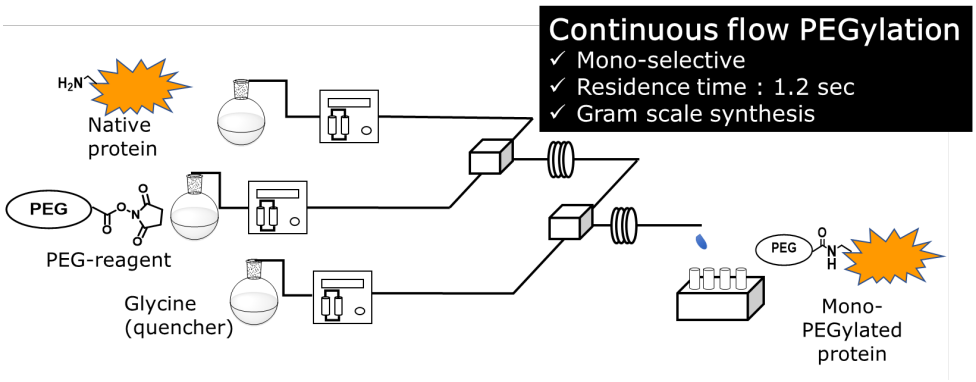

Figure 4. Illustration of homogeneous PEGylated bioconjugates produced by FMR

Protein PEGylation, a traditional bioconjugation technology, enables the enhancement of therapeutic efficacy and in vivo half-life of proteins through the formation of covalent bonds with the highly activated ester group linking polyethylene glycol (PEG). However, the high reactivity of these reagents triggers a random reaction with lysine residues on the protein surface, resulting in a heterogeneous mixture of PEGylated proteins. In addition, there are scalability and aggregation risks associated with the traditional batch mode reaction.

To overcome these limitations of traditional batch mode PEGylation, a manufacturing strategy incorporating structural analysis and a FMR reaction was investigated. Solvent exposure analysis can be used to identify the most reactive lysine of a protein, and the FMR mode allows this lysine to be modified, enabling mono-PEGylation of two different proteins within two seconds. The potential for applying this ultra-fast modification reaction to the gram-scale production of PEGylated bioconjugates without the formation of aggregates is demonstrated. A similar trend was observed between the level of protein lysine exposure and mono-selectivity as demonstrated by continuous flow PEGylation. This observation suggests the potential of this manufacturing strategy to produce a wide range of bioconjugates.

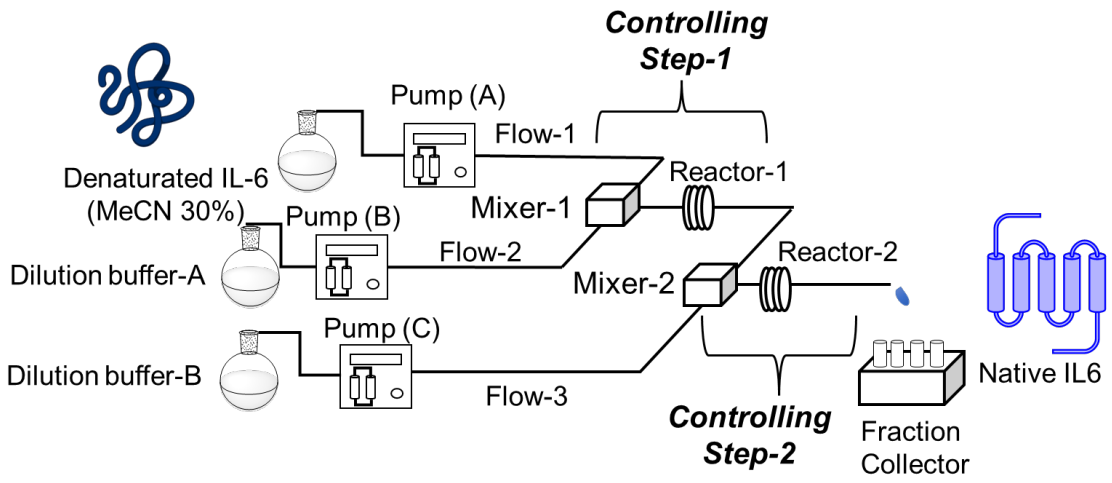

Figure 5. Illustration of protein refolding through flash-change reaction condition

Protein refolding stands as a crucial component of protein production, yet the development of a versatile and scalable method continues to pose a challenge. In this study, the presentation of a novel refolding system employing an FMR is offered, a system that grants precise control over critical parameters such as buffer pH and organic solvent content during the process.

Interleukin-6 (IL-6), a model protein, is employed to underscore the effectiveness of this system in achieving efficient refolding, generating pure monomeric protein, and facilitating gram-scale production. The facilitated flash-change of reaction conditions through the FMR system effectively curtails protein aggregation during refolding. This study is believed to represent the first report utilizing the FMR system for protein refolding, a system that holds the potential to revolutionize protein production by providing a more efficient and scalable method.

The presented results underscore the utility of the FMR system as a high-throughput screening tool for streamlined scale-up, accentuating the importance of controlling and comprehending intermediates in the refolding process. The novelty of this approach is sourced from the unique ability of the FMR to govern both spatial and temporal aspects of protein refolding, an accomplishment hitherto unattainable by any other method.

3. Application of FMR technologies for industrial use.

Finally, there will be a discussion of recent applications of FMR for industrial use.

FMR technology was used to create a continuous synthesis system for monodisperse polystyrene, representing the practical application of fundamental theories. A model reaction, controlled/living anionic polymerization, was chosen because of its high sensitivity to flow rates of monomer and initiator solutions. This polymerization of styrene was performed in tetrahydrofuran (THF)/hexane initiated by THF-diluted n-butyllithium. Larger-sized poly(styrenes) were successfully produced, and continuous operation yielded about 0.5 kg of the polymer with a narrow molecular weight distribution after four hours. These results demonstrate the feasibility of large-scale, industrially relevant applications of this continuous flow system for controlled/living anionic polymerization.

In addition to the synthesis of monodisperse polystyrene, FMR technology has been effectively applied to the synthesis of ADCs. Key factors such as optimized mixer type, reaction time, and mixer diameter were addressed, resulting in the preparation of ADCs with clinically relevant drug-to-antibody ratios. A scaled-down manufacturing approach was used, employing a stepwise mixing system for sequential reduction/conjugation processes. This established continuous flow methodology proved adaptable to various combinations of three antibodies and three payloads, with consistent trends across all nine ADC syntheses attempted. These results reinforce the potential of continuous flow chemistry in establishing reliable and robust manufacturing processes for ADCs.

From an industrial standpoint, FMR technology has been utilized by Ajinomoto OmniChem, an affiliate company. This entity has embarked on the establishment of a drug intermediate synthesis plant via flow synthesis. This venture has contributed significantly to the construction of chemical processes that are characterized by their environmental harmony and elevated safety standards.

Chapter 2

Micromixing enables chemoselective reactions of difunctional electrophiles with functional aryllithiums

Abstract

Generation of highly unstable functional aryllithiums followed by chemoselective reactions with difunctional electrophiles were successfully achieved using flow microreactor systems equipped with micromixers to give highly functionalized compounds without protecting functional groups. Extremely fast micromixing is responsible for high chemoselectivity.

Introduction

Protecting groups have been indispensable for synthesizing complex highly functionalized organic molecules, although the use of a protective group needs at least two additional synthetic steps, protection and deprotection. Recently, protecting group-free-synthesis has attracted a great deal of attention.[1]

In this regard, the generation of organolithiums[2] bearing unprotected functional groups has been investigated extensively (Scheme 1 (a)).[3] Various electrophilic functional groups can be compatible with organolithium

reactions if the author uses flow microreactors.[4] Micromixing using flow microreactors[5,6,7] enables selective lithiation without affecting the functional group, whereas the precise residence time control enables the effective use of short-lived organolithium intermediates for the subsequent reaction with electrophiles. Reactions of such functional organolithiums with electrophiles give difunctional products.

Another approach to difunctional compounds using organolithium chemistry is the reaction of unfunctionalized organolithiums with difunctional electrophiles (Scheme 1 (b)). However, it is usually difficult or impossible to achieve chemoselective reactions[8] without affecting less electrophilic functionality even if one equivalent of an organolithium is used. However, recently, the author reported extremely fast micromixing[9] dramatically improves the chemoselectivity.[10]

The combination of the first and the second approaches is also effective (Scheme 1 (c)). Chemoselective reactions of functional organolithiums with difunctional electrophiles should give trifunctional products.

In this paper, the author reports the full details of such approaches based on extremely fast micromixing using flow microreactor systems, which serve as powerful and straightforward methods for protecting group-free-synthesis of highly functionalized organic molecules.

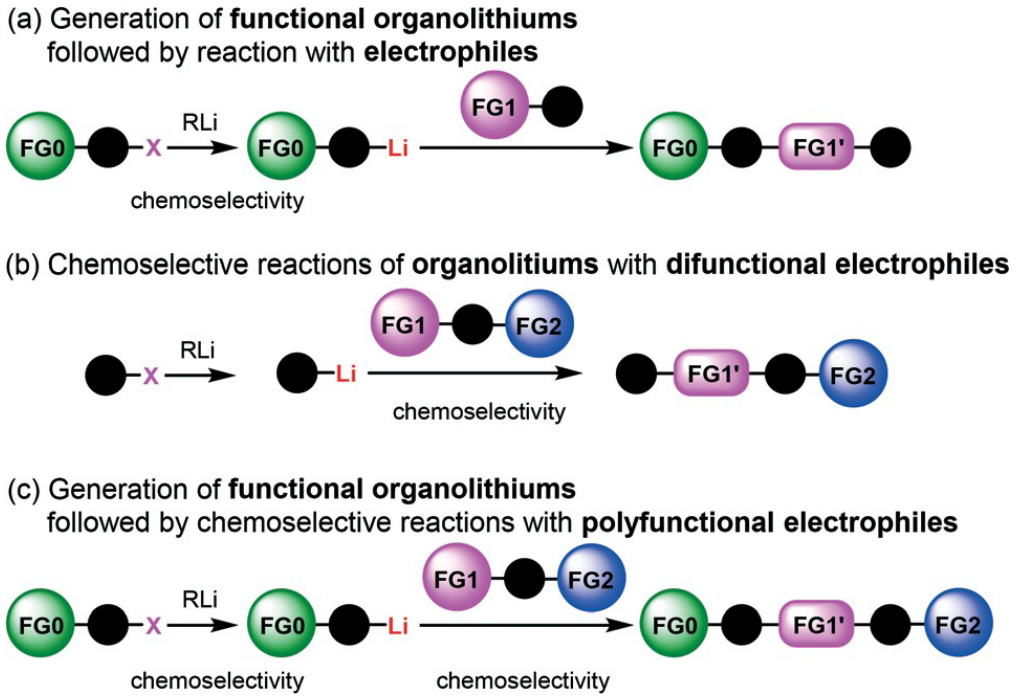

Scheme 1. Synthetic approaches to functionalized organic molecules using organolithium reactions.

Results and discussion

Generation of functional aryllithiums

First the author shows the effect of mixing on the efficiency of functional aryllithium generation. Although aryllithiums bearing various electrophilic functional groups have been successfully generated using flow microreactors, the author focuses on the generation of 4-cyanophenyllithium by bromine-lithium exchange of 4-cyanobromobenzene with *n*-butyllithium (*n*-BuLi) as a representative (Scheme 1 (a)).

The reaction of 4-cyanobromobenzene with one equivalent of *n*-BuLi was examined using a flow microreactor system composed of two micromixers (**M1** and **M2**) and two microtube reactors (**R1** and **R2**) shown in Figure 1.

As shown in Table 1, the selective generation and reaction of 4-cyanophenyllithium was achieved and the desired compound was obtained in high yields at high flow rates. This indicates that the reaction selectivity depended on the flow speed because it is well known that flow speed increases with an increase with the flow rate.[11] The decrease in the total flow rate caused the decrease of the yields presumably because n-BuLi attacked the cyano group of 4-cyanobromobenzene. In fact, at slower flow rates, the formation of 1-phenylpentan-1-one was observed by GC-Mass analysis (See supporting information for details). The present observations indicate that extremely fast mixing is responsible for the high selectivity in the generation of functional organolithiums.

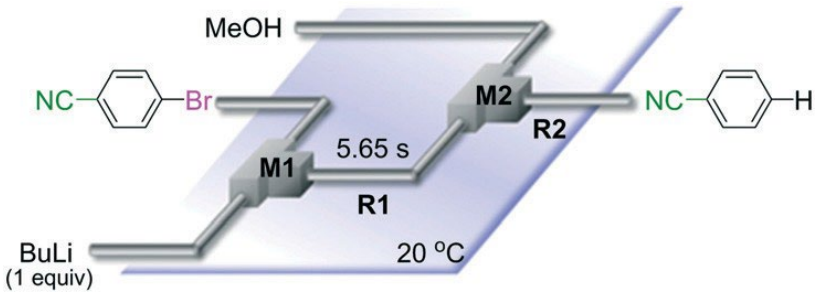

Figure 1. A flow microreactor system for bromine–lithium exchange of 4-cyanobromobenzene with *n*-BuLi followed by reaction with methanol.

Table 1. Bromine–lithium exchange of 4-cyanobromobenzene with *n*-BuLi followed by reaction with methanol

total flow rate in **M1** (ml/min)	conversion (%)	yield (%)
2.5	100	36
5.0	100	61
10	100	75
20	100	85

Reaction of phenyllithium with difunctional electrophiles

The second approach is the reaction of unfunctionalized organolithiums with difunctional electrophiles. The author choses to use phenyllithium as a representative organolithium reagent without functional groups.

First, the author focused on aliphatic compounds having two different electrophilic functional groups such as aldehyde, ketone, and ester carbonyl groups.

The reaction of phenyllithium with 6-oxo-6-phenylhexanal (**1**) (1: 1 molar ratio) was carried out using a flow microreactor system equipped with a micromixer (Figure 2). A solution of **1** (0.10 M in THF, 12 ml/min) and a solution of PhLi (0.42 M in Et_2O/cyclohexane (74/26 v/v), 3.0 ml/min) were introduced to **M** by syringe pumps, and the resulting mixture was passed through **R** (ϕ = 1000 μm, L = 100 cm). The yields of 6-hydroxy-1,6-diphenylhexan-1-one (**2**, mono-addition product), 6-hydroxy-6,6-diphenylhexanal (**3**, mono-addition product), and 1,1,6-triphenylhexane-1,6-diol (**4**, di-addition product) were determined by GC after aqueous work-up. As shown in Table 2, the reaction at a low flow rate (2.5 ml/min) at -40 ºC resulted in a low selectivity for **2**, which was formed by selective nucleophilic attack of PhLi at the aldehyde carbonyl group. A significant amount of **4**, which was derived from the nucleophilic attack of PhLi at both aldehyde and ketone carbonyl groups, was obtained. The increase in the flow rate resulted in an increase in the selectivity for **2**, indicating that the selectivity for **2** increases with the mixing efficiency, because it is known that the mixing efficiency in a micromixer increases with an increase in the flow speed.[11] The reaction at -78 ºC also showed a similar selectivity. The highest yield of **2** (48%) was observed at the flow rate of 30 ml/min at –40 ºC, although the selectivity is still not acceptable.

The reactions of methyl 6-oxohexanoate (**5**) were also examined using a flow microreactor system. The yields of methyl 6-hydroxy-6-phenylhexanoate (**6**, mono-addition product), 6-oxo-6-phenylhexanal (**1**, mono-addition product), 6-hydroxy-1,6-diphenylhexan-1-one (**2**, di-addition product), 6-hydroxy-6,6-diphenylhexanal (**3**, di-addition product), and 1,1,6-triphenylhexane-1,6-diol (**4**, tri-addition product) were determined by GC

after aqueous work-up. As shown in Table 3, the increase in the flow rate resulted in an increase in the selectivity for **6**, indicating that the increase in the mixing efficiency increases the selectivity for the attack on the aldehyde carbonyl group. The desired product **6** was obtained in 72% yield.

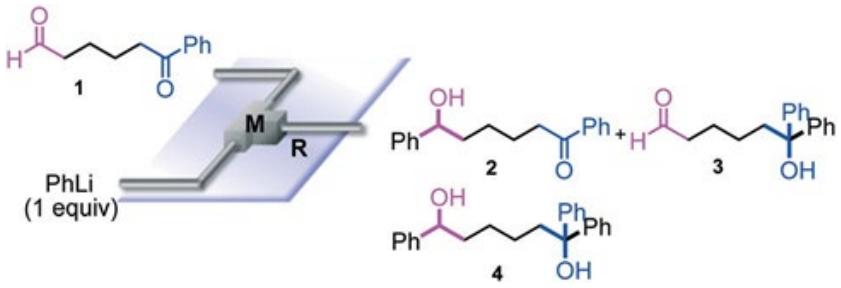

Figure 2. A flow microreactor system for the reaction of phenyllithium with 1.

Table 2. Reactions of phenyllithium with 6-oxo-6-phenylhexanal (**1**)

temperature (°C)	flow rate (ml/min)	conversion (%)	yield (%)		
			2	**3**	**4**
-40	2.5	66	10	20	29
-40	10	65	36	12	19
-40	30	77	48	10	18
-70	2.5	67	11	23	26
-70	10	72	27	18	22
-70	30	73	44	12	17

Table 3. Reactions of phenyllithium with methyl 6-oxohexanoate (**5**)

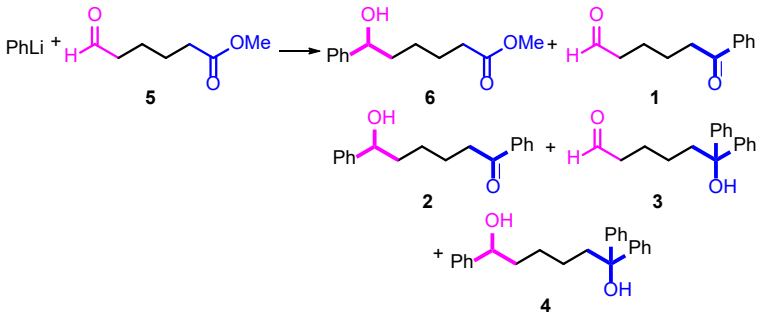

temperature (°C)	flow rate (ml/min)	conversion (%)	yield (%)				
			6	**1**	**2**	**3**	**4**
-40	2.5	59	22	0	19	9	0
-40	10	82	69	0	4	2	5
-40	30	81	72	0	3	1	5
-70	2.5	62	22	0	15	11	2
-70	10	72	52	3	6	3	5
-70	30	74	60	2	4	2	5

Next, the author turned our attention to the reactions with aromatic compounds bearing two electrophilic functional groups. In contrast to the aliphatic case, remarkable selectivity was observed in the aromatic case, although the selectivity strongly depends on the flow rate (Table 4). The yields of (4-(hydroxy(phenyl)methyl) phenyl)(phenyl)methanone (**8**, mono-addition product), 4-(hydroxydiphenylmethyl)benzaldehyde (**9**, mono-addition product), and (4-(hydroxy(phenyl)methyl)phenyl)diphenylmethanol (**10**, di-addition product) were determined by GC after aqueous work-up. The yield of **8** (mono-addition product) increases and that of **10** (di-addition product) decreases with an increase in the flow rate, indicating the importance of mixing efficiency. It is interesting to note that the yield of **9** also decreases with an increase in the flow rate, although the reason is not clear at present. Notably, the selectivity decreases with an increase in the diameter of micromixer. The mixing efficiency generally decreases with an increase in the inner diameter if the flow rate is the same. In contrast, the selectivity does not vary with the reaction temperature appreciably.

Table 4. Effect of inner diameter, temperature, and flow rate for the reaction of PhLi with 4-benzoylbenzaldehyde (**7**) using flow microreactors

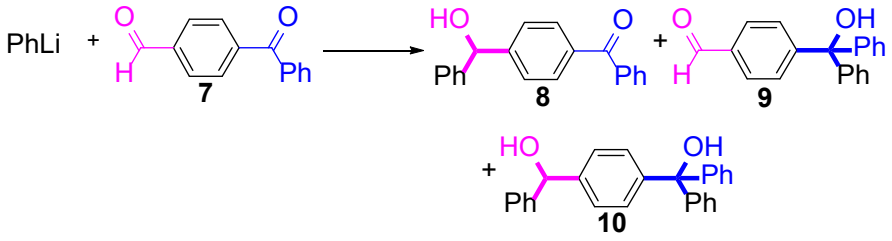

inner diameter in **M** (μm)	temperature (°C)	flow rate (ml/min)	conversion (%)	yield (%)		
				8	**9**	**10**
800	-40	15	65	23	3	40
500	-40	15	71	34	3	32
250	-40	15	83	66	2	15
250	-78	15	78	60	4	17
250	-20	15	79	57	2	18
250	0	15	81	61	2	21
250	20	15	81	57	2	22
250	-40	0.63	61	7	5	40
250	-40	1.3	56	8	5	41
250	-40	2.5	60	15	5	38
250	-40	5.0	74	42	5	29
250	-40	10	82	60	3	20
250	-40	20	84	69	3	15
250	-40	25	78	70	2	8
250	-40	30	81	73	1	7

To get a deeper insight into the effect of micromixing on the selectivity, the reaction of PhLi with 4-benzoylbenzaldehyde was carried out in a conventional macrobatch reactor (a 50 ml round bottomed flask with a magnetic stirring) at various temperatures with varying the way of addition. The results are summarized in Table 5.

The addition of one equivalent of phenyllithium to a stirred solution of **7** for 1.0 min at –78 ºC gave **8** in only 28% yield, and a significant amount of **10** (25%) was produced together with unchanged **7**. Interestingly, compound **9**, which is formed by the reaction of PhLi with the ketone carbonyl group without affecting the more reactive aldehyde carbonyl group, was also obtained in 7% yield. The increase in the temperature caused a decrease in the yield of desired product **8**. Moreover, the reverse addition resulted in lower yields of **8**, and the simultaneous addition did not give better results.

Although the selectivity should also depend on the size and shape of the reactor, the stirring speed, and the speed of the addition, the present data demonstrate the limitations of the macrobatch method for achieving this type of chemoselectivity of fast reactions.

Table 5. Reactions of 4-benzoylbenzaldehyde (**7**) with one equivalent of phenyllithium using a conventional macro batch reaction

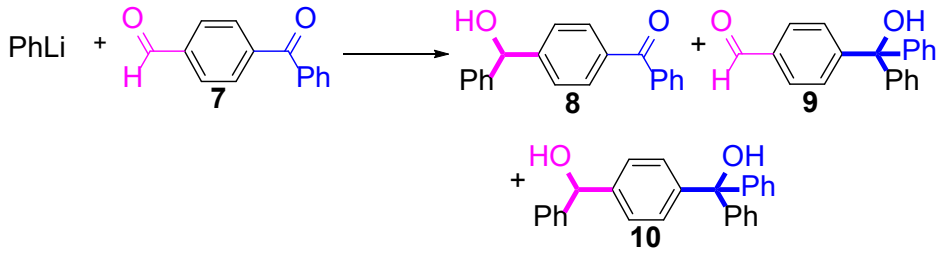

temperature (°C)	method of addition	conversion (%)	yield (%)		
			8	**9**	**10**
-78	addition of PhLi to **7**	65	28	7	25
-40	addition of PhLi to **7**	64	23	7	26
-20	addition of PhLi to **7**	64	20	7	30
0	addition of PhLi to **7**	64	12	6	30
20	addition of PhLi to **7**	61	12	5	33
-78	addition of **7** to PhLi	33	6	2	26
-40	addition of **7** to PhLi	37	5	1	27
-20	addition of **7** to PhLi	49	3	1	35
0	addition of **7** to PhLi	51	2	1	37
20	addition of **7** to PhLi	55	1	1	40
-78	simultaneous addition of **7** and PhLi	51	16	9	26

With the remarkable effect of micromixing on the selectivity in hand, the author next examined the reactions of PhLi with various benzaldehyde having different electrophilic functional groups such as ketone carbonyl, ester carbonyl, nitro[12], and cyano groups. As shown in Table 6, high chemoselectivity was obtained by using the flow microreactor system, whereas the use of a batch reactor resulted in much lower selectivity. In all cases, the faster flow rates gave better selectivity. Furthermore, the reactions of PhLi with phenylisocyanates having a cyano or an alkoxycarbonyl group were also accomplished with high chemoselectivity, although the reactions in a batch reactor gave complex mixtures.

Table 6. The reaction of aromatic compounds having two different electrophilic functional groups with PhLi using the flow microreactors

difunctional electrophiles	reaction method	flow rate (mL/min)	yield (%)[a] mono-addition product	yield (%)[a] di-addition product
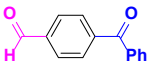	batch macro	-	28	25
	flow micro	2.5	15	38
	flow micro	10	60	20
	flow micro	30	73	7
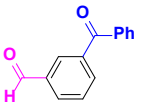	batch macro	-	29	26
	flow micro	2.5	13	35
	flow micro	10	55	14
	flow micro	30	71	7
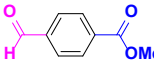	batch macro	-	56	5
	flow micro	2.5	56	13
	flow micro	10	83	0
	flow micro	30	84	0
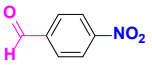	batch macro	-	36	
	flow micro	2.5	29	
	flow micro	10	72	
	flow micro	30	76	
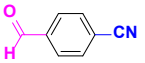	batch macro	-	65	
	flow micro	2.5	54	
	flow micro	10	88	
	flow micro	30	89	
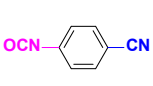	batch macro	-	5	1
	flow micro	2.5	43	0
	flow micro	10	73	0
	flow micro	30	82	0
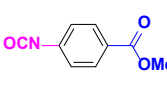	batch macro	-	18	4
	flow micro	2.5	25	8
	flow micro	10	81	2
	flow micro	30	91	1

Reactions of Functional Aryllithiums with Difunctional Electrophiles

Next, the author focused on the third case (Scheme 1 (c)); the reactions of aryllithiums bearing an electrophilic functional group (**FG0**) with difunctional electrophiles, *i.e.* compounds bearing two different electrophilic functional groups (**FG1** and **FG2**) (Scheme 2). In this case, the author has to worry about not only the competition between two electrophilic functional groups on the electrophile (**FG1** and **FG2**) but also the competition between functional groups on the electrophile (**FG1** and **FG2**) and a functional group on the nucleophile (**FG0**).[13,14]

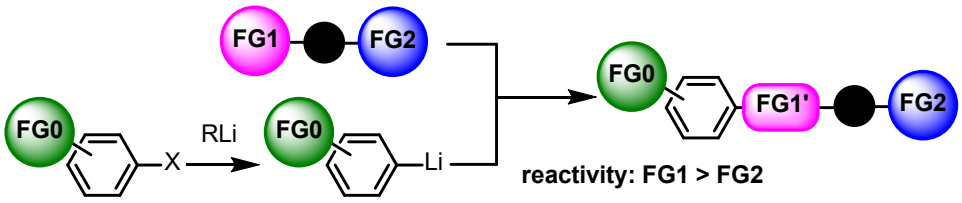

Scheme 2. Reactions of functional aryllithiums with compounds bearing two electrophilic functional groups

An aryllithium bearing an electrophilic functional group was generated by halogen-lithium exchange of the corresponding aryl halide using a flow microreactor system consisting of a T-shaped micromixer (ϕ = 250 μm) (**M1**), a V-shaped micromixer (ϕ = 250 μm) (**M2**) and two microtube reactors (**R1** and **R2**) (Figure 3). The residence time (t^{R1}) for the halogen-lithium exchange reaction was optimized individually (See experimental section for the details).

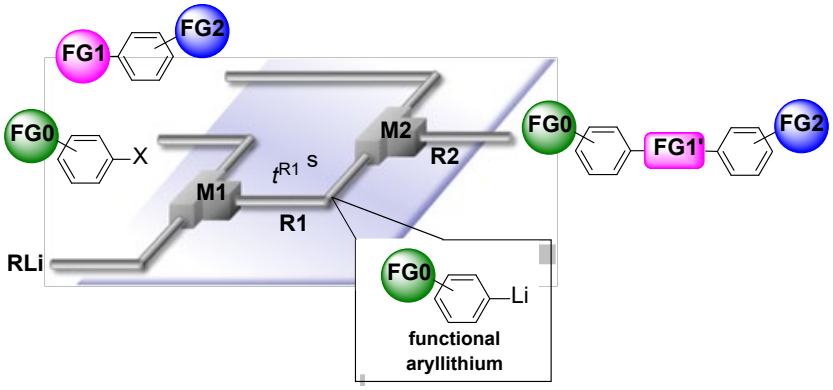

Figure 3. A flow microreactor system for the reaction of compounds bearing two different electrophilic functional groups with functional aryllithium generated by halogen-lithium exchange

As shown in Table 7, the aldehyde carbonyl group reacted selectively without affecting other electrophilic functional groups such as ketone carbonyl, ester carbonyl, nitro, and cyano groups to give desired compounds in good yields, when one equivalent of a functionalized aryllithium was used. Also, the functional groups on the aryllithiums were not affected. It is also noteworthy that aldehyde bearing two other electrophilic functional groups such an ester carbonyl group and a nitro group (a trifunctional electrophile) also reacted chemoselectively. Competition between an isocyanate group and other electrophilic functional groups using functionalized aryllithium is also interesting. As shown in Table 7, the nucleophilic addition took place selectively on the isocyanate group without affecting other functional groups on both the electrophile and the nucleophile. The reactions seem to be useful as they allow amides having two functional groups to be easily synthesized.

Table 7. Reactions of functional aryllithiums with difunctional electrophiles using the flow microreactor system.

functionalized aryl halide	lithiating agent	difunctional electrophile	product	yield (%)
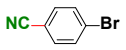	BuLi	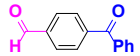	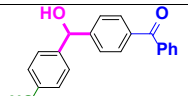	78
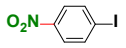	PhLi		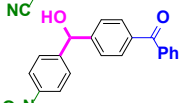	79
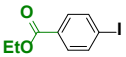	PhLi		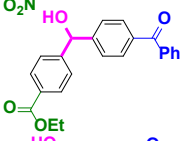	67
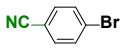	BuLi	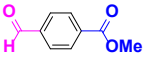	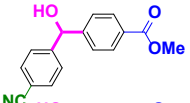	86
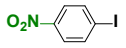	PhLi		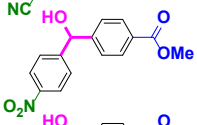	90
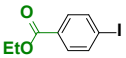	PhLi		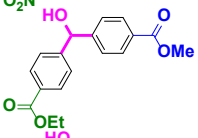	78
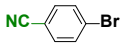	BuLi	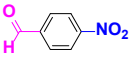	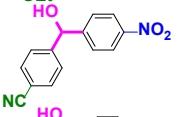	86
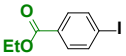	PhLi		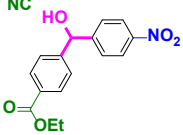	69
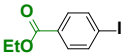	PhLi	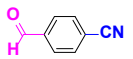	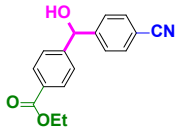	74
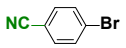	BuLi		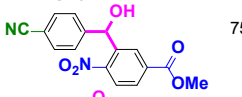	75
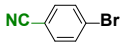	BuLi	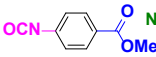	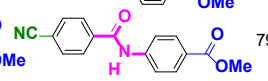	79
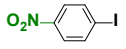	PhLi		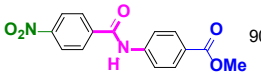	90
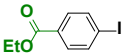	PhLi		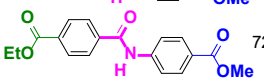	72
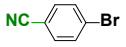	BuLi	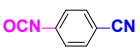	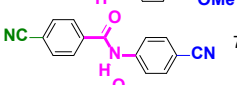	74
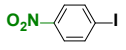	PhLi		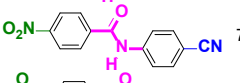	74
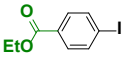	PhLi		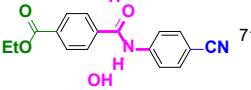	71
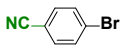	BuLi			60 (33:67)[a]
	BuLi			64

[a] Diastereomer ratio

It is well known that a ketone carbonyl group reacts with organolithiums very rapidly. Therefore, aryllithiums bearing a ketone carbonyl group are very unstable and decompose very rapidly. However, with a flow microreactor system, aryllithiums bearing ketone carbonyl groups can be generated by iodine–lithium exchange reactions of the corresponding aryl iodides with mesityllithium and can be reacted with subsequently added electrophiles. Therefore, the author examined the reactions of aryllithiums bearing a ketone carbonyl group with aromatic compounds having different electrophilic functional groups. A flow microreactor system consisting of three micromixers (**M1**, **M2**, and **M3**) and three microtube reactors (**R1**, **R2**, and **R3**) (Figure 4) was used. A solution of mesityl bromide (0.090 M in THF, 5.0 mL/min) and a solution of *n*-BuLi (0.22 M in hexane, 1.8 mL/min) were introduced to **M1**, and the mixture was passed through **R1** (ϕ = 1000 μm, L = 410 cm (200 cm at 0 °C, 10 cm at ambient temperature and 200 cm at –70 °C)). The resulting solution of mesityllithium was mixed with a solution of aryl iodide (0.10 M in THF, 3.0 mL/min) in **M2** (–70 °C), and the mixture was passed through **R2** (ϕ = 250 μm, L = 1.0 cm, –70 °C). The resulting solution of an aryllithiums bearing a ketone carbonyl group was mixed with a solution of a compound bearing two different electrophilic functional groups (0.10 M in THF, 4.2 mL/min) in **M3** (–70 °C), and the mixture was passed through **R3** (ϕ = 1000 μm, L = 200 cm, –70 °C).

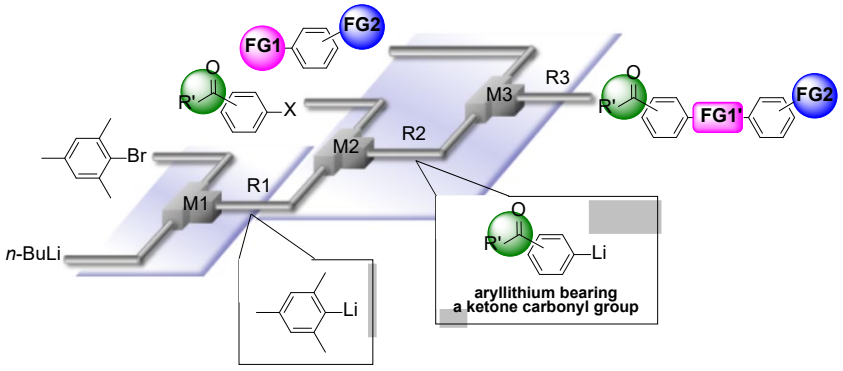

Figure 4. A flow microreactor system for the reaction of aryllithium bearing a ketone carbonyl group generated by iodine-lithium exchange with aromatic compounds having different electrophilic functional groups.

As shown in Table 8, benzaldehyde and isocyanate bearing another electrophilic functional group such as a ketone carbonyl group, an ester carbonyl group and a cyano group reacted chemoselectively without decomposition of aryllithium bearing a ketone carbonyl group.

Table 8. Reactions of compounds having different electrophilic functional groups with aryllithium bearing a ketone carbonyl group using the flow microreactor

aryl halide havig ketone carbonyl group	difunctional electrophile	product	yield (%)
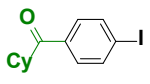	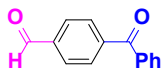	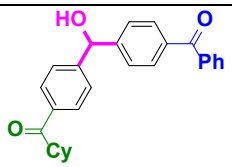	65
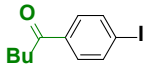	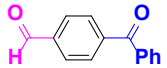	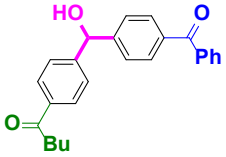	30
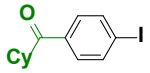	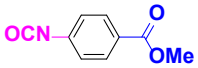	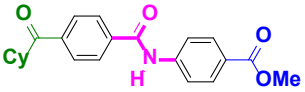	73
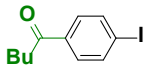	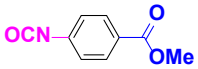	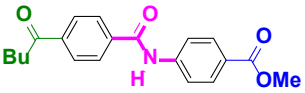	51
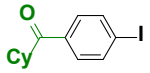	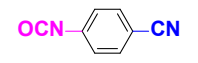	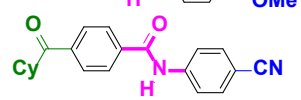	52

Chemoselective Three-Component Coupling Using an Integrated Flow Microreactor System

Integration of chemical reactions enhances the power and speed of organic synthesis, and recently it has been recognized that space-integration[15] of reactions using flow microreactors is quite effective. Thus, the author examined chemoselective three-component coupling using benzaldehyde having a ketone carbonyl group (**7**) in an integrated flow microreactor system consisting of four micromixers (**M1**, **M2**, **M3**, and **M4**) and three microtube reactors (**R1**, **R2**, **R3**, and **R4**) (Figure 5). A solution of 4-bromobenzonitrile (0.10 M in THF, 5.8 mL/min) and a solution of *n*-BuLi (0.42 M in hexane, 1.5 mL/min) were introduced to **M1**, and the mixture was passed through **R1**. The resulting solution was mixed with a solution of 4-benzoylbenzaldehyde (0.10 M in THF, 5.8 mL/min) in **M2** and passed through **R2**. A solution of 1-iodo-4-nitrobenzene (0.10 M in THF, 6.4 mL/min) and a solution of PhLi (0.42 M in Et_2O/cyclohexane (74/26 v/v), 1.6 mL/min) were introduced to **M3** by syringe pumps and the mixture was passed through **R3.** Then, the two solutions produced in **R2** and **R3** were mixed in **M4** and passed through **R4**. The reaction with *p*-cyanophenyllithium at the aldehyde carbonyl group followed by the reaction with *p*-nitrophenyllithium at the ketone carbonyl group was successfully achieved to obtain the desired product in 61% isolated yield. High productivity (156 mg/min) of the present method, because of high flow rates and short residence times, is also noteworthy.

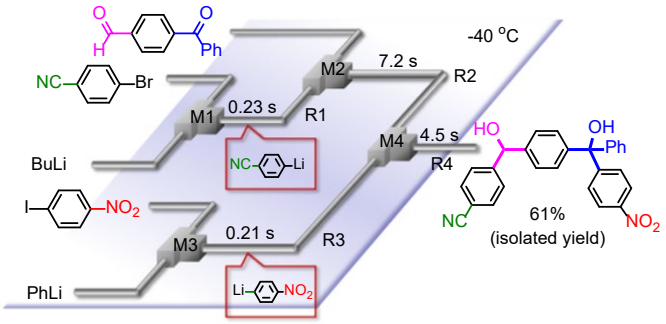

Figure 5. Chemoselective three-component coupling using an integrated flow microreactor system

Experimental Section

General information

GC analysis was performed on a SHIMADZU GC-2014 gas chromatograph equipped with a flame ionization detector using a fused silica capillary column (column, Rtx-200; 0.25 mm x 30 m). 1H and 13C NMR spectra were recorded on Varian MERCURYplus-400 (1H 400 MHz, 13C 100 MHz) spectrometer with Me4Si as an internal standard in CDCl3. ESI and APCI mass spectra were recorded on executive spectrometer. Gel permeation chromatography (GPC) was carried out on Japan Analytical Industry LC-9201. THF and Et2O were purchased from Wako as a dry solvent and used without further purification. Hexane was purchased from Wako, distilled before use, and stored over molecular sieves 4A. n-Butyllithium, phenyllithium, methanol, acetic acid, methyl 4-formylbenzoate, 4-nitrobenzaldehyde, 4-cyanobenzaldehyde, 4-isocyanatobenzonitrile, methyl 4-isocyanatobenzoate, methyl 3-formyl-4-nitrobenzoate, 4-bromobenzonitrile, 1-iodo-4-nitrobenzene, ethyl 4-iodobenzoate, and mesityl bromide were commercially available. 5-Cyanopentanal and ethyl 4-formmylcyclohexanecarbolate were purchased from a commercial supplier. 6-oxo-6-phenylhexanal1, methyl 6-oxohexanoate2, 3-benzoylbenzaldehyde3, 4-benzoylbenzaldehyde4, cyclohexyl(4-iodophenyl)methanone5, 1-(4-iodophenyl)-1-pentanone5 were synthesized according to the literature.

A Stainless steel (SUS304) T-shaped micromixer with the inner diameter of 250, 500, and 800 □m and a stainless steel (SUS304) V-shaped micromixer with inner diameter of 250 μm were manufactured by Sanko Seiki Co., Inc (Figure S1). Stainless steel (SUS316) microtube reactors with inner diameter of 250 and 1000 μm were purchased from GL Sciences. The micromixers and microtube reactors were connected with stainless steel fittings (GL Sciences, 1/16 OUW). The flow microreactor system was dipped in a cooling bath to control the temperature. Solutions were introduced to the flow microreactor system using syringe pumps, Harvard PHD 2000, Harvard PHD 4400 or Harvard PHD Ultra, equipped with gastight syringes purchased from SGE (Harvard PHD 2000 or Harvard PHD Ultra) or stainless steel syringes (Harvard PHD 4400).

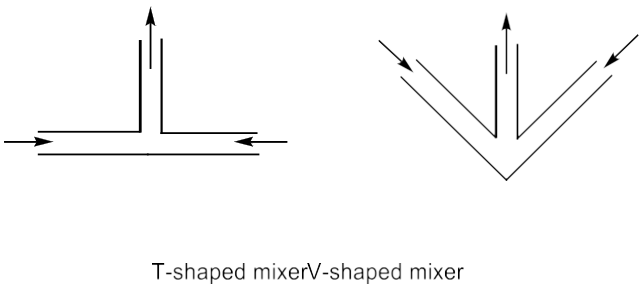

Figure 6. Schematic diagrams of the T-shaped micromixer and the V-shaped micromixer.

General Procedure for Bromine-lithium Exchange of 4-Cyanobromobenzene with *n*-BuLi followed by Reaction with Methanol

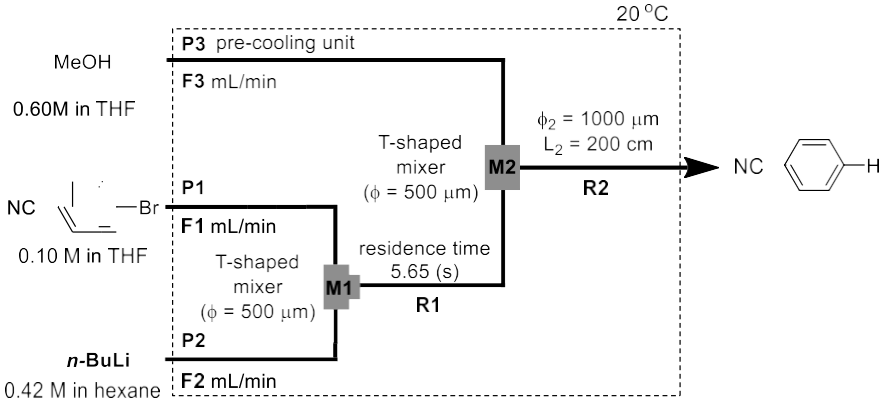

A flow microreactor system consisting of two T-shaped micromixers (ϕ = 500 μm) (**M1**, **M2**), a microtube reactor (**R1**, **R2**), and three pre-cooling units (**P1** (inner diameter ϕ = 1000 μm, length L = 100 cm), **P2** (ϕ = 1000 μm, L = 50 cm) and **P3** (ϕ = 1000 μm, L = 50 cm)) was used. When the total flow rate was 20 mL/min, three pre-cooling units (**P1** (ϕ = 1000 μm, length L = 200 cm), **P2** (ϕ = 1000 μm, L = 100 cm) and **P3** (ϕ = 1000 μm, L = 100 cm)) was used. The flow microreactor system was dipped in a cooling bath of 20 ºC. A solution of 4-bromobenzonitrile (**1**) (0.10 M in THF) (flow rate F1 mL/min) and a solution of n-BuLi (0.42 M in hexane) (flow rate F2 mL/min) were introduced to M1 by syringe pumps. The resulting solution was passed through **R1** (ϕ = 1000 μm, L1 cm) and was mixed with a solution of MeOH (1.0 M in THF) (flow rate F3 mL/min) in **M2**. The resulting solution was passed through **R2** (ϕ = 1000 μm, L = 200 cm). After a steady state was reached, an aliquot of the product solution was collected in a flask containing brine for 30 s. The conversion of 4-bromobenzonitrile (**1**) and the yields of benzonitrile were determined by GC analysis using an internal standard (tetradecane) (Table 9). In the case of slower flow rate condition (F1 = 2.0 ml/min, F2 = 0.50 ml/min, F3 = 0.50 ml/min), the formation of 1-

phenylpentan-1-one was observed by GC-Mass analysis (Figure 7).

Table 9. Bromine-lithium exchange of 4-cyanobromobenzene with *n*-BuLi followed by reaction with methanol

F1 (mL/min)	F2 (mL/min)	F3 (mL/min)	conversion (%)	yield (%)
2.0	0.50	0.50	100	36
4.0	1.0	1.0	100	61
8.0	2.0	2.0	100	75
16	4.0	4.0	100	85

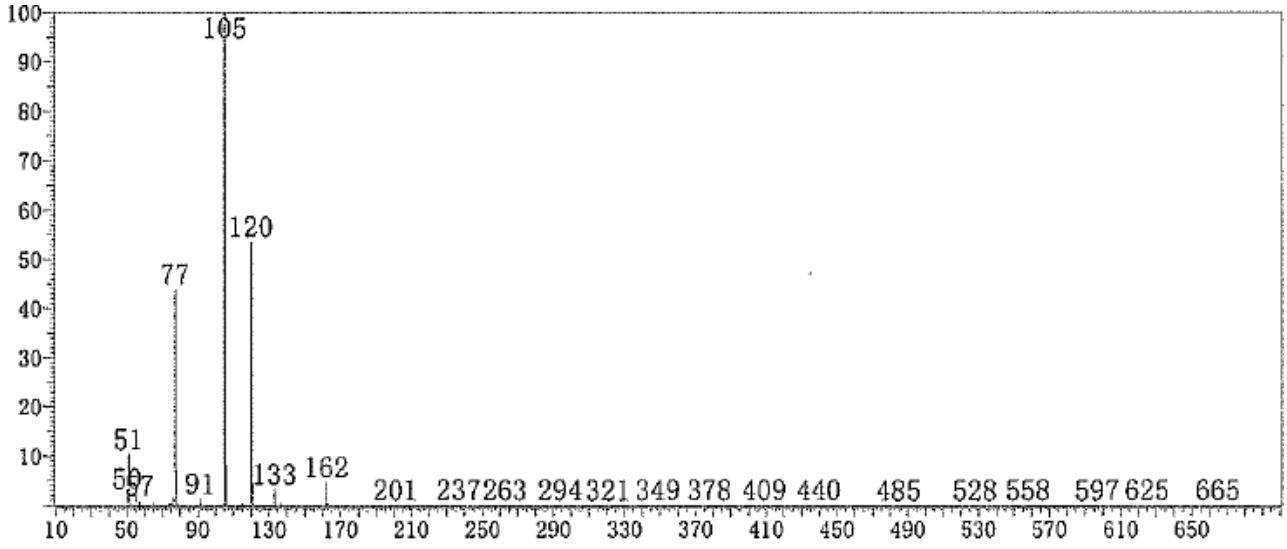

Figure 7. GC-MS analysis of the reaction of 4-bromobenznitrile with *n*-BuLi

General Procedure for Reactions of Phenyllithium with 6-Oxo-6-phenylhexanal in a Flow Microreactor System

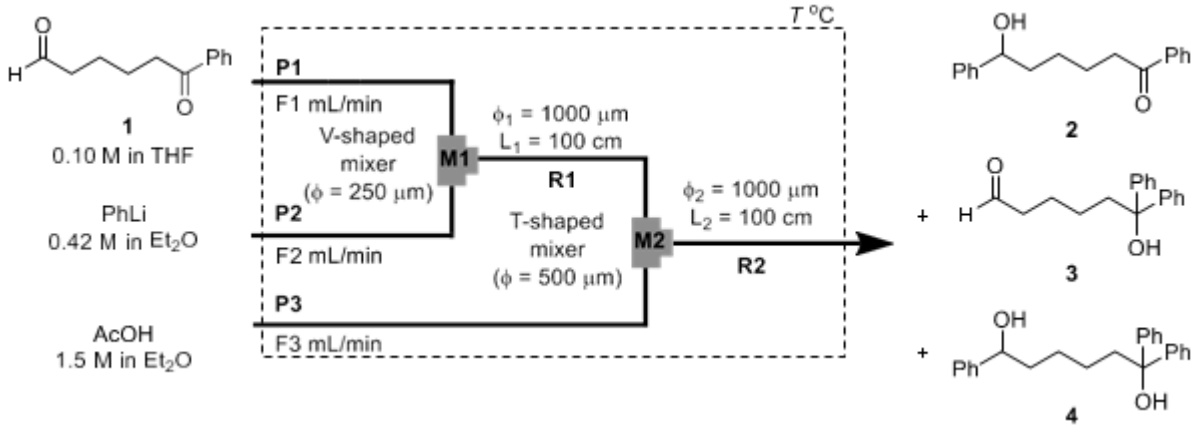

A flow microreactor system consisting of V-shaped micromixer (ϕ = 250 μm) (**M1**), T-shaped micromixer (ϕ = 500 μm) (**M2**), two microtube reactors (**R1** and **R2**), and three pre-cooling units (**P1** (inner diameter ϕ = 1000 μm, length L = 200 cm), **P2** (ϕ = 1000 μm, L = 100 cm) and **P3** (ϕ = 1000 μm, L = 50 cm)) was used. A solution of 6-oxo-6-phenylhexanal (0.10 M in THF) (flow rate: F1 mL/min) and a solution of PhLi (0.42 M in Et2O/cyclohexane (74/26 v/v)) (flow rate: F2 mL/min) were introduced to **M1** by syringe pumps. The resulting solution was passed through **R1** (residence time t^{R1} (s)) and was mixed with a solution of AcOH (1.5 M in Et2O) (flow rate: F3 mL/min) in **M2**. The resulting solution was passed through **R2** (ϕ = 1000 μm, L = 100 cm). After a steady state was reached, an aliquot of the product solution was collected to the sat. NaHCO3 aqueous solution for 30 s (when the total flow rate in **M1** was 2.5 mL/min, an aliquot of the product solution was collected for 1 min, when total flow rate in **M1** was 30 mL/min, an aliquot of the product solution was collected for 20 s) to neutralize the solution. The flow microreactor system was dipped in a cooling bath of -40 oC. The reaction mixture was analyzed by GC using an internal standard. The results are summarized in Table 10.

Table 10. Reactions of phenyllithium with 6-oxo-6-phenylhexanal

temperature (°C)	F1 (mL/min)	F2 (mL/min)	F3 (mL/min)	conversion (%)	yield (%)		
					2	**3**	**4**
-40	2.0	0.50	0.50	66	10	20	29
-40	8.0	2.0	2.0	65	36	12	19
-40	24	6.0	6.0	77	48	10	18
-70	2.0	0.50	0.50	67	11	23	26
-70	8.0	2.0	2.0	72	27	18	22
-70	24	6.0	6.0	73	44	12	17

6-Oxo-1,6-diphenylhexan-1-ol (2). Obtained by 48% yield (GC yield using an internal standard (hexadecane)) from 6-oxo-6-phenylhexanal and PhLi. GC *tR* 20.0 min (initial oven temperature, 100 °C for 2 min; rate of temperature increase, 10 °C/min; He linear velocity, 60 cm/sec. After extraction, the crude product was purified by silica-gel flash chromatography (hexane/ethyl acetate = 10/1 to 1/1) and purified by GPC to obtain a pure compound as a white solid. : GC *tR* 20.0 min (initial oven temperature, 100 °C for 2 min; rate of temperature increase, 10 °C/min; He linear velocity, 30 cm/sec); ^{1}H NMR (400 MHz, CDCl3) δ 1.34-1.60 (m, 2H), 1.72-1.94 (m, 5H), 2.97 (t, *J* = 7.4 Hz, 2H), 4.66-4.74 (m, 1H), 7.25-7.39 (m, 5H), 7.42-7.50 (m, 2H), 7.52-7.60 (m, 1H), 7.92-7.98 ppm (m, 2H); ^{13}C NMR (100 MHz, CDCl3) δ 24.0, 25.5, 38.4, 38.8, 74.3, 125.8, 127.5, 128.0, 128.4, 128.5, 132.9, 136.9, 144.7, 150.3, 200.3 ppm; HRMS (EI) *m/z* calcd for $C18H20O^{+}$ $[M]^{+}$: 268.1458, found: 268.1458.

6-Hydroxy-6,6-diphenylhexanal (3). Obtained in 10% yield (GC yield using an internal standard (dodecane)). GC *tR* 18.2 min; initial oven temperature, 100 °C for 2 min; rate of temperature increase, 10 °C/min; He linear velocity, 30 cm/sec). After extraction, the crude product was purified by silica-gel flash chromatography (hexane/ethyl acetate = 10/1 to 3/1) and purified by GPC to obtain a pure compound as a white solid. 1H NMR (400 MHz, CDCl3) δ 1.28-1.36 (m, 2H), 1.64-1.68 (m, 2H), 2.09 (s, 1H), 2.26-2.34 (m, 2H), 2.38-2.44 (m, 2H), 7.20-7.42 (m, 10H), 9.72 ppm (s, 1H); ^{13}C NMR (100 MHz, CDCl3) δ 22.3, 23.4, 41.6, 43.8, 78.0, 125.9, 126.8, 128.1, 146.9, 202.6 ppm; HRMS (EI) *m/z* calcd for C H O + [M]+: 268.1458, found: 268.1452.

1,1,6-Triphenylhexane-1,6-diol (4). Obtained in 18% yield (GC yield using an internal standard (dodecane)) GC *tR* 22.9 min (initial oven temperature, 100 °C for 2 min; rate of temperature increase, 10 °C/min; He linear velocity, 30 cm/sec). After extraction, the crude product was purified by silica-gel flash chromatography (hexane/ethyl acetate = 10/1 to 1/1) and purified by GPC to obtain a pure compound as a colorless oil. 1H NMR (400 MHz, CDCl3) δ 1.28-1.40 (m, 2H), 1.60-1.72 (m, 2H), 2.09 (s, 1H), 2.27-2.36 (m, 2H), 2.39-2.44 (m, 2H), 7.20-7.42 (m, 10H), 9.72 ppm (t, *J* = 1.6 Hz, 1H); ^{13}C NMR (100 MHz, CDCl3) δ 22.3, 23.4, 41.6, 43.8, 78.0, 125.9, 126.8, 128.1, 146.9, 202.6 ppm; HRMS (ESI) *m/z* calcd for C24H26O2Na$^+$ [M+Na]$^+$: 369.1831, found: 369.1817.

General Procedure for Reactions of Phenyllithium with Methyl 6-oxohexanoate in a Flow Microreactor System

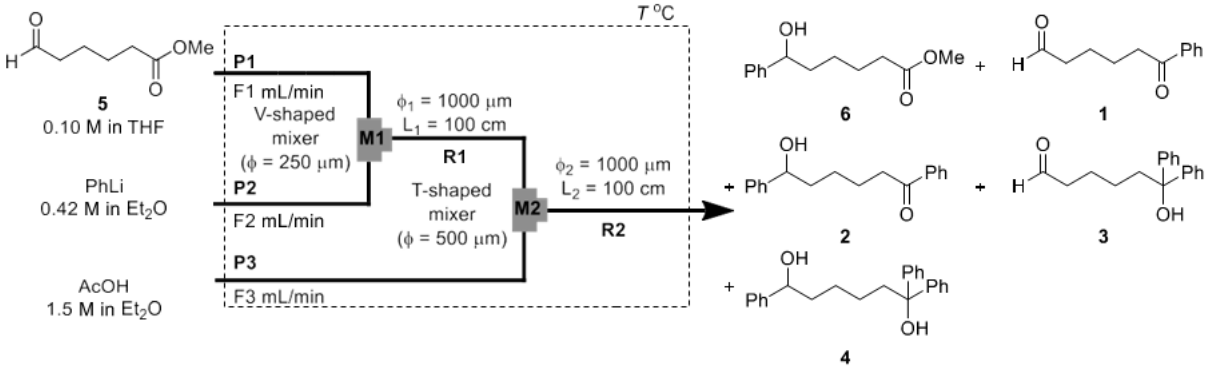

A flow microreactor system consisting of V-shaped micromixer (ϕ = 250 μm) (**M1**), T-shaped micromixer (ϕ = 500 μm) (**M2**), two microtube reactors (**R1** and **R2**), and three pre-cooling units (**P1** (inner diameter ϕ = 1000 μm, length L = 200 cm), **P2** (ϕ = 1000 μm, L = 100 cm) and **P3** (ϕ = 1000 μm, L = 50 cm)) was used. A solution of methyl 6-oxohexanoate (0.10 M in THF) (flow rate: F1 mL/min) and a solution of PhLi (0.42 M in Et2O/cyclohexane (74/26 v/v)) (flow rate: F2 mL/min) were introduced to **M1** by syringe pumps. The resulting solution was passed through **R1** (residence time t^{R1} (s)) and was mixed with a solution of AcOH (1.5 M in Et2O) (flow rate: F3 mL/min) in **M2**. The resulting solution was passed

through **R2** (ϕ = 1000 μm, L = 100 cm). After a steady state was reached, an aliquot of the product solution was collected to the sat. NaHCO3 aqueous solution for 30 s (when the total flow rate in **M1** was 2.5 mL/min, an aliquot of the product solution was collected for 1 min, when total flow rate in **M1** was 30 mL/min, an aliquot of the product solution was collected for 20 s) to neutralize the solution. The flow microreactor system was dipped in a cooling bath of -40 oC. The reaction mixture was analyzed by GC using an internal standard. The results are summarized in Table 11.

Table 11. Reactions of phenyllithium with 6-oxohexanoate

temperature (°C)	F1 (mL/min)	F2 (mL/min)	F3 (mL/min)	conversion (%)	yield (%)				
					6	**1**	**2**	**3**	**4**
-40	2.0	0.50	0.50	59	22	0	19	9	0
-40	8.0	2.0	2.0	82	69	0	4	2	5
-40	24	6.0	6.0	81	72	0	3	1	5
-70	2.0	0.50	0.50	62	22	0	15	11	2
-70	8.0	2.0	2.0	72	52	3	6	3	5
-70	24	6.0	6.0	74	60	2	4	2	5

Methyl 6-hydroxy-6-phenylhexanoate (6).

Obtained in 72% yield (GC yield using an internal standard (dodecane)) from methyl 6-oxohexanoate and PhLi. The spectral data were identical to those reported in the literature6. (GC tR 13.9 min; initial oven temperature, 100 °C for 2 min; rate of temperature increase, 10 °C/min; He linear velocity, 30 cm/sec).

Typical Procedure for the Reaction of 4-Benzoylbenzaldehyde with Phenyllithium in a Flow Microreactor System

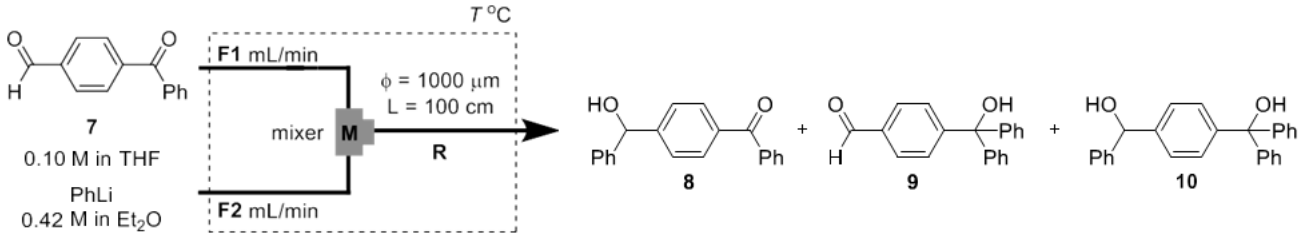

A flow microreactor system consisting of a V-shaped 45o micromixer (ϕ = 250 μm) or T-shaped micromixer (ϕ = 500, 800 μm) (M), a microtube reactor (R), and two tube pre-cooling units (P1 (inner diameter ϕ= 1000 μm, length L = 200 cm) and P2 (ϕ = 1000 μm, L = 100 cm)) was used. A solution of 4-benzoylbenzaldehyde (0.10 M in THF) (flow rate: F1 mL/min) and a solution of PhLi (0.42 M in Et2O/cyclohexane (74/26 v/v)) (flow rate: F2 mL/min)

were introduced to M by syringe pumps. The resulting solution was passed through R (ϕ = 1000 μm, L = 100 cm). After a steady state was reached, an aliquot of the product solution was collected to the sat. NH_4Cl aqueous solution for 30 s to quench the reaction. (when total flow rate in M was under 1.875 mL/min, an aliquot of the product solution was collected for 1 min, when total flow rate in M was over 20 mL/min, an aliquot of the product solution was collected for 20 s). The flow microreactor system was dipped in a cooling bath of T °C. The reaction mixture was analyzed by GC. The results are summarized in Table 12.

Table 12. Reactions of 4-benzoylbenzaldehyde with phenyllithium in a flow microreactor system

inner diameter in **M** (μm)	*T* (°C)	**F1** (mL/min)	**F2** (mL/min)	conversion of **7** (%)	yield (%)		
					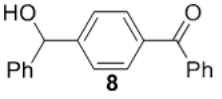 **8**	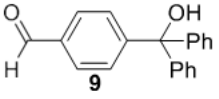 **9**	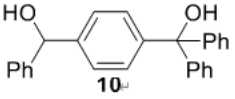 **10**
800 (90°)	-40	12	3.0	65	23	3	40
500 (90°)	-40	12	3.0	71	34	3	32
250 (45°)	-40	12	3.0	83	66	2	15
250 (45°)	-78	12	3.0	78	60	4	17
250 (45°)	-20	12	3.0	79	57	2	18
250 (45°)	0	12	3.0	81	61	2	21
250 (45°)	20	12	3.0	81	57	2	22
250 (45°)	-40	0.50	0.125	61	7	5	40
250 (45°)	-40	1.0	0.25	56	8	5	41
250 (45°)	-40	2.0	0.50	60	15	5	38
250 (45°)	-40	4.0	1.0	74	42	5	29
250 (45°)	-40	8.0	2.0	82	60	3	20
250 (45°)	-40	16	4.0	84	69	2	15
250 (45°)	-40	20	5.0	78	70	2	8
250 (45°)	-40	24	6.0	81	73	1	8

4-Benzoylbenzhydrol (8). Obtained in 73% yield (GC yield) on the condition of using V-shaped 45° micromixer, F1 = 24 mL/min, F2 = 6.0 mL/min, *T* = -40 °C. The spectral data were identical to those reported in the literature.7 (GC *tR* 21.1 min; initial oven temperature, 100 °C for 2 min; rate of temperature increase, 10 °C/min; He linear velocity, 30 cm/sec)

4-(Hydroxydiphenylmethyl)benzaldehyde (9). Obtained 1% yield (GC yield) on the condition of using V-shaped

45º micromixer, F1 = 24 mL/min, F2 = 6.0 mL/min, *T* = -40 ºC. The spectral data were identical to those reported in the literature (GC *tR* 19.2 min; initial oven temperature, 100 ºC for 2 min; rate of temperature increase, 10 ºC/min; He linear velocity, 30 cm/sec).[8]

4-(Hydroxydiphenylmethyl)benzhydrol (10). Obtained 8% yield (GC yield) on the condition of using V-shaped 45o micromixer, F1 = 24 mL/min, F2 = 6.0 mL/min, *T* = -40 oC. This product was synthesized by alternate method to make a calibration curve. A solution of methyl terephthalaldehydate (0.3283 g, 2.00 mmol) in THF (20 mL) was stirred in a flask (100 mL round bottom glass flask with a magnetic stirrer) at -78 oC. A solution of PhLi (1.07 M in Et2O/cyclohexane (30/70 v/v), 6.17 mL, 6.60 mmol) was added and a cooling bath was removed. After stirring for 15 min, sat. NH4Cl aqueous solution (15 mL) was added. The organic layer was separated and the remaining aqueous layer was extracted with Et2O (50 mL×3). The combined organic layers were dried over Na2SO4 and concentrated. The crude product was purified by silica-gel flash chromatography (hexane/ethyl acetate = 3/1) to give 4-(hydroxydiphenylmethyl)benzhydrol (0.6262 g, 86%): GC *tR* 23.1 min (initial oven temperature, 100 oC for 2 min; rate of temperature increase, 10 oC/min; He linear velocity, 30 cm/sec); 1H NMR (400 MHz, CDCl3) □ 2.20 (d, *J* = 3.6 Hz, 1H), 2.75 (s, 1H), 5.84 (d, *J* = 3.2 Hz, 1H), 7.22-7.41 ppm (m, 19H); ^{13}C NMR (100 MHz, CDCl3) □ 76.0, 81.8, 126.1, 126.5, 127.2, 127.6, 127.8, 127.9, 128.1, 128.5, 142.6, 143.6, 146.1, 146.7 ppm; HRMS (ESI) *m/z* calcd for C26H22O2Na$^+$ [M+Na]$^+$: 389.1512, found: 389.1503.

General Procedure for the Reaction of 4-Benzoylbenzaldehyde with Phenyllithium in a Batch Macro Reactor. Method A.

A cooled solution of PhLi in Et2O/cyclohexane (74/26 v/v) (0.42 M, 3.0 mL (1.05 eq), *T* ºC) was

added dropwise for 1.0 min using a glass syringe to a solution of 4-benzoylbenzaldehyde (**7**) in THF (0.10 M, 12 mL) in a 50 mL round bottom glass flask with a magnetic stirrer at *T* oC. After being stirred for 10 min at *T* oC, sat. aq. NH4Cl solution (2.0 mL) was added, and the cooling bath was removed. The conversion of 4-benzoylbenzaldehyde (**7**) and the yields of (4-(hydroxy(phenyl)methyl)phenyl)(phenyl)methanone (**8**), 4-(hydroxydiphenylmethyl)benzaldehyde (**9**), and 4-(hydroxydiphenylmethyl)benzhydrol (**10**) were determined by GC analysis using an internal standard (pentadecane). The results are summarized in Table S5.

Method B. A cooled solution of 4-benzoylbenzaldehyde (**7**) in THF (0.10 M, 12 mL, *T* oC) was added dropwise for 1.0 min using a glass syringe to a solution of PhLi in Et2O/cyclohexane (74/26 v/v) (0.42 M, 3.0 mL (1.05 eq)) in a 50 mL round bottom glass flask with a magnetic stirrer at *T* oC. After being stirred for 10 min at *T* oC, sat. aq. NH4Cl solution (2.0 mL) was added, and the cooling bath was removed. The conversion of 4-benzoylbenzaldehyde (**7**) and the yields of (4-(hydroxy(phenyl)methyl)phenyl)(phenyl)methanone (**8**), 4-(hydroxydiphenylmethyl)benzaldehyde (**9**), and 4-(hydroxydiphenylmethyl)benzhydrol (**10**) were determined by GC analysis using an internal standard (pentadecane). The results are summarized in Table S5.

Method C. A cooled solution of PhLi in Et2O/cyclohexane (74/26 v/v) (0.42 M, 3.0 mL (1.05 eq), -78 ºC) and a cooled solution of 4-benzoylbenzaldehyde (**7**) in THF (0.10 M, 12 mL, -78 oC) were added for 1.0 min to a 50 mL flask equipped with a stirring bar at -78 oC simultaneously. After the resulting solution was stirred for 10 min at -78 ºC, sat. aq. NH4Cl solution (2.0 mL) was added, and the cooling bath was removed. The conversion of 4-benzoylbenzaldehyde (**7**) and the yields of (4-(hydroxy(phenyl)methyl)phenyl)(phenyl)methanone (**8**), 4-(hydroxydiphenylmethyl)benzaldehyde (**9**), and 4-(hydroxydiphenylmethyl)benzhydrol (**10**) were determined by GC analysis using an internal standard (pentadecane). The results are summarized in Table 13.

Table 13. Reactions of 4-benzoylbenzaldehyde (**7**) and phenyllithium using a conventional macro batch reactor.

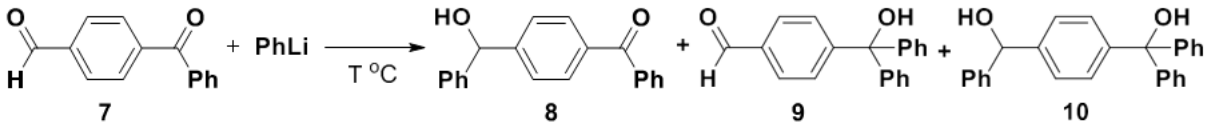

7 8 9 10

T (°C)	method of addition	conversion of **7** (%)	yield (%)		
			8	**9**	**10**
-78	addition of PhLi to **7** (method A)	65	28	7	25
-40	addition of PhLi to **7** (method A)	64	23	7	26
-20	addition of PhLi to **7** (method A)	64	20	7	30
0	addition of PhLi to **7** (method A)	64	12	6	30
20	addition of PhLi to **7** (method A)	61	12	5	33
-78	addition of **7** to PhLi (method B)	33	6	2	26
-40	addition of **7** to PhLi (method B)	37	5	1	27
-20	addition of **7** to PhLi (method B)	46	4	1	35
0	addition of **7** to PhLi (method B)	51	2	1	37
20	addition of **7** to PhLi (method B)	55	1	1	40
-78	simultaneous addition of **7** and PhLi (method C)	51	16	9	26

Conclusion

In conclusion, the author founds that extremely fast micromixing enables highly chemoselective reactions of unstable functional aryllithiums with difunctional electrophiles. The present approach based on flash chemistry serves as a powerful method for protecting-group-free synthesis using organolithium compounds and opens a new possibility in the synthesis of polyfunctional organic molecules.

References and notes

1. S. Young and P. S. Baran, *Nat. Chem.*, 2009, **1**, 193.
2. (a) J. E. Baldwin and R. M. Williams, Organolithiums: Selectivity for Synthesis; Pregamon: Amsterdam, 2002; (*b)* N. Chinkov, H. Chechik, S. Majumdar, A. Liard and I. Marek, *Synthesis*, 2002, **17**, 2473.
3. (a)P. Knochel, Handbook of Functionalized Organometallics, Wiley-VCH, Weinheim, 2005; (*b*) A. Boudier, L. O. Bromm, M. Lotz and P. Knochel, *Angew. Chem. Int. Ed.* 2000, **39**, 4414; (*c*) W. E. Parham and C. K. Bradsher, *Acc. Chem. Res.* 1982, **15**, 300.
4. A. Nagaki, H. Kim and J. Yoshida, *Angew. Chem. Int. Ed.*, 2008, **47**, 7833; *Angew. Chem.*, 2008, **120**, 7951; (*b*) A. Nagaki, H. Kim and J. Yoshida, *Angew. Chem. Int. Ed.*, 2009, **48**, 8063; *Angew. Chem.*, 2009, **121**, 8207; (*c*) A. Nagaki, H. Kim, Y. Moriwaki, C. Matsuo and J. Yoshida, *Chem. Eur. J.*, 2010, **16**, 11167; (*d*) A. Nagaki, H. Kim, C. Matsuo, H. Usutani and J. Yoshida, *Org. Biomol. Chem.*, 2010, **8**, 1212; (*e*) H. Kim, A. Nagaki and J. Yoshida, *Nat. Commun.*, 2011, **2**, 264; (*f*) A. Nagaki, Y. Tsuchihashi, S. Haraki and J. Yoshida, *Org. Biomol. Chem.*, 2015, **13**, 7140-7145.
5. Books on flow chemistry and flow microreactor synthesis: (*a*) W. Ehrfeld, V. Hessel and H. Löwe, Microreactors; Wiley-VCH: Weinheim, 2000; (*b*) V. Hessel, S. Hardt and H. Löwe, Chemical Micro Process Engineering; Wiely-VCH: Weinheim, 2004; (*c*) V. Hessel, A. Renken, J. C. Schouten and J. Yoshida, Eds, Micro Precess Engineering; Wiley-Blackwell, 2009; (*d*) T. Wirth, Ed, Microreactors in Organic Chemistry and Catalysis, 2nd Ed; Wiely-VCH: Weinheim, 2013.
6. Reviews on flow chemistry and flow microreactor synthesis: (*a*) K. Jähnisch, V. Hessel, H. Löwe and M. Baerns, *Angew. Chem. Int. Ed.*, 2004, **43**, 406; *Angew. Chem.*, 2004, **116**, 410; (*b*) G. N. Doku, W. Verboom, D. N. Reinhoudt and A. van den Berg, *Tetrahedron*, 2005, **61**, 2733; (*c*) J. Yoshida, A. Nagaki, T. Iwasaki and S. Suga, *Chem. Eng. Tech.*, 2005, **3**, 259; (*d*) P. Watts and S. J. Haswell, *Chem. Soc. Rev.*, 2005, **34**, 235; (*e*) K. Geyer, J. D. C. Codée and P. H. Seeberger, *Chem. Eur. J.*, 2006, **12**, 8434; (*f*) A. J. deMello, *Nature*, 2006, **442**, 394; (*g*) H. Song, D. L. Chen and R. F. Ismagilov, *Angew. Chem. Int. Ed.*, 2006, **45**, 7336; *Angew. Chem.*, 2006, **118**, 7494; (*h*) J. Kobayashi, Y. Mori and S. Kobayashi, *Chem. Asian. J.*, 2006, **1**, 22; (*i*) M. Brivio, W. Verboom and D. N. Reinhoudt, *Lab Chip*, 2006, **6,** 329; (*j*) B. P. Mason, K. E. Price, J. L. Steinbacher, A. R. Bogdan and D. T. McQuade, *Chem. Rev.*, 2007, **107**, 2300; (*k*) B. Ahmed-Omer, J. C. Brandt and T. Wirth,

Org. Biomol. Chem., 2007, **5**, 733; (*l*) P. Watts and C. Wiles, *Chem. Commun.*, 2007, 443; (*m*) T. Fukuyama, M. T. Rahman, M. Sato and I. Ryu, *Synlett*, 2008, 151; (*n*) R. L. Hartman and K. F. Jensen, *Lab Chip*, 2009, **9**, 2495; (*o*) J. P. McMullen and K. F. Jensen, *Annu. Rev. Anal. Chem.*, 2010, **3**, 19; (*p*) J. Yoshida, H. Kim and A. Nagaki, *ChemSusChem*, 2011, **4**, 331; (*q*) C. Wiles and P. Watts, *Green Chem.*, 2012, **14**, 38; (*r*) A. Kirschining, L. Kupracz and J. Hartwig, *Chem. Lett.*, 2012, **41**, 562; (*s*) D. T. McQuade and P. H. Seeberger, *J. Org. Chem.*, 2013, **78**, 6384; (*t*) K. S. Elvira, X. C. Solvas, R. C. R. Wootton and A. J. deMello, *Nat. Chem.*, 2013, **5**, 905; (*u*) J. C. Pastre, D. L. Browne and S. V. Ley, *Chem. Soc. Rev.*, 2013, **42**, 8849; (*v*) I. R. Baxendale, *J. Chem. Technol. Biotechnol.*, 2013, **88**, 519; (*w*) T. Fukuyama, T. Totoki and I. Ryu, *Green Chem.*, 2014, **16**, 2042; (*x*) H. P. L. Gemoets, Y. Su, M. Shang, V. Hessel, R. Luque and T. Noël, *Chem. Soc. Rev.* 2016, **45**, 83; (*y*) D. Cambié, C. Bottecchia, N. J. W. Straathof, V. Hessel, and T. Noël, *Chem. Rev.* 2016, **116**, 10276; (*z*) M. B. Plutschack, B. Pieber, K. Gilmore, and P. H. Seeberger, *Chem. Rev.*, 2017, **117**, 11796.

7. Some selected recent examples: (*a*) D. Cantillo, M. Baghbanzadeh and C. O. Kappe, *Angew. Chem. Int. Ed.*, 2012, **51**, 10190; *Angew. Chem.*, 2012, **124**, 12207; (*b*) W. Shu and S. L. Buchwald, *Angew. Chem. Int. Ed.*, 2012, **51**, 5355; *Angew. Chem.*, 2012, **124**, 5451; (*c*) A. Nagaki, Y. Moriwaki and J. Yoshida, *Chem. Commun.*, 2012, **48**, 11211; (*d*) F. Lévesque and P. H. Seeberger, *Angew. Chem. Int. Ed.*, 2012, **51**, 1706; *Angew. Chem.*, 2012, **124**, 1738; (*e*) K. C. Basavaraju, S. Sharma, R. A. Maurya and D. P. Kim, *Angew. Chem. Int. Ed.*, 2013, **52**, 6735; *Angew. Chem.*, 2013, **125**, 6867; (*f*) C. Brancour, T. Fukuyama, Y. Mukai, T. Skrydstrup and I. Ryu, *Org. Lett.*, 2013, **15**, 2794; (*g*) J. D. Nguyen, B. Reiß, C. Dai and C. R. J. Stephenson, *Chem. Commun.*, 2013, **49**, 4352; (*h*) C. Battilocchio, J. M. Hawkins and S. V. Ley, *Org. Lett.*, 2013, **15**, 2278; (*i*) A. S. Kleinke and T. F. Jamison, *Org. Lett.*, 2013, **15**, 710; (*j*) K. Asano, Y. Uesugi and J. Yoshida, *Org. Lett.*, 2013, **15**, 2398; (*k*) A. Nagaki, D. Ichinari and J. Yoshida, *Chem. Commun.*, 2013, **49**, 3242; (*l*) L. Guetzoyan, N. Nikbin, I. R. Baxendale and S. V. Ley, *Chem. Sci.*, 2013, **4**, 764; (*m*) S. Fuse, Y. Mifune and T. Takahashi, *Angew. Chem. Int. Ed.*, 2014, **53**, 851; *Angew. Chem.*, 2014, **126**, 870; (*n*) Z. He and T. F. Jamison, *Angew. Chem. Int. Ed.*, 2014, **53**, 3353; *Angew. Chem.*, 2014, **126**, 3421; (*o*) A. Nagaki, Y. Takahashi and J. Yoshida, *Chem. Eur. J.*, 2014, **20**, 7931; (*p*) M. Chen, S. Ichikawa and S. L. Buchwald, *Angew. Chem., Int. Ed.* 2015, **54**, 263; (*q*) S. Fuse, Y. Mifune, H. Nakamura and H. Tanaka, *Nat. Commun.* 2016, **7**, 13491; (*r*) A. Nagaki, Y. Takahashi and J. Yoshida, *Angew. Chem., Int. Ed.* 2016, **55**, 5327; (*s*) H. Seo, M. H. Katcher and T. F. Jamison, *Nat. Chem.* 2017, **9**, 453.

8. (a) R.W. Hoffmann, Synthesis, 2006, 3531; (b) N. A. Afagh and A. K. Yudin, Angew. Chem. Int. Ed., 2010,

49, 262; Angew. Chem., 2010, 122, 270.

9. (a) A. Nagaki, M. Togai, S. Suga, N. Aoki, K. Mae and J. Yoshida, J. Am. Chem. Soc., 2005, 127, 11666; (b) A. Nagaki, N. Takabayashi, Y. Tomida and J. Yoshida, Org. Lett., 2008, 10, 3937; (c) J. Yoshida, A. Nagaki, T. Iwasaki and S. Suga, Chem. Eng. Tech., 2005, 3, 259; (d) A. Nagaki, D. Ichinari and J. Yoshida, Chem. Commun., 2013, 49, 3242; (e) T. Noël, Y. Su, and V. Hessel, Top. Organomet. Chem. 2016, 57, 1; (f) R. L. Hartman, J. P. McMullen and K. F. Jensen, Angew. Chem. Int. Ed. 2011, 50, 7502; (g) J. Yoshida, A. Nagaki, T. Iwasaki and S. Suga, Chem. Eng. Technol. 2005, 28, 259.
10. A. Nagaki, K. Imai, S. Ishiuchi and J. Yoshida, Angew. Chem., Int. Ed., 2015, 54, 1914-1918.
11. W. Ehrfeld, K. Golbig, V. Hessel, H. Löwe and T. Richter, Ind. Eng. Chem. Res., 1999, 38, 1075.
12. It has been reported that aryllithiums react with nitroarenes to give diarylamines. T. Yang and B. P. Cho, Tetrahedron Lett., 2003, 44, 7549.
13. (a) V. Peron, E. Porhiel, V. Ferrand and H. L. Bozec, J. Org. Chem., 1997, 539, 201; (b) A. L. K. S. Shun, E. T. Chernick, S. Eisler and R. R. Tykwinski, J. Org. Chem., 2003, 68, 1339; (c) C. W. Chen and T. Y. Luh, J. Org. Chem., 2008, 73, 8357; (d) K. D. Safa, J. V. Mardipour and Y. M. Oskoei, J. Organomet. Chem., 2011, 696, 802; (e) K. D. Safa, T. Shokri, H. Abbasi and R. T. Mofrad, J. Heterocycl. Chem., 2014, 51, 80.
14. (a) V. H. Rawal, J. A. Rao and M. P. Cava, Tetrahedron Lett., 1985, 26, 4275; (b) V. B. Schmidt and D. Seebach, Angew. Chem. Int. Ed., 1991, 30, 1321; Angew. Chem., 1991, 103, 1383; (c) K. Soai, H. Hori and M. J. Kawahata, J. Chem. Soc. Chem. Commun., 1992, 106; (d) D. Seebach, A. K. Beck, B. Schmidt and Y. M. Wang, Tetrahedron, 1994, 50, 4363; (e) M. Yasuda, T. Fujibayashi, I. Shibata, A. Baba, H. Matsuda and M. Sonoda, Chem. Lett., 1995, 24, 167; (f) K. Soai, Y. Inoue, T. Takahashi and T. Shibata, Tetrahedron, 1996, 52, 13355; (g) T. C. Chan, C. P. Lau and T. H. Chan, Tetrahedron Lett., 2004, 45, 4189; (h) A. M. Piggott and P. Karuso, Tetrahedron Lett., 2005, 46, 8241; (i) J. X. Wang, K. Wang, L. Zhao, H. Li and Y. Fu, Adv. Synth. Catal., 2006, 348, 1262; (j) S. Chassaing, M. K. Stotz, G. Isorez and R. Brouillard, Eur. J. Org. Chem., 2007, 2438; (k) K. Yoshida, H. Takahashi and T. Imamoto, Chem. Eur. J., 2008, 14, 8246; (l) H. Zheng, Q. Zhang, J. Chen, M. Liu, S. Chen, J. Ding, H. Wu and W. Su, J. Org. Chem., 2009, 74, 943; (m) N. Ahlsten, A. Bartoszewicz, S. Agrawal and B. M. Matute, Synthesis, 2011, 2600; (n) M. Mineno, Y. Sawai, K. Kanno, N. Sawada and H. Mizufune, J. Org. Chem., 2013, 78, 5843; (o) W. Zeng, M. Ishida, S. Lee, Y. M. Sung, Z. Zeng, Y. Ni, C. Chi, D. Kim and J. Wu, Chem. Eur. J., 2013, 19, 16814; (p) Z. Sun, S. Lee, K. H. Park, X. Zhu, W. Zhang, B. Zheng, P. Hu, Z. Zeng, S. Das, Y. Li, C. Chi, R. W. Li, K. W. Huang, J. Ding, D. Kim and J. Wu, J.

Am. Chem. Soc., 2013, 135, 18229.

15. (a) S. Suga, D. Yamada and J. Yoshida, Chem. Lett., 2010, 39, 404; (b) A. Nagaki, A. Kenmoku, Y. Moriwaki, A. Hayashi and J. Yoshida, Angew. Chem. Int. Ed., 2010, 49, 7543; Angew. Chem., 2010, 122, 7705; (c) J. Yoshida, K. Saito, T. Nokami and A. Nagaki, Synlett, 2011, 1189.

Chapter 3

Molecular Weight Distribution of Polymers Produced by Anionic Polymerization Enables Mixability Evaluation

Abstract

In the anionic polymerization of styrene using a flow microreactor, there was a strong correlation between the molecular weight distribution (*Mw/Mn*) of the polymer and the mixing speed. By taking advantage of this relationship, a new type of mixability evaluation was developed using the flow microreactor system. The new method allowed the mixability to be evaluated at 0 °C or lower temperature with high accuracy. Being able to be applied for a wider range of reaction condition, it offers a great advantage over other evaluation procedures such as Dushman reaction, which requires reaction temperatures to be above 0 °C. The presented method is a promising alternative as a new evaluation technique for mixing efficiency.

Introduction

Flow microreactor[1,2,3] is expected to bring about revolutionary changes in chemical synthesis and manufacturing process. Therefore, it has been a technology of great interest both in academia and industry. Particularly, polymerization reactions using flow microreactors have attracted much research interests as the reaction can especially make use of its strengths. In fact, a great number of studies have been reported in various polymerizations such as cationic, anionic, radical, coordination, ring-opening polymerization, poly-condensation.[4,5]

The author previously reported that, by using flow microreactors, anionic polymerization[6,7] could lead to a precisely controlled molecular weight distribution in a more environmentally friendly way.[8] Also, the overall efficiency of polymerization was greatly improved by taking advantages of flow microreactors: fast mixing; rapid heat transfer; and precise residence time control.

Flow microreactors also offer great advantages for industrial applications. It is much easier for a newly-developed reaction to be transferred from a laboratory setting to a commercial application. It can dramatically shorten the time required for reaction scale-up. In addition, the quality control of polymers can be performed more efficiently in flow microreactors, producing polymer materials with much higher quality. In fact, some results from previous studies indicated the possibility of anionic polymerization of styrene using a flow microreactor system in a stable continuous manner.[9]

In flow microreactor process development, the mixability between several solutions can often be an important factor in terms of reaction control. Up until now, Dushman reaction[10] is the most commonly used method to evaluate mixing performance. Dushman reaction evaluates the mixability using a competitive parallel reaction between neutralization reaction and oxidation-reduction reaction.[11] When mixing of two solutions proceeds rapidly, neutralization reaction preferentially occurs. On the other hand, when the mixing is relatively slow, oxidation-reduction reaction proceeds competitively, generating iodine. The mixability is determined by measuring the absorbance (352 nm) of the generated iodine. This evaluation method has two major disadvantages: being an aqueous reactions, it cannot evaluate the mixability at 0 ^{o}C or lower temperature; and the evaluation accuracy can be significantly deteriorated as a reaction can proceed even during the absorbance measurement.

The author previously reported that ,in the addition polymerization reaction (competitive sequential reaction) using

flow microreactors, there was a strong correlation between the mixing speed and the molecular weight distribution. With low flow rates of an initiator and monomer solution, the mixability was poor, and the value for molecular weight distribution (Mw/Mn) increased. On the other hand, with high mixability, the Mw/Mn was likely to be closer to 1.0. In other words, a molecular weight distribution will be uniform when all the chains are simultaneously initiated in addition polymerization. On contrary, the polymerization can result in a non-uniform molecular weight distribution when the initiation reaction occurs disorderly.

Herein the author reports that anionic polymerization of styrene in flow microreactor system can be a very efficient new mixability evaluation method because of the strong correlation between the mixability and the molecular distribution. It is especially advantageous as the new method allows mixability to be accurately evaluated at 0 °C or lower, which is difficult by Dushman reaction. Using the new flow microreactor method, the mixability was evaluated for various shaped mixers with different inner diameters.

Using a flow microreactor consisting of a T-250-250 mixer **M1** and a tube reactor **R1**, anionic polymerization was carried out in different flow rates at 30 °C (Figure 1).

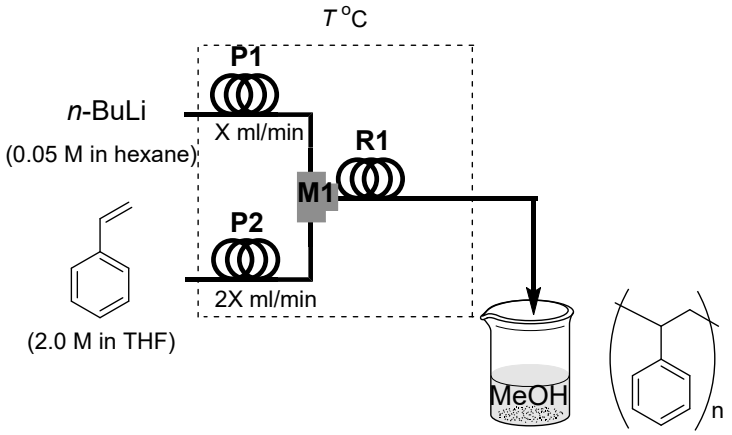

Scheme 1. Flow-microreactor-system polymerization of styrenes..

Results and discussion

Here, mixers were labeled as follows: "mixer shape-inlet inner diameter [μm]-outlet inner diameter [μm]". For example, T-250-250 stands for a T-shaped mixer with the inlet inner diameter of 250 μm and the outlet inner diameter of 250 μm. In higher flow rates, the values of molecular weight distribution were close to 1.0. On the

other hand, in lower flow rates, the values of molecular weight distribution moved away from 1.0 (Figure 2).

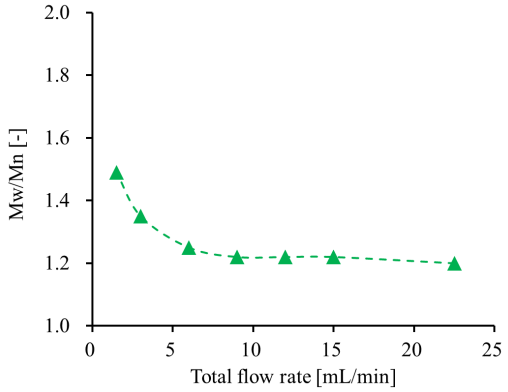

Figure 2. Relationship between total flow rate and Mw/Mn

Figure 3 shows the results of the same mixer from Dushman reaction where the mixability is determined based on absorbance values. The absorbance values were low with higher flow rates and thus higher mixability, while lower mixability conditions resulted in higher absorbance values. By comparing Figure 2 and 3, it is clear that the absorbance and molecular weight distribution had the same correlation with the flow rate mixability. Therefore, it was concluded that the molecular weight distribution of the polymer could be used for the mixability evaluation.

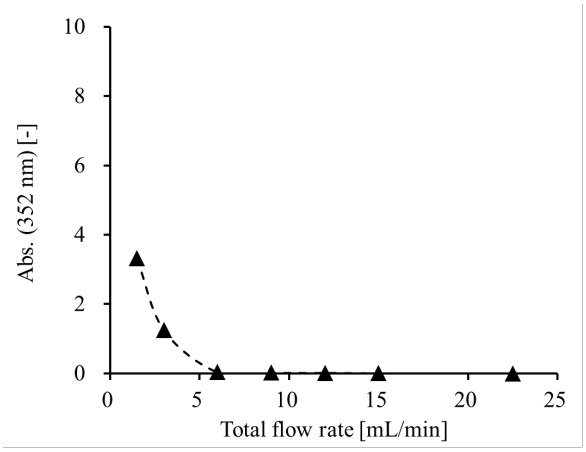

Figure 3. Relationship between total flow rate and absorbance

One of the major disadvantages of Dushman reaction is that the absorbance of reaction samples change over time. This change in absorbance deteriorates the reliability of measurement data. The absorbance dropped about 10% for one hour after sampling because the effect of sublimation of iodine (Figure 4). On the other hand, an evaluation data in anionic polymerization will not be affected by time as the molecular weight distribution of the polymer is measured after the reaction is completely stopped. For this reason, flow microreactor method is a

more reliable mixability evaluation.

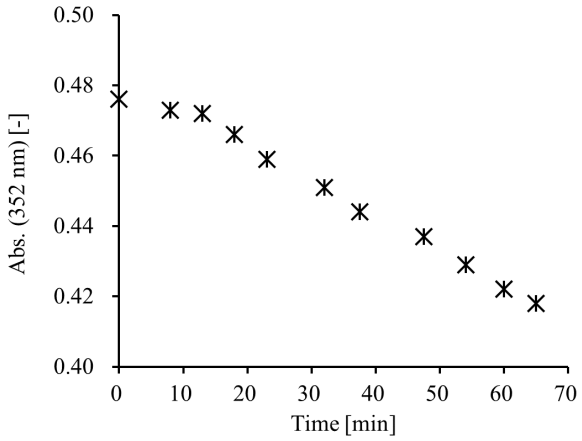

Figure 4. The changes in the absorbance of reaction solution over time

The same evaluation was conducted in various temperature conditions (-20, 0, 30 ºC). As shown in Figure 5, all three temperature conditions demonstrated no significant differences. Therefore, analysis on the molecular weight distribution of polystyrene can be used for the mixability evaluation even at 0 ºC or lower. In addition, it was decided to conduct the further evaluation at 30 ºC because it is easier to perform the evaluation under such temperature.

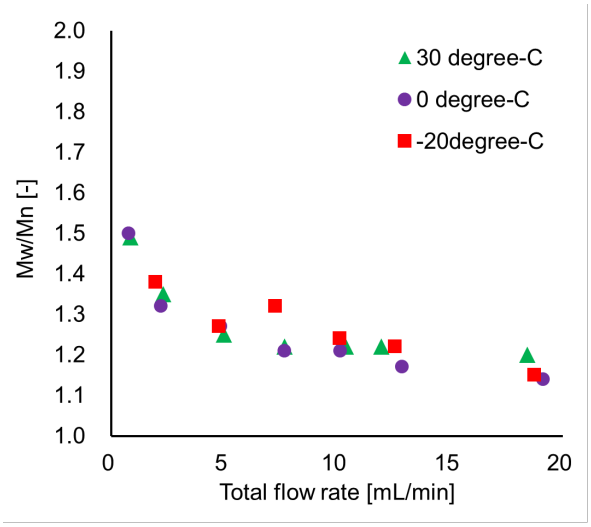

Figure 5. The results of the evaluation in various temperature condition

Next, the mixability was evaluated against mixers with different inner diameters, by comparing T-250-250 and T-500-500. The mixer with the smaller inner diameter showed higher mixability (Figure 6). In the same flow rate, a mixer with the smaller diameter has shorter diffusion distance, and mixing by diffusion is facilitated. In

addition, the smaller the inner diameter, the faster the linear velocity of solution, causing more turbulent flows.

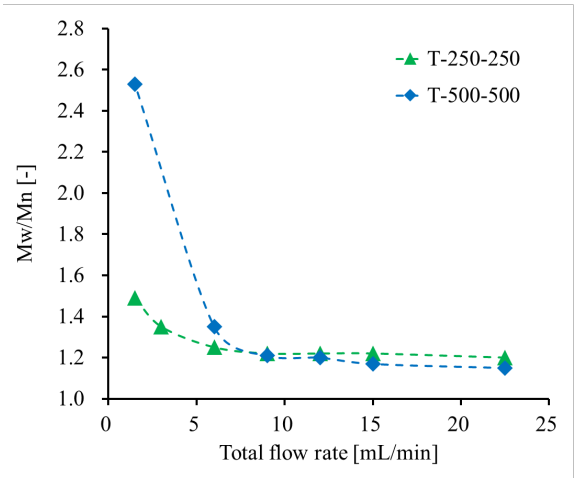

Figure 6. Comparing T-250-250 and T-500-500

The mixability was evaluated against different shaped mixers, by comparing V, T and Y-shape mixers. First, V-500-500 and T-500-500 were examined. The V-shape mixer showed slightly higher mixability than the T-shape mixer (Figure 7). Likewise, T-250-250 and Y-250-250 were examined. The T-shape mixer demonstrated higher mixability than the Y-shape mixer (Figure 8). It was clear that a shape of a mixer influenced the mixibility. The mixability of three mixers was V $\geqq$ T > Y, V-shaped mixer being the most effective and Y-shaped mixer being the least. It was presumed that when a contact area of two solutions has a more steeply curved structure, the turbulence occurs more vigorously and mixing is further improved. The obtained results were similar to those from Dushman reaction (See the Surpporitng Information for details).

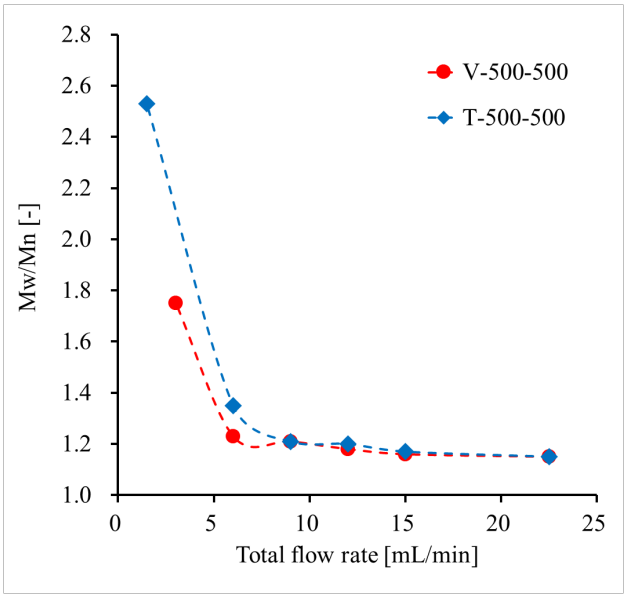

Figure 7. Comparing V-shape and T- shape mixers

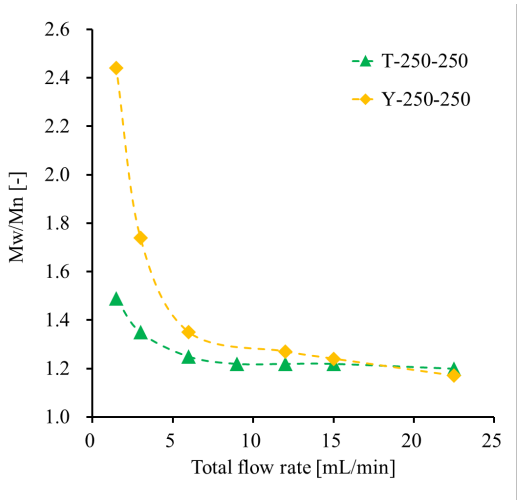

Figure 8. Comparing Y-shape and T- shape mixers

Finally, the evaluation was conducted for mixers with different inner diameters of outlet and inlet, using T-250-250, T-250-500, T-500-250 and T-500-500. The mixers with smaller inlet inner diameters, T-250-250 and T-250-500, resulted in better mixiability than the other two mixers while different outlet inner diameter sizes of these mixers caused no significant difference in mixability. The result suggested that the linear velocity at the collision area of two solutions was an important parameter influencing the mixability in anionic polymerization of polystyrenes. Between these two mixers, it can be concluded that T-250-500 is a superior mixer than T-250-250, because of its bigger outlet size, the mixer has a better ability of avoiding blockage and also suppressing pressure loss (Figure 9).

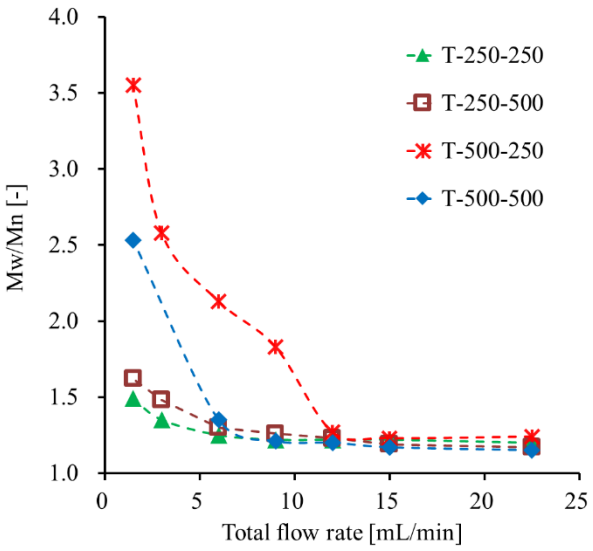

Figure 9. Evaluating the mixers of different inner diameters of inlet and outlet

On the other hand, a size difference in the outlet inner diameter clearly showed the dissimilarity in the mixability of T-500-250 and T-500-500. This was possibly caused by inefficient discharge of reaction solution at the mixer outlet. Having a much smaller inner diameter than the inlet, the outlet was presumed to act as bottleneck. As a result, the mixing was deteriorated.

Experimental Section

General.

Tetrahydrofuran (THF) and hexane was purchased from Kanto and Wako as a dry solvent and used as obtained. Styrene was purchased from TCI, and were used with further purification. 1.6 M *n*-BuLi hexane solution was purchased from Kanto, and this reagent was diluted for experiments. Stainless steel (SUS304) T, Y and V-shaped micromixers were manufactured by Sanko Seiki Co., Inc. Stainless steel (SUS316) microtube reactors having inner diameter of 1000 μm were purchased from GL Sciences. Micromixers and microtube reactors were connected with stainless type fittings (GL Sciences, 1/16 OUW). The flow microreactor system was dipped in a cooling bath to control the temperature. Solutions were introduced to a flow microreactor system using a Smoothflow pump Q-10-6T-P-S manufactured by TACMINA corporation.

Molecular Weight and Molecular Weight Distribution.

The molecular weight (*Mn*) and molecular weight distribution (*Mw/Mn*) were determined by Gel Permeation Chromatography in THF at 40 °C with a Shodex GPC-101 equipped with two LF-804L columns (Shodex) and an RI detector using a polystyrene (polySt) standard sample for calibration. And, the range of polystyrene (polySt) standard sample was 2630 to 1090000 as *Mn*.

Anionic Polymerization of Styrene Using a Flow Microreactor System.

A flow microreactor system composed of a micromixer (**M1**) and a microtube reactor (**R1**) were used. Two

precooling units (**P1**: ϕ = 1000 μm, length = 200 cm, **P2**: ϕ = 1000 μm, length = 200 cm) were connected to an inlet of the micromixers **M1**. The whole flow microreactor system was dipped in a bath to control tempuerature condition. A solution of styrene (2.00 M in THF) and *n*-BuLi (0.050 M in hexane) were introduced to **M1** by Smoothflow pumps Q. The resulting solution was passed through **R1** (ϕ = 1000 μm, length = 600 cm). The resulting solution was accepted to MeOH in vial for quenching reaction (1 min). The polymer sample was analyzed with size exclusion chromatography with the calibration using standard polystyrene samples. Detailed data were listed in Table 1 and Figure S1 – S52 in sapporting information.

Table 1. The numeric data of each graph

Mixer shape	T (°C)	Flow rate (mL/min)		[M]/[I]	Mn	Mw/Mn
		n-BuLi	Styrene			
T-250-250	30	7.5	15.0	80	11000	1.20
		5.0	10.0	80	12000	1.22
		4.0	8.0	80	11000	1.22
		3.0	6.0	80	11000	1.22
		2.0	4.0	80	12000	1.25
		1.0	2.0	80	12000	1.35
		0.5	1.0	80	11000	1.49
		4.0	8.0	80	10000	1.19
		3.0	6.0	80	10000	1.25
		2.0	4.0	80	10000	1.29
		1.0	2.0	80	10000	1.51
	0	7.5	15.0	80	11000	1.14
		5.0	10.0	80	11000	1.17
		4.0	8.0	80	11000	1.21
		3.0	6.0	80	11000	1.21
		2.0	4.0	80	11000	1.27
		1.0	2.0	80	11000	1.32
		0.5	1.0	80	11000	1.50
	-20	7.5	15.0	80	12000	1.15
		5.0	10.0	80	12000	1.22
		4.0	8.0	80	12000	1.24
		3.0	6.0	80	12000	1.32
		2.0	4.0	80	11000	1.27
		1.0	2.0	80	11000	1.38
T-500-500	30	7.5	15.0	80	11000	1.15
		5.0	10.0	80	11000	1.17
		4.0	8.0	80	11000	1.20
		3.0	6.0	80	11000	1.21
		2.0	4.0	80	11000	1.35
		0.5	1.0	80	11000	2.53
Y-250-250	30	7.5	15.0	80	11000	1.17
		5.0	10.0	80	11000	1.24
		4.0	8.0	80	11000	1.27
		2.0	4.0	80	11000	1.35
		1.0	2.0	80	11000	1.74
		0.5	1.0	80	11000	2.44
T-250-500	30	7.5	15.0	80	10000	1.17
		5.0	10.0	80	10000	1.19
		4.0	8.0	80	10000	1.23
		3.0	6.0	80	10000	1.26
		2.0	4.0	80	10000	1.30
		1.0	2.0	80	10000	1.48
		0.5	1.0	80	10000	1.62
T-500-250	30	7.5	15.0	80	10000	1.24
		5.0	10.0	80	10000	1.23
		4.0	8.0	80	10000	1.27
		3.0	6.0	80	10000	1.83
		2.0	4.0	80	10000	2.13
		1.0	2.0	80	10000	2.58
		0.5	1.0	80	10000	3.55
V-500-500	30	7.5	15.0	80	10000	1.15
		5.0	10.0	80	10000	1.16
		4.0	8.0	80	10000	1.18
		3.0	6.0	80	10000	1.21
		2.0	4.0	80	10000	1.23
		1.0	2.0	80	10000	1.75

Dushman reaction.

A flow microreactor system for dushman reaction composed of micromixer (M1) and microtube reactor (R1) used. The whole flow microreactor system was in the air. A solution A of HCl (0.03 M) and solution B (0.09 M H_3BO_3, 0.09 M NaOH, 0.032 M KI, 0.006 M KIO_3) were introduced to M1 by syringe pump (Harvard Apparatus PHD

Ultra). The reaction solution was passed through R1 (ϕ = 1000 μm, length = 50 cm). This solution was accepted to cuvette for measuring absorbance. And then, absorbance of this solution was measured by spectrophotometer. Detailed data were listed in Figure S53 – S55 and Table S1 in sapporting information.

Conclusion

In conclusion, analysis on the molecular weight distribution in polystyrene anionic polymerization can be used as a new mixability evaluation method. This newly developed method can be considered superior to Dushman Reacion because of two reasons: it can evaluate the mixability at 0 ^{o}C or lower temperature and the evaluation results are not affected by time.

Supporting information

- Size exclusion chromatography data for all polymers with the calibration using standard polystyrene samples, and, explaining the results of Dushman reaction data -

Figure S-1. *n*-BuLi Initiated Polymerization of Styrene in The Flow System (flow rate of *n*-BuLi (0.05 M) = 7.5 mL/min, flow rate of Styrene (2.0 M) = 15.0 mL/min, T-250-250 mixer, 30 degree-C)

Figure S-2. *n*-BuLi Initiated Polymerization of Styrene in The Flow System (flow rate of *n*-BuLi (0.05 M) = 5.0 mL/min, flow rate of Styrene (2.0 M) = 10.0 mL/min, T-250-250 mixer, 30 degree-C)

Figure S-3. *n*-BuLi Initiated Polymerization of Styrene in The Flow System (flow rate of *n*-BuLi (0.05 M) = 4.0 mL/min, flow rate of Styrene (2.0 M) = 8.0 mL/min, T-250-250 mixer, 30 degree-C)

Figure S-4. *n*-BuLi Initiated Polymerization of Styrene in The Flow System (flow rate of *n*-BuLi (0.05 M) = 3.0 mL/min, flow rate of Styrene (2.0 M) = 6.0 mL/min, T-250-250 mixer, 30 degree-C)

Figure S-5. *n*-BuLi Initiated Polymerization of Styrene in The Flow System (flow rate of *n*-BuLi (0.05 M) = 2.0 mL/min, flow rate of Styrene (2.0 M) = 4.0 mL/min, T-250-250 mixer, 30 degree-C)

Figure S-6. *n*-BuLi Initiated Polymerization of Styrene in The Flow System (flow rate of *n*-BuLi (0.05 M) = 1.0 mL/min, flow rate of Styrene (2.0 M) = 2.0 mL/min, T-250-250 mixer, 30 degree-C)

Figure S-7. *n*-BuLi Initiated Polymerization of Styrene in The Flow System (flow rate of *n*-BuLi (0.05 M) = 0.5 mL/min, flow rate of Styrene (2.0 M) = 1.0 mL/min, T-250-250 mixer, 30 degree-C)

Figure S-8. *n*-BuLi Initiated Polymerization of Styrene in The Flow System (flow rate of *n*-BuLi (0.05 M) = 7.5 mL/min, flow rate of Styrene (2.0 M) = 15.0 mL/min, T-250-250 mixer, 0 degree-C)

Figure S-9. *n*-BuLi Initiated Polymerization of Styrene in The Flow System (flow rate of *n*-BuLi (0.05 M) = 5.0 mL/min, flow rate of Styrene (2.0 M) = 10.0 mL/min, T-250-250 mixer, 0 degree-C)

Figure S-10. *n*-BuLi Initiated Polymerization of Styrene in The Flow System (flow rate of *n*-BuLi (0.05 M) = 4.0 mL/min, flow rate of Styrene (2.0 M) = 8.0 mL/min, T-250-250 mixer, 0 degree-C)

Figure S-11. *n*-BuLi Initiated Polymerization of Styrene in The Flow System (flow rate of *n*-BuLi (0.05 M) = 3.0 mL/min, flow rate of Styrene (2.0 M) = 6.0 mL/min, T-250-250 mixer, 0 degree-C)

Figure S-12. *n*-BuLi Initiated Polymerization of Styrene in The Flow System (flow rate of *n*-BuLi (0.05 M) = 2.0

mL/min, flow rate of Styrene (2.0 M) = 4.0 mL/min, T-250-250 mixer, 0 degree-C)

Figure S-13. *n*-BuLi Initiated Polymerization of Styrene in The Flow System (flow rate of *n*-BuLi (0.05 M) = 1.0 mL/min, flow rate of Styrene (2.0 M) = 2.0 mL/min, T-250-250 mixer, 0 degree-C)

Figure S-14. *n*-BuLi Initiated Polymerization of Styrene in The Flow System (flow rate of *n*-BuLi (0.05 M) = 0.5 mL/min, flow rate of Styrene (2.0 M) = 1.0 mL/min, T-250-250 mixer, 0 degree-C)

Figure S-15. *n*-BuLi Initiated Polymerization of Styrene in The Flow System (flow rate of *n*-BuLi (0.05 M) = 7.5 mL/min, flow rate of Styrene (2.0 M) = 15.0 mL/min, T-250-250 mixer, -20 degree-C)

Figure S-16. *n*-BuLi Initiated Polymerization of Styrene in The Flow System (flow rate of *n*-BuLi (0.05 M) = 5.0 mL/min, flow rate of Styrene (2.0 M) = 10.0 mL/min, T-250-250 mixer, -20 degree-C)

Figure S-17. *n*-BuLi Initiated Polymerization of Styrene in The Flow System (flow rate of *n*-BuLi (0.05 M) = 4.0 mL/min, flow rate of Styrene (2.0 M) = 8.0 mL/min, T-250-250 mixer, -20 degree-C)

Figure S-18. *n*-BuLi Initiated Polymerization of Styrene in The Flow System (flow rate of *n*-BuLi (0.05 M) = 3.0 mL/min, flow rate of Styrene (2.0 M) = 6.0 mL/min, T-250-250 mixer, -20 degree-C)

Figure S-19. *n*-BuLi Initiated Polymerization of Styrene in The Flow System (flow rate of *n*-BuLi (0.05 M) = 2.0 mL/min, flow rate of Styrene (2.0 M) = 4.0 mL/min, T-250-250 mixer, -20 degree-C)

Figure S-20. *n*-BuLi Initiated Polymerization of Styrene in The Flow System (flow rate of *n*-BuLi (0.05 M) = 1.0 mL/min, flow rate of Styrene (2.0 M) = 2.0 mL/min, T-250-250 mixer, -20 degree-C)

Figure S-21. *n*-BuLi Initiated Polymerization of Styrene in The Flow System (flow rate of *n*-BuLi (0.05 M) = 7.5 mL/min, flow rate of Styrene (2.0 M) = 15.0 mL/min, T-500-500 mixer, 30 degree-C)

Figure S-22. *n*-BuLi Initiated Polymerization of Styrene in The Flow System (flow rate of *n*-BuLi (0.05 M) = 5.0 mL/min, flow rate of Styrene (2.0 M) = 10.0 mL/min, T-500-500 mixer, 30 degree-C)

Figure S-23. *n*-BuLi Initiated Polymerization of Styrene in The Flow System (flow rate of *n*-BuLi (0.05 M) = 4.0 mL/min, flow rate of Styrene (2.0 M) = 8.0 mL/min, T-500-500 mixer, 30 degree-C)

Figure S-24. *n*-BuLi Initiated Polymerization of Styrene in The Flow System (flow rate of *n*-BuLi (0.05 M) = 3.0 mL/min, flow rate of Styrene (2.0 M) = 6.0 mL/min, T-500-500 mixer, 30 degree-C)

Figure S-25. *n*-BuLi Initiated Polymerization of Styrene in The Flow System (flow rate of *n*-BuLi (0.05 M) = 2.0 mL/min, flow rate of Styrene (2.0 M) = 4.0 mL/min, T-500-500 mixer, 30 degree-C)

Figure S-26. *n*-BuLi Initiated Polymerization of Styrene in The Flow System (flow rate of *n*-BuLi (0.05 M) = 0.5 mL/min, flow rate of Styrene (2.0 M) = 1.0 mL/min, T-500-500 mixer, 30 degree-C)

Figure S-27. *n*-BuLi Initiated Polymerization of Styrene in The Flow System (flow rate of *n*-BuLi (0.05 M) = 7.5 mL/min, flow rate of Styrene (2.0 M) = 15.0 mL/min, Y-250-250 mixer, 30 degree-C)

Figure S-28. *n*-BuLi Initiated Polymerization of Styrene in The Flow System (flow rate of *n*-BuLi (0.05 M) = 5.0 mL/min, flow rate of Styrene (2.0 M) = 10.0 mL/min, Y-250-250 mixer, 30 degree-C)

Figure S-29. *n*-BuLi Initiated Polymerization of Styrene in The Flow System (flow rate of *n*-BuLi (0.05 M) = 4.0 mL/min, flow rate of Styrene (2.0 M) = 8.0 mL/min, Y-250-250 mixer, 30 degree-C)

Figure S-30. *n*-BuLi Initiated Polymerization of Styrene in The Flow System (flow rate of *n*-BuLi (0.05 M) = 2.0 mL/min, flow rate of Styrene (2.0 M) = 4.0 mL/min, Y-250-250 mixer, 30 degree-C)

Figure S-31. *n*-BuLi Initiated Polymerization of Styrene in The Flow System (flow rate of *n*-BuLi (0.05 M) = 1.0

mL/min, flow rate of Styrene (2.0 M) = 2.0 mL/min, Y-250-250 mixer, 30 degree-C)

Figure S-32. *n*-BuLi Initiated Polymerization of Styrene in The Flow System (flow rate of *n*-BuLi (0.05 M) = 0.5 mL/min, flow rate of Styrene (2.0 M) = 1.0 mL/min, Y-250-250 mixer, 30 degree-C)

Figure S-33. *n*-BuLi Initiated Polymerization of Styrene in The Flow System (flow rate of *n*-BuLi (0.05 M) = 7.5 mL/min, flow rate of Styrene (2.0 M) = 15.0 mL/min, T-250-500 mixer, 30 degree-C)

Figure S-34. *n*-BuLi Initiated Polymerization of Styrene in The Flow System (flow rate of *n*-BuLi (0.05 M) = 5.0 mL/min, flow rate of Styrene (2.0 M) = 10.0 mL/min, T-250-500 mixer, 30 degree-C)

Figure S-35. *n*-BuLi Initiated Polymerization of Styrene in The Flow System (flow rate of *n*-BuLi (0.05 M) = 4.0 mL/min, flow rate of Styrene (2.0 M) = 8.0 mL/min, T-250-500 mixer, 30 degree-C)

Figure S-36. *n*-BuLi Initiated Polymerization of Styrene in The Flow System (flow rate of *n*-BuLi (0.05 M) = 3.0 mL/min, flow rate of Styrene (2.0 M) = 6.0 mL/min, T-250-500 mixer, 30 degree-C)

Figure S-37. *n*-BuLi Initiated Polymerization of Styrene in The Flow System (flow rate of *n*-BuLi (0.05 M) = 2.0 mL/min, flow rate of Styrene (2.0 M) = 4.0 mL/min, T-250-500 mixer, 30 degree-C)

Figure S-38. *n*-BuLi Initiated Polymerization of Styrene in The Flow System (flow rate of *n*-BuLi (0.05 M) = 1.0 mL/min, flow rate of Styrene (2.0 M) = 2.0 mL/min, T-250-500 mixer, 30 degree-C)

Figure S-39. *n*-BuLi Initiated Polymerization of Styrene in The Flow System (flow rate of *n*-BuLi (0.05 M) = 0.5 mL/min, flow rate of Styrene (2.0 M) = 1.0 mL/min, T-250-500 mixer, 30 degree-C)

Figure S-40. *n*-BuLi Initiated Polymerization of Styrene in The Flow System (flow rate of *n*-BuLi (0.05 M) = 7.5 mL/min, flow rate of Styrene (2.0 M) = 15.0 mL/min, T-500-250 mixer, 30 degree-C)

Figure S-41. *n*-BuLi Initiated Polymerization of Styrene in The Flow System (flow rate of *n*-BuLi (0.05 M) = 5.0 mL/min, flow rate of Styrene (2.0 M) = 10.0 mL/min, T-500-250 mixer, 30 degree-C)

Figure S-42. *n*-BuLi Initiated Polymerization of Styrene in The Flow System (flow rate of *n*-BuLi (0.05 M) = 4.0 mL/min, flow rate of Styrene (2.0 M) = 8.0 mL/min, T-500-250 mixer, 30 degree-C)

Figure S-43. *n*-BuLi Initiated Polymerization of Styrene in The Flow System (flow rate of *n*-BuLi (0.05 M) = 3.0 mL/min, flow rate of Styrene (2.0 M) = 6.0 mL/min, T-500-250 mixer, 30 degree-C)

Figure S-44. *n*-BuLi Initiated Polymerization of Styrene in The Flow System (flow rate of *n*-BuLi (0.05 M) = 2.0 mL/min, flow rate of Styrene (2.0 M) = 4.0 mL/min, T-500-250 mixer, 30 degree-C)

Figure S-45. *n*-BuLi Initiated Polymerization of Styrene in The Flow System (flow rate of *n*-BuLi (0.05 M) = 1.0 mL/min, flow rate of Styrene (2.0 M) = 2.0 mL/min, T-500-250 mixer, 30 degree-C)

Figure S-46. *n*-BuLi Initiated Polymerization of Styrene in The Flow System (flow rate of *n*-BuLi (0.05 M) = 0.5 mL/min, flow rate of Styrene (2.0 M) = 1.0 mL/min, T-500-250 mixer, 30 degree-C)

Figure S-47. *n*-BuLi Initiated Polymerization of Styrene in The Flow System (flow rate of *n*-BuLi (0.05 M) = 7.5 mL/min, flow rate of Styrene (2.0 M) = 15.0 mL/min, V-500-500 mixer, 30 degree-C)

Figure S-48. *n*-BuLi Initiated Polymerization of Styrene in The Flow System (flow rate of *n*-BuLi (0.05 M) = 5.0 mL/min, flow rate of Styrene (2.0 M) = 10.0 mL/min, V-500-500 mixer, 30 degree-C)

Figure S-49. *n*-BuLi Initiated Polymerization of Styrene in The Flow System (flow rate of *n*-BuLi (0.05 M) = 4.0 mL/min, flow rate of Styrene (2.0 M) = 8.0 mL/min, V-500-500 mixer, 30 degree-C)

Figure S-50. *n*-BuLi Initiated Polymerization of Styrene in The Flow System (flow rate of *n*-BuLi (0.05 M) = 3.0 mL/min, flow rate of Styrene (2.0 M) = 6.0 mL/min, V-500-500 mixer, 30 degree-C)

Figure S-51. *n*-BuLi Initiated Polymerization of Styrene in The Flow System (flow rate of *n*-BuLi (0.05 M) = 2.0 mL/min, flow rate of Styrene (2.0 M) = 4.0 mL/min, V-500-500 mixer, 30 degree-C)

Figure S-52. *n*-BuLi Initiated Polymerization of Styrene in The Flow System (flow rate of *n*-BuLi (0.05 M) = 1.0 mL/min, flow rate of Styrene (2.0 M) = 2.0 mL/min, V-500-500 mixer, 30 degree-C)

Figure S-53. *n*-BuLi Initiated Polymerization of Styrene in The Flow System (flow rate of *n*-BuLi (0.05 M) = 7.5 mL/min, flow rate of Styrene (2.0 M) = 15.0 mL/min, T-250-250 mixer, 30 degree-C, 2nd trial)

Figure S-54. *n*-BuLi Initiated Polymerization of Styrene in The Flow System (flow rate of *n*-BuLi (0.05 M) = 5.0 mL/min, flow rate of Styrene (2.0 M) = 10.0 mL/min, T-250-250 mixer, 30 degree-C, 2nd trial)

Figure S-55. *n*-BuLi Initiated Polymerization of Styrene in The Flow System (flow rate of *n*-BuLi (0.05 M) = 4.0 mL/min, flow rate of Styrene (2.0 M) = 8.0 mL/min, T-250-250 mixer, 30 degree-C, 2nd trial)

Figure S-56. *n*-BuLi Initiated Polymerization of Styrene in The Flow System (flow rate of *n*-BuLi (0.05 M) = 3.0 mL/min, flow rate of Styrene (2.0 M) = 6.0 mL/min, T-250-250 mixer, 30 degree-C, 2nd trial)

Figure S-57. *n*-BuLi Initiated Polymerization of Styrene in The Flow System (flow rate of *n*-BuLi (0.05 M) = 2.0 mL/min, flow rate of Styrene (2.0 M) = 4.0 mL/min, T-250-250 mixer, 30 degree-C, 2nd trial)

The reproducibility of anionic polymerization

Figure S-58. Comparing the Mw/Mn of 1st and 2nd trials

Table S-1. Numeric data of 2nd trial in the above graph

Mn	= 11492
Mw	= 13790
Mz	= 20174
Mv	= 13790
I.V	= 13790

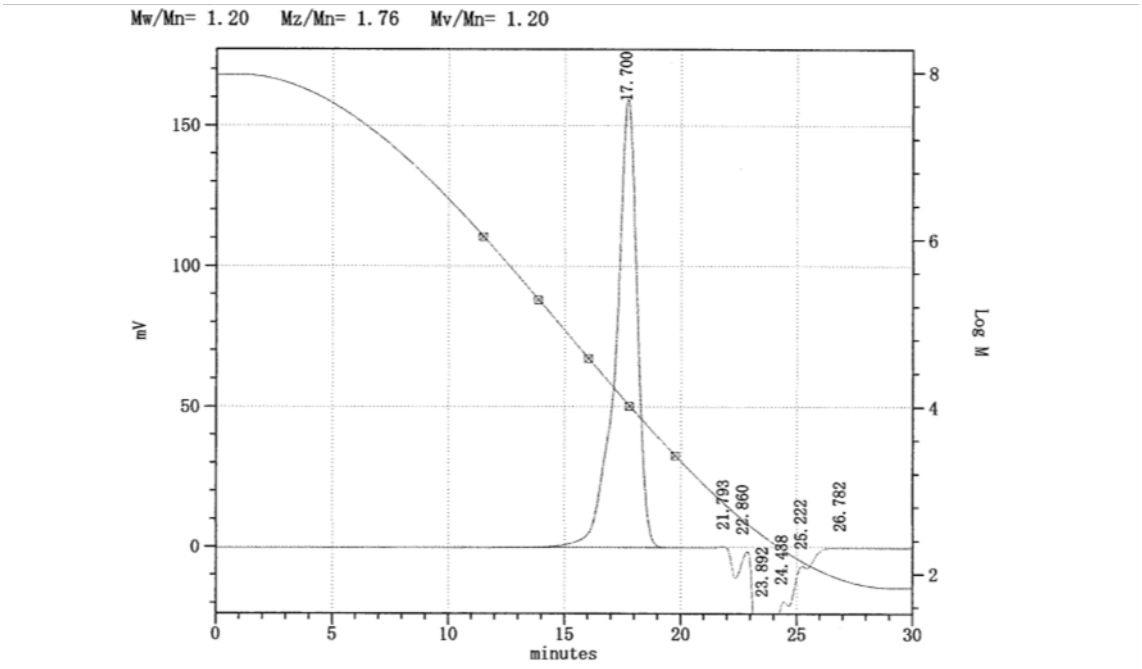

Figure S-1. *n*-BuLi Initiated Polymerization of Styrene in The Flow System (flow rate of *n*-BuLi (0.05 M) = 7.5 mL/min, flow rate of Styrene (2.0 M) = 15.0 mL/min, T-250-250 mixer, 30 degree-C)

Mn	= 11585
Mw	= 14105
Mz	= 20841
Mv	= 14105
I.V	= 14105

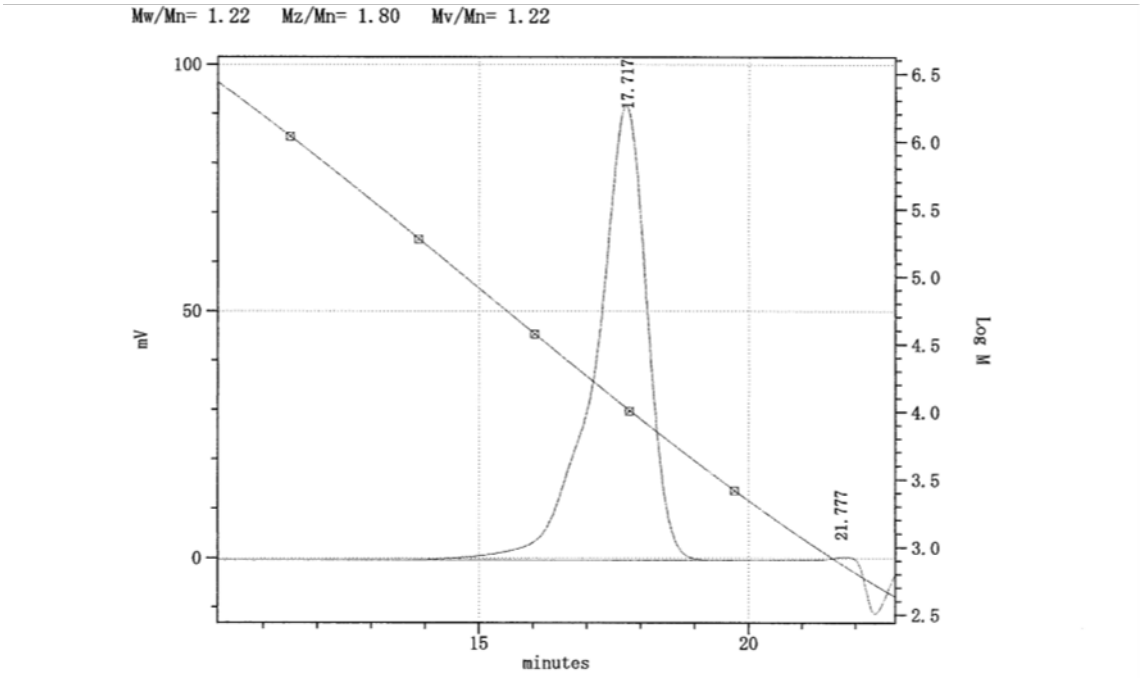

Figure S-2. *n*-BuLi Initiated Polymerization of Styrene in The Flow System (flow rate of *n*-BuLi (0.05 M) = 5.0

mL/min, flow rate of Styrene (2.0 M) = 10.0 mL/min, T-250-250 mixer, 30 degree-C)

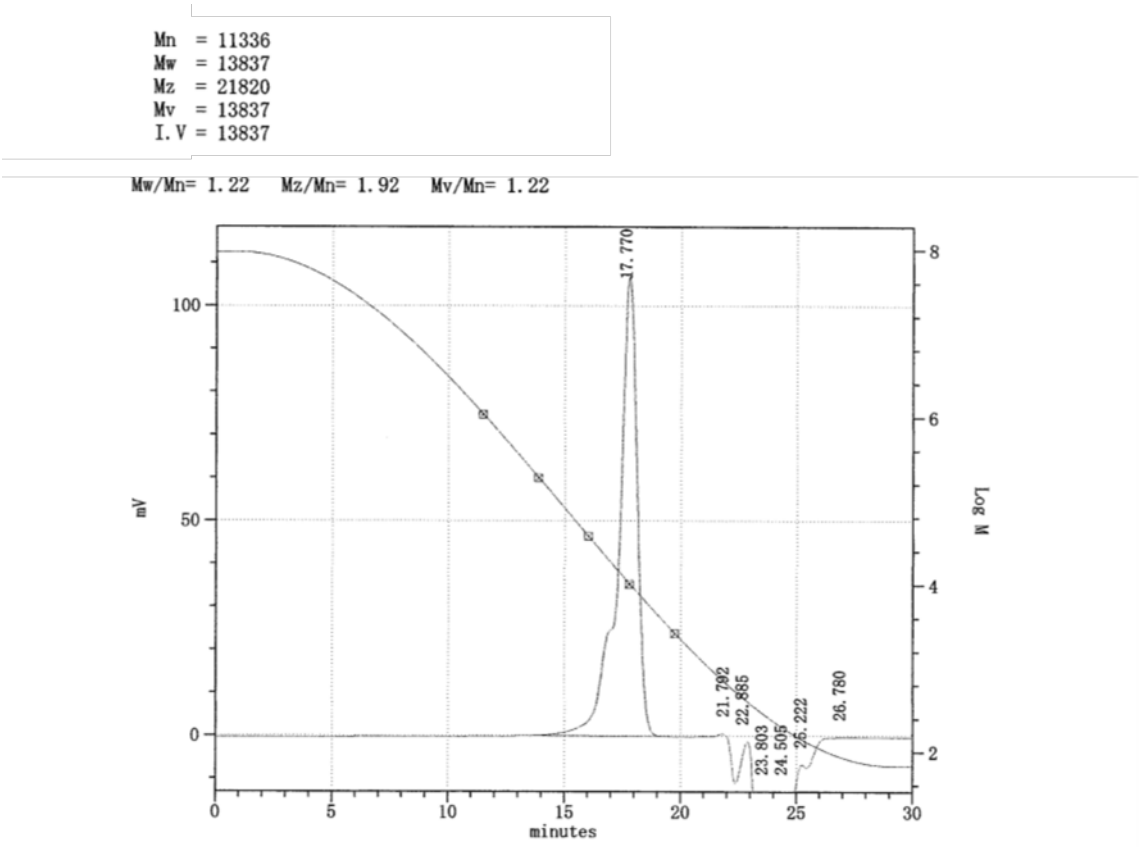

Figure S-3. *n*-BuLi Initiated Polymerization of Styrene in The Flow System (flow rate of *n*-BuLi (0.05 M) = 4.0 mL/min, flow rate of Styrene (2.0 M) = 8.0 mL/min, T-250-250 mixer, 30 degree-C)

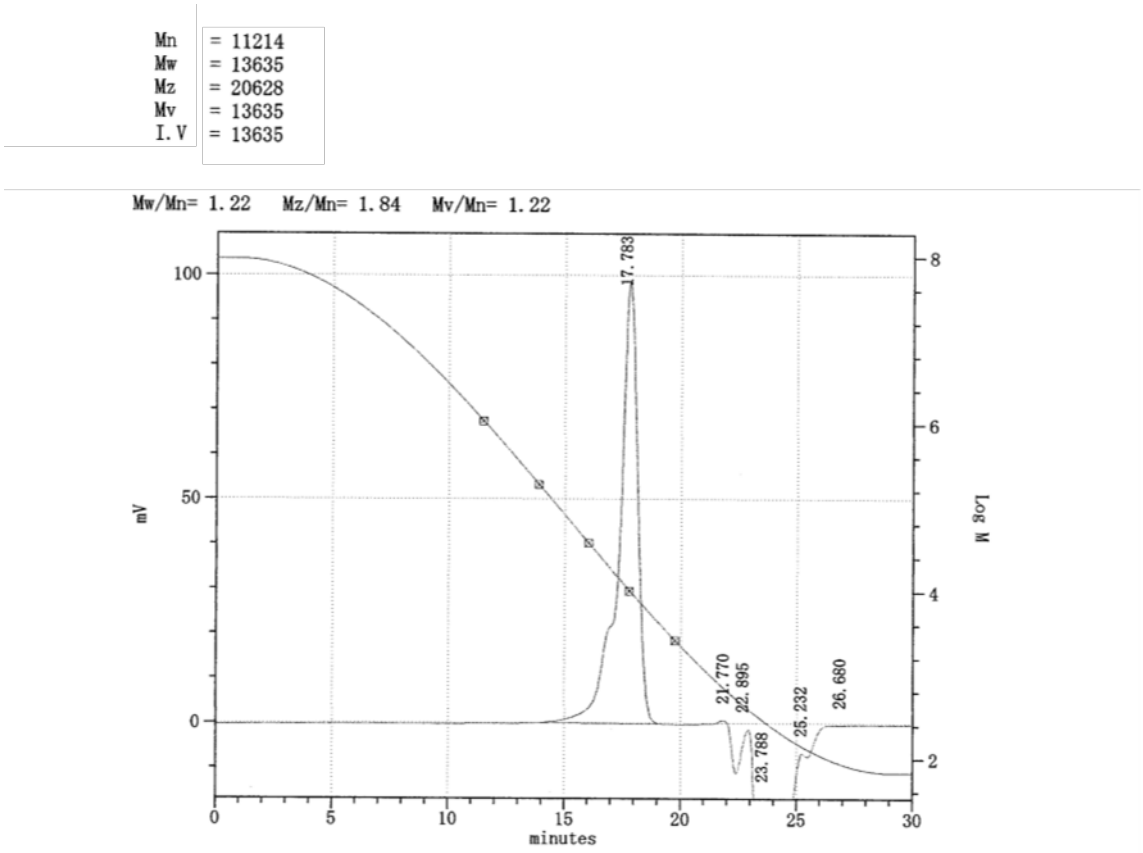

Figure S-4. *n*-BuLi Initiated Polymerization of Styrene in The Flow System (flow rate of *n*-BuLi (0.05 M) = 3.0 mL/min, flow rate of Styrene (2.0 M) = 6.0 mL/min, T-250-250 mixer, 30 degree-C)

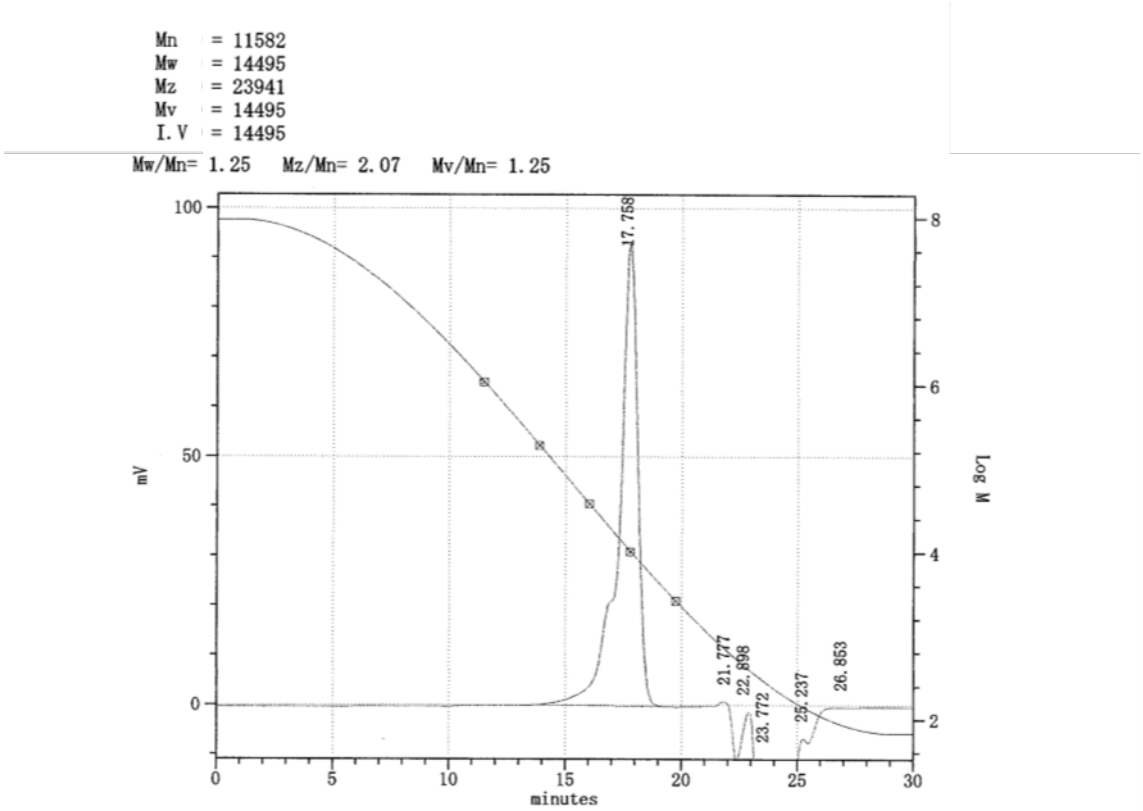

Figure S-5. *n*-BuLi Initiated Polymerization of Styrene in The Flow System (flow rate of *n*-BuLi (0.05 M) = 2.0 mL/min, flow rate of Styrene (2.0 M) = 4.0 mL/min, T-250-250 mixer, 30 degree-C)

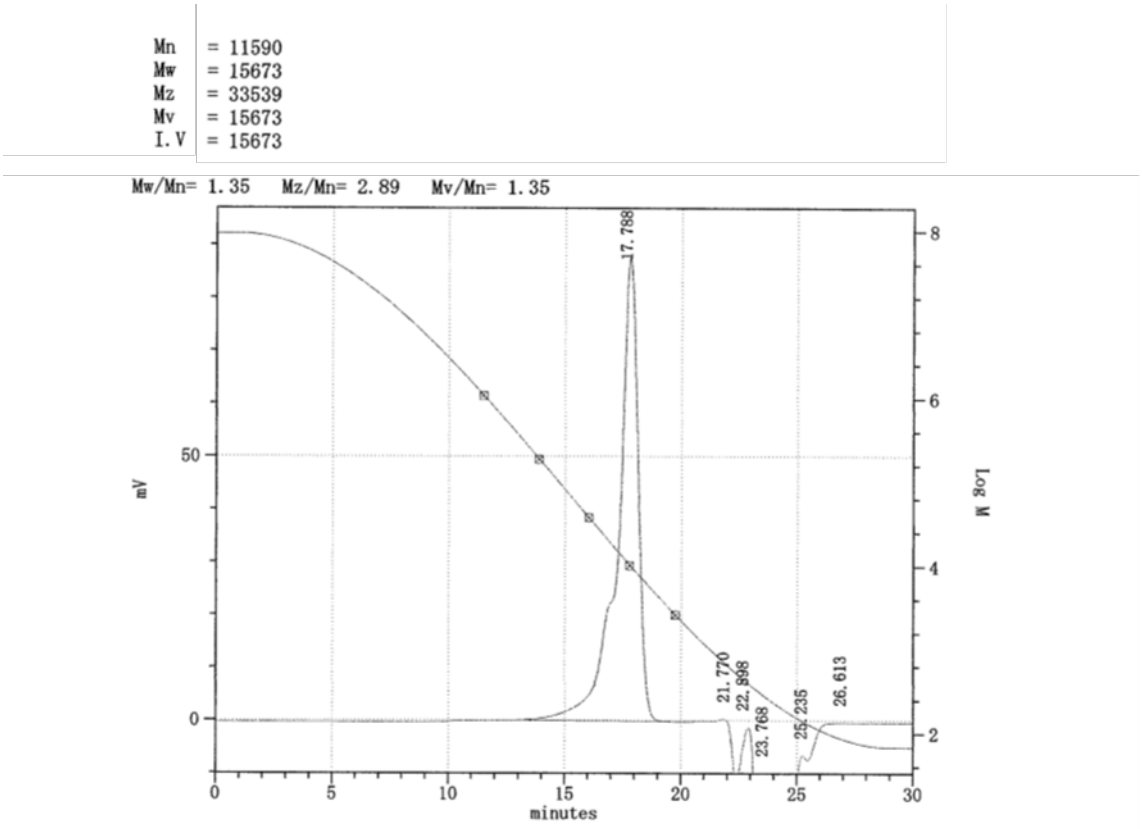

Figure S-6. *n*-BuLi Initiated Polymerization of Styrene in The Flow System (flow rate of *n*-BuLi (0.05 M) = 1.0 mL/min, flow rate of Styrene (2.0 M) = 2.0 mL/min, T-250-250 mixer, 30 degree-C)

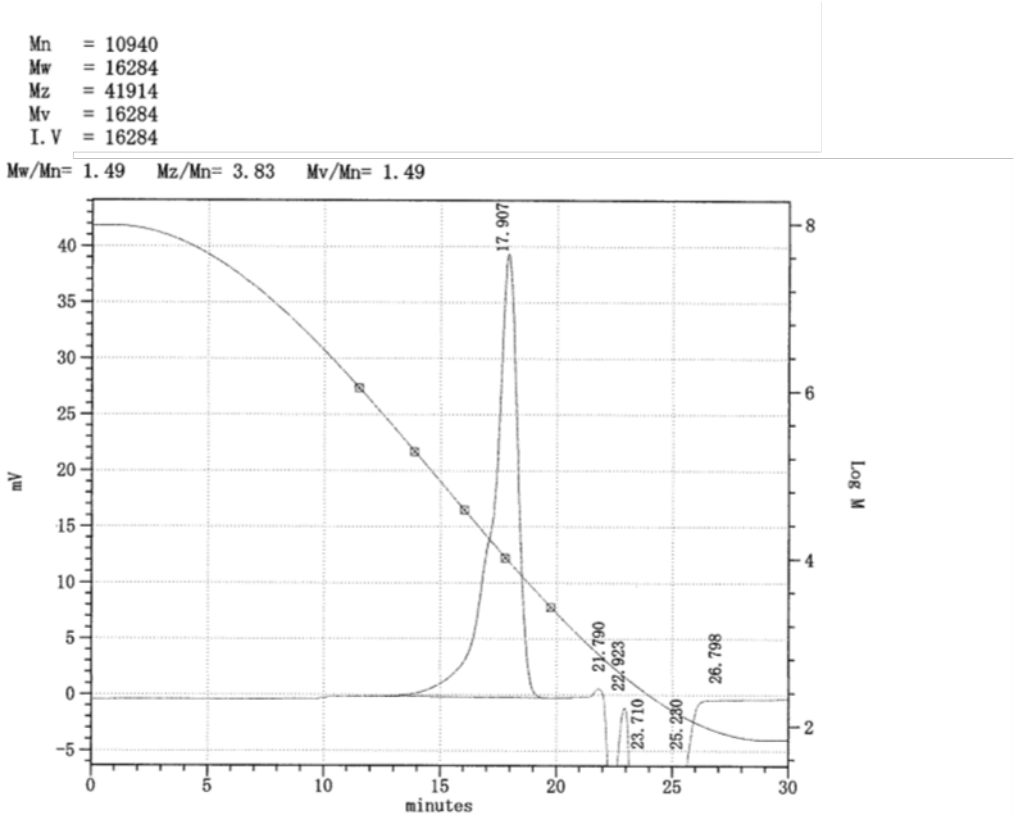

Figure S-7. *n*-BuLi Initiated Polymerization of Styrene in The Flow System (flow rate of *n*-BuLi (0.05 M) = 0.5 mL/min, flow rate of Styrene (2.0 M) = 1.0 mL/min, T-250-250 mixer, 30 degree-C)

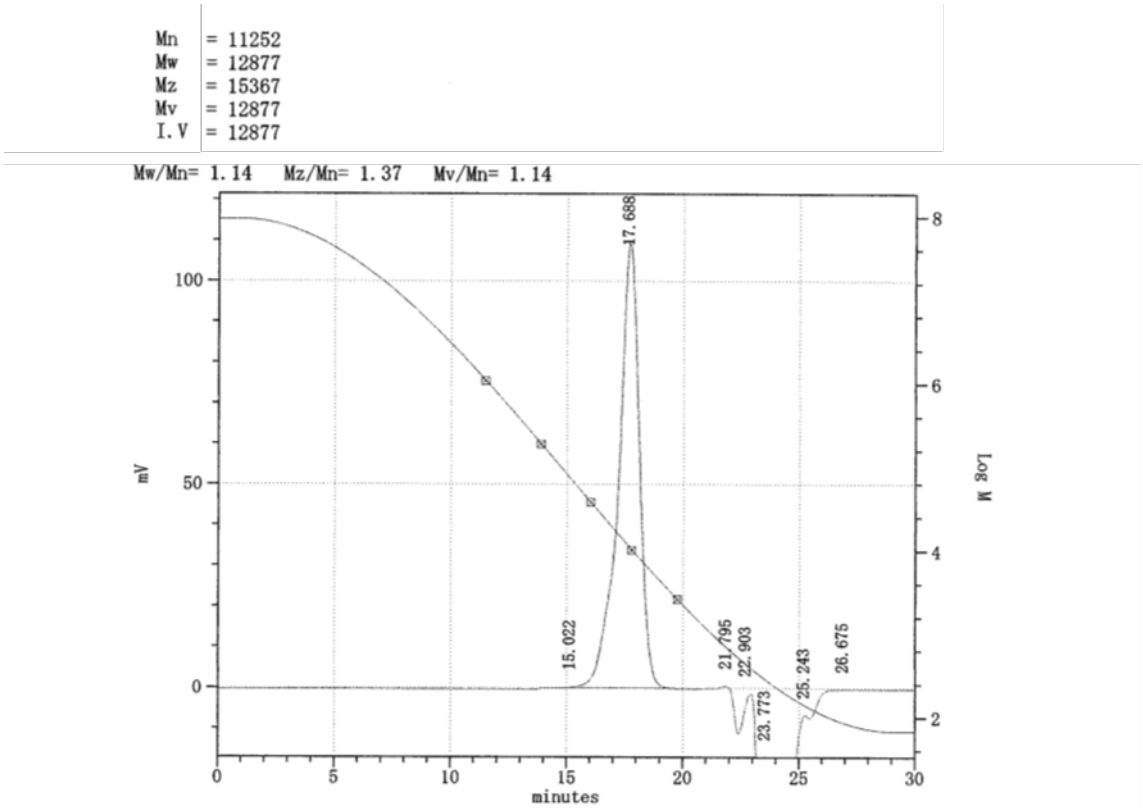

Figure S-8. *n*-BuLi Initiated Polymerization of Styrene in The Flow System (flow rate of *n*-BuLi (0.05 M) = 7.5 mL/min, flow rate of Styrene (2.0 M) = 15.0 mL/min, T-250-250 mixer, 0 degree-C)

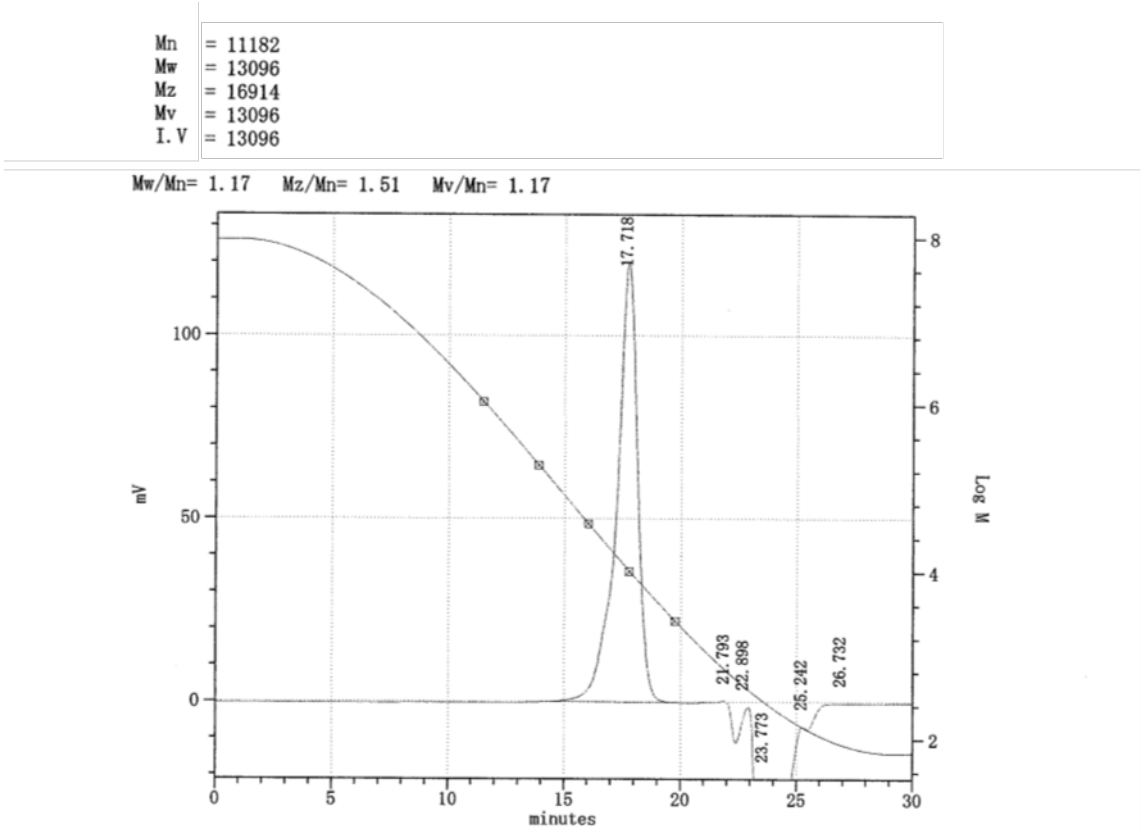

Figure S-9. *n*-BuLi Initiated Polymerization of Styrene in The Flow System (flow rate of *n*-BuLi (0.05 M) = 5.0 mL/min, flow rate of Styrene (2.0 M) = 10.0 mL/min, T-250-250 mixer, 0 degree-C)

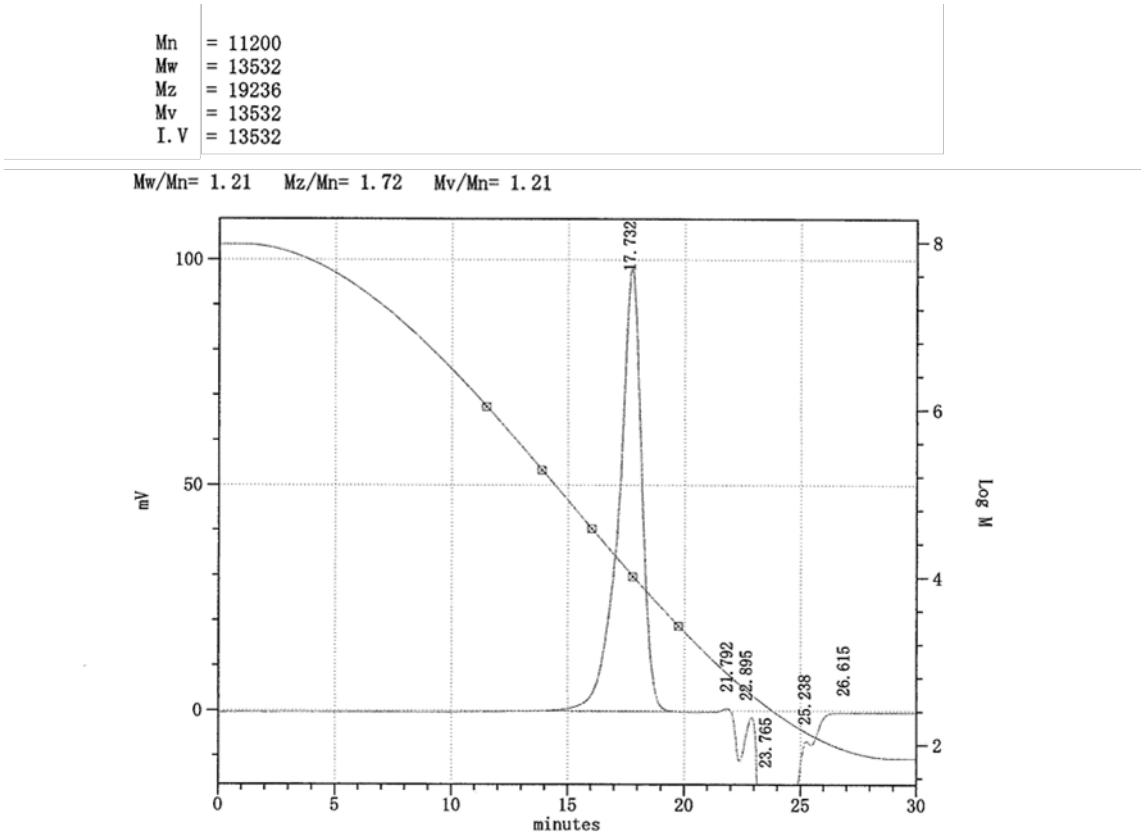

Figure S-10. *n*-BuLi Initiated Polymerization of Styrene in The Flow System (flow rate of *n*-BuLi (0.05 M) = 4.0 mL/min, flow rate of Styrene (2.0 M) = 8.0 mL/min, T-250-250 mixer, 0 degree-C)

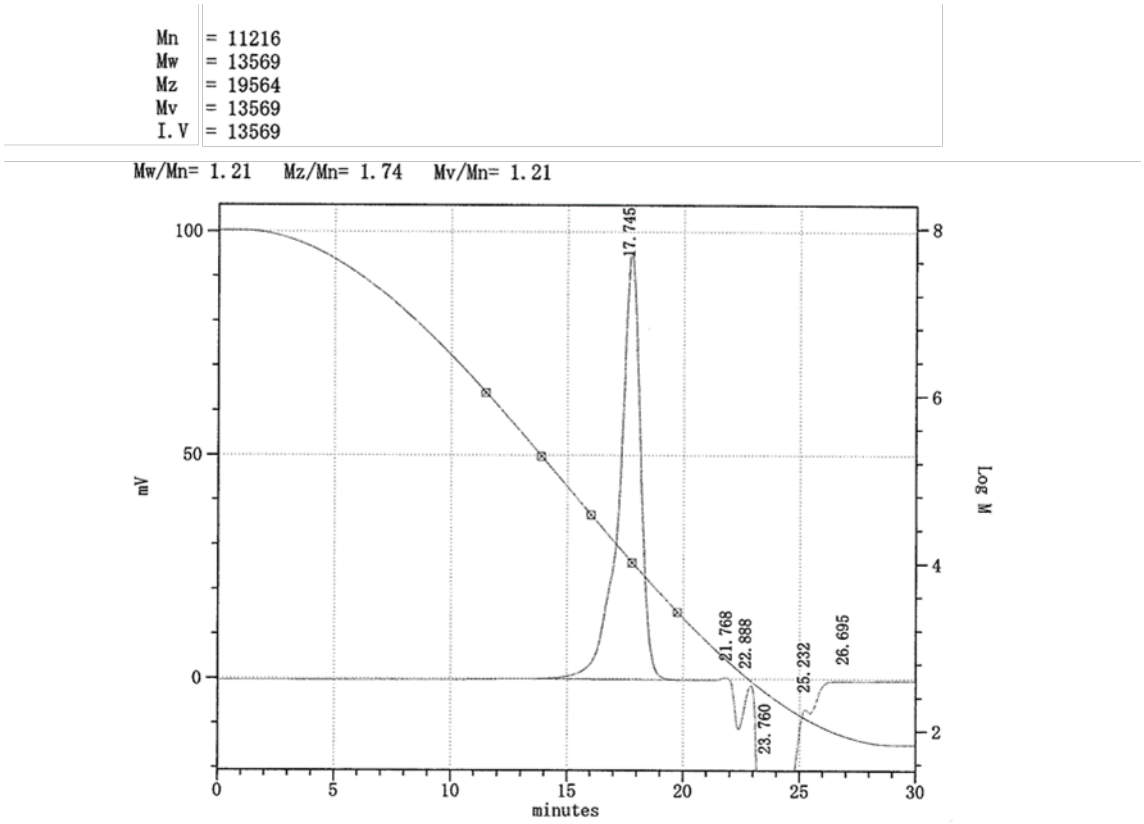

Figure S-11. *n*-BuLi Initiated Polymerization of Styrene in The Flow System (flow rate of *n*-BuLi (0.05 M) = 3.0 mL/min, flow rate of Styrene (2.0 M) = 6.0 mL/min, T-250-250 mixer, 0 degree-C)

Mn = 11239
Mw = 14218
Mz = 22783
Mv = 14218
I.V = 14218

Mw/Mn= 1.27 Mz/Mn= 2.03 Mv/Mn= 1.27

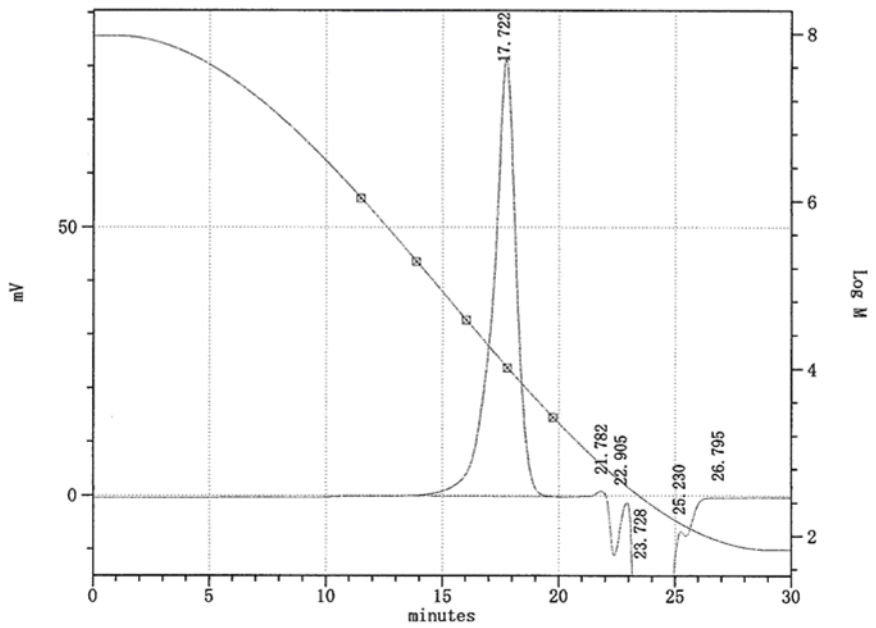

Figure S-12. *n*-BuLi Initiated Polymerization of Styrene in The Flow System (flow rate of *n*-BuLi (0.05 M) = 2.0 mL/min, flow rate of Styrene (2.0 M) = 4.0 mL/min, T-250-250 mixer, 0 degree-C)

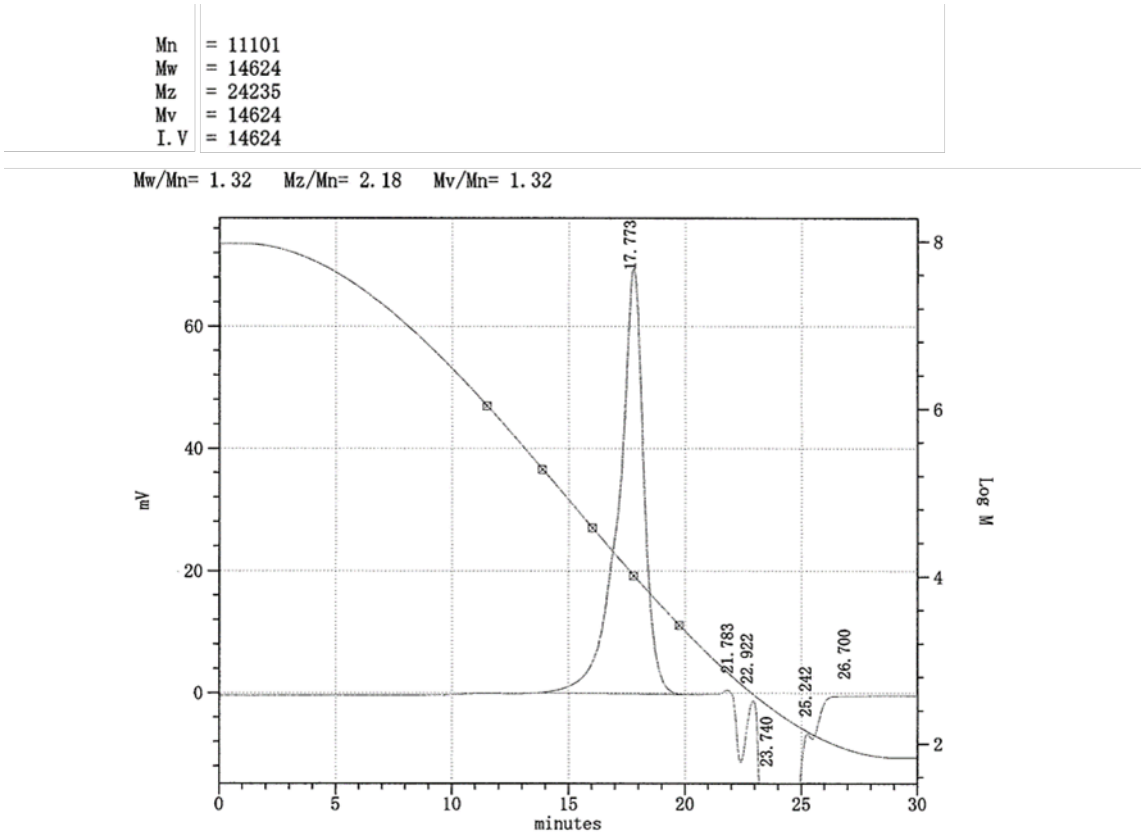

Figure S-13. *n*-BuLi Initiated Polymerization of Styrene in The Flow System (flow rate of *n*-BuLi (0.05 M) = 1.0 mL/min, flow rate of Styrene (2.0 M) = 2.0 mL/min, T-250-250 mixer, 0 degree-C)

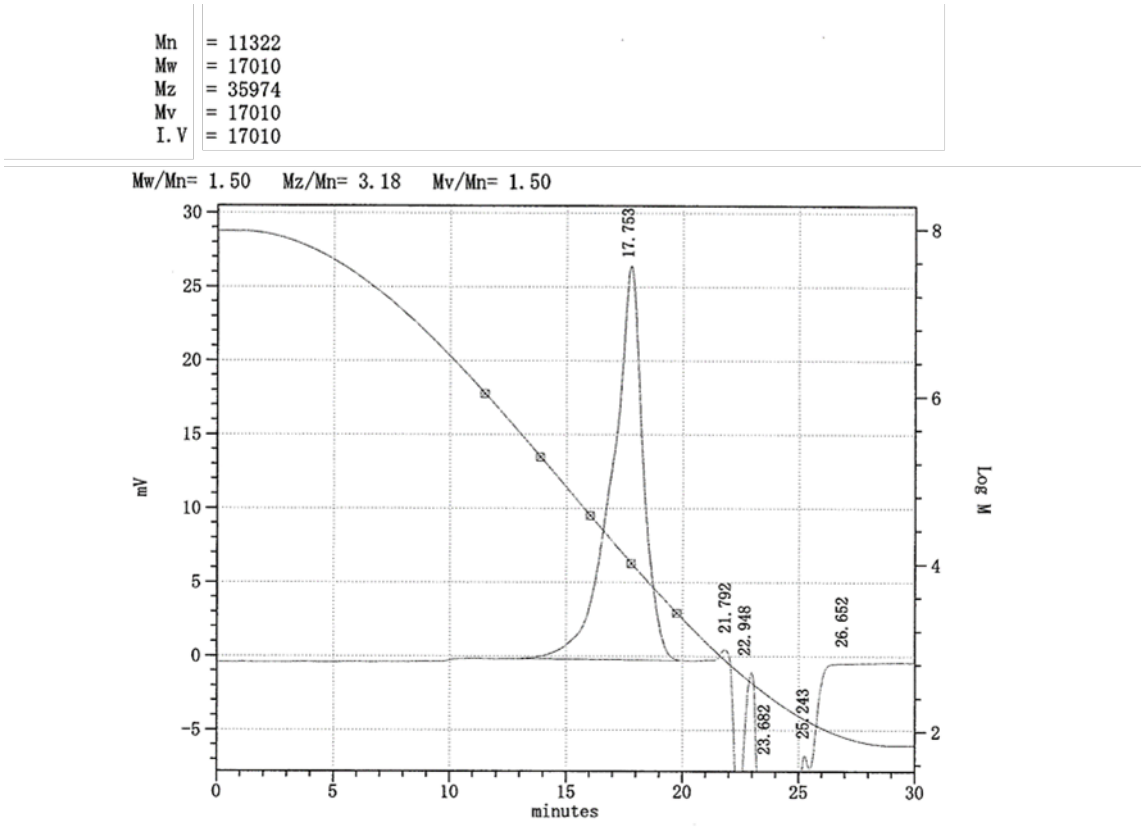

Figure S-14. *n*-BuLi Initiated Polymerization of Styrene in The Flow System (flow rate of *n*-BuLi (0.05 M) = 0.5 mL/min, flow rate of Styrene (2.0 M) = 1.0 mL/min, T-250-250 mixer, 0 degree-C)

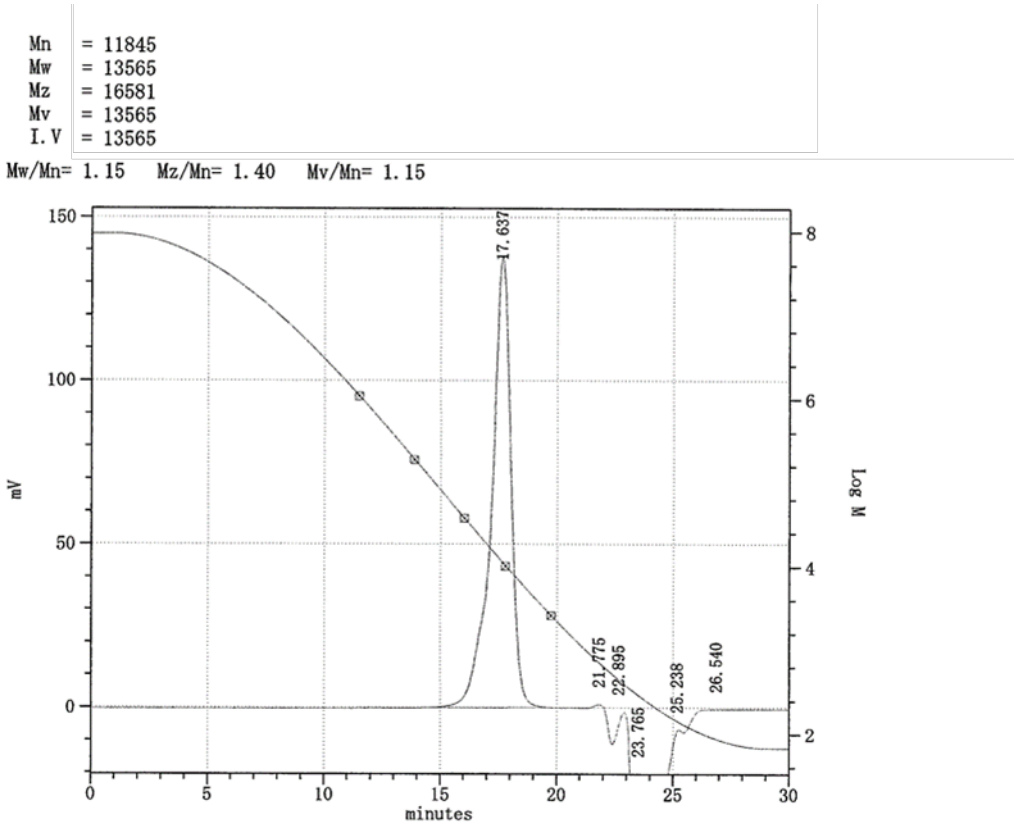

Figure S-15. *n*-BuLi Initiated Polymerization of Styrene in The Flow System (flow rate of *n*-BuLi (0.05 M) = 7.5 mL/min, flow rate of Styrene (2.0 M) = 15.0 mL/min, T-250-250 mixer, -20 degree-C)

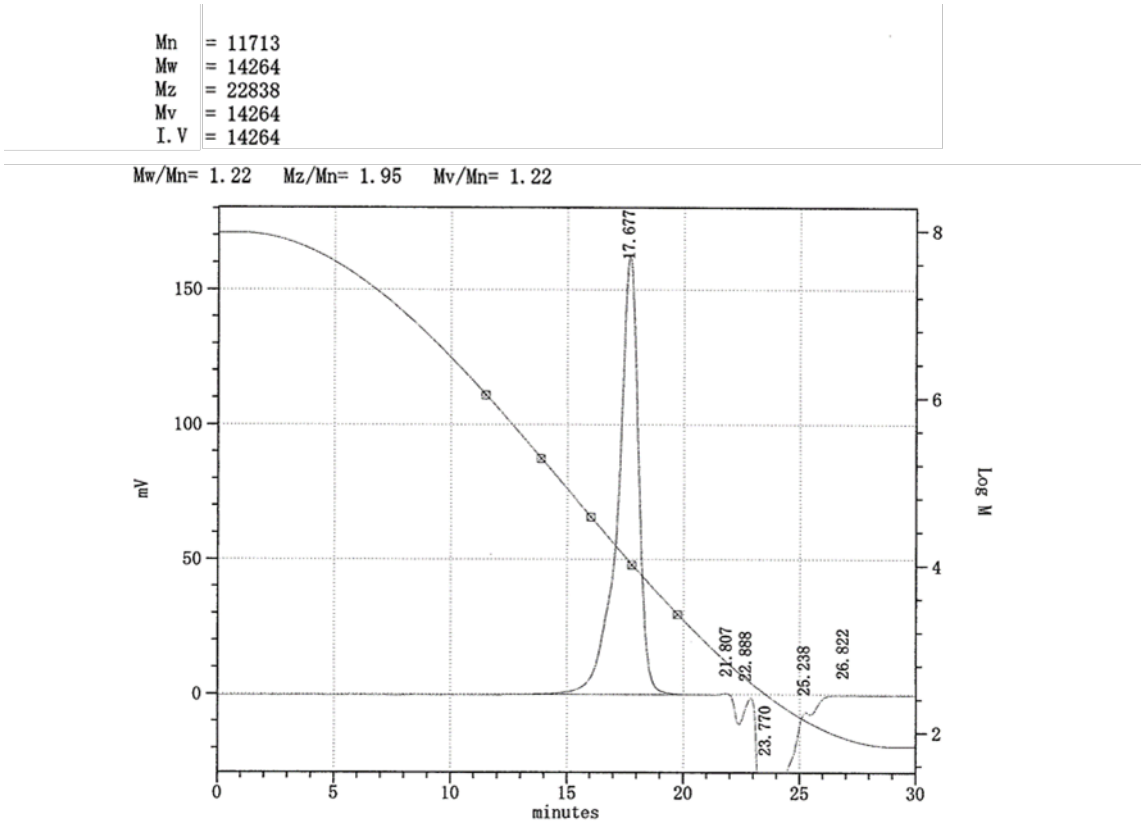

Figure S-16. *n*-BuLi Initiated Polymerization of Styrene in The Flow System (flow rate of *n*-BuLi (0.05 M) = 5.0 mL/min, flow rate of Styrene (2.0 M) = 10.0 mL/min, T-250-250 mixer, -20 degree-C)

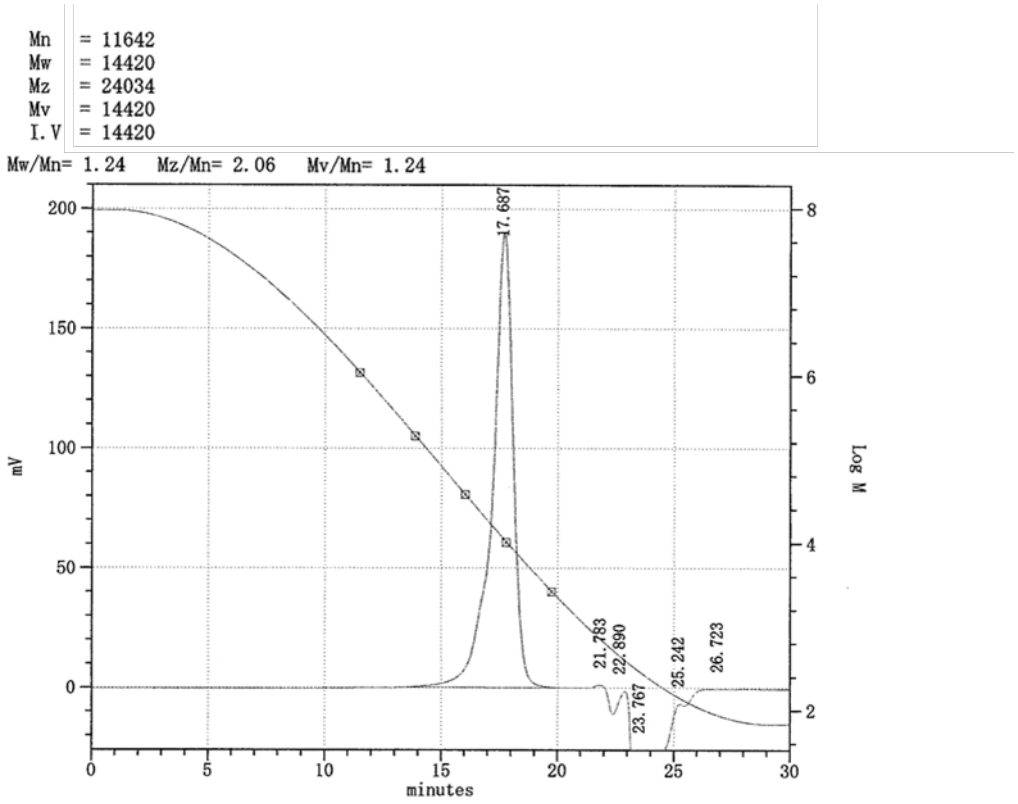

Figure S-17. *n*-BuLi Initiated Polymerization of Styrene in The Flow System (flow rate of *n*-BuLi (0.05 M) = 4.0 mL/min, flow rate of Styrene (2.0 M) = 8.0 mL/min, T-250-250 mixer, -20 degree-C)

Mn	= 11761
Mw	= 15544
Mz	= 37057
Mv	= 15544
I.V	= 15544

Mw/Mn= 1.32 Mz/Mn= 3.15 Mv/Mn= 1.32

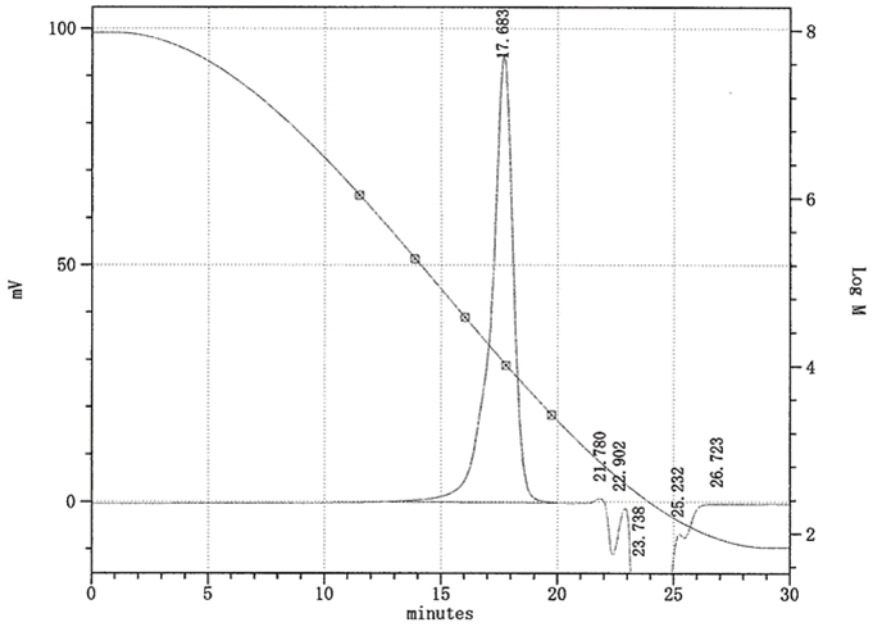

Figure S-18. *n*-BuLi Initiated Polymerization of Styrene in The Flow System (flow rate of *n*-BuLi (0.05 M) = 3.0 mL/min, flow rate of Styrene (2.0 M) = 6.0 mL/min, T-250-250 mixer, -20 degree-C)

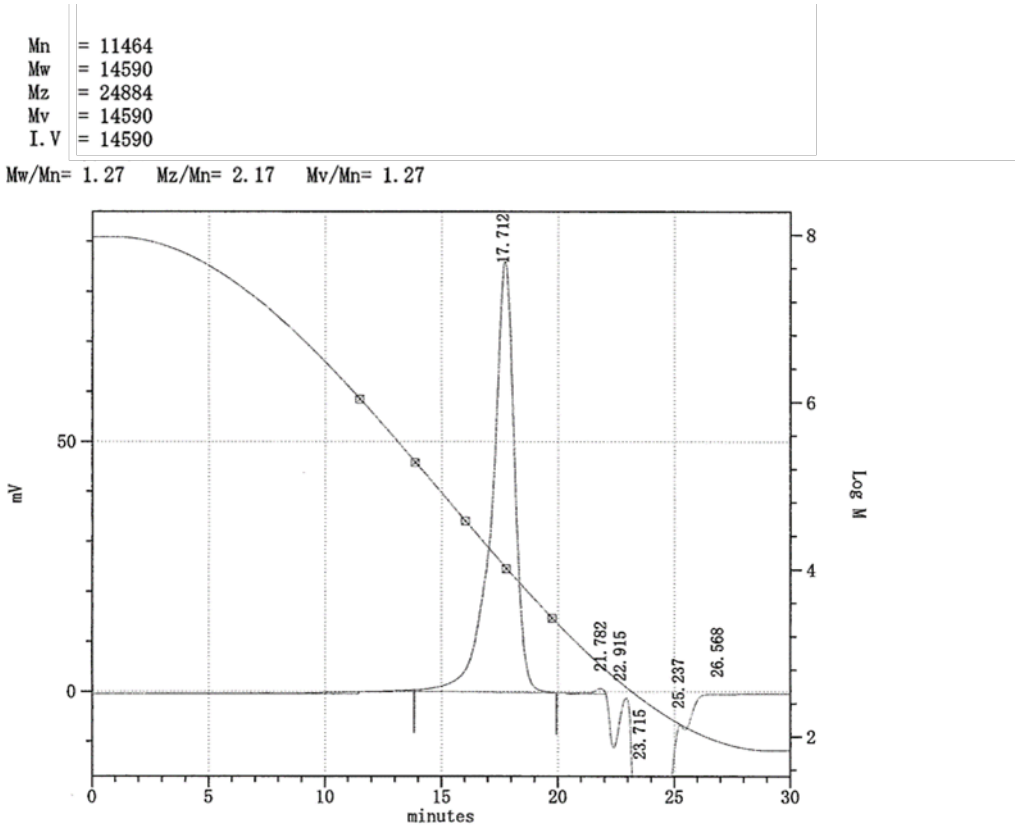

Figure S-19. *n*-BuLi Initiated Polymerization of Styrene in The Flow System (flow rate of *n*-BuLi (0.05 M) = 2.0 mL/min, flow rate of Styrene (2.0 M) = 4.0 mL/min, T-250-250 mixer, -20 degree-C)

Mn	= 11308
Mw	= 15585
Mz	= 29801
Mv	= 15585
I.V	= 15585

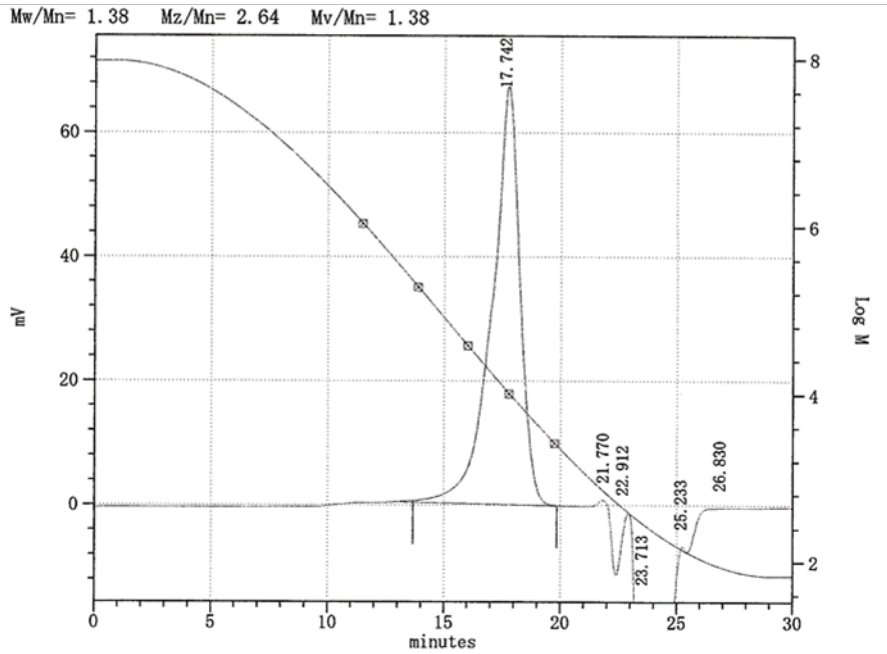

Figure S-20. *n*-BuLi Initiated Polymerization of Styrene in The Flow System (flow rate of *n*-BuLi (0.05 M) = 1.0 mL/min, flow rate of Styrene (2.0 M) = 2.0 mL/min, T-250-250 mixer, -20 degree-C)

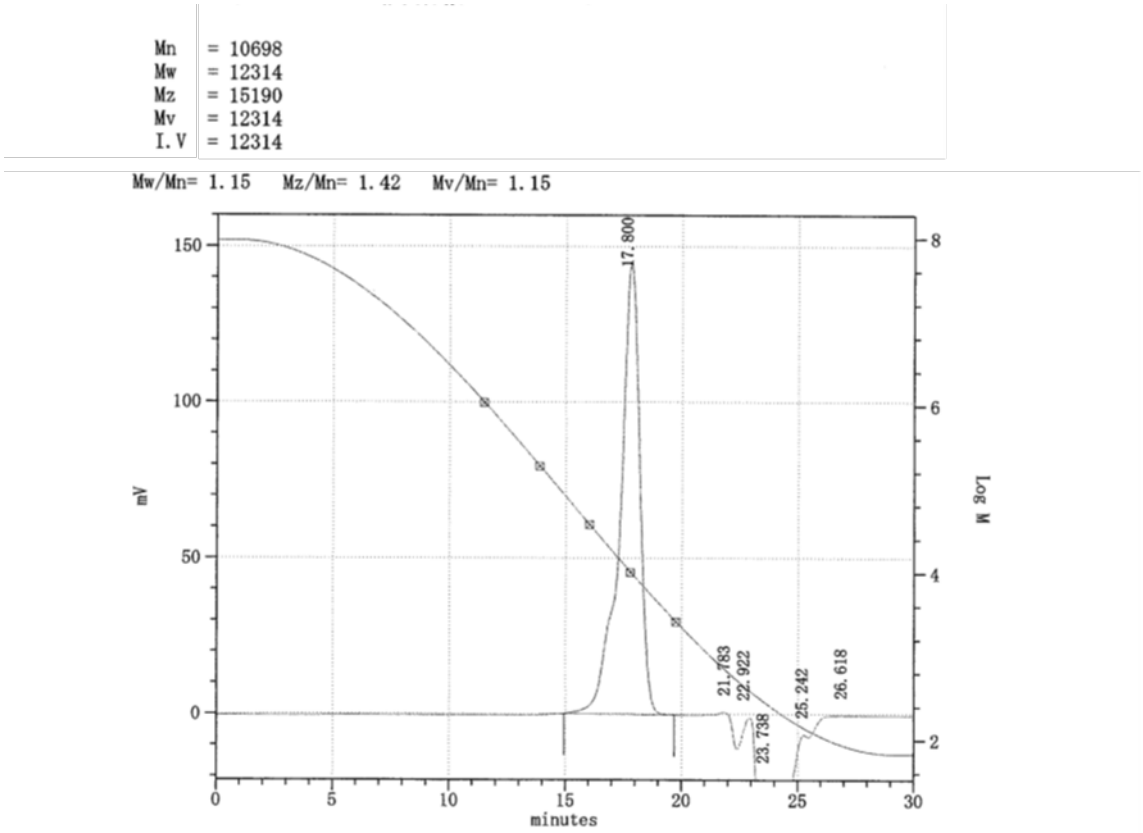

Figure S-21. *n*-BuLi Initiated Polymerization of Styrene in The Flow System (flow rate of *n*-BuLi (0.05 M) = 7.5 mL/min, flow rate of Styrene (2.0 M) = 15.0 mL/min, T-500-500 mixer, 30 degree-C)

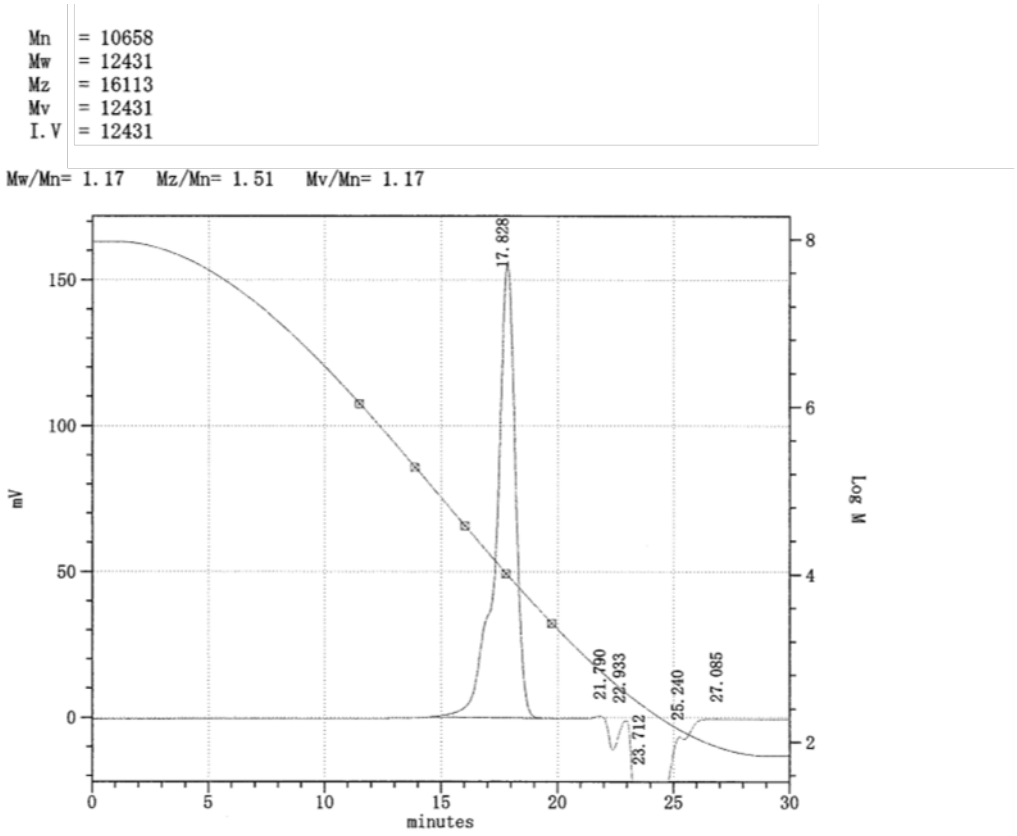

Figure S-22. *n*-BuLi Initiated Polymerization of Styrene in The Flow System (flow rate of *n*-BuLi (0.05 M) = 5.0 mL/min, flow rate of Styrene (2.0 M) = 10.0 mL/min, T-500-500 mixer, 30 degree-C)

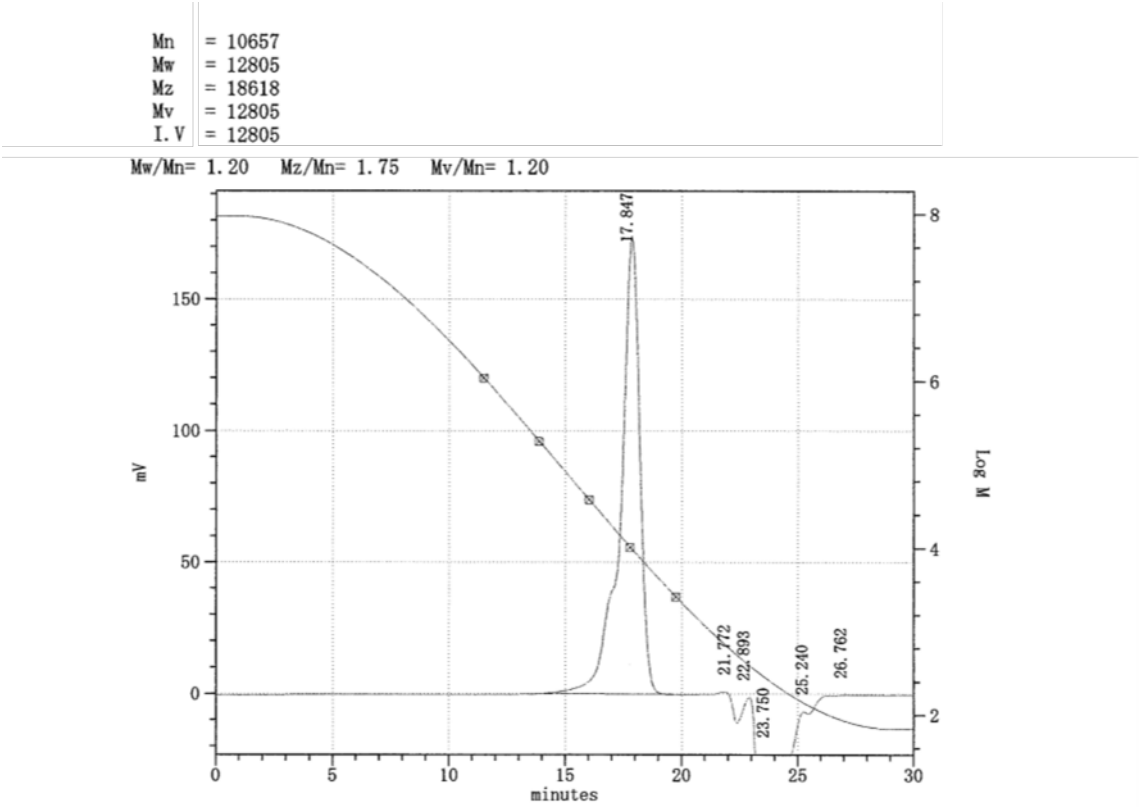

Figure S-23. *n*-BuLi Initiated Polymerization of Styrene in The Flow System (flow rate of *n*-BuLi (0.05 M) = 4.0 mL/min, flow rate of Styrene (2.0 M) = 8.0 mL/min, T-500-500 mixer, 30 degree-C)

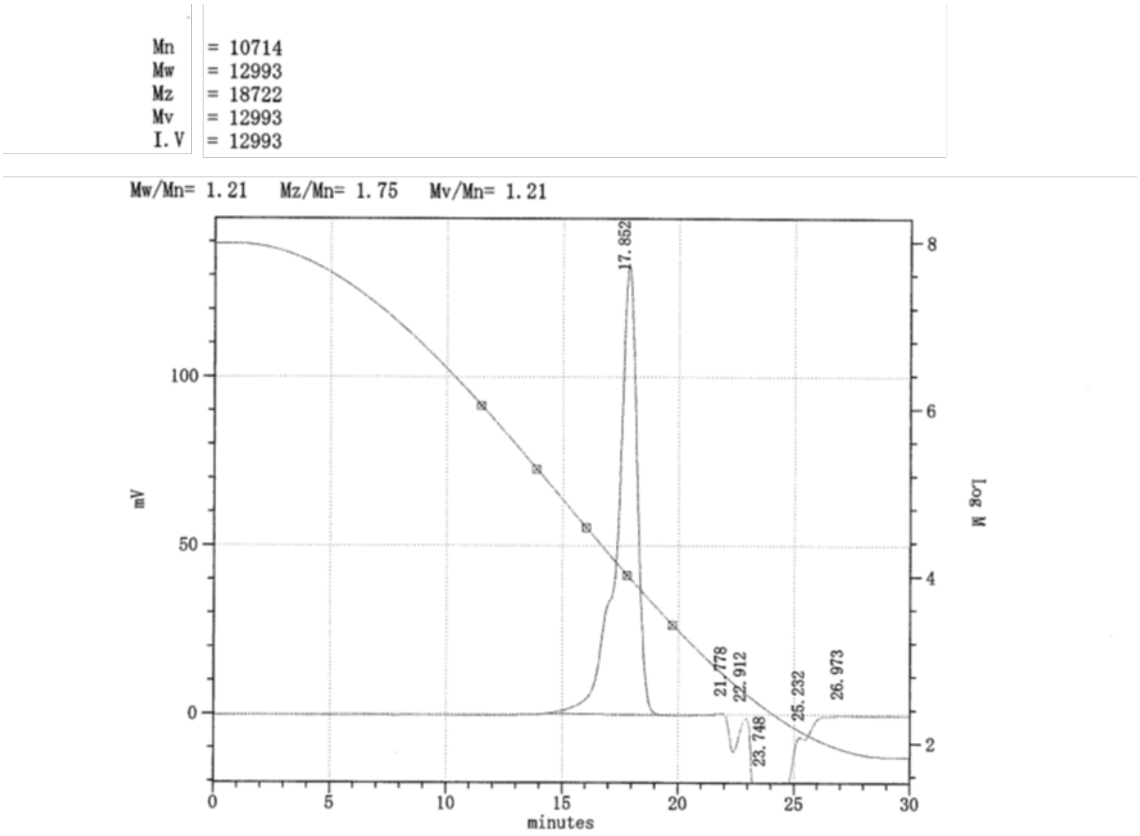

Figure S-24. *n*-BuLi Initiated Polymerization of Styrene in The Flow System (flow rate of *n*-BuLi (0.05 M) = 3.0 mL/min, flow rate of Styrene (2.0 M) = 6.0 mL/min, T-500-500 mixer, 30 degree-C)

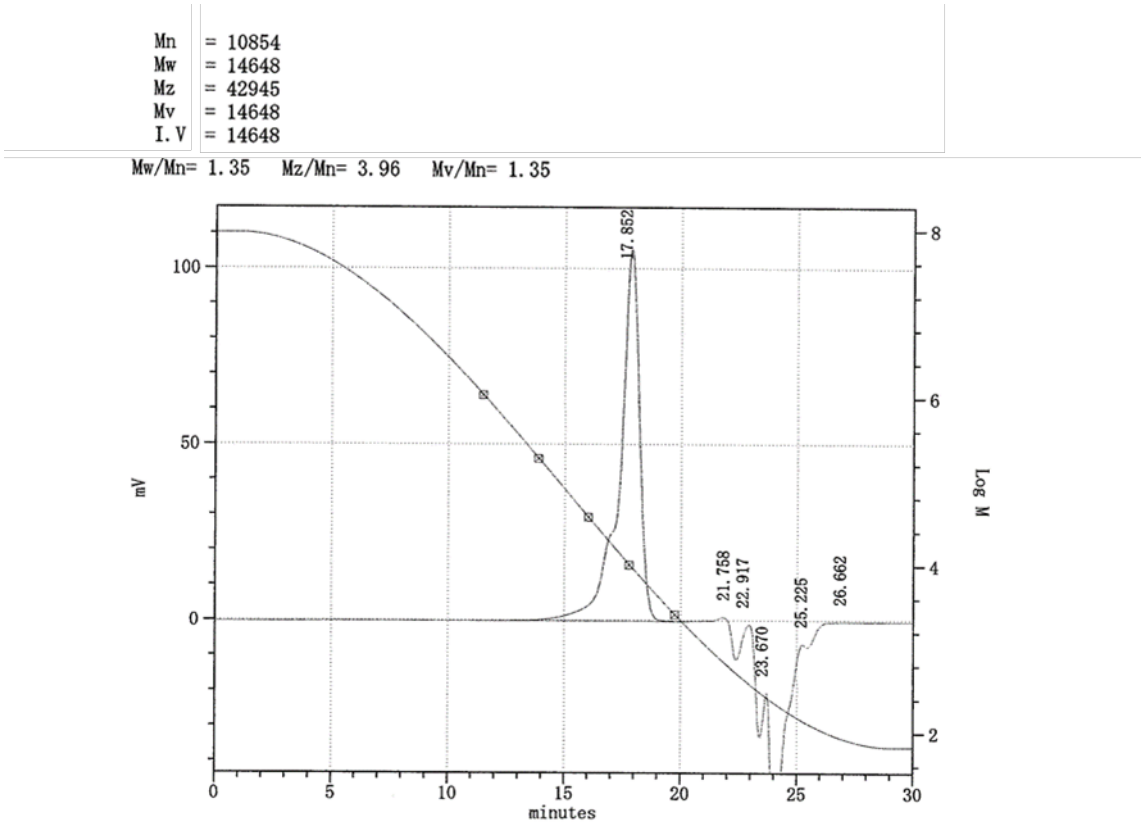

Figure S-25. *n*-BuLi Initiated Polymerization of Styrene in The Flow System (flow rate of *n*-BuLi (0.05 M) = 2.0 mL/min, flow rate of Styrene (2.0 M) = 4.0 mL/min, T-500-500 mixer, 30 degree-C)

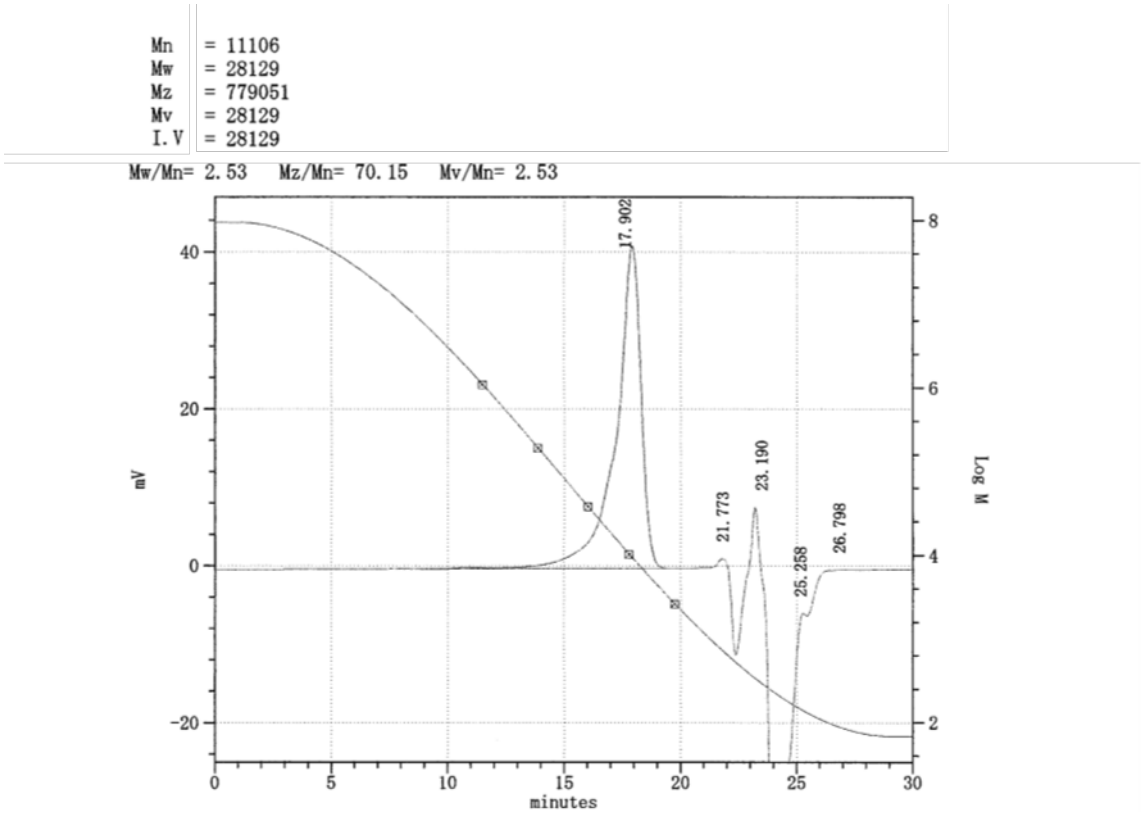

Figure S-26. *n*-BuLi Initiated Polymerization of Styrene in The Flow System (flow rate of *n*-BuLi (0.05 M) = 0.5 mL/min, flow rate of Styrene (2.0 M) = 1.0 mL/min, T-500-500 mixer, 30 degree-C)

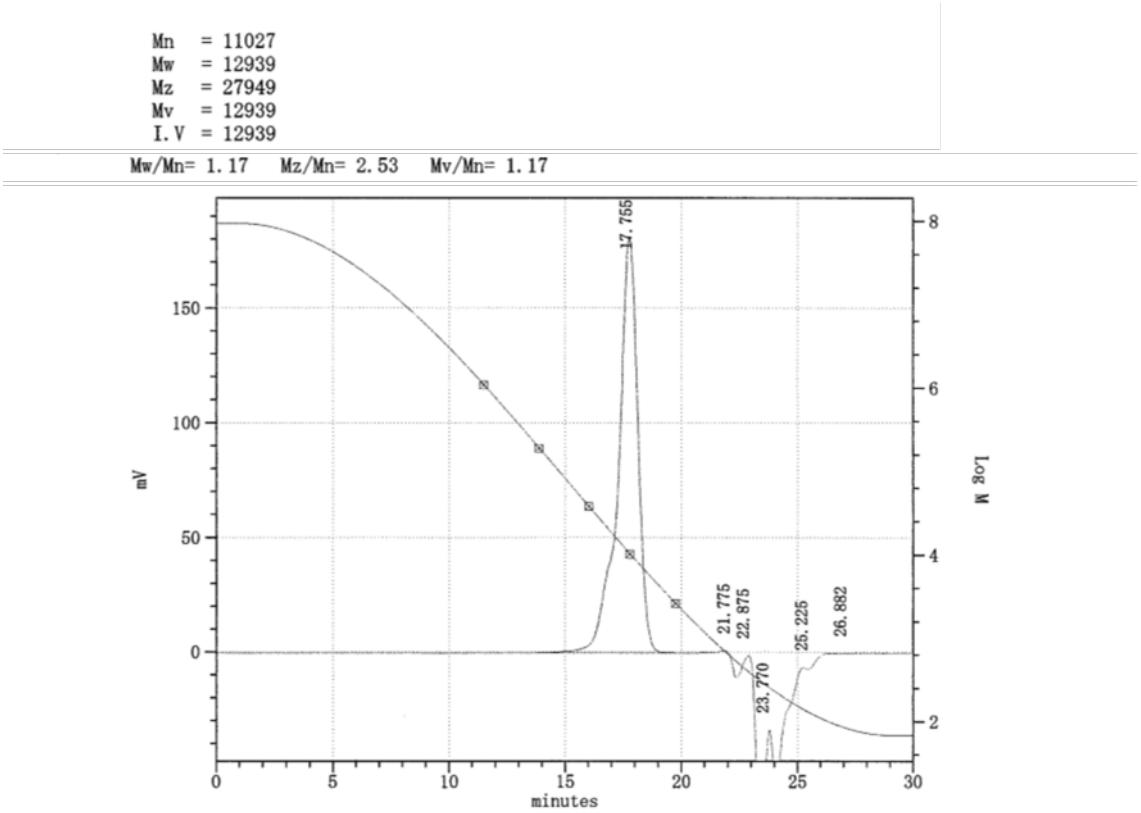

Figure S-27. *n*-BuLi Initiated Polymerization of Styrene in The Flow System (flow rate of *n*-BuLi (0.05 M) = 7.5 mL/min, flow rate of Styrene (2.0 M) = 15.0 mL/min, Y-250-250 mixer, 30 degree-C)

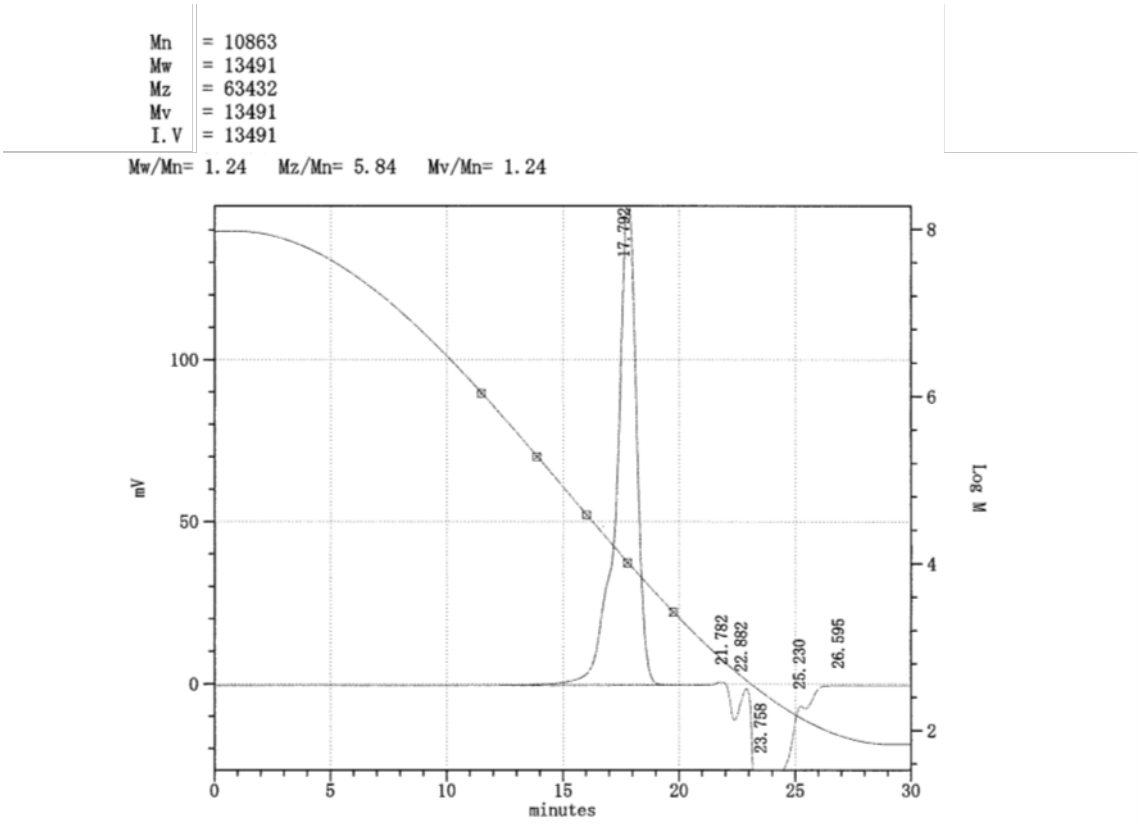

Figure S-28. *n*-BuLi Initiated Polymerization of Styrene in The Flow System (flow rate of *n*-BuLi (0.05 M) = 5.0 mL/min, flow rate of Styrene (2.0 M) = 10.0 mL/min, Y-250-250 mixer, 30 degree-C)

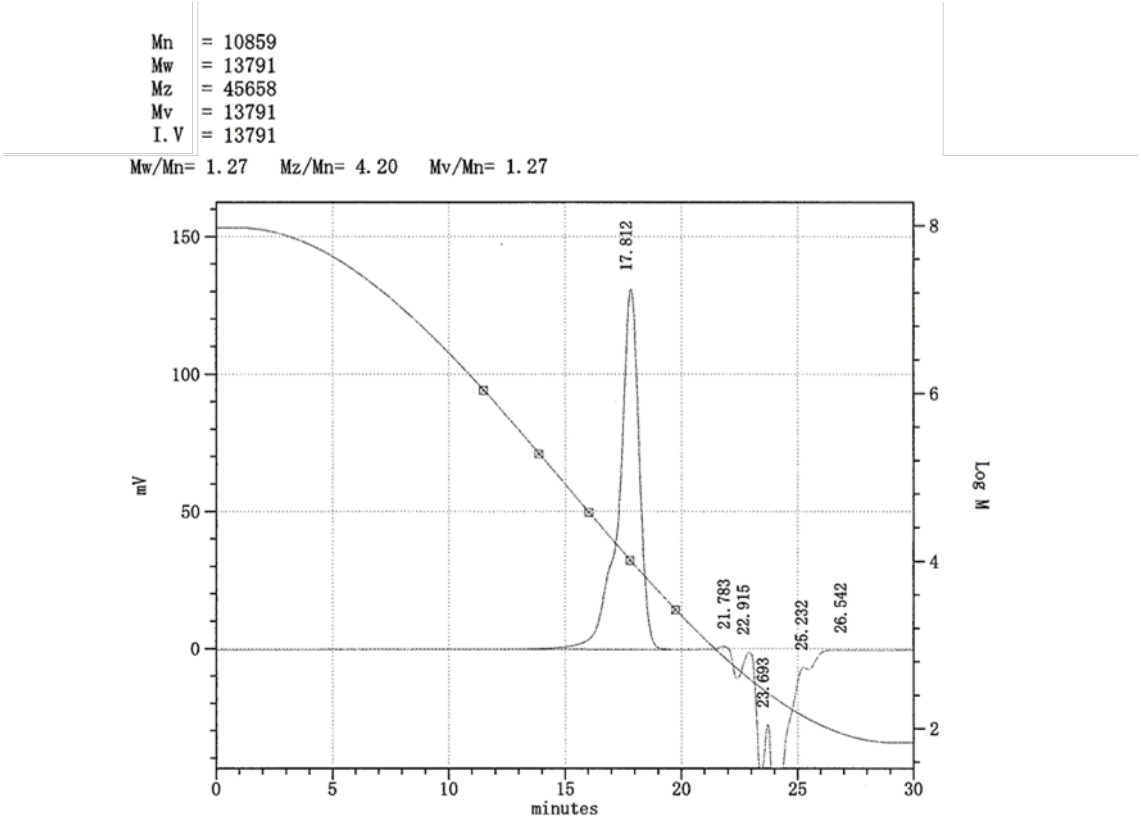

Figure S-29. *n*-BuLi Initiated Polymerization of Styrene in The Flow System (flow rate of *n*-BuLi (0.05 M) = 4.0 mL/min, flow rate of Styrene (2.0 M) = 8.0 mL/min, Y-250-250 mixer, 30 degree-C)

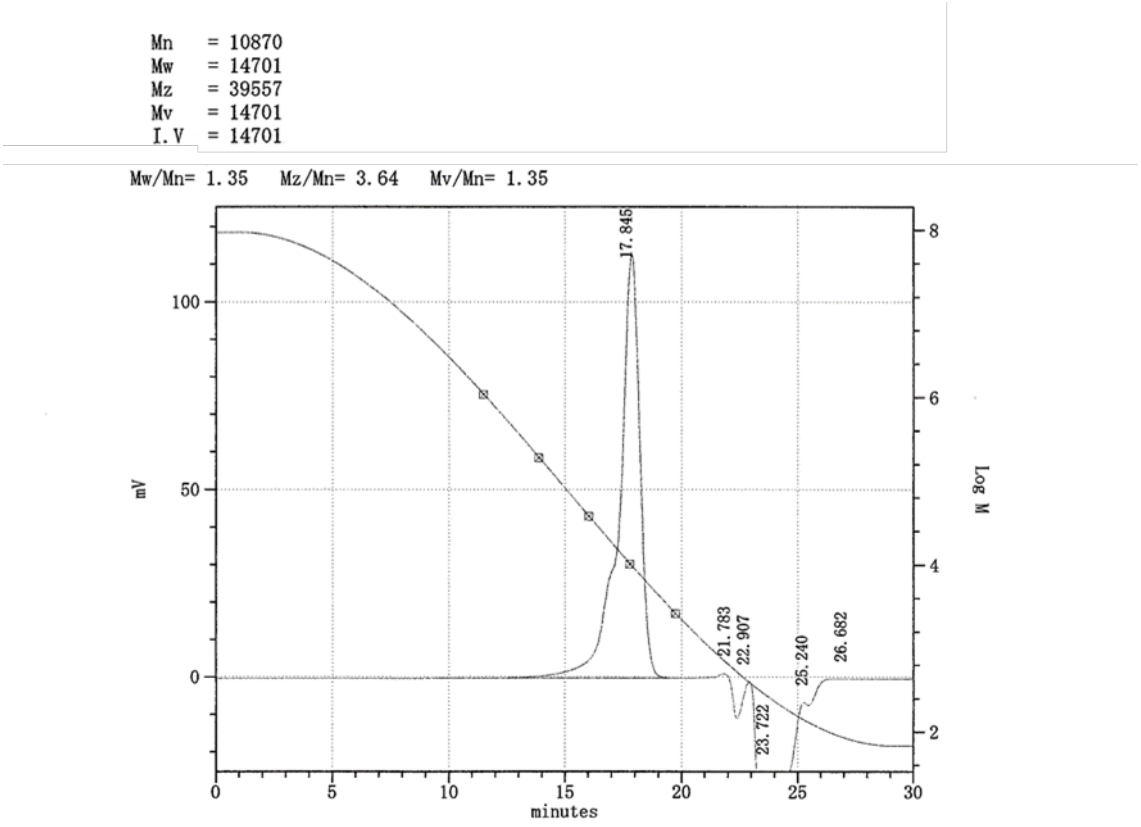

Figure S-30. *n*-BuLi Initiated Polymerization of Styrene in The Flow System (flow rate of *n*-BuLi (0.05 M) = 2.0 mL/min, flow rate of Styrene (2.0 M) = 4.0 mL/min, Y-250-250 mixer, 30 degree-C)

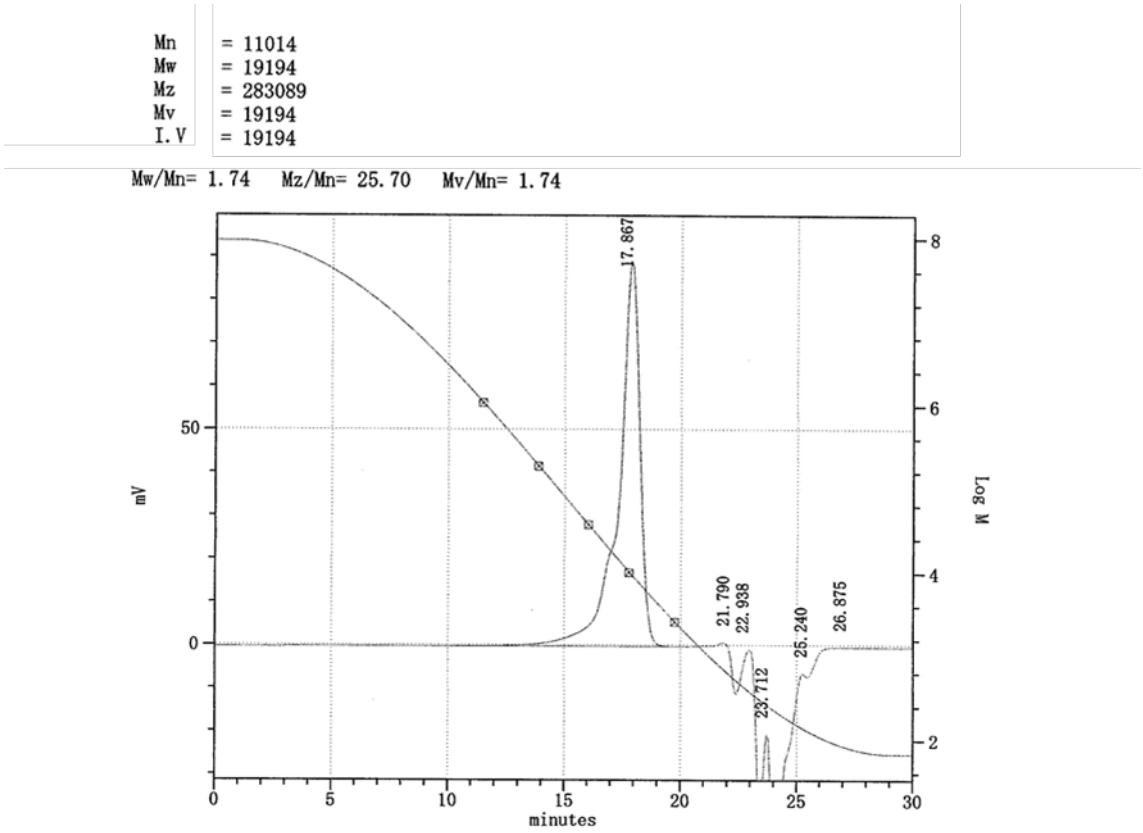

Figure S-31. *n*-BuLi Initiated Polymerization of Styrene in The Flow System (flow rate of *n*-BuLi (0.05 M) = 1.0 mL/min, flow rate of Styrene (2.0 M) = 2.0 mL/min, Y-250-250 mixer, 30 degree-C)

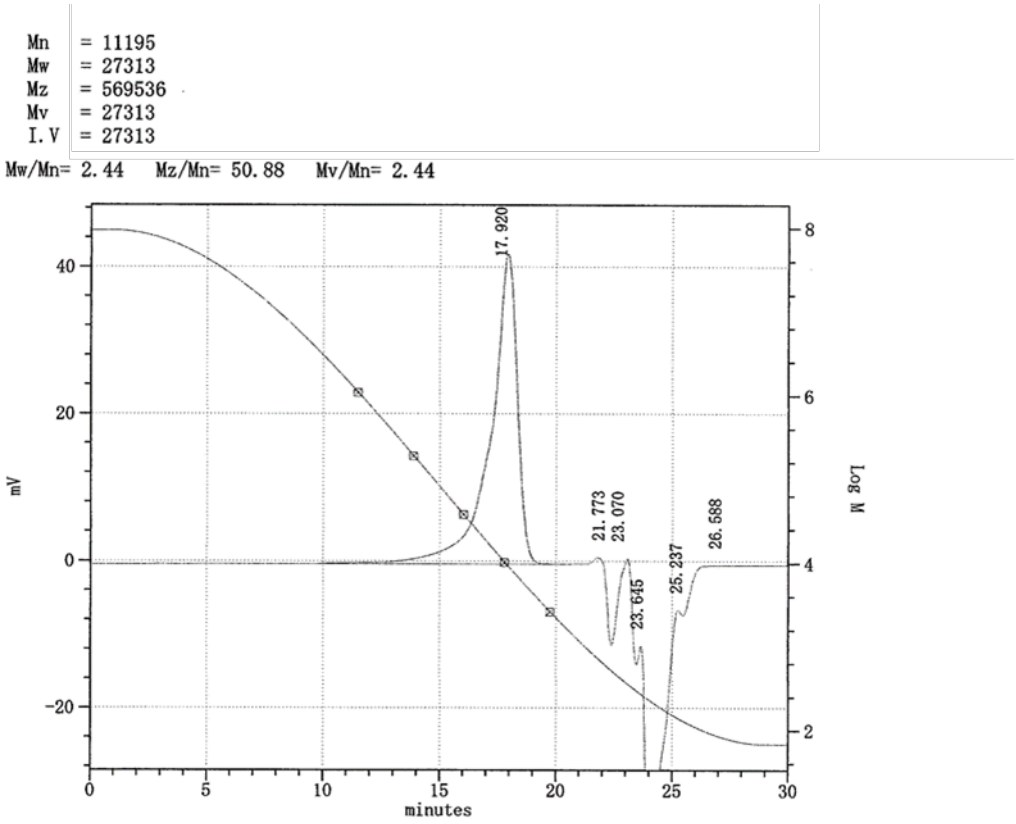

Figure S-32. *n*-BuLi Initiated Polymerization of Styrene in The Flow System (flow rate of *n*-BuLi (0.05 M) = 0.5 mL/min, flow rate of Styrene (2.0 M) = 1.0 mL/min, Y-250-250 mixer, 30 degree-C)

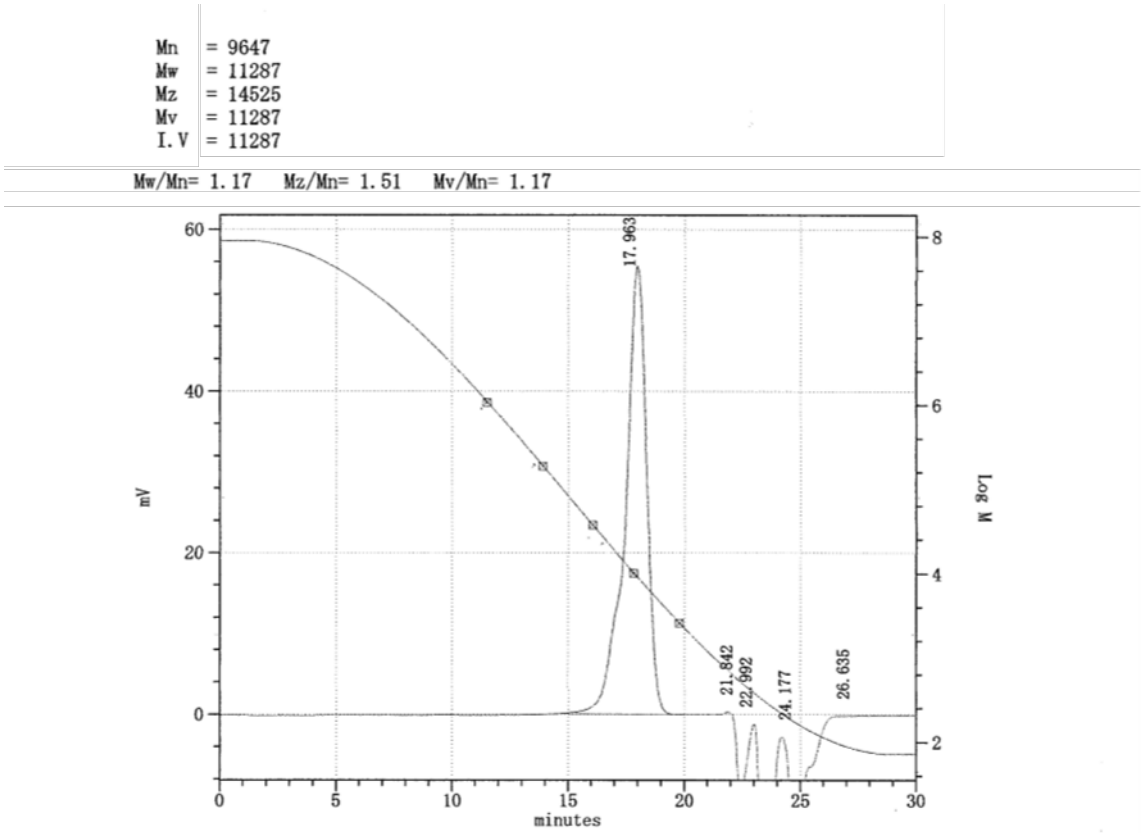

Figure S-33. *n*-BuLi Initiated Polymerization of Styrene in The Flow System (flow rate of *n*-BuLi (0.05 M) = 7.5 mL/min, flow rate of Styrene (2.0 M) = 15.0 mL/min, T-250-500 mixer, 30 degree-C)

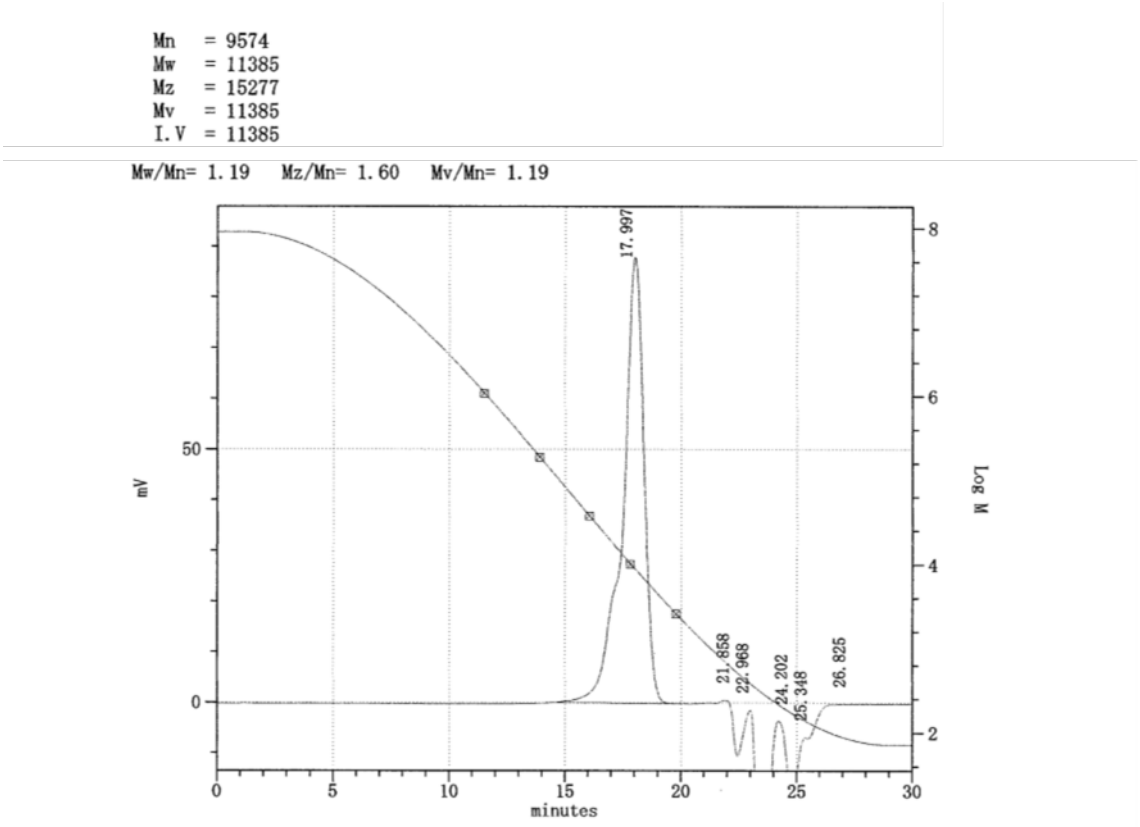

Figure S-34. *n*-BuLi Initiated Polymerization of Styrene in The Flow System (flow rate of *n*-BuLi (0.05 M) = 5.0 mL/min, flow rate of Styrene (2.0 M) = 10.0 mL/min, T-250-500 mixer, 30 degree-C)

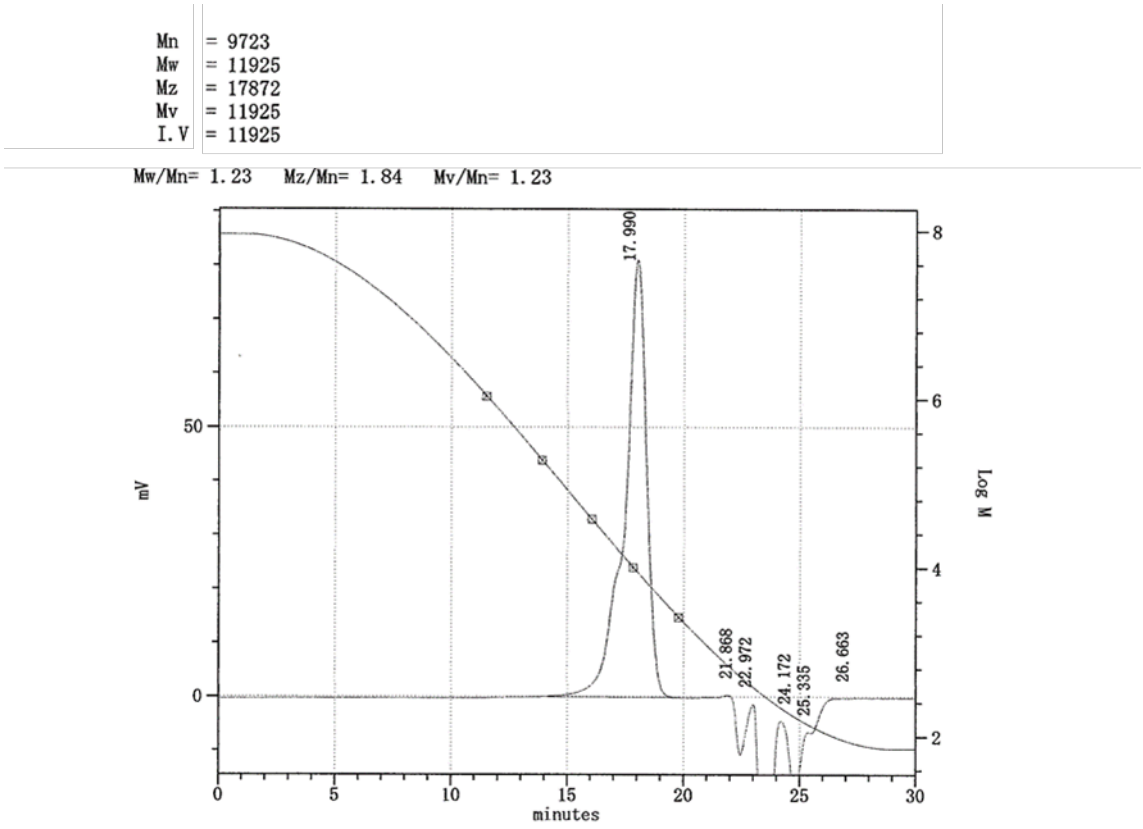

Figure S-35. *n*-BuLi Initiated Polymerization of Styrene in The Flow System (flow rate of *n*-BuLi (0.05 M) = 4.0 mL/min, flow rate of Styrene (2.0 M) = 8.0 mL/min, T-250-500 mixer, 30 degree-C)

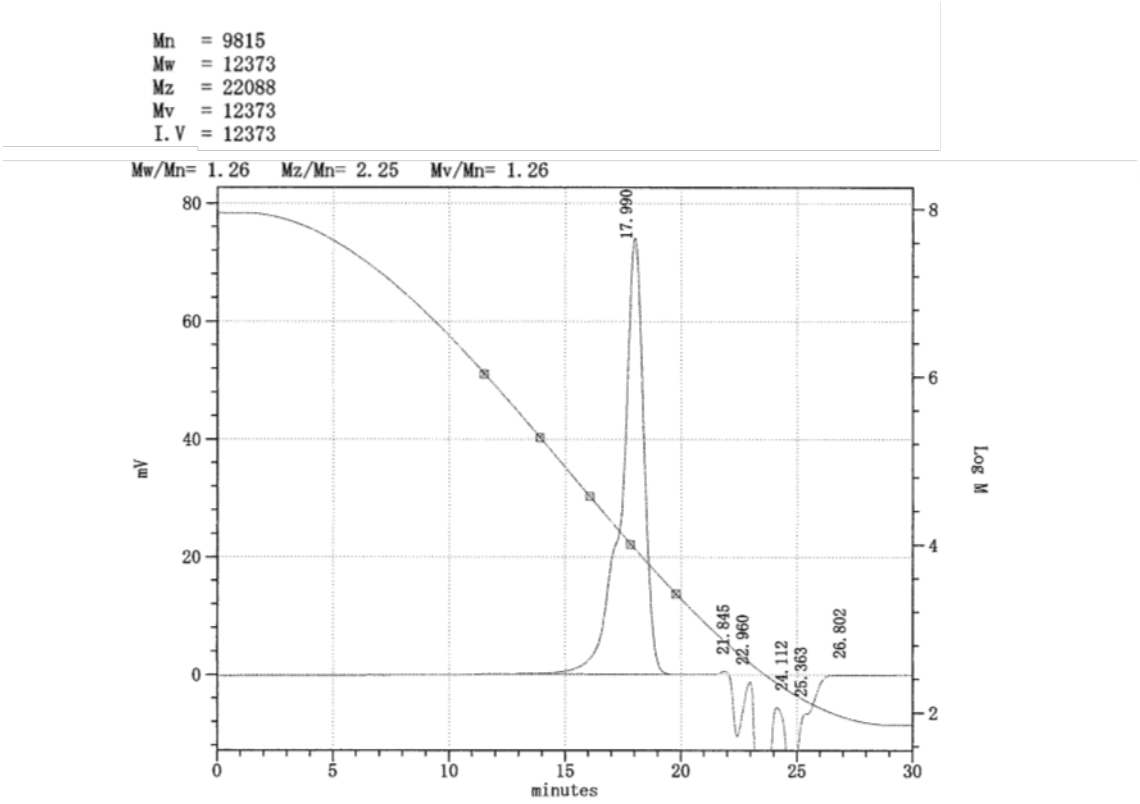

Figure S-36. *n*-BuLi Initiated Polymerization of Styrene in The Flow System (flow rate of *n*-BuLi (0.05 M) = 3.0 mL/min, flow rate of Styrene (2.0 M) = 6.0 mL/min, T-250-500 mixer, 30 degree-C)

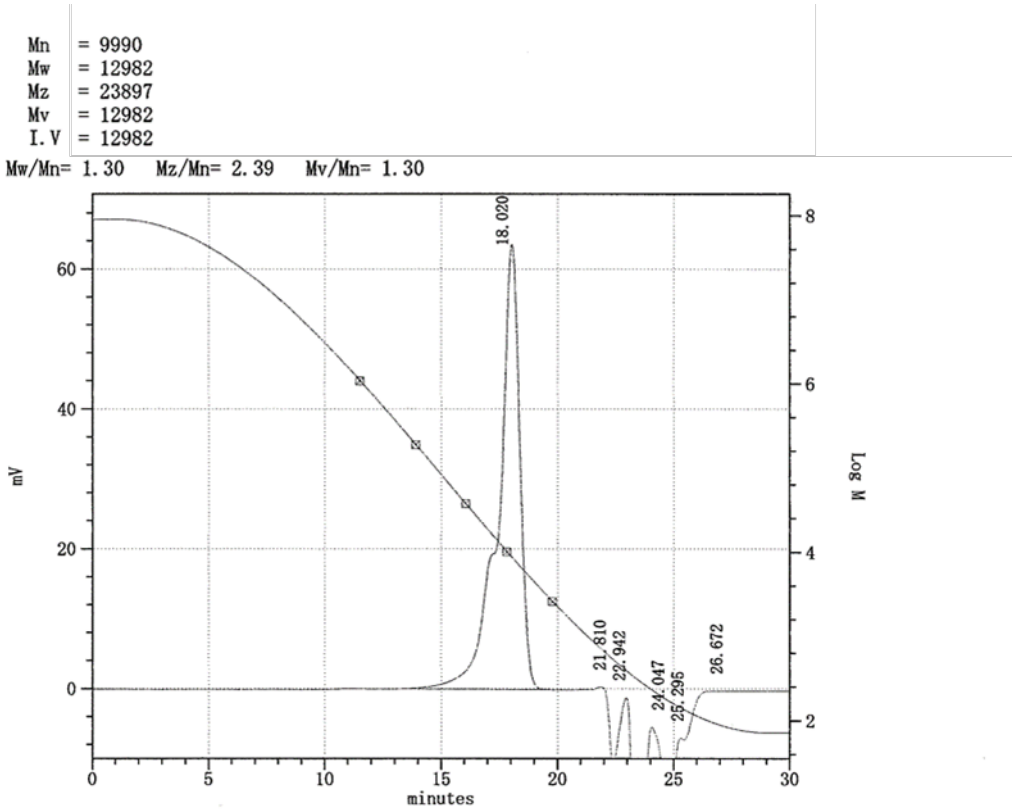

Figure S-37. *n*-BuLi Initiated Polymerization of Styrene in The Flow System (flow rate of *n*-BuLi (0.05 M) = 2.0 mL/min, flow rate of Styrene (2.0 M) = 4.0 mL/min, T-250-500 mixer, 30 degree-C)

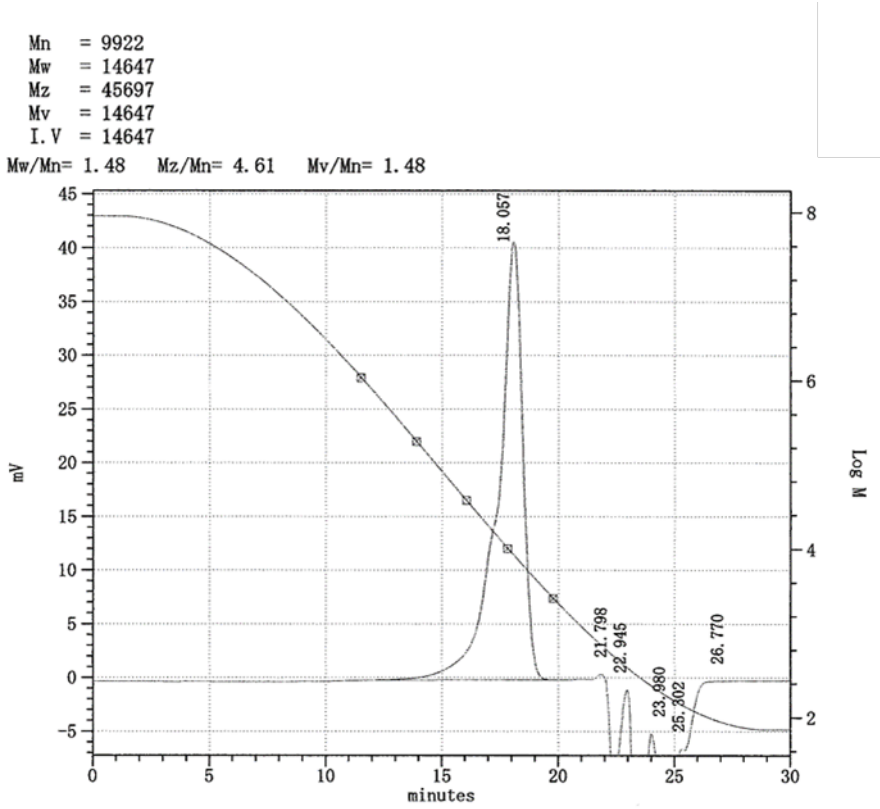

Figure S-38. *n*-BuLi Initiated Polymerization of Styrene in The Flow System (flow rate of *n*-BuLi (0.05 M) = 1.0 mL/min, flow rate of Styrene (2.0 M) = 2.0 mL/min, T-250-500 mixer, 30 degree-C)

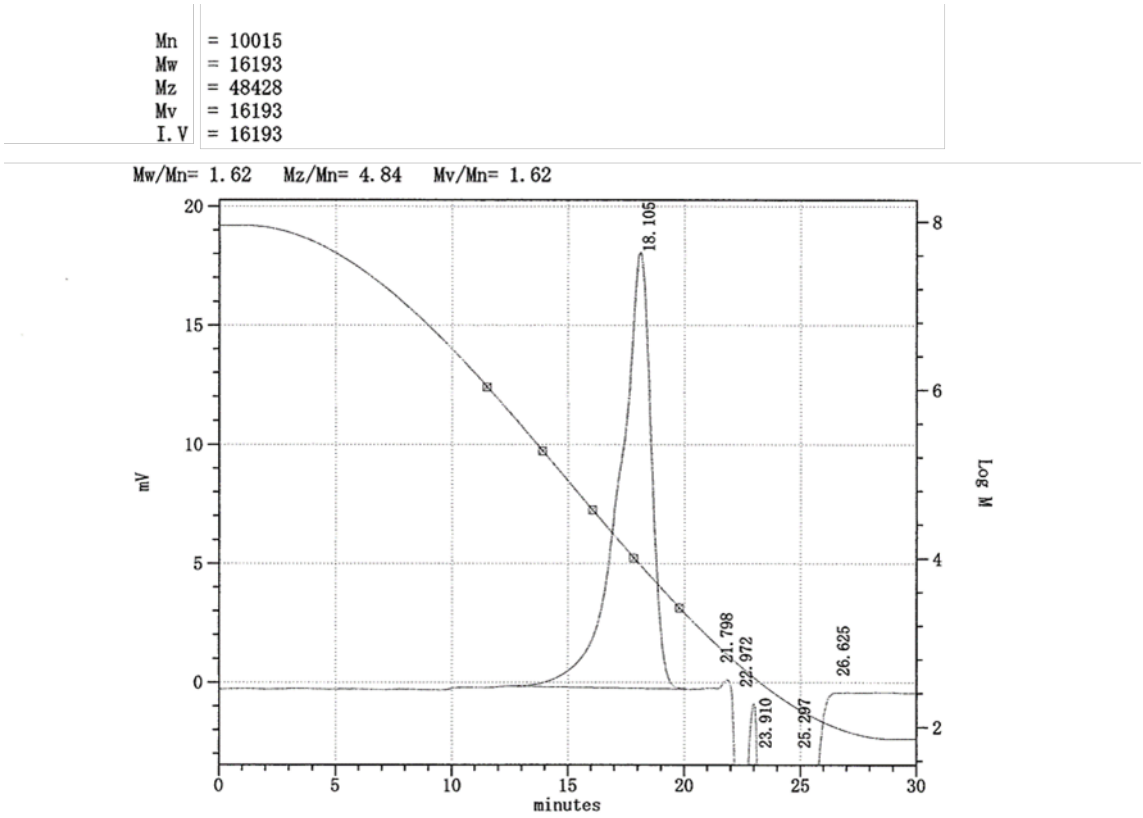

Figure S-39. *n*-BuLi Initiated Polymerization of Styrene in The Flow System (flow rate of *n*-BuLi (0.05 M) = 0.5 mL/min, flow rate of Styrene (2.0 M) = 1.0 mL/min, T-250-500 mixer, 30 degree-C)

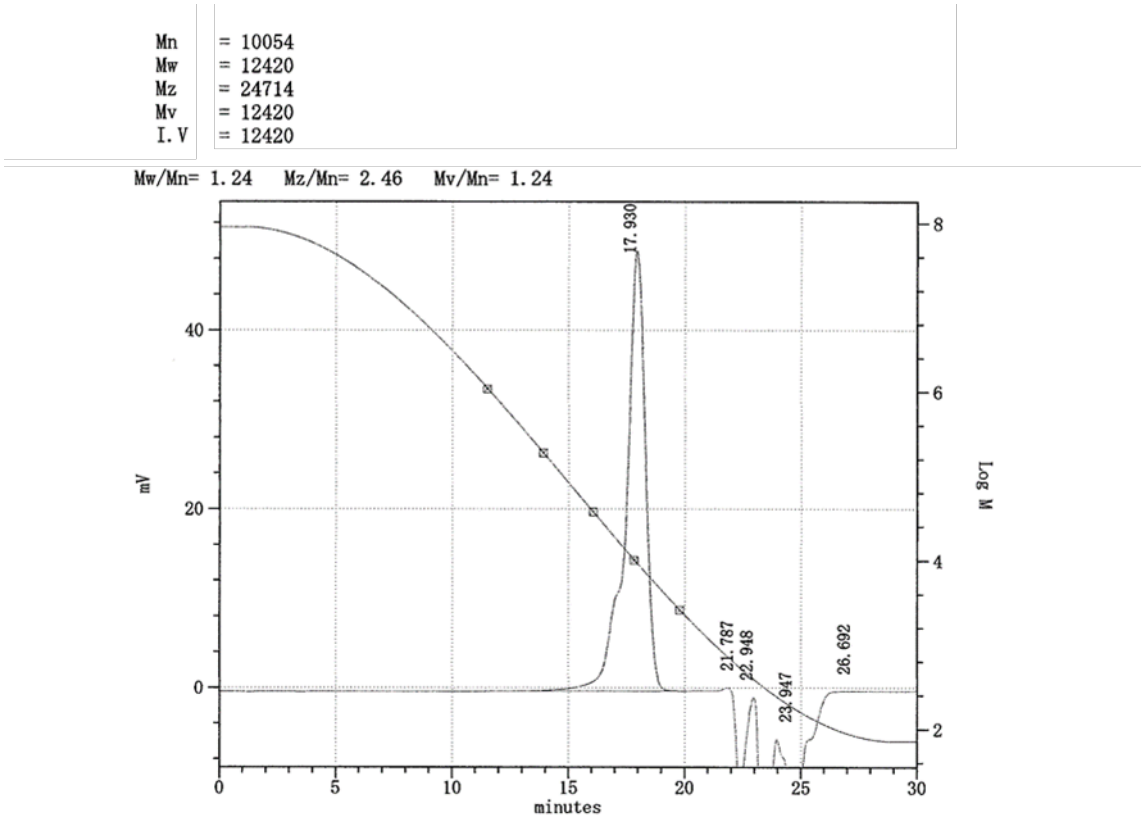

Figure S-40. *n*-BuLi Initiated Polymerization of Styrene in The Flow System (flow rate of *n*-BuLi (0.05 M) = 7.5 mL/min, flow rate of Styrene (2.0 M) = 15.0 mL/min, T-500-250 mixer, 30 degree-C)

Mn	= 9885
Mw	= 12186
Mz	= 21463
Mv	= 12186
I.V	= 12186

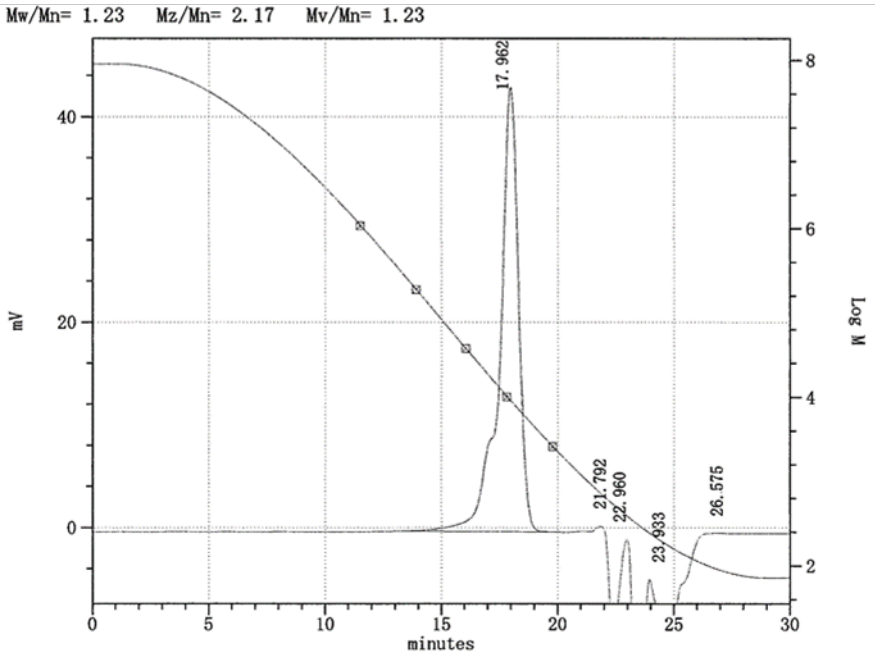

Figure S-41. *n*-BuLi Initiated Polymerization of Styrene in The Flow System (flow rate of *n*-BuLi (0.05 M) = 5.0 mL/min, flow rate of Styrene (2.0 M) = 10.0 mL/min, T-500-250 mixer, 30 degree-C)

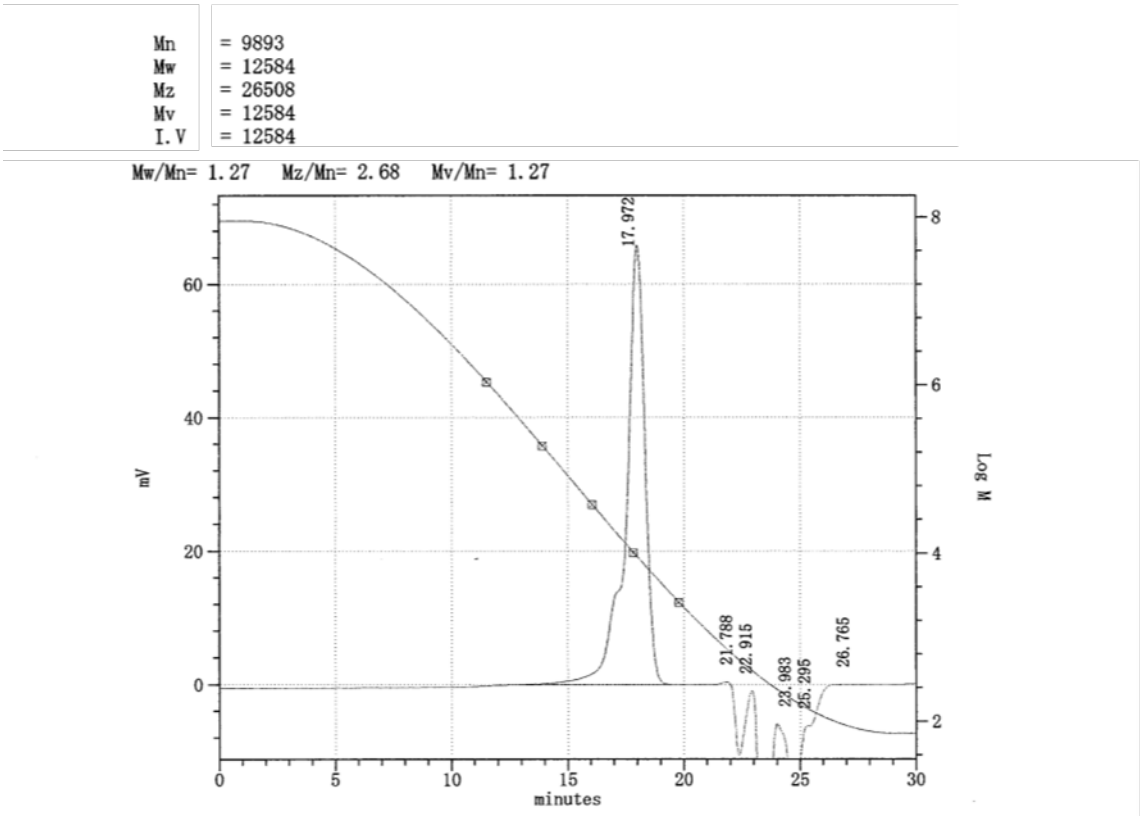

Figure S-42. *n*-BuLi Initiated Polymerization of Styrene in The Flow System (flow rate of *n*-BuLi (0.05 M) = 4.0 mL/min, flow rate of Styrene (2.0 M) = 8.0 mL/min, T-500-250 mixer, 30 degree-C)

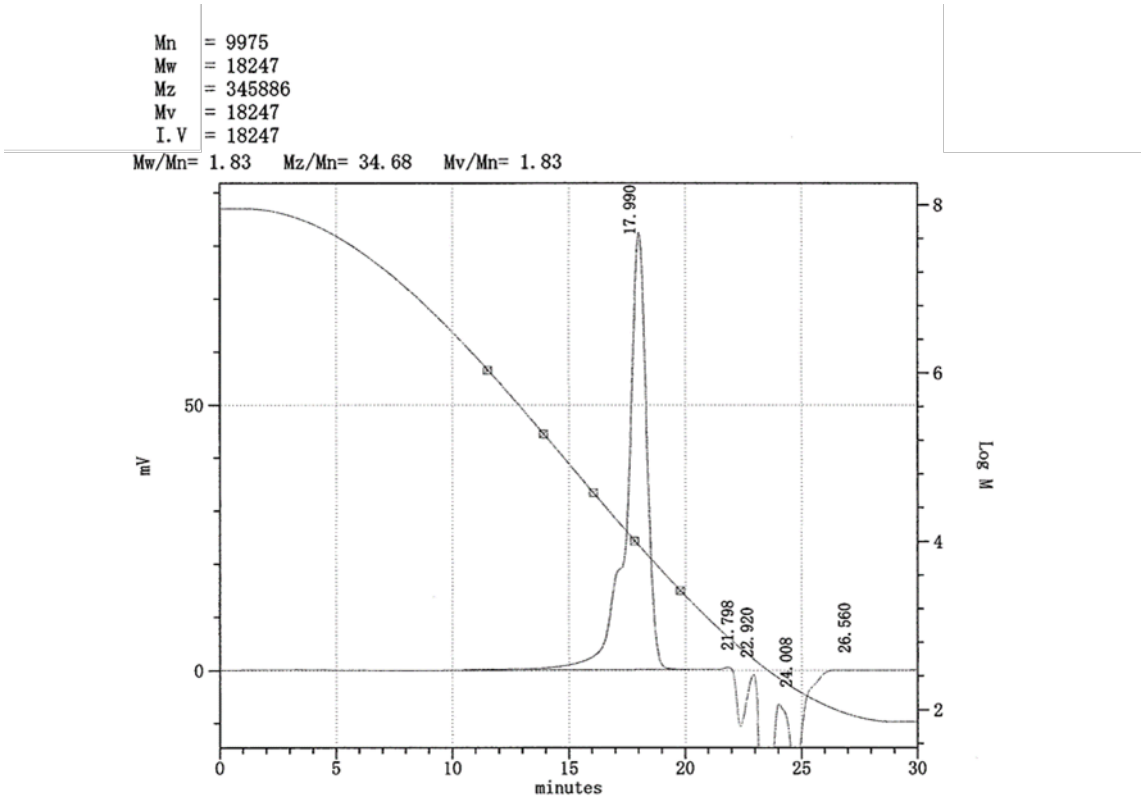

Figure S-43. *n*-BuLi Initiated Polymerization of Styrene in The Flow System (flow rate of *n*-BuLi (0.05 M) = 3.0 mL/min, flow rate of Styrene (2.0 M) = 6.0 mL/min, T-500-250 mixer, 30 degree-C)

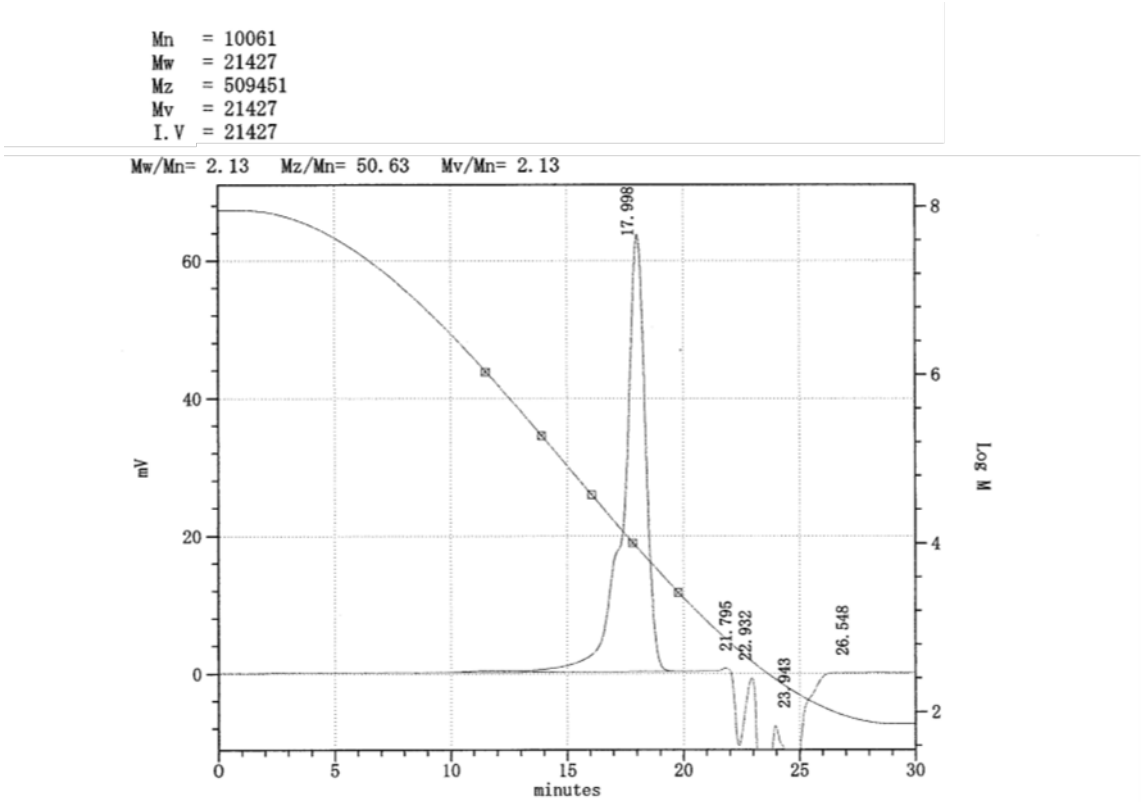

Figure S-44. *n*-BuLi Initiated Polymerization of Styrene in The Flow System (flow rate of *n*-BuLi (0.05 M) = 2.0 mL/min, flow rate of Styrene (2.0 M) = 4.0 mL/min, T-500-250 mixer, 30 degree-C)

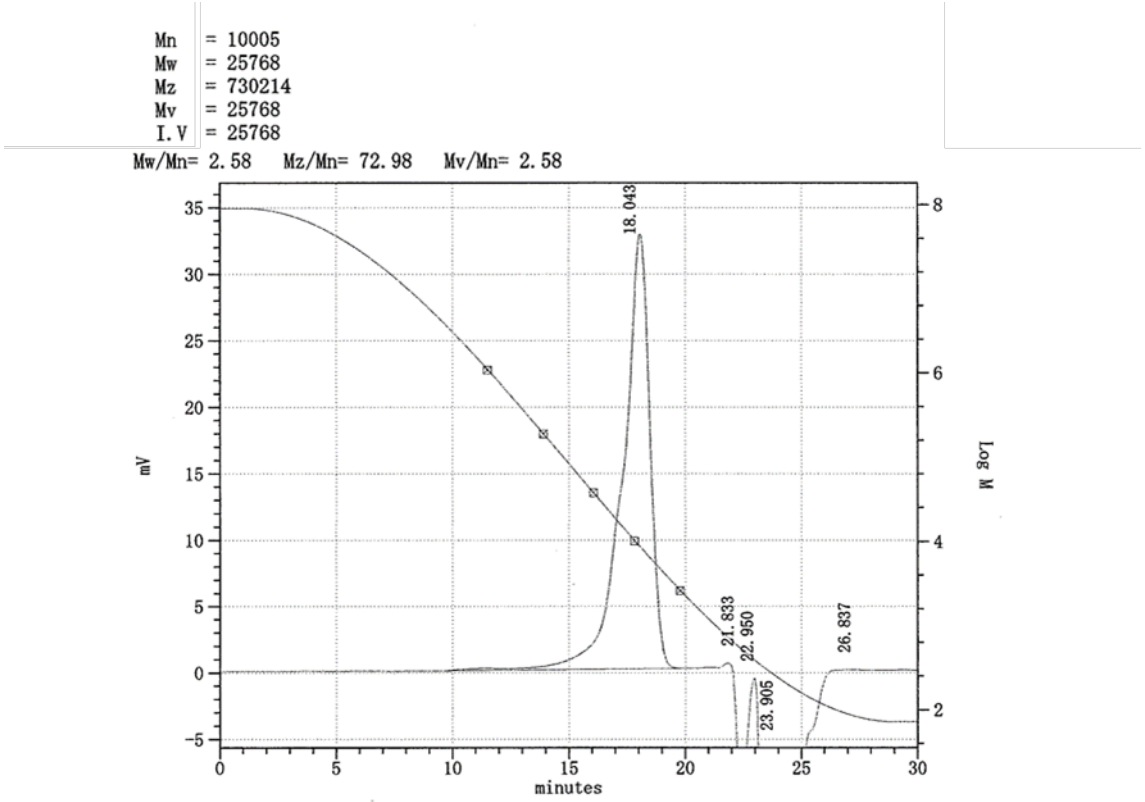

Figure S-45. *n*-BuLi Initiated Polymerization of Styrene in The Flow System (flow rate of *n*-BuLi (0.05 M) = 1.0 mL/min, flow rate of Styrene (2.0 M) = 2.0 mL/min, T-500-250 mixer, 30 degree-C)

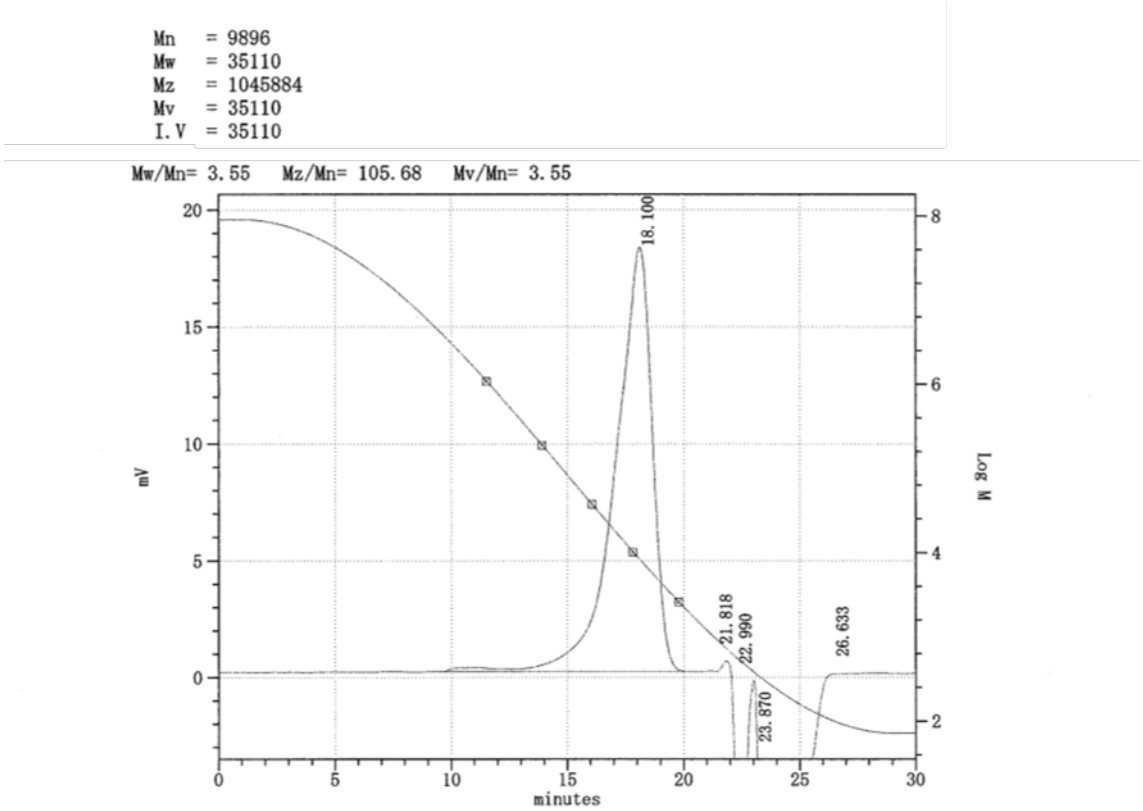

Figure S-46. *n*-BuLi Initiated Polymerization of Styrene in The Flow System (flow rate of *n*-BuLi (0.05 M) = 0.5 mL/min, flow rate of Styrene (2.0 M) = 1.0 mL/min, T-500-250 mixer, 30 degree-C)

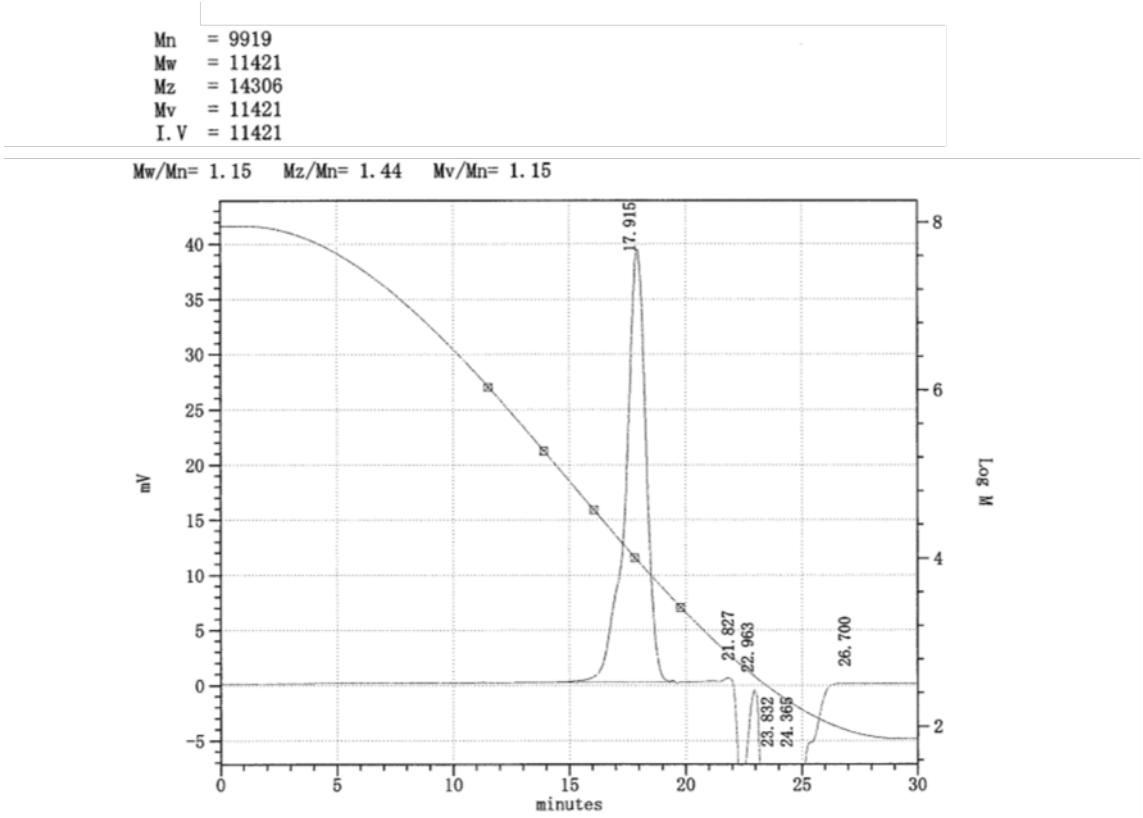

Figure S-47. *n*-BuLi Initiated Polymerization of Styrene in The Flow System (flow rate of *n*-BuLi (0.05 M) = 7.5 mL/min, flow rate of Styrene (2.0 M) = 15.0 mL/min, V-500-500 mixer, 30 degree-C)

Mn	= 9878
Mw	= 11484
Mz	= 14634
Mv	= 11484
I.V	= 11484

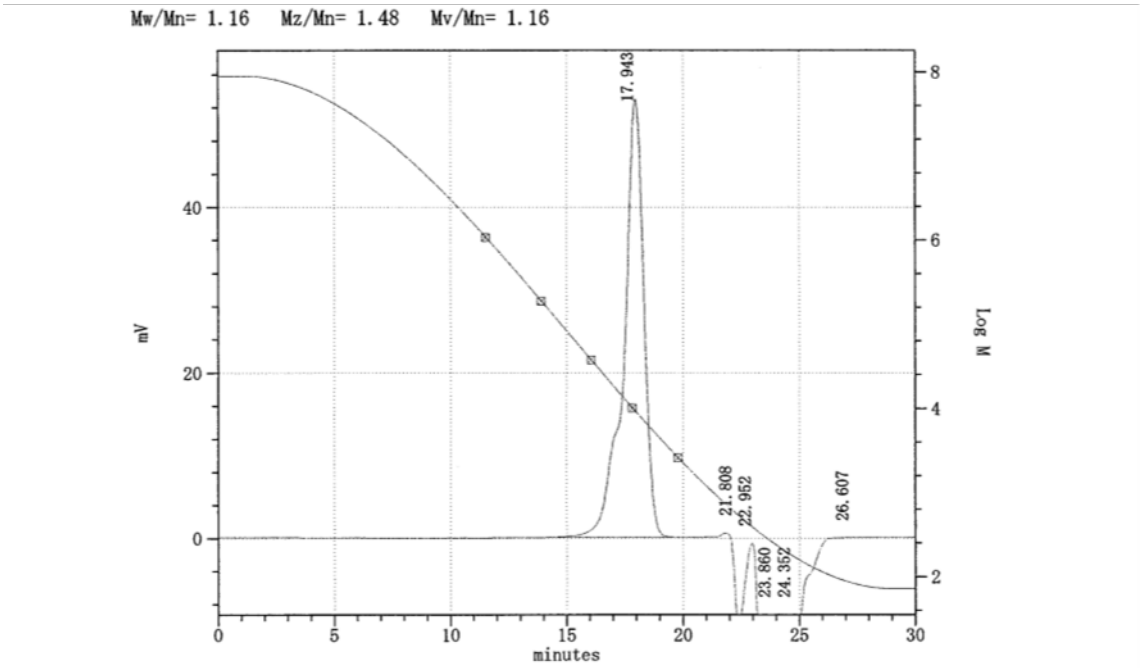

Figure S-48. *n*-BuLi Initiated Polymerization of Styrene in The Flow System (flow rate of *n*-BuLi (0.05 M) = 5.0 mL/min, flow rate of Styrene (2.0 M) = 10.0 mL/min, V-500-500 mixer, 30 degree-C)

Mn	= 9958
Mw	= 11726
Mz	= 15426
Mv	= 11726
I.V	= 11726

Mw/Mn= 1.18 Mz/Mn= 1.55 Mv/Mn= 1.18

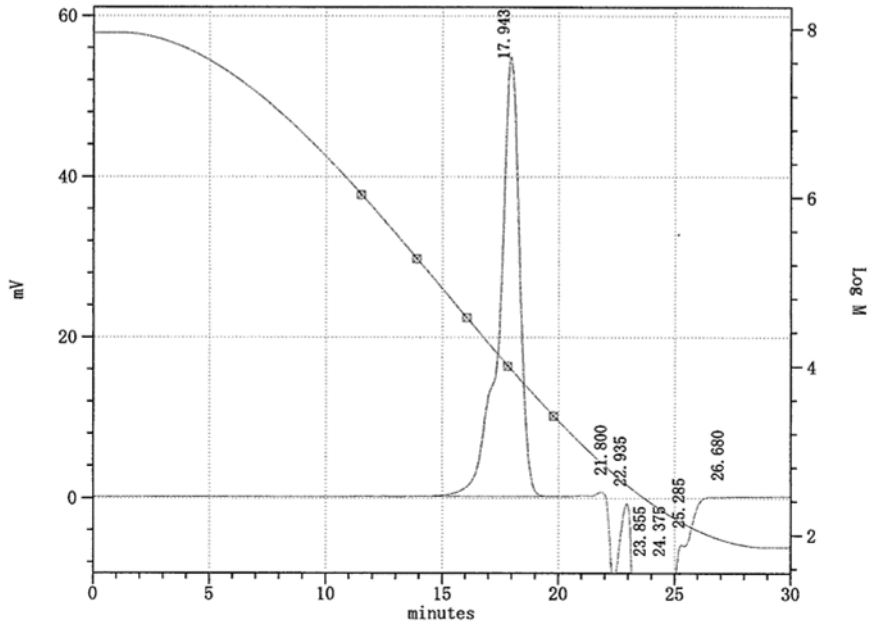

Figure S-49. *n*-BuLi Initiated Polymerization of Styrene in The Flow System (flow rate of *n*-BuLi (0.05 M) = 4.0 mL/min, flow rate of Styrene (2.0 M) = 8.0 mL/min, V-500-500 mixer, 30 degree-C)

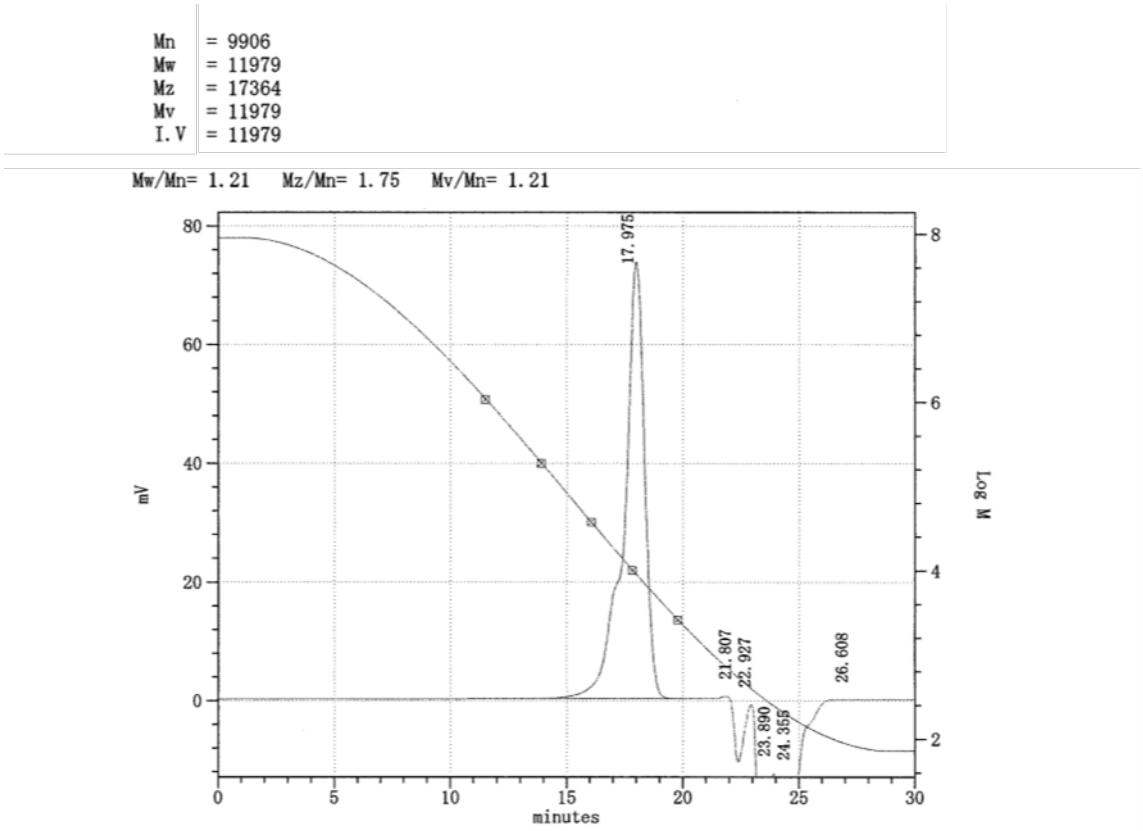

Figure S-50. *n*-BuLi Initiated Polymerization of Styrene in The Flow System (flow rate of *n*-BuLi (0.05 M) = 3.0 mL/min, flow rate of Styrene (2.0 M) = 6.0 mL/min, V-500-500 mixer, 30 degree-C)

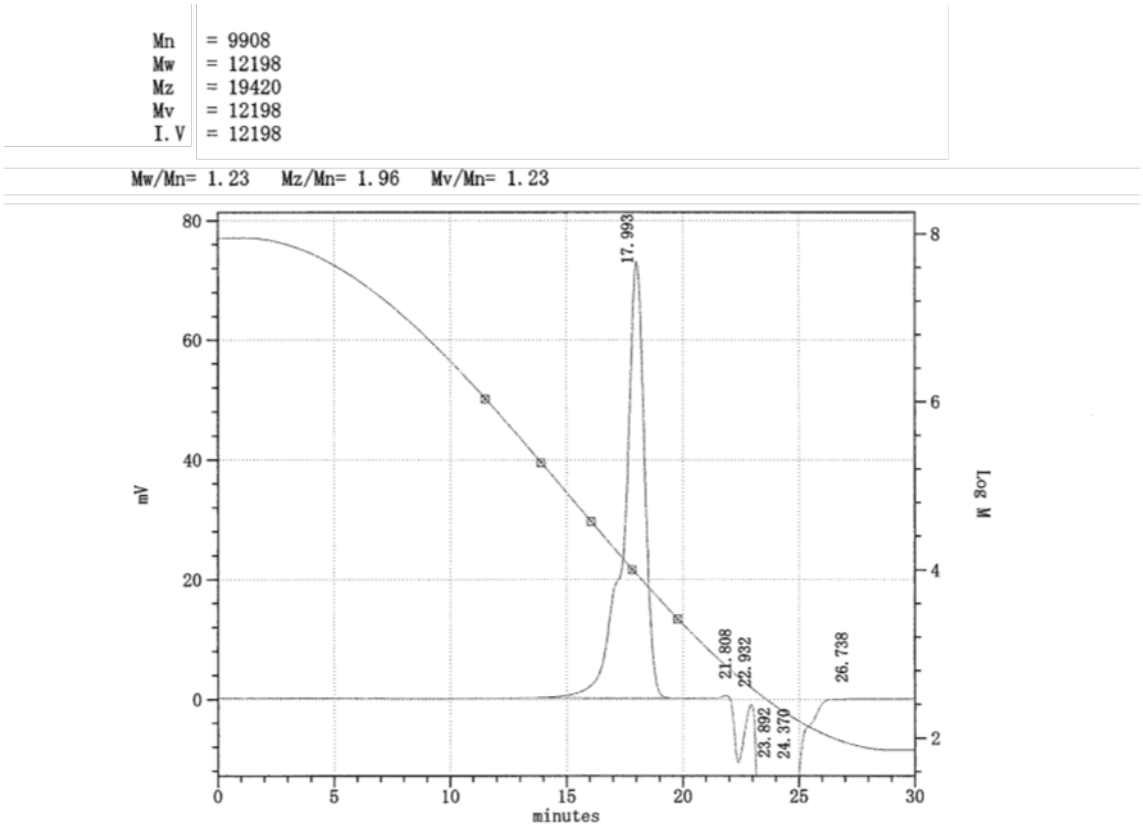

Figure S-51. *n*-BuLi Initiated Polymerization of Styrene in The Flow System (flow rate of *n*-BuLi (0.05 M) = 2.0 mL/min, flow rate of Styrene (2.0 M) = 4.0 mL/min, V-500-500 mixer, 30 degree-C)

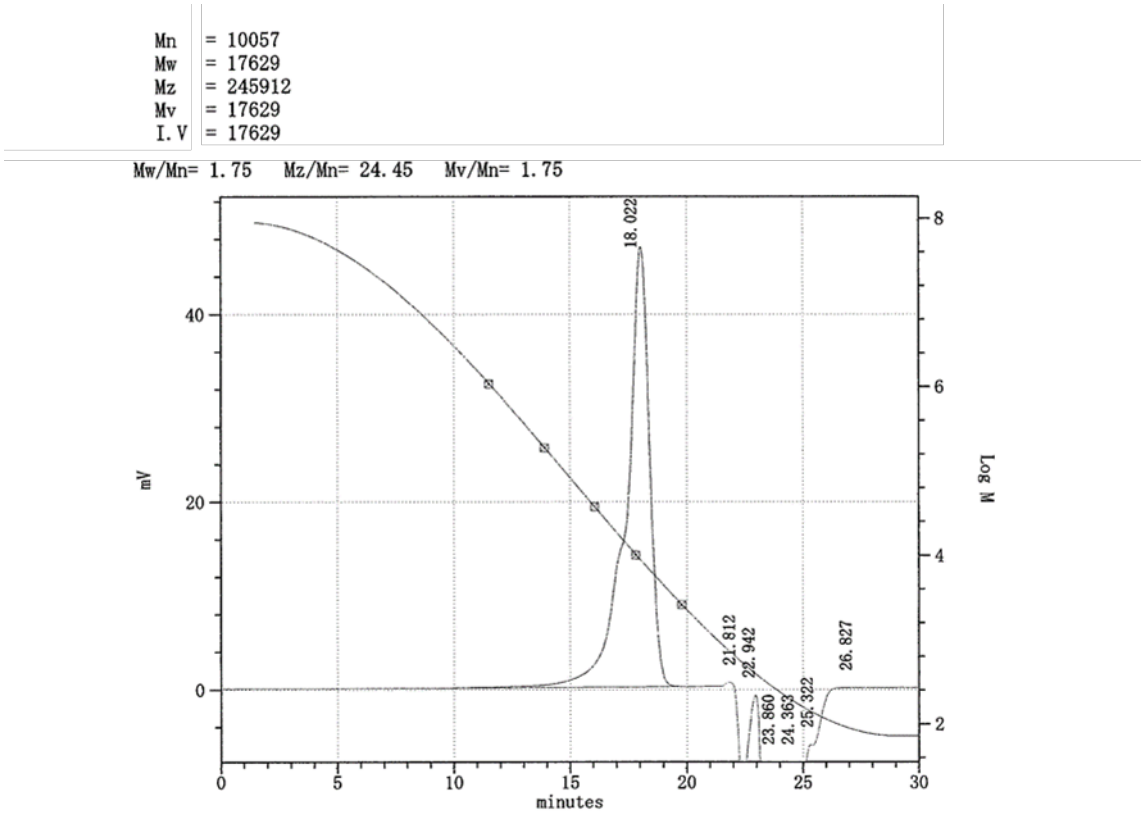

Figure S-52. *n*-BuLi Initiated Polymerization of Styrene in The Flow System (flow rate of *n*-BuLi (0.05 M) = 1.0 mL/min, flow rate of Styrene (2.0 M) = 2.0 mL/min, V-500-500 mixer, 30 degree-C)

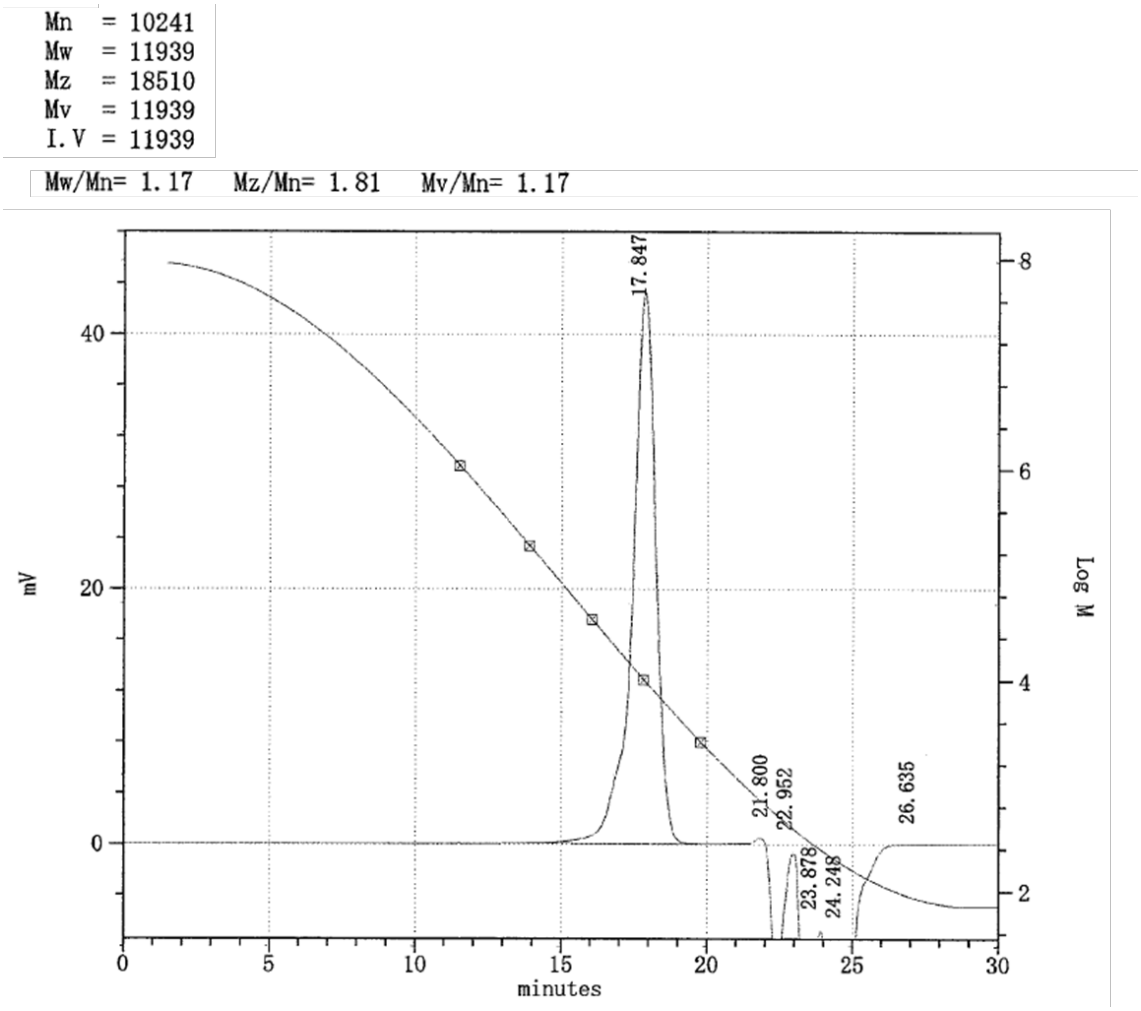

Figure S-53. *n*-BuLi Initiated Polymerization of Styrene in The Flow System (flow rate of *n*-BuLi (0.05 M) = 7.5 mL/min, flow rate of Styrene (2.0 M) = 15.0 mL/min, T-250-250 mixer, 30 degree-C, 2nd trial)

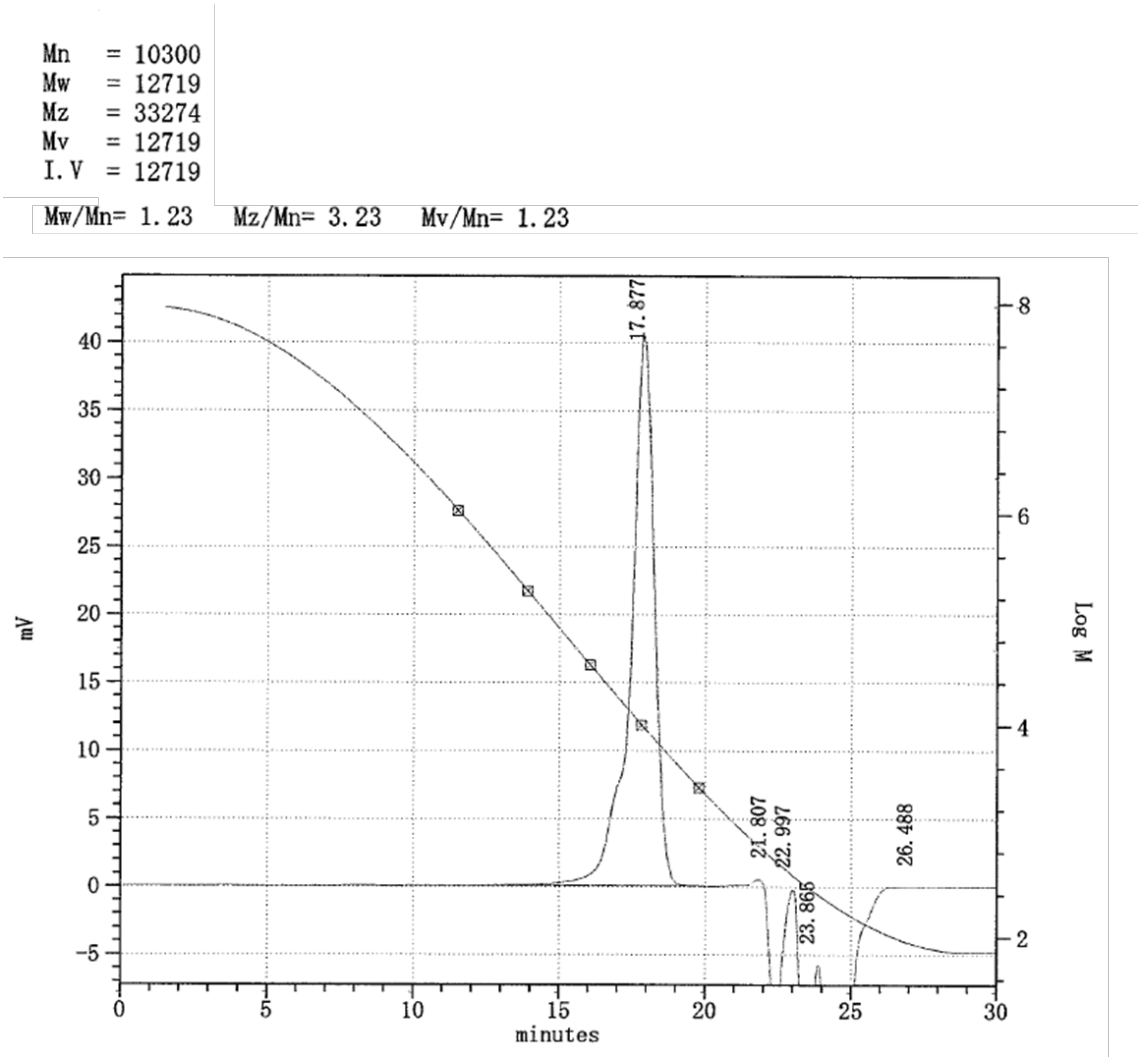

Figure S-54. *n*-BuLi Initiated Polymerization of Styrene in The Flow System (flow rate of *n*-BuLi (0.05 M) = 5.0 mL/min, flow rate of Styrene (2.0 M) = 10.0 mL/min, T-250-250 mixer, 30 degree-C, 2nd trial)

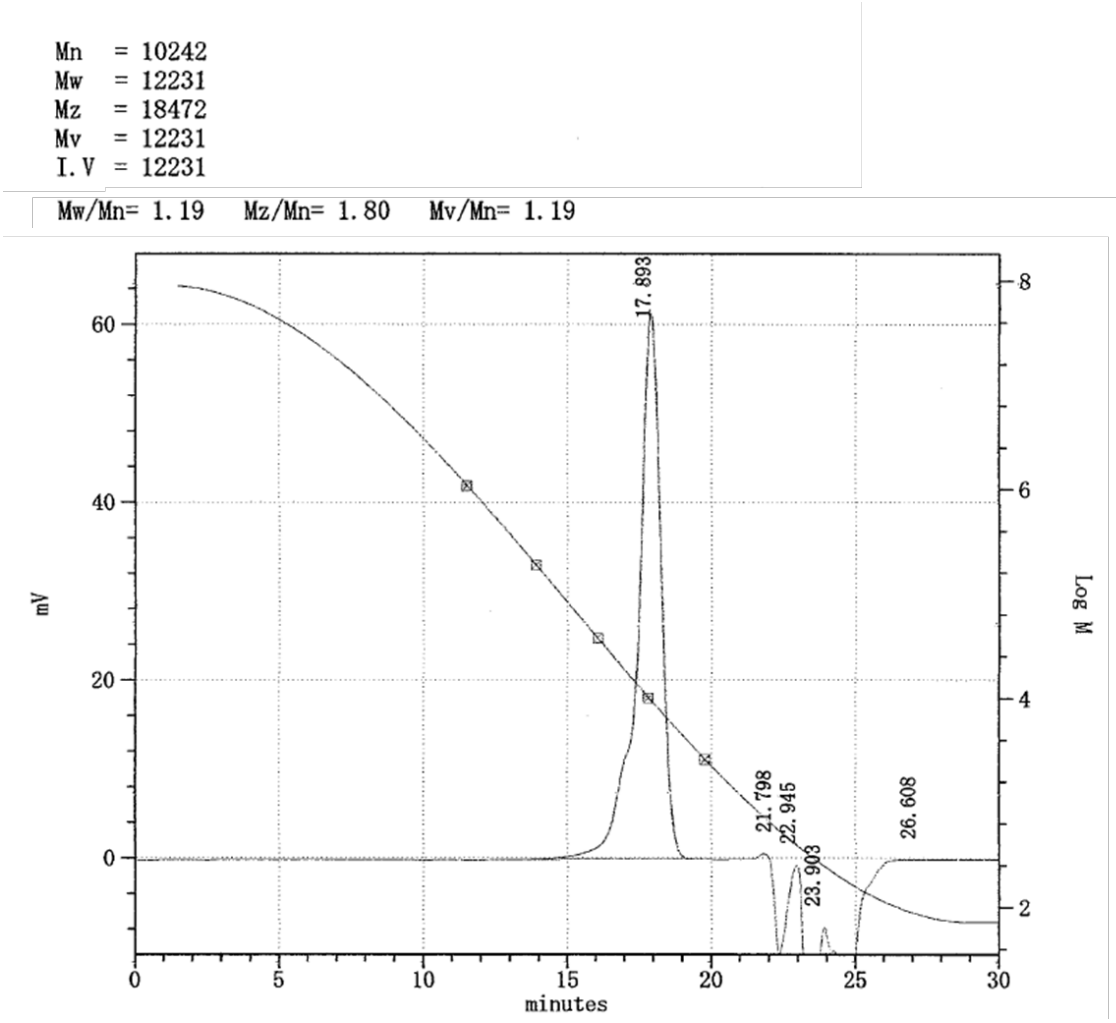

Figure S-55. *n*-BuLi Initiated Polymerization of Styrene in The Flow System (flow rate of *n*-BuLi (0.05 M) = 4.0 mL/min, flow rate of Styrene (2.0 M) = 8.0 mL/min, T-250-250 mixer, 30 degree-C, 2nd trial)

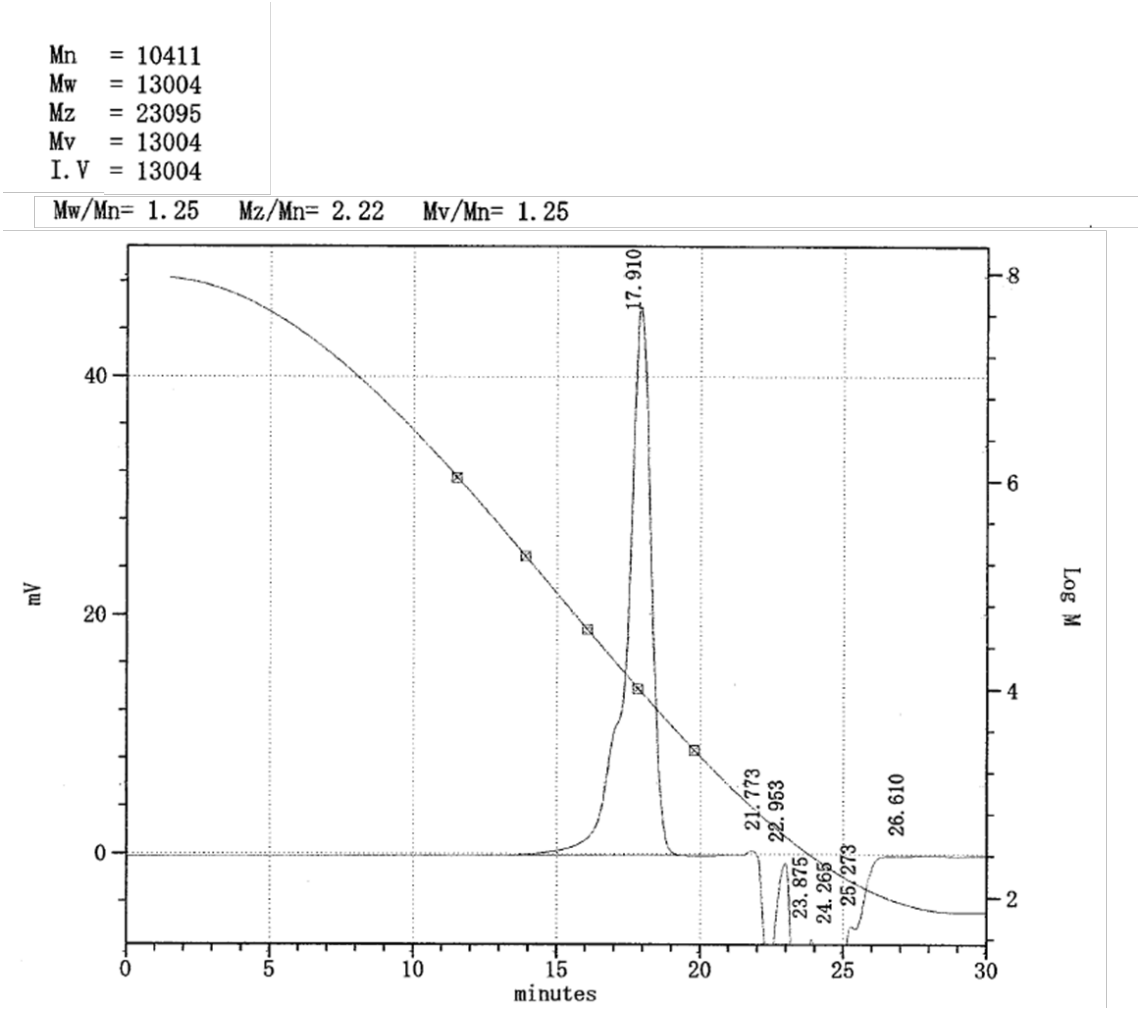

Figure S-56. *n*-BuLi Initiated Polymerization of Styrene in The Flow System (flow rate of *n*-BuLi (0.05 M) = 3.0 mL/min, flow rate of Styrene (2.0 M) = 6.0 mL/min, T-250-250 mixer, 30 degree-C, 2nd trial)

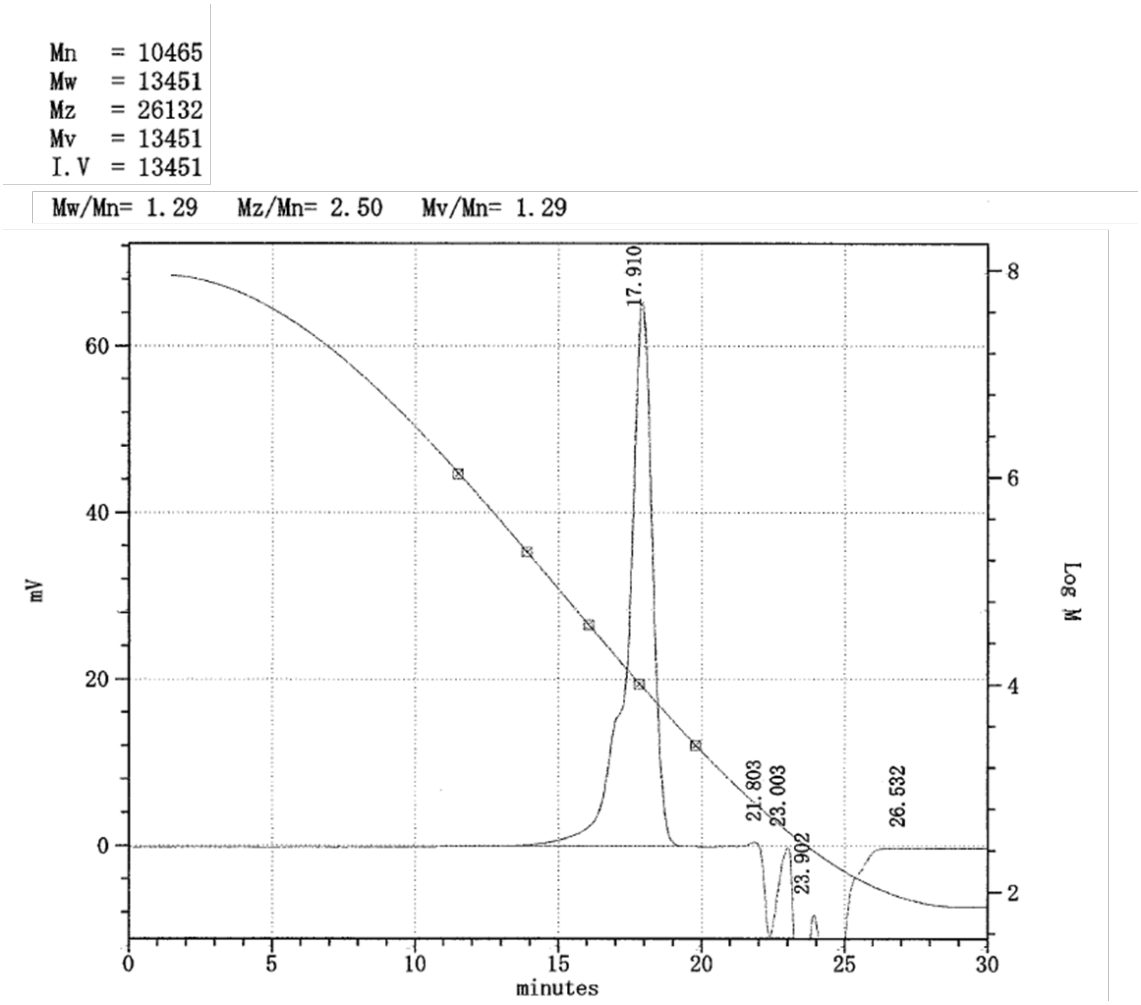

Figure S-57. *n*-BuLi Initiated Polymerization of Styrene in The Flow System (flow rate of *n*-BuLi (0.05 M) = 2.0 mL/min, flow rate of Styrene (2.0 M) = 4.0 mL/min, T-250-250 mixer, 30 degree-C, 2nd trial)

The reproducibility of anionic polymerization

2nd trial of anionic polymerization was conducted with T-250-250 mixer at 30 degree-C in some flow rate conditions to evaluate the reproducibility. The results of 2nd trial was similar to it of 1st trial which was described in the manuscript. Figure S-58 shows these results.

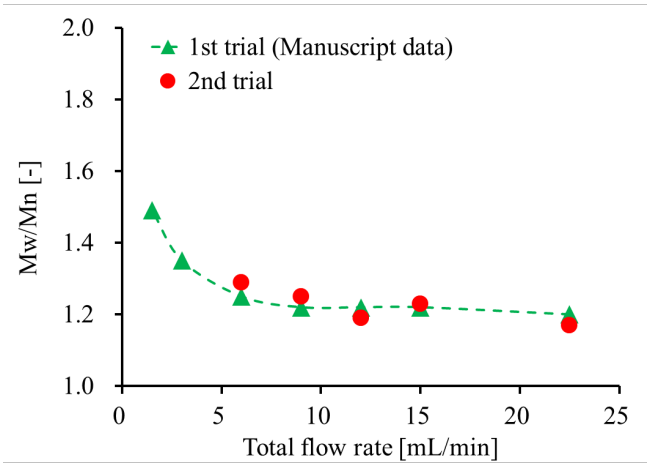

Figure S-58. Comparing the Mw/Mn of 1st and 2nd trials

Table S-1. Numeric data of 2nd trial in the above graph

Mixer shape	T (°C)	Flow rate (mL/min)		[M]/[I]	Mn	Mw/Mn
		n-BuLi	Styrene			
T-250-250	30	7.5	15.0	80	10000	1.17
		5.0	10.0	80	10000	1.23
		4.0	8.0	80	10000	1.19
		3.0	6.0	80	10000	1.25
		2.0	4.0	80	10000	1.29

Explaining the results of Dushman reaction

What the mixability of three mixers was V ≧ T > Y in terms of Mw/Mn in this study. On the other hand, figure S-59 and S-60 show results of Dushman reaction. In the result, mixability order of Dushman reaction was also V > T > Y.

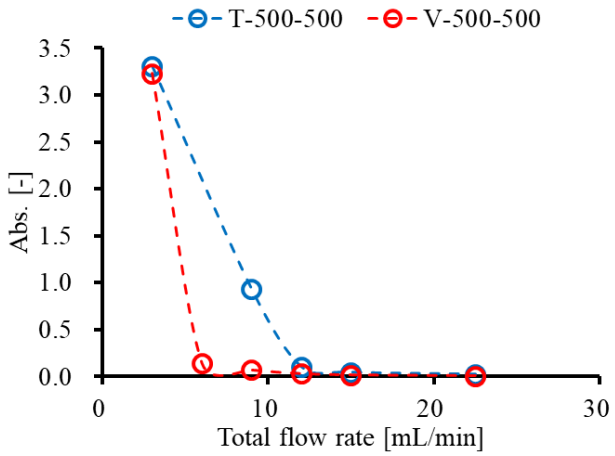

Figure S-59. Comparing V-shape and T- shape mixers in Dushman reaction

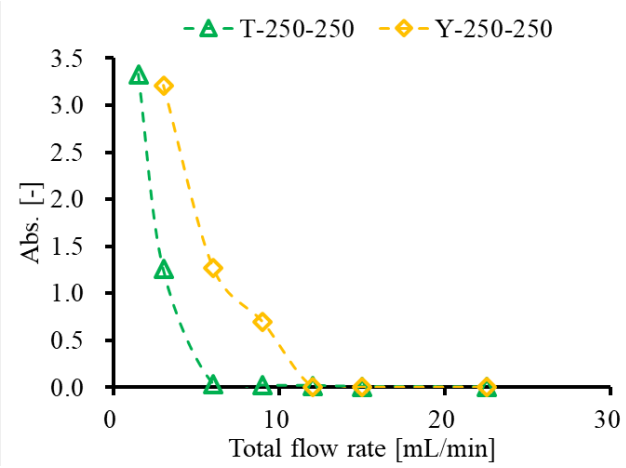

Figure S-60. Comparing Y-shape and T- shape mixers in Dushman reaction

Table S-2. Numeric data of each graph in Dushman reaction

Flow rate (mL/min)		Absorbance [352 nm] (-)			
Solution A	Solution B	T-250-250	T-500-500	V-500-500	Y-250-250
0.75	0.75	3.33	3.43	3.37	3.34
1.50	1.50	1.26	3.31	3.23	3.21
3.00	3.00	0.04	3.23	0.14	1.27
4.50	4.50	0.02	0.93	0.07	0.70
6.00	6.00	0.02	0.10	0.03	0.01
7.50	7.50	0.01	0.05	0.02	0.00

11.25	11.25	0.00	0.03	0.01	0.00

References and notes

1. (1) Books on flow microreactor synthesis: (a) Ehrfeld, W.; Hessel, V.; Löwe, H. Microreactors; Wiley-VCH: Weinheim, 2000. (b) Hessel, V.; Hardt, S.; Löwe, H. Chemical Micro Process Engineering; Wiely-VCH Verlag: Weinheim, 2004. (c) Yoshida, J. Flash Chemistry. Fast Organic Synthesis in Microsystems; Wiley-Blackwell, 2008. (d) Hessel, V.; Renken, A.; Schouten, J. C.; Yoshida, J. Eds. Micro Precess Engineering; Wiley-VCH Verlag: Weinheim, 2009. (e) Wirth T. Ed. Microreactors in Organic Chemistry and Catalysis 2nd Ed., Wiley-VCH Verlag: Weinheim, 2013.
2. (2) Reviews on flow microreactor synthesis: (a) Jähnisch, K.; Hessel, V.; Löwe, H.; Baerns, M. Chemistry in Microstructured Reactors, Angew. Chem. Int. Ed. 2004, 43, 406. (b) Doku, G. N.; Verboom, W.; Reinhoudt, D. N.; van den Berg, A. On-microchip multiphase chemistry - a review of microreactor design principles and reagent contacting modes, Tetrahedron 2005, 61, 2733. (c) Watts, P.; Haswell, S. J. The application of micro reactors for organic synthesis, Chem. Soc. Rev. 2005, 34, 235. (d) Geyer, K.; Codée, J. D. C.; Seeberger, P. H. Microreactors as Tools for Synthetic Chemists—The Chemists' Round-Bottomed Flask of the 21st Century?, Chem. Eur. J. 2006, 12, 8434. (e) deMello, A. J. Control and detection of chemical reactions in microfluidic systems, Nature 2006, 442, 394. (f) Song, H.; Chen, D. L.; Ismagilov, R. F. Reactions in Droplets in Microfluidic Channels, Angew. Chem. Int. Ed. 2006, 45, 7336. (g) Kobayashi, J.; Mori, Y.; Kobayashi, S. Multiphase Organic Synthesis in Microchannel Reactors, Chem. Asian. J. 2006, 1, 22. (h) Brivio, M.; Verboom, W.; Reinhoudt, D. N. Miniaturized continuous flow reaction vessels: influence on chemical reactions, Lab Chip. 2006, 6, 329. (i) Mason, B. P.; Price, K. E.; Steinbacher, J. L.; Bogdan, A. R.; McQuade, D. T. Greener Approaches to Organic Synthesis Using Microreactor Technology, Chem. Rev. 2007, 107, 2300. (j) Ahmed-Omer, B.; Brandt, J. C.; Wirth, T. Advanced organic synthesis using microreactor technology, Org. Biomol. Chem. 2007, 5, 733. (k) Watts, P.; Wiles, C. Recent advances in synthetic micro reaction technology, Chem. Commun. 2007, 443. (l) Fukuyama, T.; Rahman, M. T.; Sato, M.; Ryu, I. Adventures in Inner Space: Microflow Systems for Practical Organic Synthesis, Synlett 2008, 151. (m) Hartman, R. L.; Jensen, K. F. Microchemical systems for continuous-flow synthesis, Lab Chip 2009, 9, 2495. (n) McMullen, J. P.; Jensen, K. F. Integrated Microreactors for Reaction Automation: New Approaches to Reaction Development, Annu. Rev. Anal. Chem. 2010, 3, 19. (o) Yoshida, J.; Kim,

H.; Nagaki, A. Green and Sustainable Chemical Synthesis Using Flow Microreactors, ChemSusChem 2011, 4, 331. (p) Wiles, C.; Watts, P. Continuous flow reactors: a perspective, Green Chem. 2012, 14, 38. (q) Kirschining, A.; Kupracz, L.; Hartwig, J. New Synthetic Opportunities in Miniaturized Flow Reactors with Inductive Heating, Chem. Lett. 2012, 41, 562. (r) McQuade, D. T.; Seeberger, P. H. Applying Flow Chemistry: Methods, Materials, and Multistep Synthesis, J. Org. Chem. 2013, 78, 6384. (s) Elvira, K. S.; i Solvas, X. C.; Wootton, R. C. R.; deMello, A. J. The past, present and potential for microfluidic reactor technology in chemical synthesis, Nat. Chem. 2013, 5, 905. (t) Pastre, J. C.; Browne, D. L.; Ley, S. V. Flow chemistry syntheses of natural products, Chem. Soc. Rev. 2013, 42, 8849. (u) Baxendale, I. R. The integration of flow reactors into synthetic organic chemistry, J. Chem. Technol. Biotechnol. 2013, 88, 519. (v) Yoshida, J.; Nagaki, A.; Yamada, D. Continuous flow synthesis, Drug Discovery Today Technol. 2013, 10, e53. (w) Fukuyama, T.; Totoki, T.; Ryu, I. Carbonylation in microflow: close encounters of CO and reactive species, Green Chem. 2014, 16, 2042. (x) Gemoets, H. P. L.; Su, Y.; Shang, M.; Hessel, V.; Luque, R.; Noël, T. Liquid phase oxidation chemistry in continuous-flow microreactors, Chem. Soc. Rev. 2016, 45, 83. (y) Cambié, D.; Bottecchia, C.; Straathof, N. J. W.; Hessel, V.; Noël, T. Applications of Continuous-Flow Photochemistry in Organic Synthesis, Material Science, and Water Treatment, Chem. Rev. 2016, 116, 10276. (z) Plutschack, M. B.; Pieber, B.; Gilmore, K.; Seeberger, P. H. The Hitchhiker's Guide to Flow Chemistry, Chem. Rev. 2017, 117, 11796.

3. (3) Some selected recent examples: (a) Cantillo, D.; Baghbanzadeh, M.; Kappe, C. O. In Situ Generated Iron Oxide Nanocrystals as Efficient and Selective Catalysts for the Reduction of Nitroarenes using a Continuous Flow Method, Angew. Chem. Int. Ed. 2012, 51, 10190. (b) Shu, W.; Buchwald, S. L. Enantioselective β-Arylation of Ketones Enabled by Lithiation/Borylation/1,4-Addition Sequence Under Flow Conditions, Angew. Chem. Int. Ed. 2012, 51, 5355. (c) Nagaki, A.; Moriwaki, Y.; Yoshida, J. Flow Synthesis of Arylboronic Esters Bearing Electrophilic Functional Groups and Space Integration with Suzuki–Miyaura Coupling without Intentionally Added Base, Chem. Commun. 2012, 48, 11211. (d) Lévesque, F.; Seeberger, P. H. Continuous-Flow Synthesis of the Anti-Malaria Drug Artemisinin, Angew. Chem. Int. Ed. 2012, 51, 1706. (e) Basavaraju, K. C.; Sharma, S.; Maurya, R. A.; Kim, D. P. Safe Use of a Toxic Compound: Heterogeneous OsO4 Catalysis in a Nanobrush Polymer Microreactor, Angew. Chem.

Int. Ed. 2013, 52, 6735. (f) Brancour, C.; Fukuyama, T.; Mukai, Y.; Skrydstrup, T.; Ryu, I. Modernized Low Pressure Carbonylation Methods in Batch and Flow Employing Common Acids as a CO Source, Org. Lett. 2013, 15, 2794. (g) Nguyen, J. D.; Reiß, B.; Dai, C.; Stephenson, C. R. J. Batch to flow deoxygenation using visible light photoredox catalysis, Chem. Commun. 2013, 49, 4352. (h) Battilocchio, C.; Hawkins, J. M.; Ley, S. V. Org. Lett. 2013, 15, 2278. (i) Kleinke, A. S.; Jamison, T. F. Hydrogen-Free Alkene Reduction in Continuous Flow, Org. Lett. 2013, 15, 710. (j) Guetzoyan, L.; Nikbin, N.; Baxendale, I. R.; Ley, S. V. Flow chemistry synthesis of zolpidem, alpidem and other GABAA agonists and their biological evaluation through the use of in-line frontal affinity chromatography, Chem. Sci. 2013, 4, 764. (k) Fuse, S.; Mifune, Y.; Takahashi, T. Efficient Amide Bond Formation through a Rapid and Strong Activation of Carboxylic Acids in a Microflow Reactor, Angew. Chem. Int. Ed. 2014, 53, 851. (l) He, Z.; Jamison, T. F. Continuous-Flow Synthesis of Functionalized Phenols by Aerobic Oxidation of Grignard Reagents, Angew. Chem. Int. Ed. 2014, 53, 3353. (m) Nagaki, A.; Takahashi, Y.; Yoshida, J. Extremely Fast Gas/Liquid Reactions in Flow Microreactors: Carboxylation of Short-Lived Organolithiums, Chem. Eur. J. 2014, 20, 7931. (n) Chen, M.; Ichikawa, S.; Buchwald, S. L. Rapid and Efficient Copper-Catalyzed Finkelstein Reaction of (Hetero)Aromatics under Continuous-Flow Conditions, Angew. Chem., Int. Ed. 2015, 54, 263; e) Fuse, S.; Mifune, Y.; Nakamura, H.; Tanaka, H. Total synthesis of feglymycin based on a linear/convergent hybrid approach using micro-flow amide bond formation, Nat. Commun. 2016, 7, 13491; f) Nagaki, A.; Takahashi, Y.; Yoshida, J. Generation and Reaction of Carbamoyl Anions in Flow: Applications in the Three-Component Synthesis of Functionalized α-Ketoamides, Angew. Chem., Int. Ed. 2016, 55, 5327; g) Seo, H.; Katcher, M. H.; Jamison, T. F. Photoredox activation of carbon dioxide for amino acid synthesis in continuous flow, Nat. Chem. 2017, 9, 453.

4. (4) Reviews on polymerizations using microreactors: (a) Hessel, V.; Serra, C.; Lowe, H.; Hadziioannou, G. Polymerisationen in mikrostrukturierten Reaktoren: Ein Überblick, Chemie Ingenieur Technik 2005, 77, 1693. (b) Steinbacher, J. L.; Mcquade, D. T. Polymer chemistry in flow: New polymers, beads, capsules, and fibers, J. Polym. Sci. Part A Polym. Chem. 2006, 44, 6505. (c) Tonhauser, C.; Natalello, A.; Löwe, H.; Frey, H. Microflow Technology in Polymer Synthesis, Macromolecules 2012, 45, 9551. (d) Nagaki, A.; Yoshida, J. Flow-Microreactor-System Controlled Polymerization, Adv. Poly. Sci. 2013, 259, 1 and

references therein.

5. (5) Erlita M.; Junpo H. 1.Continuous Production of Multiblock Copolymers in a Loop Reactor: When Living Polymerization Meets Flow Chemistry, Macromolecules 2017, 50, 9173
6. (6) (a) Hsieh, H. L.; Quirk, R. P. Anionic polymerization: principles and practical applications; Marcel Dekker: New York, 1996. (b) Jagur-grodzinski, J. Functional polymers by living anionic polymerization, J. Polym. Sci., Part A: Polym. Chem. 2002, 40, 2116. (c) Hong, K.; Uhrig, D.; Mays, J. W. Living anionic polymerization, Current Opinion in Solid State and Material Science 4 1999, 531. (d) Smid, J. Historical perspectives on living anionic polymerization, J. Polym. Sci., Part A: Polym. Chem. 2002, 40, 2101. (e) Hirao, A.; Loykulnant, S.; Ishizone, T. Recent advance in living anionic polymerization of functionalized styrene derivatives, Prog. Polym. Sci. 2002, 27, 1399. (f) Hadjichristidis, N.; Pitsikalis, M.; Pispas, S.; Iatrou, H. Polymers with Complex Architecture by Living Anionic Polymerization, Chem. Rev. 2001, 101, 3747 and reference therein.
7. (7) (a) Szwarc, M. 'Living' Polymers, Nature 1956, 178, 1168. (b) Geacintov, C.; Smid, J.; Szwarc, M. Kinetics of Anionic Polymerization of Styrene in Tetrahydrofuran, J. Am. Chem. Soc. 1962, 84, 2508. (c) Bhattacharyya, D. N.; Lee, C. L.; Smid, J.; Szwarc, Reactivities and Conductivities of Ions and Ion Pairs in Polymerization Processes, J. Phys. Chem. 1965, 69, 612.
8. (8) Anionic polymerization using microreactors: (a) Wilms, D.; Nieberle, J.; Klos, J.; Löwe, H.; Frey, H. Synthesis of Hyperbranched Polyglycerol in a Continuous Flow Microreactor, Chem. Eng. Technol. 2007, 30, 1519. (b) Wurm, F.; Wilms, D.; Klos, J.; Löwe, H.; Frey, H. Carbanions on Tap – Living Anionic Polymerization in a Microstructured Reactor, Macromol. Chem. Phys. 2008, 209, 1106. (c) Wilms, D.; Klos, J.; Frey, H. Macromol. Chem. Phys. 2008, 209, 343. (d) Nagaki, A.; Tomida, Y.; Yoshida, J. Microflow-System-Controlled Anionic Polymerization of Styrenes, Macromolecules 2008, 41, 6322-6330. (e) Nagaki, A.; Tomida, Y.; Miyazaki, A.; Yoshida, J. Microflow System Controlled Anionic Polymerization of Alkyl Methacrylates, Macromolecules 2009, 42, 4384. (f) Iida, K.; Chastek, T. Q.; Beers, K. L.; Cavicchi, K. A.; Chun, J.; Fasolka, M. J. Living anionic polymerization using a microfluidic reactor, Lab Chip, 2009, 9, 339. (g) Tonhauser, C.; Wilms, D.; Wurm, F.; Berger-Nicoletti, E.; Maskos, M.; Löwe, H.; Frey, H. Multihydroxyl-Functional Polystyrenes in Continuous Flow, Macromolecules 2010, 43, 5582.

(h) Nagaki, A.; Miyazaki, A.; Yoshida, J. Synthesis of Polystyrenes−Poly(alkyl methacrylates) Block Copolymers via Anionic Polymerization Using an Integrated Flow Microreactor System, Macromolecules 2010, 43, 8424. (i) Nagaki, A.; Miyazaki, A.; Tomida, Y.; Yoshida, J. Anionic polymerization of alkyl methacrylates using flow microreactor systems, Chem. Eng. J. 2011, 167, 548. (j) Cortese, B.; Noel, T.; de Croon, M. H. J. M.; Schulze, S.; Klemm, E.; Hessel, V. Modeling of Anionic Polymerization in Flow With Coupled Variations of Concentration, Viscosity, and Diffusivity, Macromol. React. Eng. 2012, 6, 507. (k) Tonhauser, C.; Natalello, A.; Löwe, H.; Frey, H. Microflow Technology in Polymer Synthesis, Macromolecules 2012, 45, 9551. (l) Nagaki, A.; Takahashi, S.; Akahori, K.; Yoshida, J. Living Anionic Polymerization of tert-Butyl Acrylate in a Flow Microreactor System and Its Applications to the Synthesis of Block Copolymers, Macromol. React. Eng. 2012, 6, 467. (m) Nagaki, A.; Akahori, K.; Takahashi, Y.; Yoshida, J. Flow Microreactor Synthesis of Fluorine-Containing Block Copolymers, J. Flow Chem. 2014, 4, 168.

9. (9) Nagaki, A.; Nakahara, Y.; Furusawa, M.; Sawaki, T.; Yamamoto, T.; Toukairin, H.; Tadokoro, S.; Shimazaki, T.; Ito, T.; Otake, M.; Arai, H.; Toda, N.; Ohtsuka, K.; Takahashi, Y.; Moriwaki, Y.; Tsuchihashi, Y.; Hirose, K.; Yoshida, J. Feasibility Study on Continuous Flow Controlled/Living Anionic Polymerization Processes, Org. Process Res. Dev. 2016, 20, 1377.
10. (10) Ehrfeld, W.; Golbig, K.; Hessel, V.; Lowe, H.; Richter, T. Characterization of Mixing in Micromixers by a Test Reaction: Single Mixing Units and Mixer Arrays, Ind. Eng. Chem. Res. 1999, 38, 1075.
11. (11) Reckamp, J. M.; Bindels, A.; Duffield, S.; Liu, Y. C.; Bradford, E.; Ricci, E.; Susanne, F.; Rutter, A. Mixing Performance Evaluation for Commercially Available Micromixers Using Villermaux–Dushman Reaction Scheme with the Interaction by Exchange with the Mean Model, Org. Process Res. Dev. 2017, 21, 816.

Chapter 4

Modeling and Design of Flow Microreactor-based Process for Synthesizing Ionic Liquids

Abstract

A synthesis process for ionic liquids (ILs), 1-butyl-3-methylimidazolium chloride (BMIM.Cl), is developed using a flow microreactor (FMR) in this study. After the reaction rate analysis, FMR is efficiently designed using CFD simulation, which can shorten the process development time by reducing trial and error experiment. The designed FMR is composed of a V-shaped mixer and a tubular reactor having millimeter-scale inner diameter. From the viewpoint of process operation and control, reactors with larger inner diameter are basically preferable. The influence of three types of inner diameters of 0.75 mm, 2.16 mm, and 4.35 mm, which satisfy temperature constraints on product quality, on product yield and production volume is investigated. It is shown that as the inner diameter becomes large, the product yield becomes low because the mass transfer approaches the rate-limiting step of the reaction process. To avoid this problem, it is proposed that static mixers are built in the reactor having the inner diameter of 4.35 mm. As a result, its production volume, without lowering the product yield, could be improved about 39 times compared with the conventional one.

Introduction

Ionic liquids (ILs) are low melting salts (melting point below 100 ℃) and have several features such as low vapour pressure, easy to separate solvents and high electrical conductivity.[1,2,3] Such features make it possible to use ILs as alternative solvents for reactions and to facilitate recycling of catalyst and solvent. It is estimated that the market size of ILs will record a compound annual growth rate of 9.2% between 2016 and 2021, reaching US$ 39.6 million by 2021.[4] That is, it can be said that demand for production of ILs is increasing. Several methods for producing ILs have been developed so far, but they need improvement to realize higher

productivity.[5] For example, the revision of reaction conditions such as temperature, pressure and concentration can be mentioned. It is preferable to perform the reaction at higher temperature, pressure and concentration. The reaction rate is thereby accelerated. But, since ILs synthesis is highly exothermic, it is necessary to efficiently remove the heat of reaction to avoid quality decay or runaway conditions. Besides, promotion of mass transfer during reaction can be also mentioned. Increasing viscosity and/or biphasic formation in the reaction process of ILs synthesis are known to decline mass transfer.[6] Therefore, improving efficiency of mixing so that mass transfer does not become the rate determining step leads to improvement of productivity.

Flow microreactors (FMRs) are well known as effective tools for fast mixing, efficient heat exchange and precise residence time control.[7,8] Various applications using FMRs such as formation of alkyl lithium species,[9] anion polymerization[10] and exothermic reactions[11] have been reported. FMR can be said to be one of promising candidates for realizing highly productive processes for ILs synthesis. There have been many reports and reviews on Ils synthesis using FMRs and/or continuous flow process, [12,13,14,15] and they show that FMRs can more accuracy control reactions and drastically reduce reaction time compared to batch reactors. But the production volume is not high enough to meet real production requirement. Increasing the production of FMRs is often done by numbering-up. However, as the number of parallelized reactors becomes large, the structure of the numbering-up system becomes complicated and its stable operation may be difficult. Therefore, it is desirable to avoid thoughtlessly increasing the number of parallelized reactors through examination of appropriate design and operation conditions that make the production of a single reactor as high as possible.

Figure 1 shows a flowchart of chemical process development using FMRs. Currently, such process development is often advanced by trial and error involving repeated experiments, which take a lot of time and cost. In order to improve process development efficiency, it is important to use simulation as well as experiment. In the flowchart, after defining a design problem where objectives and requirements are given, the reaction kinetics, the optimum device and the optimum process are efficiently derived through modelling, simulation, experiment and optimization. At the stage of reaction rate analysis, which is key for chemical process development, the use of FMRs gives more accurate reaction data, which lead to realization of reaction rate analysis with higher prediction accuracy. At the stage of device and process development, it is necessary to derive design conditions such as channel shape and sizes as well as operating conditions such as flow rates and temperature that

maximize/minimize the objective functions (e.g., space time yield and deviation from desirable reaction temperature) while satisfying the constraints. Such derivation will be able to proceed efficiently by use of modelling and simulation tools. For example, Computational Fluid Dynamics (CFD) simulation is one of effective tools for estimating the detailed distributions of velocity, temperature, and concentration in the reactors.[16] CFD simulation is superior in that it can visualize and quantitatively evaluate how the design modification influences chemical processing. There are many reports on application of CFD modeling to microreactors and microfluidic devices.[17,18] It can be applied not only to the reactor design but also to the improvement of the process design.[19,20] But, there have been no report aiming to shorten the development time of ILs synthesis processes by using CFD simulation.

In this research, an FMR-based process of synthesizing ILs is designed according to Figure 1. In chapter 2, our constructed experimental system and reaction rate analysis are described. In chapter 3, the design of FMR-based process is efficiently investigated by using CFD simulation. In the final chapter, summary of the results obtained, discussion and future prospects will be stated.

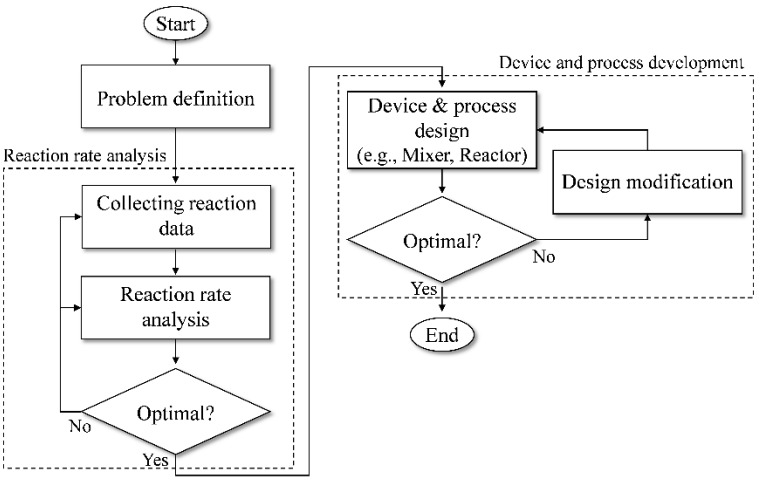

Figure 1. Flowchart of developing chemical processes

2. Reaction rate analysis

The accuracy of simulation models for reactors depends on reaction rate analysis. In this chapter, a targeted reaction system, a constructed experimental setup and the result of reaction rate analysis are shown.

2.1 Targeted reaction system

BMIM.Cl **3** is a short for 1-butyl-3-methylimidazolium chloride, which is one of ILs of current interest in industry due to its ability to be infinitely recycled and its solubility at room temperature, making it an excellent green solvent. BMIM.Cl is also the most common starting material for room temperature ILs BMIM.BF4, BMIM.PF6 and many others via ion exchange reaction. **3** was produced from **1 (**1-Methyl imidazole, MIM) and **2** (1-chlorobutane, BuCl) as starting materials (Scheme 1.).

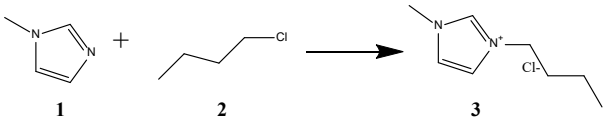

1 2 3

Scheme 1. Synthesis of BMIM.Cl

2.2 Experimental system

Figure 2 shows a constructed FMR-based experimental system. The FMR mainly consisted of mixers (M1 and M2) and tubular reactors (R1, R2, R3 and R4).

(a)

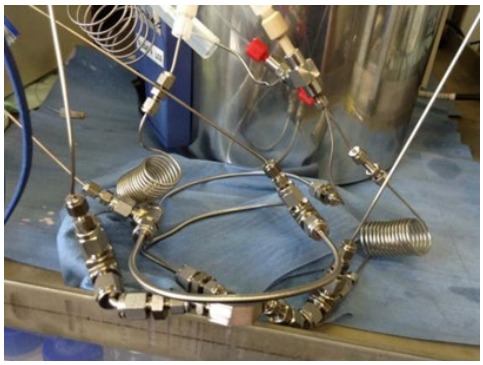

(b)

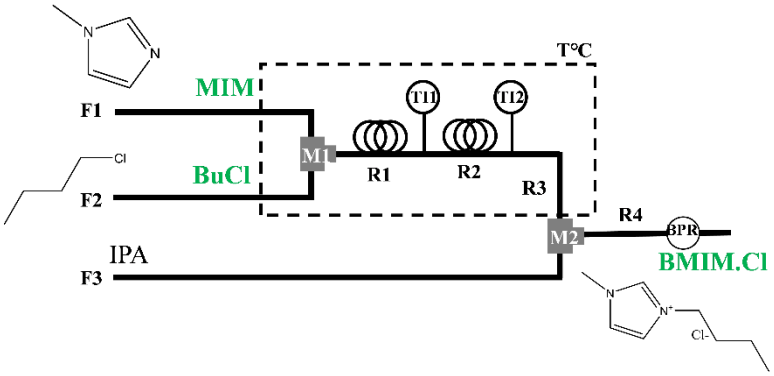

Figure 2. FMR-based experimental system: (a) photo of the part immersed in the oil bath and (b) process flow diagram.

F1, F2, F3 : plunger pump, M1, M2 : micromixer, R1, R2, R3, R4 : coiled reactor, TI1, TI2 : K-type thermocouple

Results and Discussion

The relationship between temperature, residence time, and the product yield was examined using the developed experimental system. Reaction temperature was controlled by the oil bath, and residence time was controlled by adjusting the feed flow rates (For example, when the total flow rate is 1.32 mL/min, the residence time is 1 min.). The examination result is shown in Figure 3. Over the whole experiment, the feed molar ratio of MIM and BuCl was fixed at 1:1.1, and the back pressure was set at 0.7 MPa. It was shown that as the reaction temperature becomes high, the yield at each residence time becomes high. But, when the reaction temperature was 180°C, the product quality was deteriorated due to coloration.

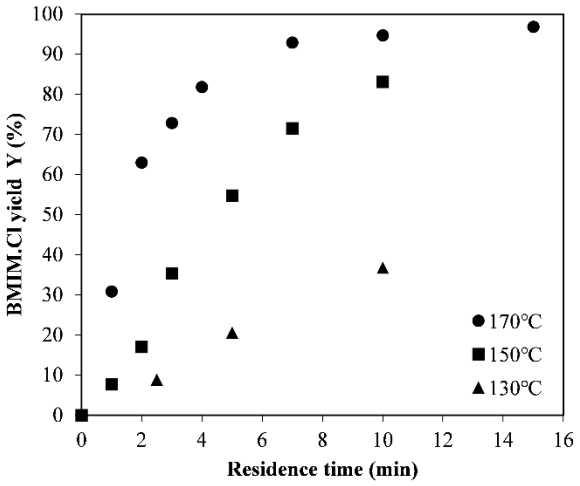

Figure 3. Yield profiles of ILs synthesis at different temperatures

▲ : 130°C, ■ : 150°C, ● : 170°C

In this study, reaction rate analysis was performed using an isothermal plug flow reactor (PFR) model. As will be explained later, the CFD simulation result shows that the temperature distribution in the reactor used is almost uniform. Therefore, the reactor was assumed to be isothermal. In addition, when the dispersion in the reactor was evaluated on the basis of the dimensionless parameter Pe (Péclet number), Pe of the present system was considerably larger than 1. This means that the deviation from plug flow is small. Therefore, PFR model was selected in this study.

The rate expression in the PFR model can be written as a product of a temperature-dependent term and a

composition-dependent term. In this study, it was assumed that the rate of disappearance of MIM is given by

$$-r_{\mathrm{MIM}} = kC_{\mathrm{MIM}}C_{\mathrm{BuCl}} \quad (1)$$

where k is the temperature-dependent term, i.e., the reaction rate constant, which is well presented by Arrhenius law:

$$k = k_0 e^{-E/\mathrm{R}T} \quad (2)$$

where k_0 is called the frequency or pre-exponential factor and E is called the activation energy of the reaction. The temperature dependency of reactions is determined by the activation energy and temperature level of the reaction. The Arrhenius plot is obtained by plotting the logarithm of the rate constant, k, versus the inverse temperature, $1/T$. Figure 4 shows the result of Arrhenius plot in this study. The plot of ln k vs $1/T$ gave a straight line. As a result, E = 104.75 kJ/mol and $k_0 = 4.99\times10^6$ m^3/(mol s) were derived. To validate the derived Arrhenius parameters, the experimental and simulation results when the reaction temperature was 170°C were compared in Figure 5. Since the experimental result and the PFR simulation result were almost in agreement, the validity of the obtained Arrhenius parameters was confirmed. The CFD simulation shown in Figure 5 is explained in Chapter 3.

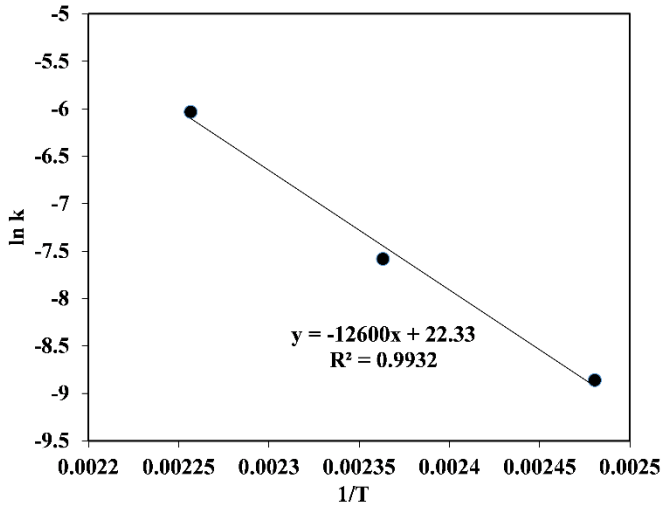

Figure 4. Arrhenius Plot of reaction rate

3 temperature condition (130, 150, and 170°C) was used.

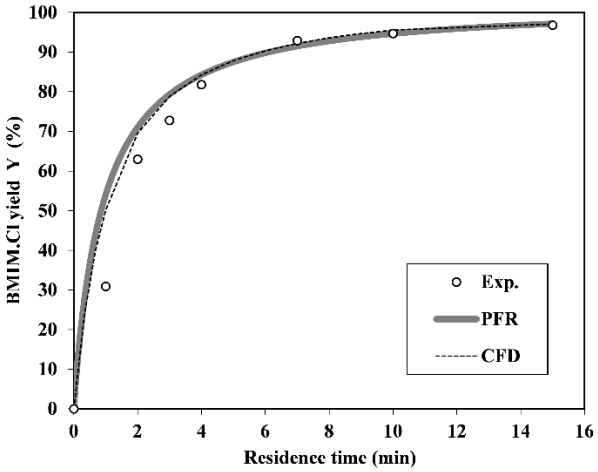

Figure 5. Comparison between simulation and experiment on product yield profile at 170℃

3. FMR-based process design

In this chapter, the FMR-based process of synthesizing ILs is efficiently analysed and designed using CFD simulation. The design objective is to increase the production volume while suppressing the decline in product yield and product quality.

3.1 Basic settings of CFD simulation

CFD allows to model heat and fluid flow processes in FMRs with different channel shapes and sizes. In this study, CFD simulation was performed using ANSYS Fluent® v17.0, which is based on the finite volume method. The common settings of CFD simulation performed in this study are as follows: In the FMR, modelling of hydrodynamics, heat and mass transfer, and chemical reactions is important. Reynolds number based on the fluid velocity and channel diameter is a low value making the flow definitely laminar. The energy equation and the species conservation equations are solved along with the momentum and continuity equations for steady state laminar and incompressible flow. Negligible gravity is used to evaluate the flow characteristics. The physical properties of species and reaction enthalpy are summarized in Table 1, and the result obtained in Chapter 2 is used for the reaction rate expression. Table 1 was obtained from literature.[21, 22, 23] The channel geometry of mixers and tubular reactors is presented in the following sections. The device under consideration is divided into some control volumes (cells) that are discretized by means of an unstructured numerical grid.

The conservation equations for mass, momentum, energy, and species are solved on this set of control volumes. The typical size of each cell element is 75 □m and the total number of cells are roughly 5,000,000 in this study. As for boundary conditions, uniform distribution of velocity, temperature and species mass fraction is stated at each channel inlet. Their specific values are given according to the experiment. Atmospheric pressure is stated at each channel outlet. The temperature of the wall is assumed to be equal to the temperature of the oil bath. Zero velocity is imposed on the wall. Regarding solver settings, ANSYS Fluent® is used in double precision, which will result in less round-off errors and may improve accuracy and convergence. The SIMPLE (Semi-Implicit Method for Pressure Linked Equations) algorithm is used to solve the pressure-velocity coupling equation. The second-order upwind difference scheme is employed for spatial discretization related to variables such as pressure, momentum, and temperature.

Under the above-mentioned conditions, CFD simulation using ANSYS Fluent® was carried out in this study. Figure 5 shows that CFD simulation can accurately predict the product concentration profile in the FMR used in this study. It can be said that CFD simulation is effective, and it is used in the following sections to reduce trial and error experiment.

Table 1. Physical properties of components

	Molecular weight (g/mol)	Density (kg/m^3)	Reaction enthalpy (kJ/kmol)	Heat Capacity (J/kg·K)
MIM	82.11	1030	-	1794
BuCl	82.57	873	-	1716
BMIM.Cl	174.67	1080	-1.49×10^7	1711

Mixing of raw materials is one of the important unit operations in the FMR-based process of synthesizing ILs. In the previous report, [13] the vortex-shaped mixer, to which each raw material is supplied after being divided into four, was used, as shown in Figure. 6 (c). The vortex-shaped mixer can be a good candidate for use in this research, but other candidates include T- and V-shaped mixer, as shown in Figure. 6 (a) and (b). T- and V-shaped mixers are simpler in channel structure than vortex-shaped mixers and have been widely used in micro chemical processes so far. Mixers with simpler channel structure are preferable from an operational point of view. In this section, the effects of T-, V-, and vortex-shaped mixers on the product yield distribution along the

R1 were examined by CFD simulation. T- and V-shaped mixers were assumed to have the almost same inner diameter as the previously reported vortex-shaped mixer having the inner diameter of 0.45 mm. Regarding the total flow rate, 0.13 mL/min corresponding to the lower limit of the assumed range was set. The mixing performance of mixers basically increases as the flow rates increase. In this research, a mixer that can achieve high mixing performance and high product yield even at low flow rate is selected. Regarding the temperature, the temperature of the oil bath was set to 170°C. The other design and operation conditions were set in the same way as the experimental conditions in Chapter 2.

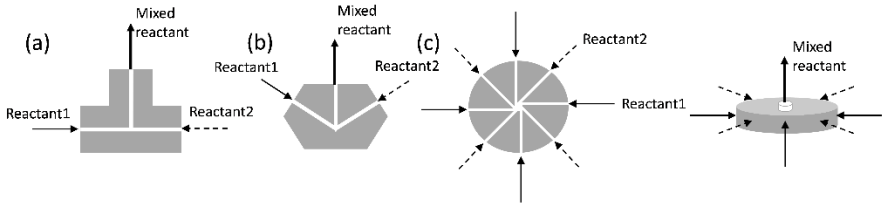

Figure 6. Schematic diagram of mixers:T-shaped mixer (0.5 mm I.D.), (b) V-shaped mixer (0.5 mm I.D.), (c) Vortex shaped mixer (0.45 mm I.D.)

Figure 7 shows the CFD simulation results where the mass-averaged concentrations of BMIM.Cl at channel cross sections are plotted along the flow direction of R1. While the result of the V-shaped mixer showed the same result as the vortex-shaped mixer, the result of the T-shaped mixer was slightly declined among the three. This is because the V- and vortex-shaped mixers is superior in mixing efficiency. As in this simulation result, there is other report that the mixing performance of V-shaped mixers is higher than that of T-shaped mixers.[24] From the result of this CFD simulation study, it was decided that V-shaped mixers are selected because its channel structure is simpler while exhibiting the same mixing performance as the vortex-shaped mixer.

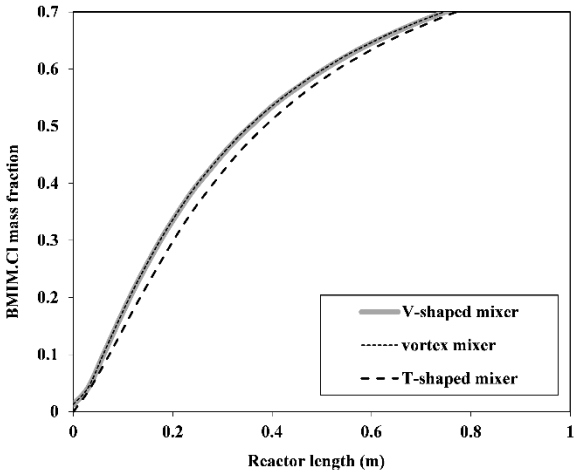

Figure 7. CFD simulation result of product distribution along the reactor connected with different mixers: T-, V-, and vortex-shaped mixers

3.3 Reactor design

After mixing the stating materials, the reaction of synthesizing ILs proceeds in the reactor. An increase in the production volume of the reactor is basically achieved by an increase in the reaction temperature, the flow rate, the size of the reactor and so on. By making the reactor length longer as the flow rate is increased, the desired residence time (reaction time) is maintained, but the pressure loss increases. If the inner diameter of the reactor is increased instead of the length of the reactor, the ability to remove the heat of reaction is reduced. In this section, the effects of reactors having four different inner diameters of 0.75 mm, 2.16 mm, 4.35 mm, and 7.53 mm on the temperature and product concentration distributions were examined by CFD simulation. In every case, the V-shaped mixer was used, and the temperature of the oil bath and the residence time were fixed at 170°C and 10 min., respectively. The other design and operation conditions were set in the same way as the experimental conditions in Chapter 2.

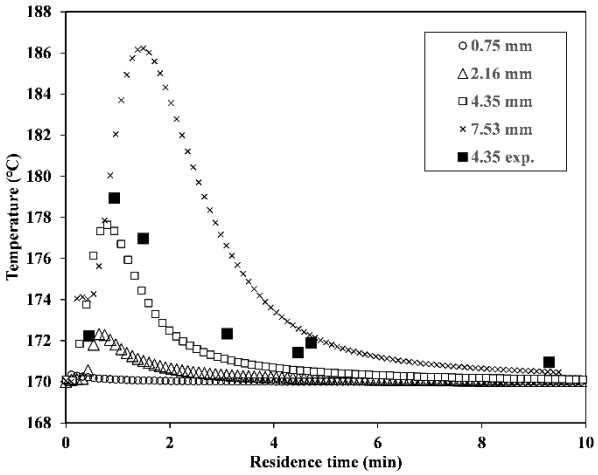

Figure 8. CFD simulation result of temperature distribution along the reactors with different inner diameters

○ : 0.75 mm I.D. (0.13 mL/min), △ : 2.16 mm I.D. (1.0 mL/min),

□ : 4.35 mm I.D. (4.5 mL/min), ■ : 4.35 mm I.D. (Experimental)

× : 7.53 mm I.D. (12.0 mL/min)

Figure 8 shows the CFD simulation result of temperature profiles. Each profile was derived by calculating mass-averaged values at the channel cross sections in the flow direction of each reactor. The temperature distribution measured by experiment in the case of the reactor having an inner diameter of 4.35 mm as a representative of four kinds of reactors was also shown. At this time, it can be seen that the experimental result and the simulation result almost agree. In addition, it was confirmed that the temperature distribution in the reactor having an inner diameter of 0.75 mm, which was used for reaction rate analysis, was almost uniform. Among the four kinds of reactors, it was shown that the reaction temperature in the reactor having an inner diameter of 7.53 mm greatly exceeded 180°C due to decrease in the heat exchange performance and that the product quality was deteriorated due to coloration. In addition, it was shown that the unevenness of temperature distribution in the radial direction tended to increase as the inner diameter increased (data not shown).

Figure 9 shows the CFD simulation result of product concentration profiles for reactors having three different inner diameters of 0.75 mm, 2.16 mm, and 4.35 mm, which satisfy temperature constraints on product quality. Although reactors with larger inner diameter are preferable from an operational point of view, it was shown that the product yield tended to decrease as the inner diameter increased. This is because mass transfer decreased as

the inner diameter became large.

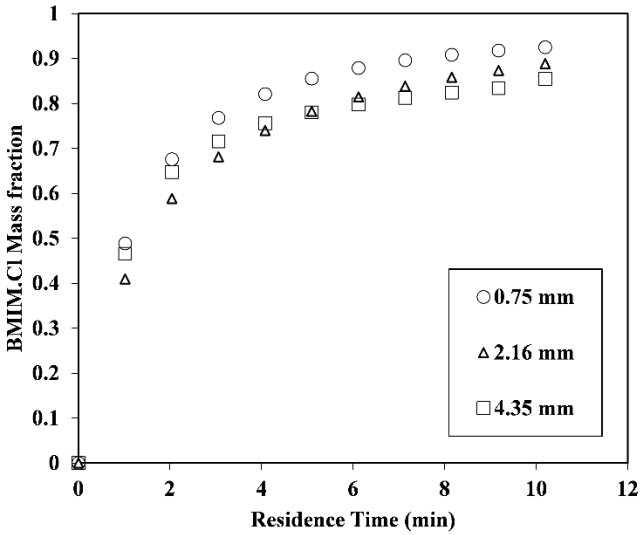

Figure 9. ILs synthesis profiles on tubular diameter

○ : 0.75 mm, △ : 2.16 mm, □ : 4.35 mm

3.4 Reactor with built-in static mixers

From the results in the previous section, it is suggested that improvement of not only heat transfer but also mass transfer performance is necessary when the inner diameter is increased. In this study, it was proposed that PTFE helical static mixers (SMs; 3.0 mm diameter, 37 mm length; Stamixco, Switzerland) are built in the second half of each reactor having the inner diameter of 4.35 mm. In this section, experimental investigation was proceeded to evaluate the usefulness of the proposed method. Figure 10 shows the results of the product yield when the reactors with/without SMs were used. It is demonstrated that use of SMs makes it possible to solve the problem of lowering the product yield when the inner diameter of the reactor is large. Table 2 shows comparison of production volume. As a result, the production volume of the reactor with built-in SMs, without lowering the product yield, could be improved about 39 times compared with the conventional one.

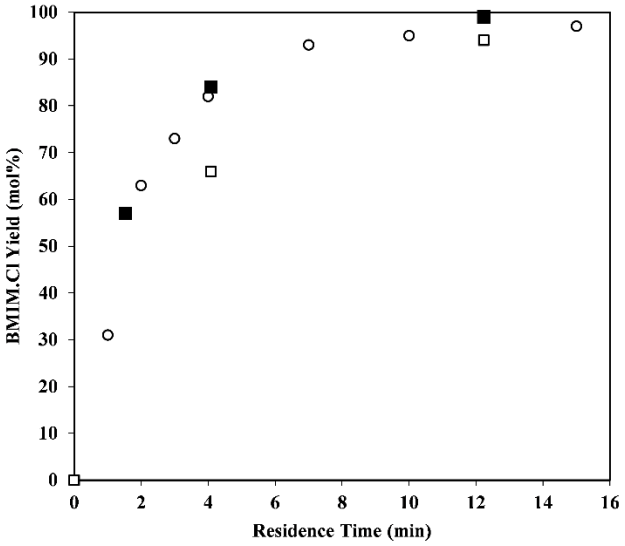

Figure 10. Experimental result of ILs synthesis

○ : 0.75 mm I.D. without build-in SMs, □ : 4.35 mm I.D. without build-in SMs, ■ : 4.35 mm I.D. with build-in SMs

Table 2. Reaction condition and experimental results for the SMs condition

	I.D. (mm)	Flow rate (mL/min)	Conversion (%)	Yield (%)	Production volume (kg/day)
FMR	0.75	0.13	100	94.4	0.19
FMR + SMs	4.35	4.50	100	>99	6.93

Experimental Section

V-shaped stainless mixers with an inner diameter of 0.5 mm (Sankoh-seiki, Japan) were used as M1 and M2. R1, R2 and R3 were made of Hastelloy® (0.75 mm ID, 1.0 m length). R4 is made of Hastelloy® (0.75 mm ID, 1.0 m length) and PFA (1.00 mm ID, 1.0 m length), respectively, coupled by standard ETFE and PEEK unions and ETFE fittings and ferrules from IDEX. A back pressure valve pre-set at 0.7 MPa was attached to the outlet of R4. The FMR excluding M2 and R4 was immersed in an oil bath with a constant temperature, and the fluid temperatures at the outlets of R1 and R2 were measured by K-type thermocouples (Sukegawa-denki, Japan),

which were denoted as TI1 and TI2. Reagents were pumped with automated plunger pumps (Vapourtec R-series). In this study, neat MIM and BuCl were constantly supplied to M1 through F1 and F2 lines, respectively. At the outlet of R3 the reaction mixture and IPA, which was delivered through F3 line, were mixed at M2. The IPA was used to quench the reaction and to prevent precipitation of product.

The product stream after M2 was sampled into 20 mL vials. Each sample was analyzed in the following two ways. The first one is the use of NMR. The resulting NMR spectra were used to determine the weight percentages of BMIM.Cl, MIM, BuCl and IPA. Another one is to measure the weight of BMIM.Cl after washing and drying of the product stream. Specifically, the contents of the vials were first concentrated by separating starting materials and IPA using a V-10 Evaporator (Biotage) and then dried under vacuum at 60°C for a long period (> 48 hours) to remove traces of them. Based on these analysis results, the next defined variable is calculated:

$$Y = \frac{W_{\mathrm{BMIM.Cl}}}{F_{\mathrm{MIM}} \cdot t_{\mathrm{sampling}}} \times 100 \tag{3}$$

where t_{sampling} sampling time of the product stream, F_{MIM} mass flow rate of MIM supplied to M1, and $W_{\mathrm{BMIM.Cl}}$ weight of BMIM.Cl obtained after washing and drying of the product stream.

Conclusion

A synthesis process of ionic liquids (ILs), 1-bythyl-3-methylimidazolium chloride (BMIM.Cl), was developed using a flow microreactor (FMR) in this study. After the reaction rate analysis, FMR was efficiently designed using CFD simulation. As for the mixer selection, through the CFD simulation, the V-shaped mixer was efficiently selected from several mixer candidates. This means that the time and cost consumed in experiments with various mixers have been reduced. In addition, CFD simulation showed that management of the reaction temperature inside the tubular reactor and acceleration of mass transfer are important for improvement of product yield and product quality. Utilizing the knowledge obtained in this way, the reactor with larger inner diameter incorporating the static mixer has been successfully developed. Reactors with larger inner diameter are desirable from the viewpoints of stable operation and increase in production volume, and it is expected that studies toward practical application of this process will be made in the future.

References and notes

1. Wasserscheid, P.; Keim, W. Ionic Liquids—new “Solutions” for Transition Metal Catalysis. Angew. Chemie Int. Ed. 2000, 39 (21), 3772–3789.
2. (2) Welton, T. Room-Temperature Ionic Liquids . Solvents for Synthesis and Catalysis. Chem. Rev. 1999, 99, 2071−2083.
3. (3) Holbrey, J. D.; Seddon, K. R. Ionic Liquids. Clean Prod. Process. 1999, 1 (4), 223–236.
4. (4) https://www.marketreport.jp/research/mam-ch-4297 (Access 2019.Jan.18)
5. (5) Große Böwing, A.; Jess, A. Kinetics of Single-and Two-Phase Synthesis of the Ionic Liquid 1-Butyl-3-Methylimidazolium Chloride. Green Chem., 2005, 7, 230–235.
6. (6) Fendt, S.; Padmanabhan, S.; Blanch, H. W.; Prausnitz, J. M. Viscosities of Acetate or Chloride-Based Ionic Liquids and Some of Their Mixtures with Water or Other Common Solvents. J. Chem. Eng. Data 2011, 56, 31–34.
7. (7) Abe, A.; Lee, K.; Leibler, L.; Kobayashi, S.; Nagaki, A.; Yoshida, J. Controlled Polymerization and Polymeric Structures. Adv. Polym. Sci. 2013, 259, 1–50.
8. (8) Wilms, D.; Klos, J.; Frey, H. Microstructured Reactors for Polymer Synthesis: A Renaissance of Continuous Flow Processes for Tailor-Made Macromolecules? Macromol. Chem. Phys. 2008, 209 (4), 343–356.
9. (9) Nagaki, A.; Imai, K.; Ishiuchi, S.; Yoshida, J. Reactions of Difunctional Electrophiles with Functionalized Aryllithium Compounds: Remarkable Chemoselectivity by Flash Chemistry. Angew. Chemie Int. Ed. 2015, 54 (6), 1914–1918.
10. (10) Nagaki, A.; Tomida, Y.; Yoshida, J. Microflow-System-Controlled Anionic Polymerization of Styrenes. Macromolecules 2008, 41 (17), 6322–6330.
11. (11) Rosenfeld, C.; Serra, C.; Brochon, C.; Hadziioannou, G. High-Temperature Nitroxide-Mediated Radical Polymerization in a Continuous Microtube Reactor: Towards a Better Control of the Polymerization Reaction. Chem. Eng. Sci. 2007, 62 (18–20), 5245–5250.
12. (12) Waterkamp, D. A.; Heiland, M.; Schlüter, M.; Sauvageau, J. C.; Beyersdorff, T.; Thöming, J.

Synthesis of Ionic Liquids in Micro-Reactors - A Process Intensification Study. Green Chem., 2007, 9, 1084–1090.

13. (13) Renken, A.; Hessel, V.; Löb, P.; Miszczuk, R.; Uerdingen, M.; Kiwi-Minsker, L. Ionic Liquid Synthesis in a Microstructured Reactor for Process Intensification. Chemical Engineering and Processing, 2007, 46, 840–845.
14. (14) Löwe, H.; Axinte, R. D.; Breuch, D.; Hofmann, C.; Petersen, J. H.; Pommersheim, R.; Wang, A. Flow Chemistry: Imidazole-Based Ionic Liquid Syntheses in Micro-Scale. Chemical Engineering Journal 2010, 163, 429–437.
15. (15) Eduardo García-Verdugo, Belen Altava, M. Isabel Burguete, Pedro Lozanob and S. V. Luisa, Ionic liquids and continuous flow processes: a good marriage to design sustainable processes. Green Chem., 2015, 17, 2693-2713.
16. (16) Patankar, S. V. Numerical Heat Transfer and Fluid Flow Hemisphere, New York, 1980, 41–135.
17. (17) Gravesen, P.; Branebjerg, J.; Jensen, O, S.; Microfluidics-a review, Journal of Micromechanics and Microengineering, 1993, 3 (4), 168-182
18. (18) Song, Y.; Cheng, D.; Zhao, L. Microfluidics: Fundamentals, Devices, and Applications" John Wiley & Sons, 2018, Jan 4
19. (19) Tonomura, O.; Tanaka, S.; Noda, M.; Kano, M; Hasebe, S.; Hashimoto, I. CFD based optimal design of manifold in plate-fin microdevices. Chem. Eng. J., 2004, 101, 397–402
20. (20) Wang, K.; Lu, Y.; Xia, Y.; Shao, H.; Luo, G. Kinetics research on fast exothermic reaction between cyclohexanecarboxylic acid and oleum in microreactor. Chem. Eng. J., 2011, 169, 290-298
21. (21) Dharaskar, S. A.; Varma, M. N.; Shende, D. Z.; Yoo, C. K.; Wasewar, K. L. Synthesis, Characterization and Application of 1-Butyl-3 Methylimidazolium Chloride as Green Material for Extractive Desulfurization of Liquid Fuel. Sci. World J. 2013, 1-9.
22. (22) Mariano, A.; Camacho, A.; Postigo, M.; Valen, A.; Artigas, H.; Royo, F. M.; Urieta, J. S. Viscosities and Excess Energy of Activation for Viscous Flow for Binary Mixtures of Tetrahydrofuran with 1-Butanol, 2-Butanol and 1-Chlorobutane at 283.15, 298.15 and 313.15 K. Brazilian J. Chem. Eng. 2000, 17, 4-7.

23. (23) Verevkin, S. P.; Zaitsau, D. H.; Emel, V. N.; Ralys, R. V; Yermalayeu, A. V; Schick, C. Thermochimica Acta Does Alkyl Chain Length Really Matter ? Structure – Property Relationships in Thermochemistry of Ionic Liquids. Thermochim. Acta 2013, 562, 84–95.
24. (24) Siconolfi, L.; Fani, A.; Camarri, S.; Salvetti, M. V. Fluids Effect of Geometry Modifications on the Engulfment in Micromixers : Numerical Simulations and Stability Analysis. European Journal of Mechanics B 2016, 55, 360–366.

Chapter 5

A Manufacturing Strategy Utilizing a Continuous Mode Reactor toward Homogeneous PEGylated Bioconjugate Production

Abstract

Protein PEGylation is a traditional bioconjugation technology that enhances the therapeutic efficacy and *in vivo* half-life of proteins by the formation of covalent bonds with highly activated ester group linking polyethylene glycol (PEG). However, the high reactivity of these reagents induces a random reaction with lysine residues on the protein surface, resulting in a heterogeneous mixture of PEGylated proteins. Moreover, the traditional batch-mode reaction has risks relating to scalability and aggregation. To overcome these risks of traditional batch-mode PEGylation, a manufacturing strategy utilizing structural analysis and a continuous-flow-mode reaction was examined. A solvent exposure analysis revealed the most reactive lysine of a protein, and the continuous flow mode modified this lysine to achieve the mono-PEGylation of two different proteins within two seconds. This ultra-rapid modification reaction can be applied to the gram-scale manufacturing of PEGylated bioconjugates without generating aggregates. A similar trend of the exposure level of protein lysine and mono-selectivity performed by continuous-flow PEGylation was observed, which indicated that this manufacturing strategy has the potential to be applied to the production of a wide variety of bioconjugates.

Introduction

Protein PEGylation is a modification technique that forms a covalent link between polyethylene glycol (PEG) and a protein. [1-3] This traditional conjugation approach enhances the therapeutic efficacy and safety profile of protein-based biopharmaceutics due to the hydrophilic nature of PEG molecules. Currently, many PEGylated proteins are approved by the US Food and Drug Administration[4]. PEG reagents possessing activated esters, such as N-hydroxysuccinimide (NHS), are widely used in this technique. These reagents modify the lysine residues of proteins to form covalent bonds and create PEGylated conjugates. The conjugation concept is simple; however, most PEGylated proteins currently on the market have wide heterogeneity owing to nonspecific protein modifications, resulting in clinical insufficiencies. Furthermore, this heterogeneous nature of current PEGylated proteins may be problematic in terms of chemistry, manufacturing, and control (CMC) challenges. The wide distribution of PEGylation sites and structural complexity make batch-to-batch consistency analysis challenging. In addition to the heterogeneous nature of PEGylated proteins, the chemical reaction to install PEG poses a risk of aggregation generation.[5] In particular, several sensitive proteins may have limited compatibility with chemical reactions such as PEGylation; therefore, mild reaction conditions with short reaction times should allow for more reliable conjugations. Furthermore, kinetic reactions, such as amidation by activated ester reagents such as NHS, can cause scalability issues.[6] To overcome the aggregation and scale gap issues in protein PEGylation, a variety of chemical reactions are required during the early stages of manufacturing, including screening of functional groups to react with the amino acid residues of the target protein and/or careful process development. A promising option for achieving homogeneous PEGylation is to utilize a continuous-mode flow reaction. The continuous flow reaction is a rapidly growing manufacturing process in industry.[7,8] This process enables chemical reactions in designated systems consisting of tubes, mixers, and pipes. Flow-mode manufacturing equipment can perform sensitive novel chemical reactions that cannot to be controlled in traditional stirred-batch reactors[9]. Furthermore, this process is environmentally friendly, as it reduces the risk of accidental exposure to toxic chemicals,[10] and is straightforwardness to scale-up.[11] Based on these advantages, a flow microreactor (FMR) system can reduce operating expenditures and facilitate automated manufacturing of industrial materials. PEGylation in continuous mode has been attempted by several groups using proprietary systems such as the on-column counter-current chromatograph,[12] hollow-fiber membrane reactor,[13,14] and coiled flow inverter reactor.[15] These fundamental

studies demonstrated the feasibility of protein PEGylation using FMR to achieve bioconjugation with native lysine amino acid side chains. However, this type of lysine conjugation produces a heterogeneous mixture of conjugate molecules. For example, typical IgG1 antibody proteins have greater than 80 exposed and reactive lysine residues[16] indicating that careful optimization of the reaction conditions is required despite the use of an FMR system. Amino acid nature differs among protein bases; therefore, careful reaction optimization that is dependent on protein characteristics is required. These results prompted us to investigate a versatile manufacturing strategy that supports continuous-mode PEGylation. To establish a practical strategy for homogeneous PEGylated protein manufacturing, the author conducted demonstration studies using traditional lysine-based PEGylation with PEG reagents functionalized by an activated ester group. The author hypothesized that the exposed lysine groups would have higher reactivity to PEGylation; therefore, the author investigated the relationship between the exposure level of each lysine in the protein and the reaction selectivity. Solvent exposure analysis[17] enabled us to predict the reactivity of each lysine in the protein, and the resultant trends were compared with the site selectivity of PEGylation produced using a continuous mode reaction. For this demonstration, a V-shaped mixing system that can be easily applied at the manufacturing scale was selected. Feasibility flow system trials enabled the mono-PEGylation of therapeutic proteins such as lysozyme and interleukin-6 (IL-6) within two seconds (Figure 1). Furthermore, this "ultra-rapid" and mild reaction condition was successfully applied to a gram-scale synthesis of the PEGylated protein without aggregation generation, whereas batch mode synthesis revealed scale-gap issues.

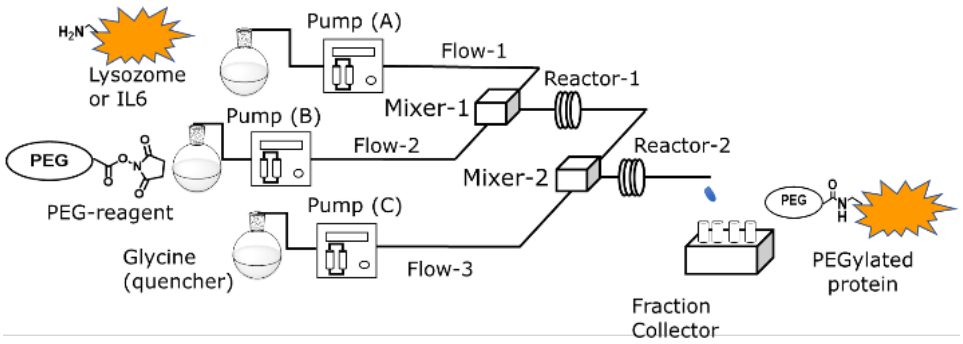

Figure 1. Flow diagram of continuous flow protein PEGylation.

Results and discussion

Lysozyme has only six lysine groups in its sequence; therefore, the PEGylated product has a relatively low distribution (from mono-to hexa-conjugates). This inexpensive (USD 23 per gram; Millipore Sigma, accessed Jan 29, 2023) protein has been subjected to continuous PEGylation in several previous studies[14]. To predict the reactivity difference of each lysine, the author conducted solvent exposure analysis of the lysozyme structure reported in the Protein Data Bank (PDB) (Figure 2).[17,18] The results indicated that although all six lysozyme lysines were well exposed to the solvent, the solvent-accessible surface areas (SASAs) differed slightly. The most exposed lysine (Lys116) showed a 10 % higher SASA level than that of the second most exposed lysine (Lys97).

In addition to lysozyme, IL-6 levels were analyzed. IL-6 has a higher molecular weight and a greater number of lysine residues (14) than lysozyme. PEGylation of IL-6 enhanced the therapeutic efficacy of native IL-6;[19] however, only limited pharmaceutical applications were identified due to the heterogeneous nature of the conjugate[20]. First, the author attempted to apply the same calculation procedure as that used for lysozyme; however, 52–60 amino acid disorders were observed in the IL-6 structure reported in the PDB (PBD: 1ALU) (Supporting Information (SI), Figure S1).[21] To understand the actual structure, the author utilized the AlphaFold-2 database,[22,23] which contains a modified IL-6 monomer structure (AlphaFold Protein Structure Database: AF-P05231-F1-model_v4) that can be used for structural and SASA analyses. These analyses showed that all 14 lysines of IL-6 were well exposed to the solvent; however, the SASA levels of each lysine differed slightly. The most exposed lysine (Lys159) showed an SASA that was only 4 % higher than that of the second most exposed lysine (Lys98). These analyses revealed that IL-6 is a more challenging target than lysozyme for demonstrating this strategy.

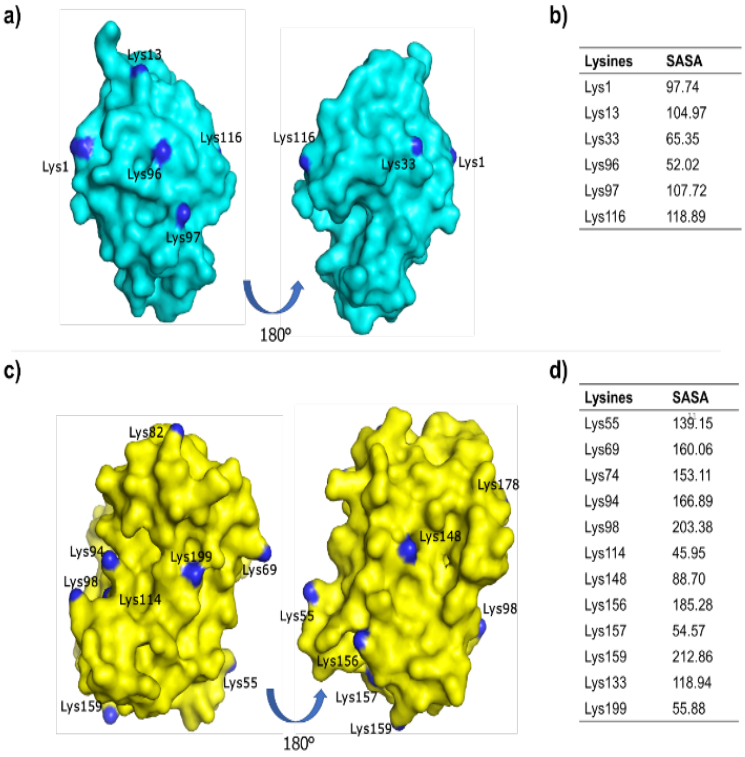

Lysines	SASA
Lys1	97.74
Lys13	104.97
Lys33	65.35
Lys96	52.02
Lys97	107.72
Lys116	118.89

Lysines	SASA
Lys55	139.15
Lys69	160.06
Lys74	153.11
Lys94	166.89
Lys98	203.38
Lys114	45.95
Lys148	88.70
Lys156	185.28
Lys157	54.57
Lys159	212.86
Lys133	118.94
Lys199	55.88

Figure 2 Predictions of exposure levels for lysines, a) structural analysis of lysozyme (PBD: 1dpx), b) SASA analysis of lysine residues in lysosome, c) structural analysis of IL-6 (AlphaFold-2: AF-P05231-F1-model_v4.pdb), d) SASA analysis of lysine residues in IL-6

Next, the author attempted to determine whether a continuous-flow system could be used to identify small reactivity differences and perform selective lysine modifications. Several studies [11,24] have reported that the FMR reaction is suitable for kinetically controlled reactions; therefore, our first attempt used PEG reagent screening. NOF Corporation, a main PEG reagent company in the bioconjugation field, provides reagents in different PEG units.[25] Batch-mode reaction screening revealed that methoxy-PEG-CH2-COO-NHS (5 kDa, catalog number SUNBRIGHT ME-050AS) showed the highest reactivity. The PEGylation reaction was completed in less than 1 min using SUNBRIGHT ME-050AS, whereas the other PEG reagents continued to react after 3 min (Supporting Information (SI) Figure S2). These reactivity trends were similar to that of the half-life of these PEG reagents[25] and supported the hetero-functional group placing in neighboring positions, which enhanced the reactivity of the NHS group and reduced hydrolysis resistance.

In the development of continuous reactions, several parameters must be considered[26, 27] such as the tube length, time, pH, and temperature of the reaction. However, the appropriate parameter depends on the target protein

behavior and this experimental design approach is beyond the scope of the current feasibility study. The purpose of this study was to demonstrate the developability of this modification strategy (SASA analysis scouting the target lysine followed by a continuous flow reaction). For this purpose, the author selected a tentative condition to apply to the PEGylation. The most important factors affecting mixability in flow systems are the geometry and diameter of the mixer unit, and the author selected conditions previously reported as effective for early selection[11, 26]. The iodide-iodate reaction, termed the Dushman reaction, is commonly used to evaluate mixing efficiencies[28,29] and the author previously confirmed the high reproducibility of this method,[25] whereby V-shaped mixers produced the most efficient mixability for several geometric types (Vortex-shaped, T-shaped, and V-shaped; Figure S3). Therefore, a V-shaped mixer was selected for PEGylation. Diameter is also a critical factor that affects the mixability of the flow system. Based on our previous study[10], a diameter of 0.25 mm was selected for use in the present investigation. Previously, our group succeeded in performing a tandem reaction (reduction of disulfide bonds of an antibody followed by conjugation with a cytotoxic drug) in continuous mode to produce antibody-drug conjugates (ADCs). A 0.25 mm diameter V-shaped mixer sufficiently converted naked antibodies to ADCs, while a mixer with a diameter greater than 0.5 mm did not reach the target drug-to-antibody ratio. The author expected that the 0.25 mm diameter V-shaped mixer that was applied to a complicated tandem bioconjugation to produce ADC could also be applied to a single reaction PEGylation. The flow system consisted of two V-shaped mixers (Mixer-1 and Mixer-2 in Figure 1) and two 0.25 mm reactors (Reactor-1 and Reactor-2 in Figure 1). The diameter of the reactors was 1.0 mm, and using a high flow rate (8 mL/min for lysozyme and 2 mL/min for PEG reagent), PEGylation was completed in 1.17 s (residence time in Reactor-1). The detailed calculations are below.

- reactor length; 250 mm = 0.25 m
- reactor diameter; 1 mm = 1×10^{-3} m
- reactor volume; 0.196 mL
- flow rate; 8 mL/min (Lysozyme) and 2 mL/min (PEG)
- reaction time = 1.17 s = 0.196 (mL)/10 (mL/min)

This rapid reaction mode enabled the production of a gram-scale PEGylated lysozyme within 15 min. The conversion yield and mono-PEGylation selectivity were analyzed using RP-HPLC (Figure 3 and Figure S4).

Additionally, a direct comparison was conducted between the PEGylated lysozyme produced using the batch-mode approach and that synthesized through the continuous flow system.

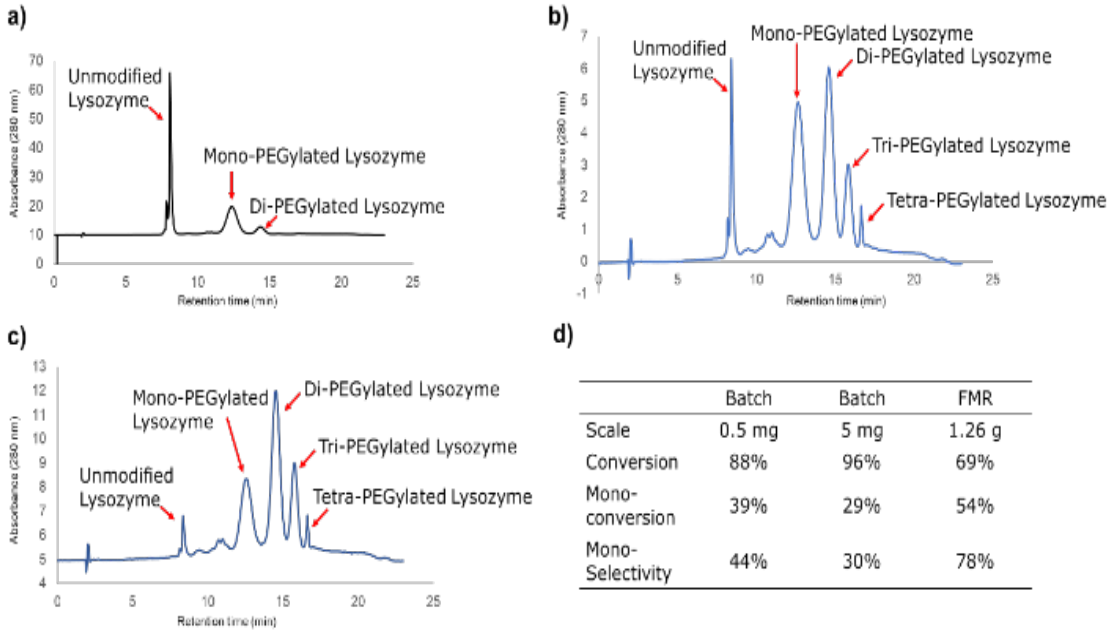

d)

	Batch	Batch	FMR
Scale	0.5 mg	5 mg	1.26 g
Conversion	88%	96%	69%
Mono-conversion	39%	29%	54%
Mono-Selectivity	44%	30%	78%

Figure 3 PEGylation of lysozyme a) HPLC analysis of PEGylated lysozyme produced with continuous flow mode (1.26 g scale), b) HPLC analysis of PEGylated lysozyme produced with batch mode (0.5 mg scale), c) HPLC analysis of PEGylated lysozyme produced with batch mode (5 mg scale), d) summary of mono-PEGylation

Continuous flow mode converted 54 % of the lysozyme to mono-PEGylated conjugates, showing a mono-selectivity of 78 %. In contrast, batch mode provided less than 40 % mono-conversion. In addition, the reproducibility and scalability of batch mode were clearly problematic. In larger-scale syntheses, the mono-conversion rate decreased, and an overreaction was observed. In addition to conversion yield, the ineffective mixability of the batch mode triggered aggregate generation (greater than 44 % by size-exclusion chromatography analysis (SEC),[30] Figure S5 in SI), whereas no aggregates were observed in the gram-scale conjugates produced in continuous mode. The author also performed a comparative SDS-PAGE analysis of these two PEGylated proteins to confirm their mono-selectivity. Due to the complex structure of bioconjugates, it is recommended to use several analytical methods to obtain more accurate results[31]. A comparison of the SDS-PAGE results supported the mono-selectivity of the PEGylated conjugates produced by FMR (Figure S6).

Next, continuous mono-PEGlylation was performed to modify IL-6 (Figure 4).

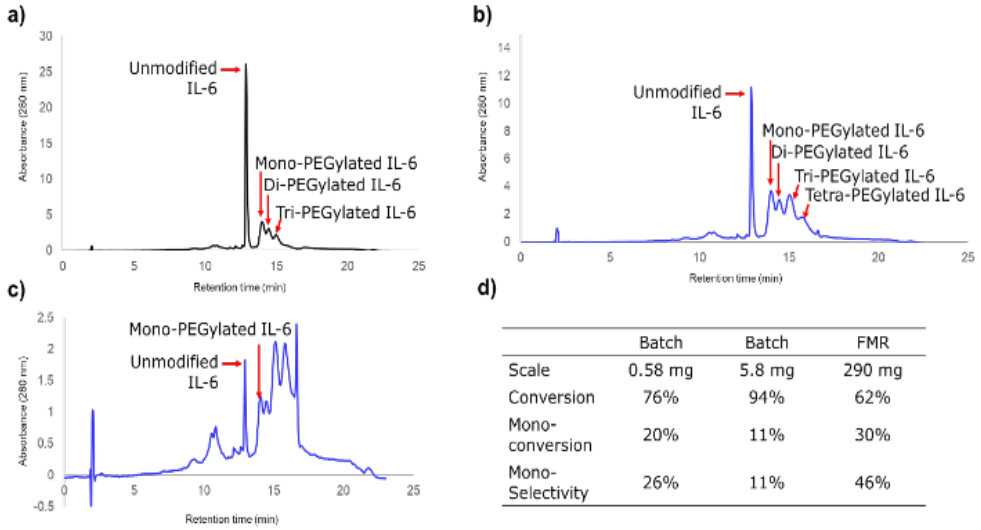

	Batch	Batch	FMR
Scale	0.58 mg	5.8 mg	290 mg
Conversion	76%	94%	62%
Mono-conversion	20%	11%	30%
Mono-Selectivity	26%	11%	46%

Figure 4. PEGylation of IL-6 a) HPLC analysis of PEGylated IL-6 produced with continuous flow mode (290 mg scale), b) HPLC analysis of PEGylated IL-6 produced with batch mode (0.58 mg scale), c) HPLC analysis of PEGylated IL-6 produced with batch mode (5.8 mg scale), d) summary of mono-PEGylation

Similar comparisons were obtained for the batch and continuous flow modes as those observed with lysozyme. Continuous flow mode converted 30 % of IL-6 to mono-PEGylated conjugates with a mono-selectivity of 46 %, while batch mode presented several issues (low mono-selectivity, reproducibility, and scalability, and high aggregation generation (greater than 54 % by SEC analysis, Figure S4 in SI)). IL-6 has more lysine residues, all of which are more exposed to solvent than those of lysozyme. Based on previously reported results[32,33], lysine residues with more than 20-25 SASAs can be defined as solvent exposed. This means that all lysine residues of both lysozyme and IL-6 used in this study are well exposed. However, the highest SASA value for lysozyme on lysine was 118.9 for Lys116, whereas IL-6 has eight lysine residues with higher SASA values. In addition, scatter plots and box plots were created for clear comparison of the variability of SASA values for each lysine residue in the respective proteins (Figure S6 in SI). It can be hypothesized that if the variability of SASA values for each lysine residue is low, it may be difficult to achieve selective PEGylation. However, the results showed that lysosome had lower variability in SASA values compared to IL6, indicating that lysosome had a higher prevalence of lysine residues with similar SASA values. On the other hand, IL6 showed higher variability in SASA values, but had a higher prevalence of highly exposed lysine residues compared to lysosome, as

mentioned earlier. Therefore, it can be speculated that the decrease in selectivity may be attributed to the higher prevalence of highly exposed lysine residues. Therefore, this exposure level difference caused a relatively lower mono-conversion rate in the IL-6 modification. Although this speculation requires further examples for conclusive assertions, the present results provide valuable guidance for evaluating the relationship between the kinetics-dominant reaction mediated by active groups such as NHS ester and SASA. The author also performed an SDS-PAGE analysis comparison of these two PEGylated proteins showing the mono-selectivity of PEGylated conjugates (Figure S7).

Experimental Section

Materials

Lysozyme (Chicken egg-white) was purchased from Sigma-Aldrich (USA). IL6 protein was expressed and purified as previously reported.[36] The PEG reagent (Methoxy-PEG-CH_2-COO-NHS, 5 kDa, catalog number SUNBRIGHT ME-050AS) was purchased from NOF Corporation (Japan). All other chemical reagents were purchased from Sigma-Aldrich (USA).

SASA Calculation

The SASA calculations were performed using the Bioluminate software suite (Bioluminate, version 2022-2, Schrödinger, Inc.). The initial structures of lysozyme (PDB:1DPX)[37] and IL-6 (AlphaFold Protein Structure Database: AF-P05231-F1-model_v4)[22,23] were protonated and minimized, and the SASA score was calculated using the Residue Analysis module.

Molecular modeling

The model structure of the proteins was generated as described previously.[38]

Experimental procedure for PEGylation using batch reactor

PEG reagent in DMSO (10.5 mg/mL, 1.66 mg or 16.6 mg) was added to a solution of protein (0.5 mg or 5 mg) in 20 mM Borate buffer (pH 9.0). The mixture was then incubated for 5 min at 20 °C. An excess of 50 mM glycine and 1 M acetate buffer (pH 4.7) was added to adjust the pH of the reaction mixture (to approximately pH 7.0) and the mixture was stirred for an additional 15 min. Subsequently, the reaction mixture was purified using a PD-10 desalting column and eluted with 50 mM acetate buffer (pH 5.5).

Experimental procedure for PEGylation using flow reactor

V- and T-shaped stainless-steel mixers with inner diameters of 0.25 mm (Sankoh-seiki, Tokyo, Japan) were used as Mixer-1 and Mixer-2, respectively, as shown in Figure 1. Reactor-1 (1.0 mm i.d., 0.25 m length) and Reactor-2 (1.0 mm i.d., 0.5 m length) were also made of stainless steel. The 50m M borate buffer containing the protein (1.05 mg/mL for lysozyme, 1.47 mg/mL for IL-6, pH 9.0) was added to Mixer-1 through Flow-1 (flow rate: 8 mL/min). The PEG reagent in DMSO (3.5 mg/mL, 4.2 g for lysozyme, 690 mg for IL-6) was added to Mixer-1 through Flow-2 (flow rate: 2 mL/min). The output mixture from Reactor-1 and that delivered from Flow-3 were mixed in Mixer-2. The glycine in the phosphate buffer (50 mM, excess, pH 7.4) was added to Mixer-2 through Flow-3. The output mixture of Reactor-2 was eluted into a fraction collector, to which an excess of 1 M acetate

buffer (pH 4.7) was added for neutralization. This elution was combined and purified using large desalting columns as previously reported.[39]

RP-HPLC methods

RP-HPLC analysis was performed on an PLRP-S 300A, 3 μm, 150 mm × 4.6 mm (Agilent Technologies, USA), connected to an Agilent 1260 HPLC system containing a binary gradient pump, temperature-controlled column compartment, autosampler, and a diode array detector. The system ran at 1.0 mL/min at 70 °C using 0.1% trifluoroacetic acid (TFA) in water (mobile phase A, MPA) and 0.1% TFA in acetonitrile (ACN) (mobile phase B, MPB), and absorbance was monitored at 280 nm (reference wavelength at 450 nm). All protein samples (2.0 mg/mL, 20 μL) were injected into the system sequentially and eluted with a 25 min method consisting of a 2 min isocratic hold at 24% MPB, a 18 min linear gradient from 24% to 56% MPB, a 3 min wash using 95% MPB, and a 2 min re-equilibration at 24% MPB.

Other instruments/analytical methods

The concentration of proteins was determined using the Slope Spectroscopy® method with a Solo-VPE system.[40] Size exclusion chromatography[30] was performed as previously reported.

Conclusion

In conclusion, a manufacturing strategy utilizing SASA analysis and continuous-flow process-mediated PEGylation was achieved using two proteins that have potential for clinical use. The selected 0.25 mm diameter V-shaped mixer performed rapid (1.17 s) protein modification to achieve mono-selective PEGylation without inducing appreciable aggregation. All flow processes were conducted using a scaled-down manufacturing approach with a sequential mixing system. Furthermore, these early stage (not thoroughly optimized) reaction conditions were able to generate gram-scale PEGylated lysozymes within 15 min. The exposed lysine trend calculated by SASA analysis was similar to that of mono-selective production in the continuous mode. The results described herein indicate that the strategy of using an SASA with continuous-flow chemistry has the potential for application in a wide variety of protein modifications[34].

To establish a robust and reliable PEGylation using the continuous mode, some challenges still remain. For example, process development including understanding critical process parameters, PEG reagent screening to replace NHS ester having risk of overreactions[35], detailed conjugation site analysis by peptide mapping, and normal operating range identification was not complete in the present study. Further investigations to establish the ideal continuous mode-mediated PEGylation are currently underway.

Supporting information

Structural analysis of IL-6

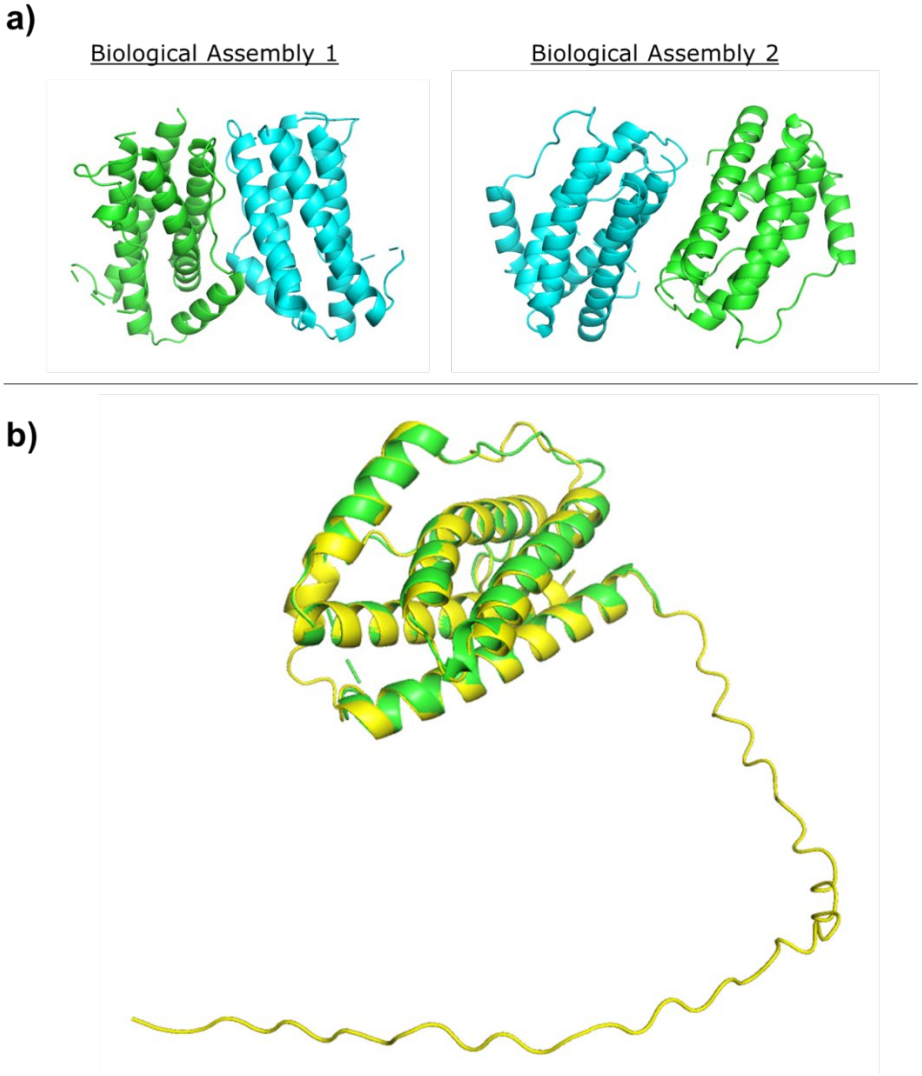

Figure S1. Structural analysis of IL-6 (a) dimer structure reported in PDB (PBD: 1ALU), (b) Structural comparison of PDB (green) and AlphaFold-2 (yellow), root mean square deviation = 0.359Å

Comparison of PEG reagent reactivity

a)

Product name	Structure	Half-life (Ref 20)
SUNBRIGHT ME-050PS	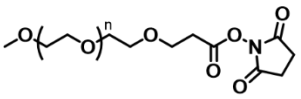	17.1 min
SUNBRIGHT ME-050CS	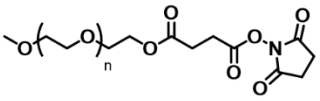	14.7 min
SUNBRIGHT ME-050AS	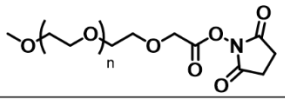	0.7 min

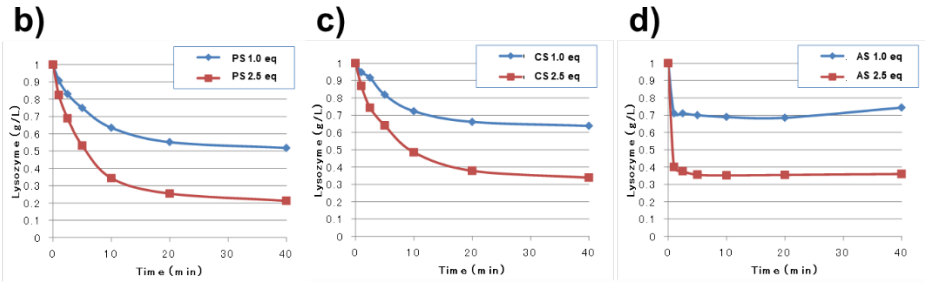

Figure S2. Comparison of PEG reagent reactivity (a) summary of PEG reagents and their half-life (b) PEGylation rate of lysozyme by batch mode using SUNBRIGHT ME-050PS (c) PEGylation rate of lysozyme by batch mode using SUNBRIGHT ME-050CS. (d) PEGylation rate of lysozyme by batch mode using SUNBRIGHT ME-050AS.

The schematic diagrams of the mixers

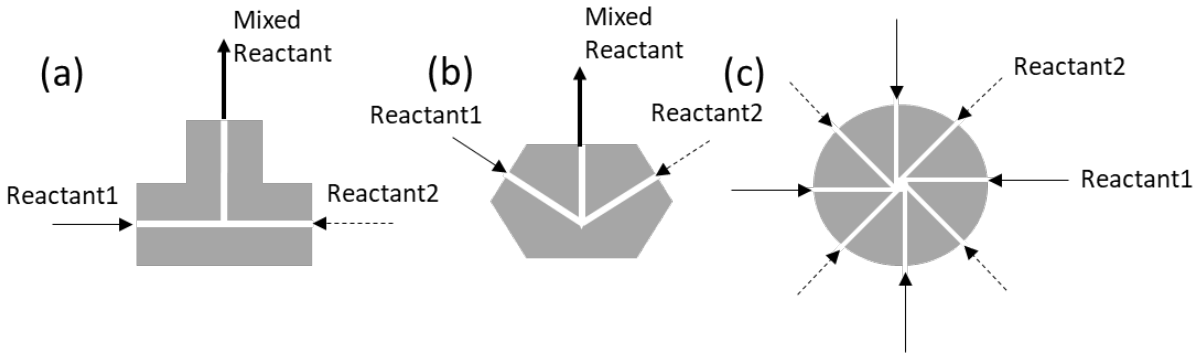

Figure S3. (a) T-shaped mixer (φ 500 μm), (b) V-shaped mixer (φ 500 μm), (c) vortex shaped mixer (φ450μm) in vortex shaped mixer, each reactant was divided by 4 feeding lines.

Full length chromatograms RP-HPLC

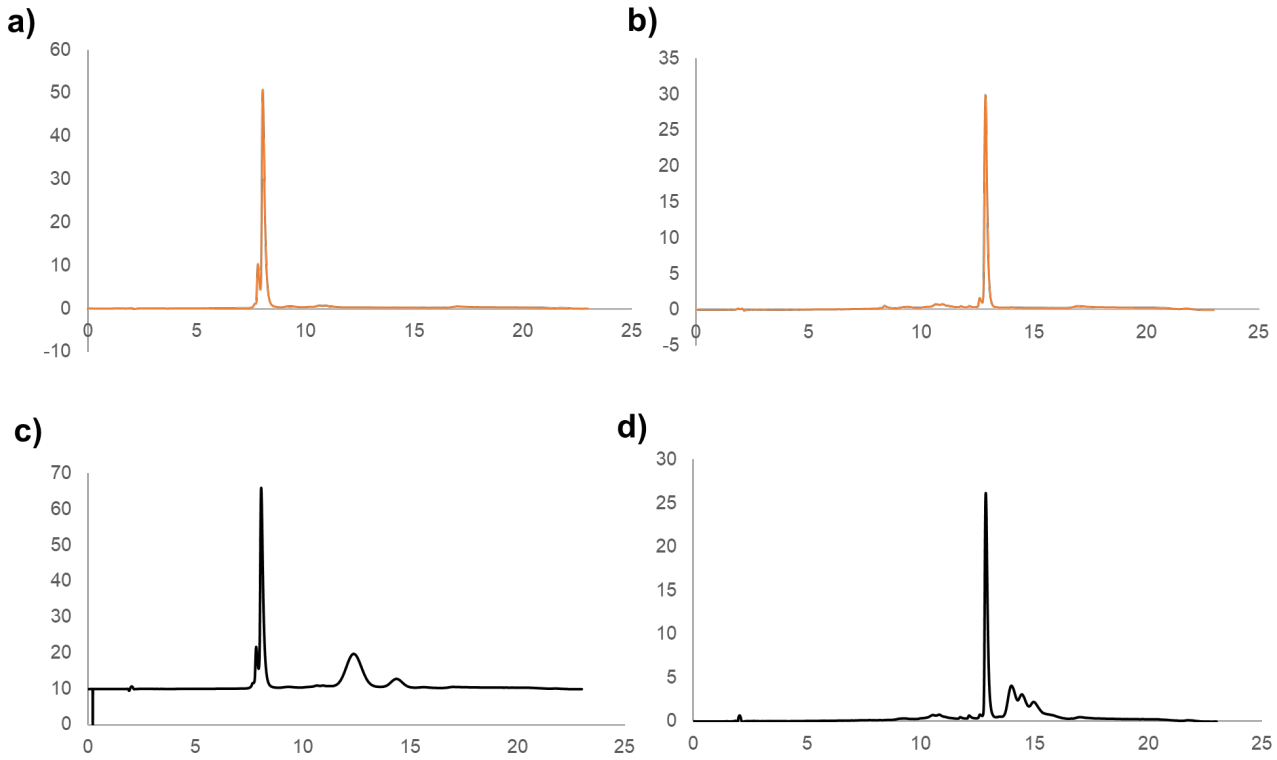

Figure S4. RP-HPLC analysis (a) naked lysozyme (b) naked IL-6 (c) PEGylated lysozyme produced by continuous flow mode (d) PEGylated IL-6 produced by continuous flow mode

Full length chromatograms SEC-HPLC

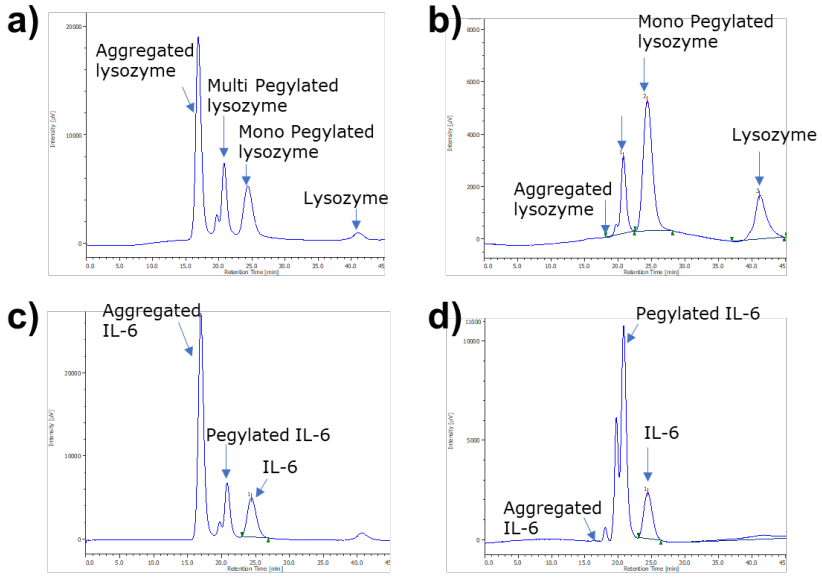

Figure S5. SEC analysis (a) PEGylated lysozyme produced by batch mode (aggregation: 44%) (b) PEGylated lysozyme produced by continuous flow mode (aggregation: <1%) (c) PEGylated IL-6 produced by batch mode (aggregation: 54%) (d) PEGylated IL-6 produced by continuous flow mode (aggregation: <1%)

Comparison of SASA values

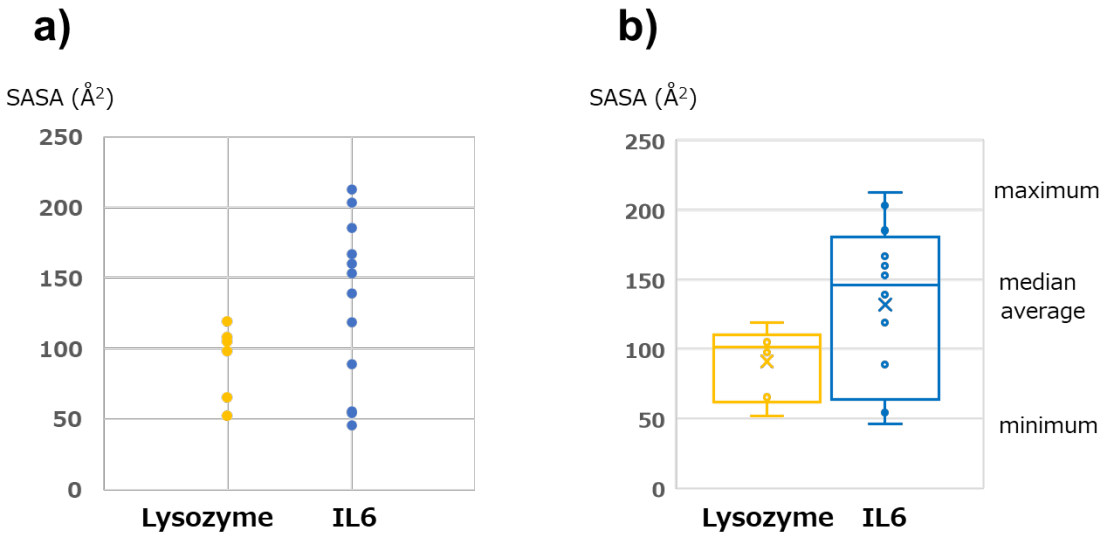

Figure S6. Comparison analysis of SASA values (a) scatter plots (b) box pots

SDS-PAGE analysis

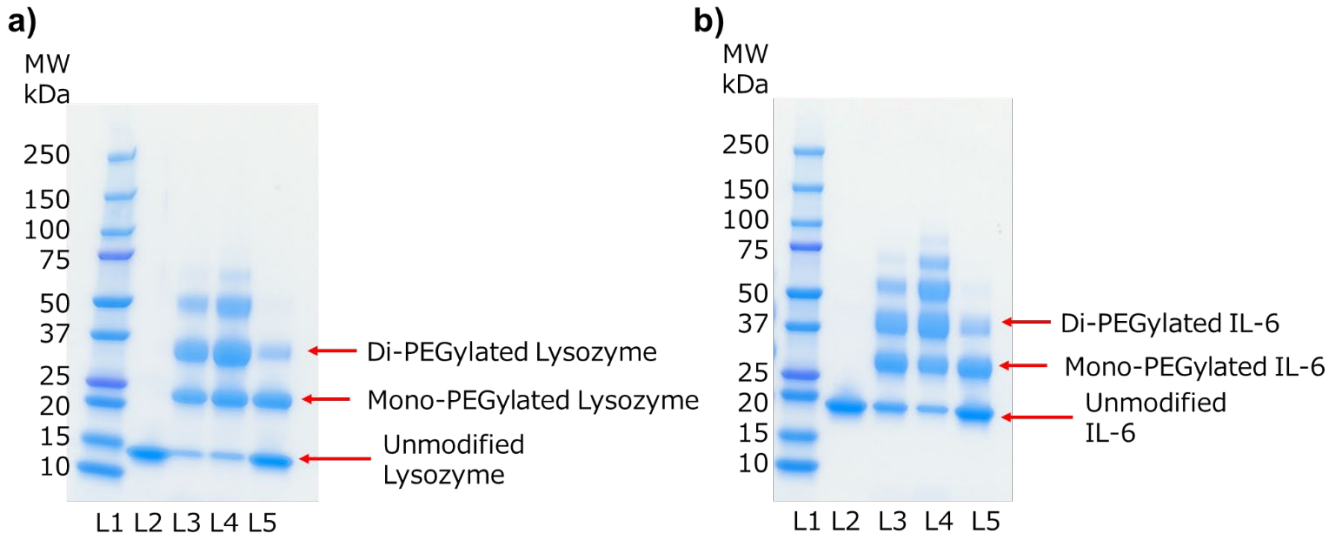

Figure S7. SDS-PAGE analysis SEC analysis (a) Lysozyme, L1= molecular maker, L2= naked lysozyme (non-reduced), L3= PEGylated lysozyme produced by batch mode (non-reduced, 0.5 mg scale), L4= PEGylated lysozyme produced by batch mode (non-reduced, 5.0 mg scale), L5= PEGylated lysozyme produced by continuous flow mode (non-reduced, 1.26 g scale), (b) IL-6, L1= molecular maker, L2= naked IL-6 (non-reduced), L3= PEGylated IL-6 produced by batch mode (non-reduced, 0.58 mg scale), L4= PEGylated IL-6 produced by batch mode (non-reduced, 5.8 mg scale), L5= PEGylated IL-6 produced by continuous flow mode (non-reduced, 290 mg scale)

References and notes

1. Turecek, P. L.; MBossard, M. J.; Schoetens, F.; Ivens, I. A. *J. Pharm. Sci.* **2016**, *105*, 460−475.
2. Mishra, P.; Nayak, B.; Dey, R. K. *Asian J. Pharm. Sci.* **2016**, *11*, 337−348.
3. Mao, L.; Russell, A. J.; Carmali, S. *Bioconjugate Chem.* **2022***, 33,* 1643–1653.
4. Armengol, E. S.; Unterweger, A.; Laffleur, F. *Drug Dev. Ind. Pharm.* **2022**, *48*, 129-139.
5. Rajan, R.; Ahmed, S.; Sharma, N.; Kumar N.; Debas, A.; Matsumura, K. *Mater. Adv.*, **2021**, *2*, 1139-1176.
6. Rossetti, I.; Compagnoni, M. *Chem. Eng. J*. **2016**, *296*, 56–70.
7. Baumann, M.; Moody, T. S.; Smyth, M.; Wharry, S. *Org. Process Res. Dev.* **2020,** *24*, 1802–1813.
8. Hughes, D. L. *Org. Process Res. Dev.* **2020,** *24*, 1850–1860.
9. Takahashi, Y.; Nagaki, A. *Molecules* **2019**, *24*, 1532.
10. Movsisyan, M.; Delbeke, E. I.; Berton, J. K.; Battilocchio, C.; Ley, S. V.; Stevens, C. V. *Chem. Soc. Rev.* **2016,** *45*, 4892–4928.
11. Nakahara, Y.; Mendelsohn, B. A.; Matsuda, Y. *Org. Process Res. Dev.* **2022**, *26*, 2766–2770.
12. Ingold, O.; Pfister, D.; Morbidelli, M. *React. Chem. Eng*., **2016**, *1*, 218–228.
13. Shang, X.; Ghosh, R. *J. Memb. Sci*. **2014**, *451*, 177–184.
14. Madadkar, P.; Selvaganapathy, P. R.; Ghosh, R. *Biomicrofluidics* **2018**, *12*, 44114.
15. Kateja, N.; Nitika, Dureja, S.; Rathore, A. S. *J. Biotechnol.* **2020**, *322*, 79–89.
16. Matsuda, Y.; Leung, M.; Tawfiq, Z.; Fujii, T.; Mendelsohn, B. A. *Anal. Sci.* **2021,** *37*, 1171–1176.
17. Yamazaki, S.; Shikida, N.; Takahashi, K.; Matsuda, Y.; Inoue, K.; Shimbo, K.; Mihara, Y. *Bioorg. Med. Chem. Lett.* **2021**, *51*, 128360.
18. Matsuda, Y.; Chakrabarti, A.; Takahashi, K.; Yamada, K.; Nakata, K.; Okuzumi, T.; Mendelsohn, B. A. *J. Chromatogr. B Analyt. Technol. Biomed. Life Sci.* **2021,** *1177*, 122753.
19. Tsutsumi, Y. E.; Tsunoda, S. S.; Kamada, H.; Kihira, T.; Kaneda, Y.; Ohsugi, Y.; Mayumi, M. *Thromb. Haemost.* **1997**, *77*, 168–173.
20. Tsunoda, S.; Ishikawa, T.; Watanabe, M.; Kamada, H.; Yamamoto, Y.; Tsutsumi, Y.; Hirano, T.; Mayumi, T. *Br. J. Haematol.* **2001**, *112*, 181-188.
21. Somers, W.; Stahl, M.; Seehra, J. S. *EMBO J.* **1997**, *16*, 989–997.

22. Jumper, J.; Evans, R.; Pritzel, A.; Green, T.; Figurnov, M.; Ronneberger, O.; Tunyasuvunakool, K. Bates, R.; Žídek, A.; Potapenko, A. *et. al. Nature*, **2021**, *596*, 583–589.
23. Varadi M. *et. al Nucleic Acids Res.* **2022***, 50*, D439–D444.
24. Konermann, L. *J. Phys. Chem. A* **1999**, *103*, 7210–7216.
25. Homepage of NOF Corporation. https://www.nofamerica.com/store/index.php?dispatch=categories.view&category_id=7.
26. Endo, Y.; Furusawa, M.; Shimazaki, T.; Takahashi, Y.; Nakahara, Y.; Nagaki, *Org. Process Res. Dev.* **2019,** *23*, 635–640.
27. Taylor, C. J.; Baker, A.; Chapman, M. R.; Chapman, M. R.; Reynolds, W. R.; Jolley, K. E.; Clemens, G.; Smith, G. E.; Blacker, A. J.; Chamberlain, T. W.;. Christie, S. D. R.; Taylor, B. A.; Bourne R. A. *J. Flow. Chem.* **2021**, *11*, 75–86.
28. Reckamp, J. M.; Bindels, A.; Duffield, S.; Liu, Y. C.; Bradford, E.; Ricci, E.; Susanne, F.; Rutter, A. *Org. Process Res. Dev.* **2017,** *21*, 816–820.
29. Ehrfeld, W.; Golbig, K.; Hessel, V.; Löwe, H.; Richter, T. *Ind. Eng. Chem. Res.* **1999,** *38*, 1075–1082.
30. Fujii, T.; Reiling, C.; Quinn, C.; Kliman, M.; Mendelsohn, B. A.; Matsuda, Y. *Explor. Target. Anti-Tumor Ther.* **2021**, *2*, 576–585.
31. Tawfiq, Z.; Matsuda, Y.; Alfonso, M. J.; Clancy, C.; Robles, V.; Leung, M.; Mendelsohn, B. A. *Anal. Sci.* **2020,** *36*, 871–875.
32. Savojardo, C.; Manfredi, M.; Martelli, P. L.; Casadio, R. *Front. Mol. Biosci.* **2021** *7*, 626363.
33. Kajander, T.; Kahn, P. C.; Passila, S. H.; Cohen, D. C.; Lehtiö, L.; Adolfsen, W.; Warwicker, J.; Schell, U.; Goldman, A.; *Structure* **2000** *8*, 1203-1214.
34. FMR has the advantage of high throughput to find appropriate reaction conditions. As a hypothetical case study, we have attempted to compare the estimated development time for both batch and FMR cases. In the case of batch development, it is assumed that each parameter study takes 10 min to find ideal scale-up conditions, so a total of 300 min is required if 30 parameter studies are performed. On the other hand, in the case of FMR development, the run time for each parameter study is less than 1 min. Therefore, a total of only 30 min is required to complete 30 parameter studies.
35. Fujii T., Matsuda Y., Seki T., Shikida N., Iwai Y., Ooba Y., Takahashi K., Isokawa M., Kawaguchi S., Hatada N., Watanabe T., Takasugi R., Nakayama A., Shimbo K., Mendelsohn B. A., Okuzumi T., Yamada K.; *Bioconjugate Chem.*; **2023**, *34*, 728–738.

36. Ejima, D.; Watanabe, M.; Sato, Y.; Date, M.; Yamada, N.; Takahara, Y. *Biotechnol. Bioeng.* **1999**, *62*, 301–310.

37. Weiss, M. S.; Palm, G. J.; Hilgenfeld. R. *Acta Cryst.* **2000**. *D56*, 952–958.

38. Matsuda, Y.; Seki, T.; Yamada, K.; Ooba, Y.; Takahashi, K.; Fujii, T.; Kawaguchi, S.; Narita, T.; Nakayama, A.; Kitahara, Y.; Mendelsohn, B. A.; Okuzumi, T. *Mol. Pharm.* **2021,** *18*, 4058–4066.

39. Matsuda, Y.; Tawfiq, Z.; Leung, M.; Mendelsohn, B. A. *ChemistrySelect.* **2020,** *5*, 8435–8439.

40. Seki, T.; Yamada, K.; Ooba, Y.; Fujii, T.; Takahiro, N.; Nakayama, A.; Kitahara, Y.; Mendelsohn, B. A.; Matsuda, Y.; Okuzumi, T. *Front. Biosci. (Landmark Ed)* **2022**, *27*, 234.

Chapter 6

Spatial and Temporal Control in Protein Refolding through Flash-change Reaction Conditions

Abstract

Protein refolding is a critical aspect of protein production, but the development of a versatile and scalable method remains a challenge. In this study, the author presents a novel refolding system using a flow micro reactor (FMR) that allows precise control of key parameters such as buffer pH and organic solvent content during the process. The author uses interleukin-6 (IL-6) as a model protein to demonstrate the effectiveness of this system in achieving efficient refolded highly pure protein (96% monomer) and enabling gram-scale production. This FMR system facilitates flash-change of reaction conditions, which effectively circumvents protein aggregation during refolding. To the best of our knowledge, this is the first report using FMR system for protein refolding, which has the potential to revolutionize protein production by providing a more efficient and scalable method. The present results highlight the utility of the FMR system as a high-throughput screening tool for streamlined scale-up, emphasizing the importance of controlling and understanding intermediates in the refolding process. The novelty of this approach is derived from FMR's unique ability to control both spatial and temporal aspects of protein refolding, a feat previously unattainable by any other method.

Introduction

Protein function depends on primary, secondary, and tertiary structures[1]. The tertiary structure, influenced by external factors like pH, is crucial. In recombinant protein production, proper refolding is necessary to restore this structure.[2] Current refolding technologies suffer from a major drawback: the formation of protein aggregates [3-5]. Optimization of protein folding conditions is a critical aspect of recombinant protein production and is typically achieved through laboratory experimentation and observation [6-9]. High throughput screening methods are essential to streamline the protein folding process and several approaches have been developed. However, these methods are primarily used in early-stage research and are not widely adopted by contract development and manufacturing organizations, making the development of a high-throughput and scalable protein refolding screening system a challenging and innovative task.

The limitations of existing protein refolding systems prompted us to develop a versatile and straightforward refolding system that is compatible with various proteins. The continuous-mode flow reaction holds considerable promise for achieving high-throughput protein refolding. This manufacturing process is gaining popularity in industry and allows chemical reactions to take place in dedicated systems consisting of tubes, mixers and pipes [10-12]. However, its application in the biotherapeutic field is limited. Pivotal groundwork carried out by Rathore and co-workers in 2016 presented the viability of a continuous refolding system employing a coiled flow inverter[13]. Rathore's team managed to boost protein yield, although the protein's purity level paralleled that achieved by batch-mode refolding. This research invites subsequent advancements: the implementation of continuous processes for more pragmatic applications.

In this study, the author present a novel application of flow microreactor (FMR) system to protein refolding, overcoming the limitations of current technologies. Using the cytokine IL-6 as a model protein [14], the author studied its conformational changes under different pH levels and organic solvents [15, 16]. Our aim was to determine the most effective way to generate the optimal conformation of IL-6 by manipulating these variables. IL-6 is known for its α-helix-rich structure and its tendency to dimerize and form aggregates, making it a suitable model protein for our study.

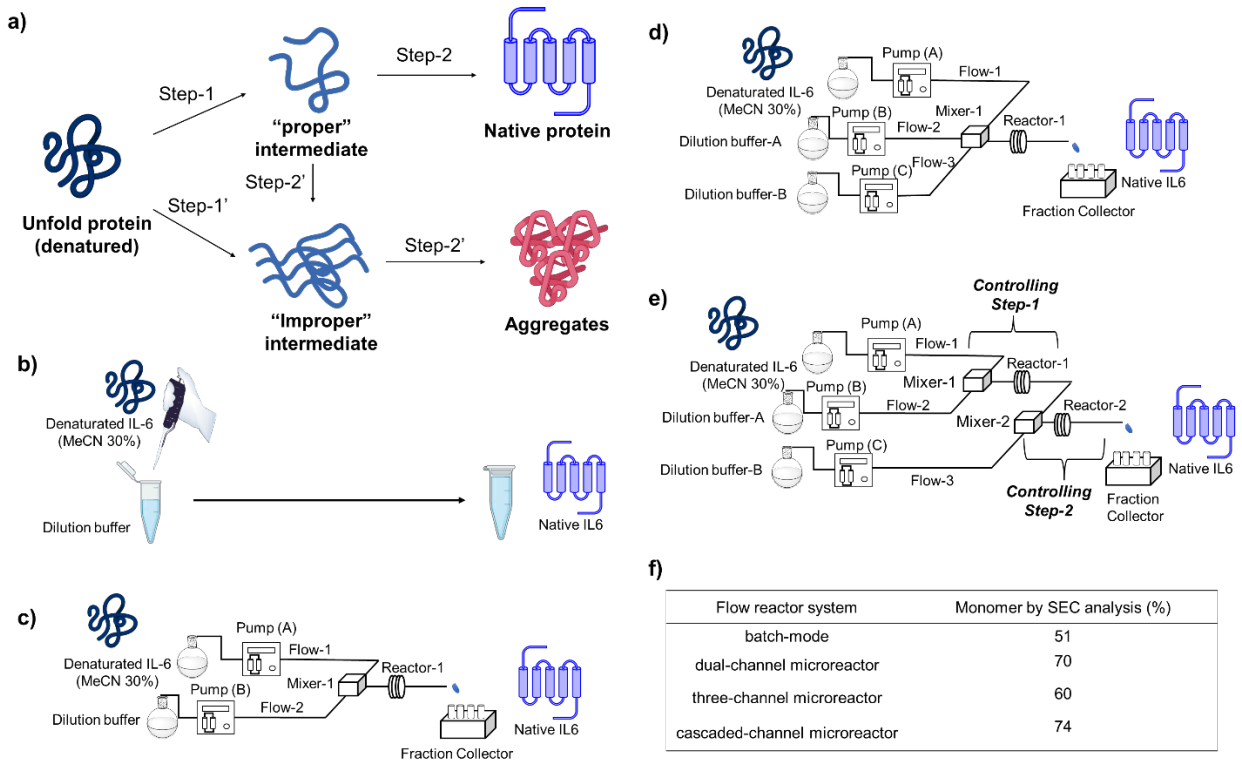

f)

Flow reactor system	Monomer by SEC analysis (%)
batch-mode	51
dual-channel microreactor	70
three-channel microreactor	60
cascaded-channel microreactor	74

Figure 1. Overview of FMR mode refolding, a) illustration of "proper" and "improper" intermediates b) illustration of batch-mode refolding system, c) illustration of FMR refolding system using a dual-channel microreactor, d) illustration of FMR refolding system using a triple-channel microreactor, e) illustration of FMR refolding system using a cascaded-channel microreactor, f) Summary of feasibility study results

Results and Discussion

In general, protein refolding involves intermediates that ultimately lead to the native state protein structure [17]. Our hypothesis suggests that certain challenges exist in IL-6 refolding, which may lead to aggregation. Firstly, the author proposes that there are 'proper' and 'improper' intermediates, with only the former giving rise to the monomer (Step-1 and Step-2 in Figure 1a). Secondly, appropriate treatment conditions are required for denatured IL-6 to obtain the proper intermediates. Otherwise, improper intermediates are generated and converted to aggregates (Step-2' in Figure 1a). Lastly, the appropriate intermediate has a short shelf-life, and if not treated correctly, it will denature into an inappropriate intermediate (Step-2' in Figure 1a). To address these challenges, the author designed a FMR system (Figure 1c-1e) to obtain the proper intermediate in Step-1 and convert it into a monomer in Step-2. Our initial aim is to determine the candidate mixing system for refolding; therefore, the author first performed a comparative experiment using different types of flow reactors. For batch dilution refolding, denatured IL-6 is added to the dilution buffer and stirred for an appropriate time (Figure 1b). The author used this batch dilution method as a control and compared it with microreactor systems (Figure 1b-1e). the author evaluated the two-channel microreactor (Figure 1c), the three-channel microreactor (Figure 1d), which allows the simultaneous mixing of larger or different amounts of buffer components, and the cascaded-channel microreactor (Figure 1e), which allows the sequential mixing of different buffer components. All three flow reactors showed improvements in monomer ratio compared to the batch method, with the three-channel microreactor showing the highest performance (Figure 1f). Consequently, the author aimed to further optimize the reaction conditions using the three-channel microreactor.

Next, the author attempted to identify the critical factors using this system, which deserves a high throughput system. This cascade-lined FMR system consisted of two T-shaped mixers and two reactors following the previous report (Figure 1e) [18]. The refolding was completed in 8.83 s (residence time in Reactor-1 and -2).

The detailed calculations are below.

· reactor length; Reactor-1: 250 mm = 0.25 m, Reactor-2: 250 mm = 0.25 m

· reactor diameter; 1 mm = 1×10^{-3} m

· reactor volume; Reactor-1: 0.196 mL, Reactor-2: 0.196 mL

· flow rate; 0.2 mL/min (IL-6), 1.8 mL/min (buffer-A), and 2.0 mL/min (buffer-B)

· total residence time = 8.83 s = 0.196 (mL)/2.0 (mL/min) + 0.196 (mL)/4.0 (mL/min)

This rapid reaction mode enabled theoretically more than 100 reaction condition screenings within 20 min.

To identify critical factors for refolding denatured IL-6, the author conducted a feasibility study in a FMR system, exploring a range of parameters and conditions (Table 1 and Table S1 in Supporting information, SI). Because of the various factors that can contribute to protein aggregation, the author focused our investigation on pH and organic solvent content. Structural analysis of IL-6 revealed a significant disorder, primarily due to the protein's dimerization tendency [19]. However, changes in pH can disrupt this undesired dimerization, with neutral pH being particularly effective in stabilizing refolded IL-6. Surprisingly, the author observed increased aggregation when denatured IL-6 was neutralized in step 1, indicating improper intermediate formation (entries 1-3). These results suggest that neutral pH can stabilize refolded IL-6 but does not necessarily induce proper intermediate formation. To determine the aggregation ratio of IL-6, the author employed size exclusion chromatography (SEC), using a Superdex® 75 column composed of highly cross-linked agarose [20], a material commonly used for protein purification. After exploring various analytical conditions, the author identified the optimal combination that provided the best resolution. To minimize potential adsorption to the column surface and ensure reproducible measurements, the author followed a previous report and added arginine to the mobile phase [21]. This approach allowed us to achieve optimal separation with high protein recovery rates, enabling us to obtain accurate and reliable measurements of the aggregation ratio of IL-6.

Our analysis of entries 4 and 5 revealed that final buffer pH plays a crucial role in determining the selective formation of monomers, with a pH of approximately 4.5 proving optimal. Previous studies on IL-6 formulation have suggested that the protein has a narrow ionization environment window, making it particularly sensitive to pH conditions. Based on this understanding, the author proposes that a pH of around 4.5, which avoids protonation of the imidazole group of histidine residues and deprotonation of carboxylic acid amino acid residues [22], stabilizes the proper intermediate of IL-6 and facilitates selective monomer formation.

To further improve monomer selectivity, the author explored ways to reduce the organic solvent content in step 1. Ultimately, the author founds that a process consisting of dilution to pH 2.0 in step 1, followed by pH adjustment to 4.3 in step 2, was optimal, resulting in more than 81% monomer selectivity in our feasibility study

(entry 8). The present study supported that neither the type of dilution buffer employed nor the counter ions utilized in Step 1 had a noteworthy impact (entries 10-11). Based on these findings, it was inferred that the monomer yield could be enhanced by reducing the ACN concentration while sustaining a pH of approximately 2.0-3.0 during step 1 and elevating the pH to around 4.0-4.5 during step 2 (Figure S1 in SI).

Table-1. Feasibility study on FMR mode refolding

Entry	Step-1				Step-2			Result
	Initial pH	Dilution buffer-A	Mixer-1 pH	Mixer-1 ACN conc. (%)	Dilution buffer-B	Mixer-2 pH	Mixer-2 ACN conc. (%)	Monom (%)
1	2.5	50 mM Citrate-ACN (pH 3.0)	2.9	30	500 mM Acetate (pH 4.5)	4.3	1.5	53
2	2.5	50 mM Citrate-ACN (pH 4.5)	4.3	30	500 mM Acetate (pH 4.5)	4.5	1.5	42
3	2.5	50 mM Citrate-ACN (pH 6.0)	5.8	30	500 mM Acetate (pH 4.5)	4.6	1.5	35
4	2.5	50 mM Citrate-ACN (pH 3.0)	2.9	30	500 mM Citrate (pH 3.0)	3.0	1.5	42
5	2.5	50 mM Citrate-ACN (pH 3.0)	2.9	30	500 mM Acetate (pH 5.5)	5.1	1.5	38
6	2.5	0.1 % TFA in ACN-water (pH 2.0)	2.3	30	500 mM Acetate (pH 4.5)	4.3	1.5	54
7	2.5	0.1% TFA (pH 2.0)	2.2	1.5	500 mM Acetate (pH 3.0)	2.8	< 0.1%	69
8	2.5	0.1% TFA (pH 2.0)	2.2	1.5	500 mM Acetate (pH 4.5)	4.3	< 0.1%	81
9	2.5	0.1% TFA (pH 2.0)	2.2	1.5	500 mM Acetate (pH 5.5)	5.1	< 0.1%	60
10	2.5	50 mM Glycine-HCl (pH 2.2)	2.3	1.5	500 mM Acetate (pH 4.5)	4.3	< 0.1%	75
11	2.5	50 mM Citrate (pH 2.2)	2.3	1.5	500 mM Acetate (pH 4.5)	4.3	< 0.1%	75

This feasibility study also revealed that the refolding process required to form suitable intermediates for IL-6 is susceptible, with even subtle changes in conditions significantly impacting aggregation formation. These findings led us to hypothesize that the lifetime of appropriate intermediates is extremely short, emphasizing the need for rapid pH and organic solvent changes, such as flash change buffers, to obtain high-purity IL-6

monomers.

To address these challenges, the author determined that a FMR mode system is the most viable solution, as it allows for easy adjustment of flow rates for flash changes and the residence time in the FMR mode unit. The authors conducted additional screening studies to identify the optimal flow rate and residence time, ultimately generating a comprehensive dataset (Table S2 in SI) to inform future experiments and process optimization efforts.

Table 2. Exploration to flush change buffer conditions

	Step-1				Step-2			Result
Entry	Flow rate of IL-6	Flow rate of dilution buffer-A	Reactor-1 length	Residence time	Flow rate of dilution buffer-B	Reactor-2 length	Residence time	Monom (%)
1	0.2 mL/min	1.8 mL/min	5 cm	1.2 S	2.0 mL/min	25 cm	2.94 S	54
2	0.2 mL/min	1.8 mL/min	25 cm	5.9 S	2.0 mL/min	25 cm	2.94 S	81
3	0.2 mL/min	1.8 mL/min	50 cm	11.8 S	2.0 mL/min	25 cm	2.94 S	55
4	0.4 mL/min	3.6 mL/min	100 cm	11.8 S	4.0 mL/min	25 cm	2.94 S	80
5	1.0 mL/min	9.0 mL/min	100 cm	4.7 S	10.0 mL/min	25 cm	1.2 S	66
6	1.0 mL/min	9.0 mL/min	50 cm	2.4 S	10.0 mL/min	25 cm	0.59 S	84
7	1.0 mL/min	9.0 mL/min	25 cm	1.2 S	10.0 mL/min	25 cm	0.59 S	86
8	1.0 mL/min	9.0 mL/min	5 cm	0.2 S	10.0 mL/min	25 cm	0.59 S	96

Our investigations into the refolding of IL-6 revealed that the residence time in step 1 is the most critical factor for forming monomer IL-6, indicating that the appropriate intermediate form is unstable and quickly converted to the inappropriate intermediate (entries 1-3). Additionally, the author found that the flow rate to realize flash-change of buffer is the most significant factor in improving monomer selectivity. Notably, the maximum flow rate required to maintain mixability, as assessed by the Villermaux-Dushman reaction [23], resulted in monomer selectivity of over 95% (entry 8), representing a significant improvement in our process. The flash buffer change achieved by cascade mixing system allowed for precise control of step 1 and step 2, which suggested the existence of proper but unstable intermediates.[24]

In addition to evaluating the FMR system for refolding screening, the author assessed its scalability for future protein production applications. Experiments were conducted in triplicate at three different scales (10 mg, 100 mg, and 500 mg), demonstrating a stable monomer yield of over 95% with an error range of less than 1% in all investigations (Table S3 in SI). Furthermore, the author investigated gram-scale preparation, which involved FMR refolding followed by polishing using SEC purification, with the goal of obtaining highly monomeric IL6 comparable to commercially available standards (with a purity exceeding 95%). Starting with 1.3 grams of denatured IL-6, the author performed a FMR refolding process at a gram-scale production level. Our optimized residence time for this FMR refolding process was 0.79 seconds. By running the process continuously, we were able to process 1.3 grams of denatured IL-6 in approximately 4 hours. After FMR refolding, the author used tangential flow filtration (TFF) and SEC purification to remove impurities and obtain more than 1.25 grams of IL-6 in a over 99% monomer format, which met commercially available specifications (Table 3, Figure 2). In addition, the Limulus amebocyte lysate assay showed that the purified IL-6 had only a minimal amount of endotoxin, indicating that our FMR system, with its closed reactor design featuring tubes and pumps, may also help mitigate the risk of endotoxin contamination. These findings demonstrate the practicality and potential of our refolding system for future protein production in the pharmaceutical industry.

Table 3. Summary of gram-scale IL-6

Quantity	Residence time (Reactor-1 and -2)	Monomer % After Flow reactor	Monomer % Final product	Endotoxin conc.
1.25 g	0.79 S	96%	99%	<0.100 EU/mL

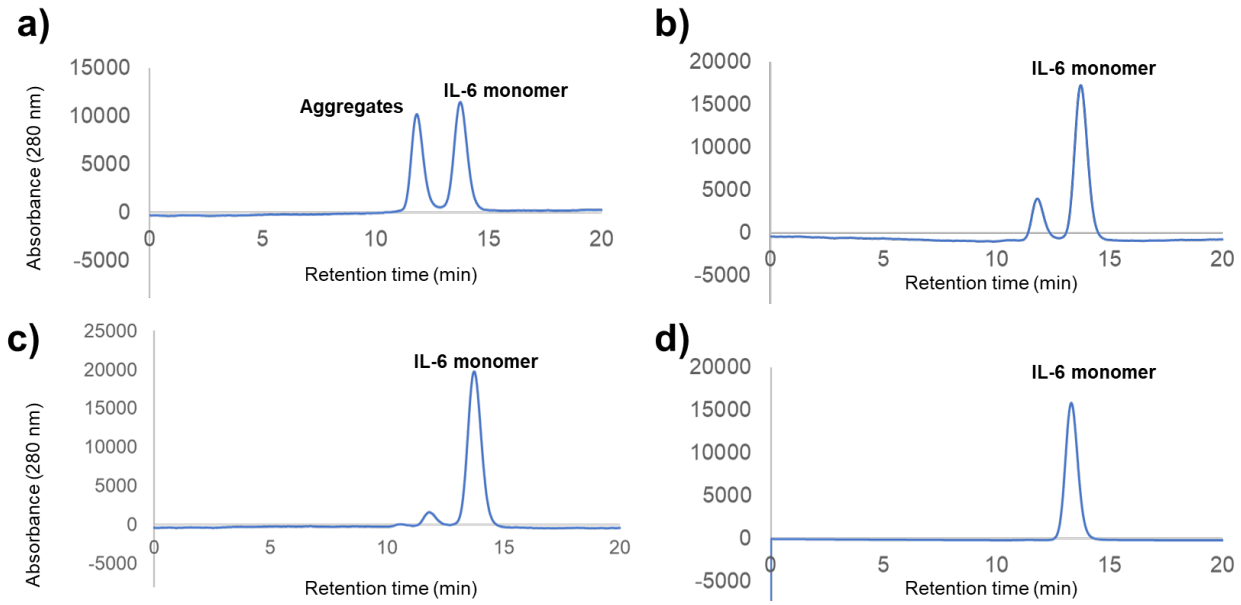

Figure 2. SEC-HPLC analysis of refolded IL-6, a) refolded IL-6 produced by batch mode mixing (51% monomer), b) refolded IL-6 produced by cascade-mode mixing with non-flush change (Table-1 entry 8, 91% monomer), c) gram scale refolded IL-6 produced by cascade-mode mixing with flush change (Table-2 entry 8, 96% monomer), d) gram scale refolded IL-6 after SEC purification (Table-2 entry 8, 99% monomer).

Experimental Section

Materials.

Recombinant human IL-6 was prepared based on the previous report. All chemicals were purchased from FujifilmWako (Japan).

Preparation of denatured IL-6

Recombinant Human IL-6 (final concentration approximately 1.6 mg/mL) was prepared in a solution containing acetonitrile (ACN) (final concentration 40 vol%) and a 0.1% trifluoroacetic acid (TFA) solution and left to stand overnight at room temperature.

Batch-mode refolding.

Denatured IL-6 (3.47 mg/mL) in water with 30 v/v was diluted rapidly by 20 diavolume of 50 mM acetate buffer (pH 4.5) based on previous report[20]. After shaking by vortex, SEC and SDS-PAGE analysis were conducted.

Representative experimental procedure for IL-6 refolding using the two-channel microreactor

T-shaped stainless-steel mixers with inner diameters of 0.5 mm (Sankoh-seiki, Tokyo, Japan) were used as Mixer as shown in Figure 1c. Reactor-1 (1.0 mm i.d., 0.5 m length) were also made of stainless steel. The denatured IL-6 solution (1.6 mg/mL in water containing 30 v/v % ACN) was added to Mixer through Flow-1 whose flow rate was 0.2 mL/min. The 500 mM Acetate (pH 4.5) was added to Mixer-1 through Flow-2 whose flow rate was 1.8 mL/min. The output mixture was eluted into a fraction collector, to which an excess of 1 M Tris buffer (pH 7.4) was added for neutralization. This elution was combined and purified using large desalting columns as previously reported.

Representative experimental procedure for IL-6 refolding using the three-channel microreactor

T-shaped stainless-steel mixers with inner diameters of 0.5 mm (Sankoh-seiki, Tokyo, Japan) were used as Mixer as shown in Figure 1e. Reactor-1 (1.0 mm i.d., 0.5 m length) were also made of stainless steel. The denatured IL-6 solution (1.6 mg/mL in water containing 30 v/v % ACN) was added to Mixer through Flow-1 whose flow rate was 0.2 mL/min. The 0.1% TFA (pH 2.0) was added to Mixer-1 through Flow-2 whose flow rate was 0.9 mL/min. The 500 mM Acetate (pH 4.5) was added to Mixer-1 through Flow-3 whose flow rate was 0.9 mL/min. The output mixture was eluted into a fraction collector, to which an excess of 1 M Tris buffer (pH

7.4) was added for neutralization. This elution was combined and purified using large desalting columns as previously reported.

Representative experimental procedure for IL-6 refolding using cascaded-channel microreactor

T-shaped stainless-steel mixers with inner diameters of 0.5 mm (Sankoh-seiki, Tokyo, Japan) were used as Mixer as shown in Figure 1e. Reactor-1 (1.0 mm i.d., 0.25 m length) and Reactor-2 (1.0 mm i.d., 0.5 m length) were also made of stainless steel. The denatured IL-6 solution (1.6 mg/mL in water containing 30 v/v % ACN) was added to Mixer through Flow-1 whose flow rate was 1.0 mL/min. The 0.1% TFA (pH 2.0) was added to Mixer-1 through Flow-2 whose flow rate was 9.0 mL/min. The 500 mM Acetate (pH 4.5) was added to Mixer-2 through Flow-3 whose flow rate was 10 mL/min. The output mixture was eluted into a fraction collector, to which an excess of 1 M Tris buffer (pH 7.4) was added for neutralization. This elution was combined and purified using large desalting columns as previously reported.

CD Spectrum analysis.

Each sample (0.5 mg/mL in 50 mM acetate) was analyzed by J-820 spectrometer (JASCO) with previously reported procedure[20].

SEC analysis.

The refolded IL-6 was analyzed by SEC-HPLC with previously reported methods[19].

SEC-HPLC data was acquired an Superdex 75 10/300 GL column (GE Healthcare). Each sample (1 mg/mL, 20 μL) was injected into the system and ran at 0.8 mL/min at 25 °C over a 11 min using 0−25 min: isocratic 100 mM Phosphate, 200 mM Argine/HCl, 1 M urea, pH 6.8. The absorbance was monitored at 280 nm (reference wavelength at 450 nm).

TFF purification.

The elution from FMR was purified by TFF with a Vivaflow 50R Hydrosart (5 kDa, Sartorius) and 10 diavolumes of PBS buffer (pH 7.4) as the diafiltration (DF) buffer at an IL6 concentration of 20 mg/mL.

SEC purification

SEC purification was performed by ÄKTA purifier (GE Healthcare) was performed under the following conditions.

Column: Superdex 200 Increase 10 / 300GL (GE Healthcare)

Buffer: pH 7.4 PBS buffer flow rate: 0.4 ml / min

Detector: Detected at wavelengths of 215 and 280 nm.

Conclusion

In this manuscript, the author have demonstrated that FMR mode is an effective method for refolding IL-6, revealing the critical factors for refolding and the existence of the "proper but unstable" intermediate. A flush change tandem mixing system is essential for the proper handling of this unique intermediate. In addition, a scale-down manufacturing model involving a FMR refolding system and SEC purification provided 1 g of 95% monomeric IL-6.

The successful implementation of our FMR system in the refolding of IL-6 demonstrates its potential application to a wide range of proteins. The high-throughput screening capabilities of this system can significantly streamline the scale-up process in protein production, reducing the time and resources required for optimization. In addition, the improved understanding of protein production intermediates facilitated by the FMR system can lead to improved quality control and more effective therapeutic protein development. By providing simultaneous spatial and temporal control during the refolding process, this FMR system has the potential to transform protein manufacturing, promoting future advancements in protein-based therapeutics, and enhancing our understanding of protein folding mechanisms.

To put it more boldly, perhaps even to the point of hyperbole, the author believe that the most remarkable discovery in this manuscript is the elucidation of the existence of intermediates in the transformation of proteins, which serve as the basic building blocks of life, and our ability to control them. Capturing and understanding intermediates in protein reactions has the potential to serve as a guide that may shed light on the origins of life. It is with satisfaction that the author has discovered the potential of the FMR system as a tool to unlock this door, and with this the author would like to conclude this Ph. D. thesis.

Supporting information

Detailed refolding condition screening

Table S1. Refolding buffer condition screening

Entry	Step-1				Step-2			Results
	Initial (pH)	Dilution buffer-A	Mixer-1 (pH)	Mixer-1 ACN conc. (%)	Dilution buffer-B	Mixer-2 (pH)	Mixer-2 ACN conc. (%)	Monomer (%)
1	2.5	50 mM Acetate-ACN (pH 3.0)	2.9	30	500 mM Acetate (pH 4.5)	4.3	1.5	53
2	2.5	50 mM Acetate-ACN (pH 3.5)	3.3	30	500 mM Acetate (pH 4.5)	4.3	1.5	50
3	2.5	50 mM Acetate-ACN (pH 4.0)	3.7	30	500 mM Acetate (pH 4.5)	4.4	1.5	45
4	2.5	50 mM Acetate-ACN (pH 4.5)	4.3	30	500 mM Acetate (pH 4.5)	4.5	1.5	42
5	2.5	50 mM Acetate-ACN (pH 5.0)	4.8	30	500 mM Acetate (pH 4.5)	4.5	1.5	40
6	2.5	50 mM Acetate-ACN (pH 5.5)	5.2	30	500 mM Acetate (pH 4.5)	4.5	1.5	36
7	2.5	50 mM Acetate-ACN (pH 6.0)	5.6	30	500 mM Acetate (pH 4.5)	4.6	1.5	35
8	2.5	50 mM Citrate-ACN (pH 2.5)	2.5	30	500 mM Acetate (pH 4.5)	4.2	1.5	53
9	2.5	50 mM Citrate-ACN (pH 3.0)	2.9	30	500 mM Acetate (pH 4.5)	4.3	1.5	53
10	2.5	50 mM Citrate-ACN (pH 3.5)	3.3	30	500 mM Acetate (pH 4.5)	4.3	1.5	50
11	2.5	50 mM Citrate-ACN (pH 4.0)	3.7	30	500 mM Acetate (pH 4.5)	4.4	1.5	45
12	2.5	50 mM Citrate-ACN (pH 4.5)	4.3	30	500 mM Acetate (pH 4.5)	4.5	1.5	42
13	2.5	50 mM Citrate-ACN (pH 5.0)	4.8	30	500 mM Acetate (pH 4.5)	4.5	1.5	40

Entry	Step-1				Step-2			Results
	Initial (pH)	Dilution buffer-A	Mixer-1 (pH)	Mixer-1 ACN conc. (%)	Dilution buffer-B	Mixer-2 (pH)	Mixer-2 ACN conc. (%)	Monomer (%)
14	2.5	50 mM Citrate-ACN (pH 5.5)	5.2	30	500 mM Acetate (pH 4.5)	4.5	1.5	36
15	2.5	50 mM Citrate-ACN (pH 6.0)	5.8	30	500 mM Acetate (pH 4.5)	4.6	1.5	33
16	2.5	50 mM Citrate-ACN (pH 2.5)	2.5	30	500 mM Citrate (pH 4.5)	4.2	1.5	53
17	2.5	50 mM Citrate-ACN (pH 3.0)	2.9	30	500 mM Citrate (pH 4.5)	4.3	1.5	53
18	2.5	50 mM Citrate-ACN (pH 3.5)	3.3	30	500 mM Citrate (pH 4.5)	4.3	1.5	50
19	2.5	50 mM Citrate-ACN (pH 4.0)	3.7	30	500 mM Citrate (pH 4.5)	4.4	1.5	45
20	2.5	50 mM Citrate-ACN (pH 4.5)	4.3	30	500 mM Citrate (pH 4.5)	4.5	1.5	42
21	2.5	50 mM Citrate-ACN (pH 5.0)	4.8	30	500 mM Citrate (pH 4.5)	4.5	1.5	40
22	2.5	50 mM Citrate-ACN (pH 5.5)	5.2	30	500 mM Citrate (pH 4.5)	4.5	1.5	36
23	2.5	50 mM Citrate-ACN (pH 6.0)	5.8	30	500 mM Citrate (pH 4.5)	4.6	1.5	33
24	2.5	50 mM Gly HCl-ACN (pH 2.5)	2.5	30	500 mM Acetate (pH 4.5)	4.2	1.5	53
25	2.5	50 mM Gly HCl-ACN (pH 3.0)	2.9	30	500 mM Acetate (pH 4.5)	4.3	1.5	53
26	2.5	50 mM Gly HCl-ACN (pH 3.5)	3.3	30	500 mM Acetate (pH 4.5)	4.3	1.5	50
27	2.5	50 mM Gly HCl-ACN (pH 4.0)	3.7	30	500 mM Acetate (pH 4.5)	4.4	1.5	45
28	2.5	50 mM Gly HCl-ACN (pH 4.5)	4.3	30	500 mM Acetate (pH 4.5)	4.5	1.5	42
29	2.5	50 mM Gly HCl-ACN (pH 5.0)	4.8	30	500 mM Acetate (pH 4.5)	4.5	1.5	40
30	2.5	50 mM Gly HCl-ACN (pH 5.5)	5.2	30	500 mM Acetate (pH 4.5)	4.5	1.5	36

Entry	Step-1				Step-2			Results
	Initial (pH)	Dilution buffer-A	Mixer-1 (pH)	Mixer-1 ACN conc. (%)	Dilution buffer-B	Mixer-2 (pH)	Mixer-2 ACN conc. (%)	Monomer (%)
31	2.5	50 mM Gly HCl-ACN (pH 6.0)	5.8	30	500 mM Acetate (pH 4.5)	4.6	1.5	33
32	2.5	50 mM Gly HCl-ACN (pH 2.5)	2.5	30	500 mM Gly HCl (pH 4.5)	4.2	1.5	53
33	2.5	50 mM Gly HCl-ACN (pH 3.0)	2.9	30	500 mM Gly HCl (pH 4.5)	4.3	1.5	53
34	2.5	50 mM Gly HCl-ACN (pH 3.5)	3.3	30	500 mM Gly HCl (pH 4.5)	4.3	1.5	50
35	2.5	50 mM Gly HCl-ACN (pH 4.0)	3.7	30	500 mM Gly HCl (pH 4.5)	4.4	1.5	45
36	2.5	50 mM Gly HCl-ACN (pH 4.5)	4.3	30	500 mM Gly HCl (pH 4.5)	4.5	1.5	42
37	2.5	50 mM Gly HCl-ACN (pH 5.0)	4.8	30	500 mM Gly HCl (pH 4.5)	4.5	1.5	40
38	2.5	50 mM Gly HCl-ACN (pH 5.5)	5.2	30	500 mM Gly HCl (pH 4.5)	4.5	1.5	36
39	2.5	50 mM Gly HCl-ACN (pH 6.0)	5.8	30	500 mM Gly HCl (pH 4.5)	4.6	1.5	33
40	2.5	50 mM Citrate-ACN (pH 3.0)	2.9	30	500 mM Citrate (pH 3.0)	3.0	1.5	42
41	2.5	50 mM Citrate-ACN (pH 3.0)	2.9	30	500 mM Acetate (pH 3.5)	3.2	1.5	42
42	2.5	50 mM Citrate-ACN (pH 3.0)	2.9	30	500 mM Acetate (pH 4.0)	3.8	1.5	51
43	2.5	50 mM Citrate-ACN (pH 3.0)	2.9	30	500 mM Acetate (pH 5.0)	4.8	1.5	40
44	2.5	50 mM Citrate-ACN (pH 3.0)	2.9	30	500 mM Acetate (pH 5.5)	5.1	1.5	38
45	2.5	50 mM Citrate-ACN (pH 3.0)	2.9	30	500 mM Acetate (pH 6.0)	5.8	1.5	33
46	2.5	50 mM Citrate-ACN (pH 3.0)	2.9	30	500 mM Citrate (pH 3.5)	3.2	1.5	42
47	2.5	50 mM Citrate-ACN (pH 3.0)	2.9	30	500 mM Citrate (pH 4.0)	3.8	1.5	51

Entry	Step-1				Step-2			Results
	Initial (pH)	Dilution buffer-A	Mixer-1 (pH)	Mixer-1 ACN conc. (%)	Dilution buffer-B	Mixer-2 (pH)	Mixer-2 ACN conc. (%)	Monomer (%)
48	2.5	50 mM Citrate-ACN (pH 3.0)	2.9	30	500 mM Citrate (pH 5.0)	4.8	1.5	40
49	2.5	50 mM Citrate-ACN (pH 3.0)	2.9	30	500 mM Citrate (pH 5.5)	5.1	1.5	38
50	2.5	50 mM Citrate-ACN (pH 3.0)	2.9	30	500 mM Citrate (pH 6.0)	5.8	1.5	33
51	2.5	50 mM Citrate (pH 3.0)	2.9	1.5	500 mM Acetate (pH 3.5)	3.2	< 0.1%	60
52	2.5	50 mM Citrate (pH 3.0)	2.9	1.5	500 mM Acetate (pH 4.0)	3.8	< 0.1%	63
53	2.5	50 mM Citrate (pH 3.0)	2.9	1.5	500 mM Acetate (pH 4.5)	4.3	< 0.1%	70
54	2.5	50 mM Citrate (pH 3.0)	2.9	1.5	500 mM Acetate (pH 5.0)	4.7	< 0.1%	55
55	2.5	50 mM Citrate (pH 3.0)	2.9	1.5	500 mM Acetate (pH 5.5)	5.2	< 0.1%	52
56	2.5	50 mM Glycine HCl-ACN (pH 3.0)	2.9	30	500 mM Acetate (pH 3.5)	3.2	1.5	42
57	2.5	50 mM Glycine HCl-ACN (pH 3.0)	2.9	30	500 mM Acetate (pH 4.0)	3.8	1.5	51
58	2.5	50 mM Gly HCl-ACN (pH 3.0)	2.9	30	500 mM Acetate (pH 4.5)	4.3	1.5	53
59	2.5	50 mM Gly HCl-ACN (pH 3.0)	2.9	30	500 mM Acetate (pH 5.0)	4.7	1.5	40
60	2.5	50 mM Gly HCl-ACN (pH 3.0)	2.9	30	500 mM Acetate (pH 5.5)	5.2	1.5	38
61	2.5	50 mM Gly HCl-ACN (pH 3.0)	2.9	30	500 mM Acetate (pH 6.0)	5.8	1.5	33
62	2.5	50 mM Citrate-ACN (pH 3.0)	2.9	30	500 mM Acetate (pH 3.5)	3.2	1.5	41
63	2.5	50 mM Citrate-ACN (pH 3.0)	2.9	30	500 mM Acetate (pH 4.0)	3.8	1.5	52
64	2.5	50 mM Citrate-ACN (pH 3.0)	2.9	30	500 mM Acetate (pH 4.5)	4.3	1.5	52

Entry	Step-1				Step-2			Results
	Initial (pH)	Dilution buffer-A	Mixer-1 (pH)	Mixer-1 ACN conc. (%)	Dilution buffer-B	Mixer-2 (pH)	Mixer-2 ACN conc. (%)	Monomer (%)
65	2.5	50 mM Citrate-ACN (pH 3.0)	2.9	30	500 mM Acetate (pH 5.0)	4.7	1.5	40
66	2.5	50 mM Citrate-ACN (pH 3.0)	2.9	30	500 mM Acetate (pH 5.5)	5.2	1.5	36
67	2.5	50 mM Citrate-ACN (pH 3.0)	2.9	30	500 mM Acetate (pH 6.0)	5.8	1.5	33
68	2.5	50 mM Citrate-ACN (pH 3.0)	2.9	30	500 mM Succinate (pH 4.5)	4.3	1.5	52
69	2.5	50 mM Citrate-ACN (pH 3.0)	2.9	30	500 mM Formate (pH 4.5)	4.3	1.5	52
70	2.5	50 mM Glycine HCl-ACN (pH 3.0)	2.9	30	500 mM Succinate (pH 4.5)	4.3	1.5	52
71	2.5	50 mM Glycine HCl-ACN (pH 3.0)	2.9	30	500 mM Formate (pH 4.5)	4.3	1.5	51
72	2.5	0.1 % TFA in ACN-water (pH 2.0)	2.3	30	500 mM Acetate (pH 4.5)	4.3	1.5	54
73	2.5	0.1 % TFA in ACN-water (pH 2.0)	2.3	30	500 mM Acetate (pH 5.5)	5.1	1.5	52
74	2.5	0.1% TFA (pH 2.0)	2.2	1.5	500 mM Acetate (pH 3.0)	2.8	< 0.1%	69
75	2.5	0.1% TFA (pH 2.0)	2.2	1.5	500 mM Acetate (pH 4.5)	4.3	< 0.1%	81
76	2.5	0.1% TFA (pH 2.0)	2.2	1.5	500 mM Acetate (pH 5.5)	5.1	< 0.1%	60
77	2.5	0.1% TFA (pH 2.0)	2.2	1.5	500 mM Citrate (pH 4.5)	4.3	< 0.1%	80
78	2.5	0.1% TFA (pH 2.0)	2.2	1.5	500 mM Glycine-HCl (pH 4.5)	4.3	< 0.1%	80
79	2.5	0.1% TFA (pH 2.0)	2.2	1.5	500 mM Succinate (pH 4.5)	4.3	< 0.1%	80
80	2.5	0.1% TFA (pH 2.0)	2.2	1.5	500 mM Formate (pH 4.5)	4.3	< 0.1%	80

Entry	Step-1				Step-2			Results
	Initial (pH)	Dilution buffer-A	Mixer-1 (pH)	Mixer-1 ACN conc. (%)	Dilution buffer-B	Mixer-2 (pH)	Mixer-2 ACN conc. (%)	Monomer (%)
81	2.5	50 mM Gly HCl (pH 2.5)	2.5	1.5	500 mM Acetate (pH 4.5)	4.3	< 0.1%	75
82	2.5	50 mM Citrate (pH 2.5)	2.5	1.5	500 mM Acetate (pH 4.5)	4.3	< 0.1%	75
83	2.5	50 mM Gly HCl (pH 2.5)	2.3	1.5	500 mM Acetate (pH 4.5)	4.3	< 0.1%	78
84	2.5	50 mM Citrate (pH 2.2)	2.3	1.5	500 mM Acetate (pH 4.5)	4.3	< 0.1%	78

Table S2. Flow condition optimization

	Step-1				Step-2			Results
Entry	Flow rate of IL-6 (mL/min)	Flow rate of dilution buffer-A (mL/min)	Reactor-1 length (cm)	Residence time (s)	Flow rate of dilution buffer-B (mL/min)	Reactor-2 length (cm)	Residence time (s)	Monomer (%)
1	0.2	1.8	5	1.2	2.0	25	2.94	54
2	0.2	1.8	10	2.4	2.0	25	2.94	58
3	0.2	1.8	15	3.5	2.0	25	2.94	65
4	0.2	1.8	20	4.7	2.0	25	2.94	70
5	0.2	1.8	25	5.9	2.0	25	2.94	81
6	0.2	1.8	30	7.1	2.0	25	2.94	68
7	0.2	1.8	35	8.2	2.0	25	2.94	65
8	0.2	1.8	40	9.4	2.0	25	2.94	62
9	0.2	1.8	50	11.8	2.0	25	2.94	55
10	0.4	3.6	25	2.9	4.0	25	1.47	85
11	0.4	3.6	50	5.9	4.0	25	1.47	86
12	0.4	3.6	75	8.8	4.0	25	1.47	83
13	0.4	3.6	100	11.8	4.0	25	1.47	80
14	0.4	3.6	125	14.7	4.0	25	1.47	73
15	1	9.0	100	4.7	10.0	25	0.588	81
16	1	9.0	50	2.4	10.0	25	0.59	84
17	1	9.0	25	1.2	10.0	25	0.59	86
18	1	9.0	10	0.5	10.0	25	0.59	91
19	1	9.0	7.5	0.4	10	25	0.59	93
20	1	9.0	5	0.2	10	25	0.59	96
21	1	9.0	3.5	0.2	10	25	0.59	90
22	1	9.0	2.5	0.1	10	25	0.59	80
23	1	9.0	5	0.2	10	12.5	0.295	93
24	1	9.0	5	0.2	10	50	1.18	95
25	1	9.0	5	0.2	10	100	2.36	95

Table S3. Flow condition optimization

	Scale (mg)	Denatured IL-6 conc.	Run	Monomer (%)	SD
1	10	1.6 mg/mL	1st	95	0.5
2	10	1.6 mg/mL	2nd	95	
3	10	1.6 mg/mL	3rd	96	
4	10	3.2 mg/mL	1st	96	0
5	10	3.2 mg/mL	2nd	96	
6	10	3.2 mg/mL	3rd	96	
7	10	4.8 mg/mL	1st	96	0
8	10	4.8 mg/mL	2nd	96	
9	10	4.8 mg/mL	3rd	96	
10	10	5.6 mg/mL	1st	93	0.8
11	10	5.6 mg/mL	2nd	91	
12	10	5.6 mg/mL	3rd	92	
13	100	4.8 mg/mL	1st	96	0
14	100	4.8 mg/mL	2nd	96	
15	100	4.8 mg/mL	3rd	96	
16	500	4.8 mg/mL	1st	96	0
17	500	4.8 mg/mL	2nd	96	
18	500	4.8 mg/mL	3rd	96	
19	1300	4.8 mg/mL	1st	96	N.D.

Experimental strategy for flash-change refolding

a)

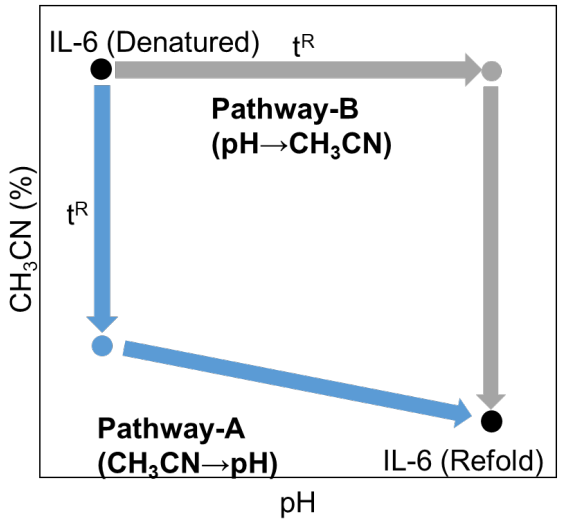

b)

t^R(sec)	1.77	8.83
Pathway-A	86% monomer	81% monomer
Pathway-B	61% monomer	42% monomer

T^R=total residence time

Figure S1. Experimental strategy for flash-change refolding. a) This panel illustrates the experimental strategy for flash-change refolding. Pathway-A represents the sequence of decreasing acetonitrile contents followed by pH adjustment, while Pathway-B represents pH adjustment followed by a decrease in acetonitrile contents. b) This panel provides a summary of the two strategies, indicating that Pathway-A results in higher monomer selectivity.

Detailed conditions

The cascade-lined FMR system consisted of two T-shaped mixers and two reactors (Figure 1e in main text). The other parameters are below.

- buffer-A: 0.1% TFA for Pathway-A, 50 mM acetate (pH4.5) for pathway-B
- buffer-B: 500 mM acetate (pH4.5) for pathway-B
- reactor length; Reactor-1: 250 mm = 0.25 m, Reactor-2: 250 mm = 0.25 m
- reactor diameter; 1 mm = 1×10-3 m
- reactor volume; Reactor-1: 0.196 mL, Reactor-2: 0.196 mL

• flow rate; 0.2 mL/min or 1.0 mL/min (IL-6), 1.8 mL/min or 9.0 mL/min (buffer-A), and 2.0 mL/min or 10.0 mL/min (buffer-B)

• total residence time: 8.83 s = 0.196 (mL)/2.0 (mL/min) + 0.196 (mL)/4.0 (mL/min) or 1.77 s = 0.196 (mL)/10.0 (mL/min) + 0.196 (mL)/20.0 (mL/min)

References and notes

1. Beygmoradi, A.; Homaei, A.; Hemmati, R.; Fernandes, P., Recombinant protein expression: Challenges in production and folding related matters. *Int J Biol Macromol* **2023,** *233*, 123407.

2. Buscajoni, L.; Martinetz, M. C.; Berkemeyer, M.; Brocard, C., Refolding in the modern biopharmaceutical industry. *Biotechnol Adv* **2022,** *61*, 108050.

3. Nabiel, A.; Yosua, Y.; Sriwidodo, S.; Maksum, I. P., Overview of refolding methods on misfolded recombinant proteins from Escherichia coli inclusion bodies. *Journal of Applied Biology & Biotechnology* **2022**.

4. Singh, A.; Upadhyay, V.; Upadhyay, A. K.; Singh, S. M.; Panda, A. K., Protein recovery from inclusion bodies of Escherichia coli using mild solubilization process. *Microb Cell Fact* **2015,** *14*, 41.

5. Yamaguchi, H.; Miyazaki, M., Refolding techniques for recovering biologically active recombinant proteins from inclusion bodies. *Biomolecules* **2014,** *4* (1), 235-51.

6. Samuel, D.; Kumar, T. K.; Ganesh, G.; Jayaraman, G.; Yang, P. W.; Chang, M. M.; Trivedi, V. D.; Wang, S. L.; Hwang, K. C.; Chang, D. K.; Yu, C., Proline inhibits aggregation during protein refolding. *Protein Sci* **2000,** *9* (2), 344-52.

7. Kudou, M.; Yumioka, R.; Ejima, D.; Arakawa, T.; Tsumoto, K., A novel protein refolding system using lauroyl-l-glutamate as a solubilizing detergent and arginine as a folding assisting agent. *Protein Expr Purif* **2011,** *75* (1), 46-54.

8. Yamaguchi, S.; Yamamoto, E.; Mannen, T.; Nagamune, T.; Nagamune, T., Protein refolding using chemical refolding additives. *Biotechnol J* **2013,** *8* (1), 17-31.

9. Otzen, D. E.; Pedersen, J. N.; Rasmussen, H. O.; Pedersen, J. S., How do surfactants unfold and refold proteins? *Adv Colloid Interface Sci* **2022,** *308*, 102754.

10. Porta, R.; Benaglia, M.; Puglisi, A., Flow Chemistry: Recent Developments in the Synthesis of Pharmaceutical Products. *Organic Process Research & Development* **2015,** *20* (1), 2-25.

11. Baumann, M.; Moody, T. S.; Smyth, M.; Wharry, S., A Perspective on Continuous Flow Chemistry in the Pharmaceutical Industry. *Organic Process Research & Development* **2020,** *24* (10), 1802-1813.

12. Al Azri, N.; Patel, R.; Ozbuyukkaya, G.; Kowall, C.; Cormack, G.; Proust, N.; Enick, R.; Veser, G., Batch-to-Continuous transition in the specialty chemicals Industry: Impact of operational differences on the production of dispersants. *Chemical Engineering Journal* **2022,** *445*.

13. Sharma, A. K.; Agarwal, H.; Pathak, M.; Nigam, K. D. P.; Rathore, A. S., Continuous refolding of a biotech therapeutic in a novel Coiled Flow Inverter Reactor. *Chemical Engineering Science* **2016,** *140*, 153-160.

14. Van Snick, J., Interleukin-6: an overview. *Annu Rev Immunol* **1990,** *8*, 253-78.

15. Ahmed, N.; Abbas, R.; Khan, M. A.; Bashir, H.; Tahir, S.; Zafar, A. U., Enhancing recombinant interleukin-6 production yield by fermentation optimization, two-step denaturing, and one-step purification. *Biotechnol Appl Biochem* **2018,** *65* (3), 490-496.

16. Ji, B.-J.; Song, G.; Zhang, Z.; Guo, Z.-Y., Efficient overexpression of human interleukin-6 in Escherichia coli using nanoluciferase as a fusion partner. *Process Biochemistry* **2015,** *50* (10), 1618-1622.

17. Tsumoto, K.; Ejima, D.; Kumagai, I.; Arakawa, T., Practical considerations in refolding proteins from inclusion bodies. *Protein Expr Purif* **2003,** *28* (1), 1-8.

18. Nakahara, Y.; Mendelsohn, B. A.; Matsuda, Y., Antibody–Drug Conjugate Synthesis Using Continuous Flow Microreactor Technology. *Organic Process Research & Development* **2022,** *26* (9), 2766-2770.

19. Somers, W.; Stahl, M.; Seehra, J. S., 1.9 A crystal structure of interleukin 6: implications for a novel mode of receptor dimerization and signaling. *EMBO J* **1997,** *16* (5), 989-97.

20. Fujii, T.; Reiling, C.; Quinn, C.; Kliman, M.; Mendelsohn, B. A.; Matsuda, Y., Physical characteristics comparison between maytansinoid-based and auristatin-based antibody-drug conjugates. *Explor Target Antitumor Ther* **2021,** *2* (6), 576-585.

21. Ejima, D.; Watanabe, M.; Sato, Y.; Date, M.; Yamada, N.; Takahara, Y., High yield refolding and purification process for recombinant human interleukin-6 expressed inEscherichia coli. *Biotechnology and Bioengineering* **1999,** *62* (3), 301-310.

22. Sumikawa, H.; Suzuki, E., Tertiary structural models of human interleukin-6 and evaluation by comparison with X-ray and NMR structures. *Chem Pharm Bull (Tokyo)* **1998,** *46* (1), 136-8.

23. Reckamp, J. M.; Bindels, A.; Duffield, S.; Liu, Y. C.; Bradford, E.; Ricci, E.; Susanne, F.; Rutter, A., Mixing Performance Evaluation for Commercially Available Micromixers Using Villermaux–Dushman Reaction Scheme with the Interaction by Exchange with the Mean Model. *Organic Process Research & Development* **2017,** *21* (6), 816-820.

24. To establish these monomer-selective conditions, our research group evaluated over 100 reaction conditions, including mixing system, pH, organic solvent ratio, ionic strength, and additives, as outlined in Table S1-S3 in the Supplementary Information.

List of Publications

1) Nagaki, A., Ishiuchi, S., Imai, K., Sasatsuki, K., Nakahara, Y., & Yoshida, J.-I. Micromixing enables chemoselective reactions of difunctional electrophiles with functional aryllithiums. Reaction Chemistry and Engineering, (2017), 862-870, 2(6)

2) Endo, Y., Furusawa, M., Shimazaki, T., Takahashi, Y., Nakahara, Y., & Nagaki, A. Molecular Weight Distribution of Polymers Produced by Anionic Polymerization Enables Mixability Evaluation. *Organic Process Research and Development*, (2019), 635-640, 23(4)

https://doi.org/10.1021/acs.oprd.8b00403

3) Nakahara, Y., Metten, B., Tonomura, O., Nagaki, A., Hasebe, S., & Yoshida, J.-I. Modeling and Design of a Flow-Microreactor-Based Process for Synthesizing Ionic Liquids. *Organic Process Research and Development*, (2019), 635-640, 23(4)

https://doi.org/10.1021/acs.oprd.8b00436

4) Nakahara, Y.; Endo, Y.; Takahashi, K.; Kawaguchi, T.; Kato, K.; Matsuda, Y.; Nagaki, A. A Manufacturing Strategy Utilizing a Continuous Mode Reactor toward Homogeneous PEGylated Bioconjugate Production

Synthesis, (2023), In press. DOI: 10.1055/a-2077-6187

Other Publications

1) Nagaki, A., Nakahara, Y., Furusawa, M., Sawaki, T., Yamamoto, T., Toukairin, H., Tadokoro, S., Shimazaki, T., Ito, T., Otake, M., Arai, H., Toda, N., Ohtsuka, K., Takahashi, Y., Moriwaki, Y., Tsuchihashi, Y., Hirose, K., & Yoshida, J.-I. Feasibility Study on Continuous Flow Controlled/Living Anionic Polymerization Processes. *Organic Process Research and Development*, (2016), 1377-1382, 20(7)

https://doi.org/10.1021/acs.oprd.6b00158

2) Nakahara, Y., Furusawa, M., Endo, Y., Shimazaki, T., Ohtsuka, K., Takahashi, Y., Jiang, Y., & Nagaki, A. Practical Continuous-Flow Controlled/Living Anionic Polymerization. *Chemical Engineering & Technology*, (2019), 2154-2163, 42(10)

https://doi.org/10.1002/ceat.201900160

3) Inoue, I., Chiba, M., Ito, K., Okamatsu, Y., Suga, Y., Kitahara, Y., Nakahara, Y., Endo, Y., Takahashi, K., Tagami, U., & Okamoto, N. One-step construction of ferritin encapsulation drugs for cancer chemotherapy. *Nanoscale*, (2021), 1875-1883, 13(3)

https://doi.org/10.1039/d0nr04019c

4) Nakahara, Y., Inoue, I., Endo, Y. Construction protocol of drug-protein cage complexes for drug delivery system. *Methods in Molecular Biology*, (2022), Article in Press

5) 中原祐一. 連続フロー生産に向けたプロセスモニタリング技術の適用, *化学工学*, (2021), 627-630, 85(11)

6) Nakahara, Y., Mendelsohn, B. A., Matsuda, Y. Antibody–Drug Conjugate Synthesis Using Continuous Flow Microreactor Technology. *Organic Process Research and Development*, (2022), 2766-2770, 26(9) https://doi.org/10.1021/acs.oprd.2c00217

7) フローマイクロ合成の実用化への展望 (吉田潤一監修), シーエムシー出版, p. 73-84 (2017)

8) マイクロリアクター/フロー合成による反応条件を最適化した導入と目的に応じた実生産への適用、サイエンス&テクノロジー, p195-216 (2020)

9) 月刊ファームステージ, 技術情報協会, p7-12 (2020)

List of patents

Domestic patents

1) 複合素子及びセンサ 特願 2019-8897

2) 圧電シートおよびその製造方法 特願 2019-9797

3) ポリマーの製造方法 特願 2020-33034

4) 有機化合物封入フェリチンの製造方法 特願 2020-553874

5) フローマイクロリアクターを用いるリフォールディングされたタンパク質の製造方法及びタンパク質のリフォールディング装置 特願 2020-556076

International patents

6) 位置選択的に修飾された抗体中間体、および生体直交性官能基または機能性物質を位置選択的に有する抗体誘導体の製造方法 PCT/JP2022/033613

7) 抗体薬物複合体の製造方法 PCT/JP2021/039001

8) 相性予測方法、相性予測装置および相性予測プログラム PCT/JP2021/018932

9) 品質予測方法、品質予測装置および品質予測プログラム PCT/JP2021/024864

10) L-アミノ酸の製造方法 PCT/JP2010/051071

List of presentations at conferences

Invited presentations

1) 化学工学会関西支部　マイクロプロセス最前線シリーズ　(2017 年 10 月 31 日)

2) The First International Conference on Automated Flow and Microreactor Synthesis (ICAMS-1), January 18-20, 2018 (Osaka, Japan)

3) 化学工学会関西支部　マイクロプロセス最前線シリーズ　(2018 年 11 月 20 日)

4) 近畿化学協会フロー・マイクロ合成研究会　第 81 回研究会(2019 年 2 月 8 日)

5) 京都大学マイクロ化学生産研究コンソーシアム講演会　(2021 年 7 月 8 日)

6) 岡山マイクロリアクターネット 第 35 回例会 (2021 年 12 月 3 日)

7) 近畿化学協会フロー・マイクロ合成研究会　第 93 回研究会(2022 年 1 月 28 日)

Oral presentations

1) 日本化学会　第 98 春季年会 2018, フローマイクロリアクタを用いた選択性制御有機リチウム種と二官能性求電子剤の反応

2) 日本化学会　第 99 春季年会 2019, マイクロリアクタによるイオン液体合成におけるモデリングとプロセス設計

Poster presentations

1) 14th International Conferences on MicroREaction technology (IMRET14)

(September 12-14, 2016, Beijing, China)

2) 日本プロセス化学会 2017 サマーシンポジウム

フローマイクロリアクタによる有機リチウム種の官能基選択性制御

Seminar Presentations

1) シーエムシー出版 フローマイクロ合成の基礎・反応制御と応用技術動向

(2019 年 03 月 13 日)

2) 技術情報協会 フロー合成の装置選定と条件設定、トラブル対策

(2021 年 10 月 19 日)

3) サイエンス&テクノロジー マイクロリアクター/フロー合成による反応条件を最適化した導入と目的に応じた実生産への適用(2020 年 12 月 4 日)

4) サイエンス&テクノロジー　マイクロリアクターにおける合成操作で起こる不具合とトラブル対策および活用に向けた課題(2022 年 1 月 20 日)

Other books and chapters

1) フローマイクロ合成の実用化への展望　(吉田潤一監修), シーエムシー出版,　p. 73-84 (2017)

2) マイクロリアクター/フロー合成による反応条件を最適化した導入と目的に応じた実生産への適用、サイエンス&テクノロジー, p195-216 (2020)

3) 月刊ファームステージ, 技術情報協会, p7-12 (2020)

Press release

1) Ajinomoto OmniChem Launches Flow Chemistry for API Commercial Manufacturing

https://www.ajibio-pharma.com/news-post/ajinomoto-omnichem-launches-flow-chemistry-for-api-commercial-manufacturing/

2) ADC 迅速製造装置の実現 -フローリアクタによる抗体薬物複合体の迅速合成-

https://www.chem-station.com/blog/2023/03/adc.html

Acknowledgement

Firstly, I would like to express my sincerest gratitude to Professor Aiichiro Nagaki for his excellent guidance, valuable discussions, and warm words of encouragement throughout this work. The studies presented in this thesis were carried out during 2011-2023 in Ajinomoro Co., Inc., as part of investigations on novel applications of flow flash chemistry for biopharmaceutical compounds.

Some studies were completed as collaborations with members of Micro Chemical Production Study Consortium in Kyoto University and Ajinomoto Omnichem and Ajinomoto Althea. I am grateful to Ms. Mai Furusawa (TOHO CHEMICAL INDUSTRY COMPANY, LIMITED), Mr. Toshiya Shimazaki (TACMINA CORPORATION), Dr. Bert Metten, Dr. Eric De Vos (Ajinomoto Omnichem) and Assistant Professor Osamu Tonomura (Kyoto University), Professor Shinji Hasebe (Kyoto University) and Professor Kazuhiro Mae (Kyoto University).

I am greatly indebted to all former/present members of the management at Ajinomoto Co. Inc., during my research period. Notably, Dr. Yutaka Matsuda (currently director antibody-drug conjugate chemistry at Exelixis Inc.,), Dr. Ippei Inoue (currently senior principal researcher at Suntory Global Innovation Center), Mr. Keisuke Kato, Dr. Yuta Endo, Dr. Kazutoshi Takahashi, Mr. Takahiro Okasora, Dr. Masoyo Date, Dr. Naoyuki Yamada (currently chief technology officer at Synplogen), Dr. Daisuke Ejima (currently senior director at Sysmex), Dr. Yoshimi Kikuchi, Dr. Teruhisa Mannen, Dr. Akira Okano, Dr. Fumihiko Takatsuki, and Dr. Atsushi Konishi, Mr. Takahiro Terawaki, Mr. Kazuhiro Hioki, and Mr. Junya Wakuda, Mr. Osamu Nishikawa, Dr. Kazuhiro Hasegawa, Dr. Shinrtaro Iwatani, Dr. Akito Chinen, Dr. Hiroshi Itaya, Dr. Takayuki Ito, Mr. Ryuichi Sasaki,

Dr. Tomoyuki Ohnishi, Dr. Tatsuya Okuzumi and Mr. Yosuke Koyama, Dr. Hiroshi Miyano, Dr. Kazuya Onomichi, Dr. Toshihisa Kato for his technical, linguistic and for their invaluable contributions.

I would also like to express my sincere thanks to Professor Masaya Sawamura of Hokkaido University, Professor Takanori Suzuki of Hokkaido University, Associate Professor Hisanori Senboku of Hokkaido University, Ms. Tomoko Kawaguchi of Hokkaido University, Associate Professor Minami Atsushi of Hokkaido University and Lecturer Kazuhiro Okamoto of Hokkaido University and Lecturer Yosuke Ashikari of Hokkaido University for all their valuable discussions and encouragement.

Furthermore, I wish to express sincere thanks to my manager and colleagues at Ajinomoto Co. Inc., Dr. Ikuo Kira, Dr. Masaru Takayanagi, Dr. Kazuhiro Nakanishi, Dr. Takashi Kayahara, Mr. Hirohisa Narahashi and Mr. Masahiro Karakawa, Mr. Kenichi Kasumi, Ms. Megumi Kaneko, Mr. Hiroshi Umishio, Mr. Takumi Yoshida, Mr, Shota Ino, Ms. Kaori Kobayashi, Ms. Kaoru Ogawa and Mr. Hiroshi Orikabe.

I gratefully dedicate the achievements of my studies to Emeritus Professor Jun-ichi Yoshida of Kyoto University and express my deepest appreciation for his extremely valuable guidance over many years, especially for establishing the concept of Flash Chemistry.

Last but not least, I wish to express my deepest appreciation to my family, Ms. Yukiko Nakahara, Mr. Yuki Nakahara, Ms. Miku Nakahara, Ms. Natsuki Nakahara, Mr. Akio Nakahara, Ms. Yasuko Nakahara and Ms. Harue Kitagawa, for their affectionate encouragement and constant assistance throughout this work. Without their support and love, I could not have completed the doctoral thesis.

Yuichi Nakahara

Hokkaido University